AD_____

Award Number: DAMD17-00-1-0042

TITLE: A Novel Member of the Insulin-like Growth Factor Binding Protein Superfamily in Prostate Cancer

PRINCIPAL INVESTIGATOR: Ron G. Rosenfeld, M.D.

CONTRACTING ORGANIZATION: Oregon Health Sciences University
Portland, OR 97201-3098

REPORT DATE: February 2004

TYPE OF REPORT: Final

PREPARED FOR: U.S. Army Medical Research and Materiel Command
Fort Detrick, Maryland 21702-5012

REPORT DOCUMENTATION PAGE

Form Approved
OMB No. 074-0188

1. AGENCY USE ONLY (Leave blank)	2. REPORT DATE	3. REPORT TYPE AND DATES COVERED
	February 2004	Final (1 Feb 2000 - 31 Jan 2004)

4. TITLE AND SUBTITLE

A Novel Member of the Insulin-like Growth Factor Binding Protein Superfamily in Prostate Cancer

5. FUNDING NUMBERS

DAMD17-00-1-0042

6. AUTHOR(S)

Ron G. Rosenfeld, M.D.

7. PERFORMING ORGANIZATION NAME(S) AND ADDRESS(ES)

Oregon Health Sciences University
Portland, OR 97201-3098

E-Mail: rosenfer@ohsu.edu

8. PERFORMING ORGANIZATION REPORT NUMBER

9. SPONSORING / MONITORING AGENCY NAME(S) AND ADDRESS(ES)

U.S. Army Medical Research and Materiel Command
Fort Detrick, Maryland 21702-5012

10. SPONSORING / MONITORING AGENCY REPORT NUMBER

11. SUPPLEMENTARY NOTES

12a. DISTRIBUTION / AVAILABILITY STATEMENT

Approved for Public Release; Distribution Unlimited

12b. DISTRIBUTION CODE

13. ABSTRACT (Maximum 200 Words)

The insulin-like growth factors (IGFs) are potent mitogens for normal and cancerous prostatic cells. The IGFs are found complexed to IGF binding proteins (IGFBPs) which modulate IGF bioactivity, but also may themselves act in an IGF-independent manner. We have recently characterized a series of IGFBP-related proteins (IGFBP-rPs) which share homology with the IGFBPs in the amino-terminus, bind IGFs with low affinity, and regulate cell growth through both IGF-dependent and IGF-independent actions. This grant is directed at the study of IGFBP-rP2 (also known as connective tissue growth factor) as a regulator of normal and malignant prostatic growth. The specific aims are to: 1) analyze IGFBP-rP2 mRNA and protein expression and distribution in normal and malignant prostatic tissues; 2) determine the transcriptional, translational and post-translational regulation of IGFBP-rP2; and 3) determine the mechanisms by which IGFBP-rP2 regulates prostatic growth.

14. SUBJECT TERMS

Growth factors, insulin-like growth factors, binding proteins, tumor suppressors

15. NUMBER OF PAGES

82

16. PRICE CODE

17. SECURITY CLASSIFICATION OF REPORT	18. SECURITY CLASSIFICATION OF THIS PAGE	19. SECURITY CLASSIFICATION OF ABSTRACT	20. LIMITATION OF ABSTRACT
Unclassified	Unclassified	Unclassified	Unlimited

Table of Contents

INTRODUCTION:

The insulin-like growth factors (IGFs) are potent mitogens for normal and cancerous prostatic cells. The IGFs are found complexed to IGF binding proteins (IGFBPs), which modulate IGF bioactivity, but may themselves act in an IGF-independent manner. We have characterized recently a series of IGFBP-related proteins (IGFBP-rPs) which share homology with the IGFBPs in the amino-terminus, bind IGFs with low affinity, and regulate cell growth through both IGF-dependent and IGF-independent actions. This grant is directed at the study of IGFBP-rP2 (more commonly known as connective tissue growth factor) as a regulator of normal and malignant prostatic growth. The specific aims are to: 1) analyze IGFBP-rP2 mRNA and protein expression and distribution in normal and malignant prostatic tissues; 2) determine the transcriptional, translational and post-translational regulation of IGFBP-rP2; and 3) determine the mechanisms by which IGFBP-rP2 regulates prostatic growth.

BODY:

Over the course of this grant, we have succeeded in the following accomplishments related to the approved Statement of Work (references indicated in parentheses):

Task 1: Analyze IGFBP-rP2 mRNA and protein expression and distribution in normal and malignant prostatic tissue (months 1-12):

IGFBP-rP2 mRNA and protein expression were analyzed in a panel of prostate cells, including human prostate epithelial cells (HPEC), immortalized prostate epithelial cells (P69), a tumorigenic prostate subline of P69 (M12), as well as the established prostate cancer cell lines, PC-3, DU145 and LNCaP. Cellular localization of IGFBP-rP2 protein expression in these same cells was also performed, although conclusive data were only obtained to permit a determination that IGFBP-rP2 was secreted and/or cell-associated. Thus, Task 1 was completed as indicated in the grant proposal, with the most important results obtained from this series of investigations published in Reference 2 (Lopez-Bermejo, *et al*, ENDOCRINOLOGY 141:4072-4080, 2000.

In brief, IGFBP-rP2 was detected in most of the normal and malignant prostatic epithelial cells tested. Of the cancer cells, expression at the mRNA level was most pronounced in M12 and PC3 cells, with low expression in DU145 and LNCaP cells. Moderate expression was detected in non-malignant P69 cells and early passage of HPEC (HPEC4), and, somewhat surprisingly, expression at least equivalent to that observed in M12 and PC3 cells was detected in late passage of HPEC (HPEC9). Protein expression, as determined from immunoblot analysis, corresponded with mRNA expression, with protein readily detected in conditioned media (CM) from HPEC9. Additionally, cell-associated IGFBP-rP2 was immunodetected in all cell lines. It is of note that a more quantitative method for detecting IGFBP-rP2, employing ELISA, was developed subsequently in our laboratory, employing the antibodies that we generated (Reference 4; Twigg, *et al*, ENDOCRINOLOGY 142:1760-1769, 2001). We have concluded, on the

basis of this series of investigations, that expression of IGFBP-rP2 could not be correlated with the degree of tumorigenicty, unlike our observations with the structurally related IGFBP-rP1, whose expression decreased in malignant cells, compared to normal cells (Reference 2; Lopez-Bermejo, *et al,* ENDOCRINOLOGY 141:4072-4080, 2000). On the other hand, it appears that IGFBP-rP2 expression increases with passaging of HPEC (at least form HPEC4 to HPEC9), perhaps representing a marker of senescence in HPEC. Indeed, we characterized HPEC as a "senescing" prostate epithelial cell, both by growth profile and by increases in the senescence marker, $p16^{INK4a}$. These findings, together with data on the regulation of IGFBP-rP2 (see Task 2, below) suggest that IGFBP-rP2 may be involved in either growth or senescence of normal and prostate cancer cells. These findings represent the first characterization in the literature of IGFBP-rP2/connective tissue growth factor (CTGF) mRNA and protein expression in normal and malignant prostate cells. All aspects of Task 1 have been completed.

A critical goal of our research has been the development of appropriate reagents for investigation of IGFBP-rP protein levels in various cancers and human biological fluids. We had previously generated specific antisera for IGFBP-rP1/mac25, IGFBP-rP2/CTGF and IGFBP-rP3/novH, which were employed in immunoblotting studies. Efforts then turned to development of highly specific antibodies which could be employed to generate sensitive and specific assays and be used for specific immunostaining studies. We have now succeeded in producing both polyclonal and monoclonal antibodies which can differentiate between IGFBP-rP1 and IGFBP-rP2, and have developed an assay which is capable of quantifying concentrations of IGFBP-rP1/mac25 in human biological fluids (Reference 7; Lopez-Bermejo, *et al,* JOURNAL OF CLINICAL ENDOCRINOLOGY AND METABOLISM 88:3401-3408, 2003). Employing baculovirus-generated IGFBP-rP1, we generated a panel of 11 monoclonal antibodies; 10/11 were of sufficient sensitivity to identify nanomolar amounts of IGFBP-rP1, and none cross-reacted with the six high-affinity IGFBPs nor with IGFBP-rP2 or –3. Evaluation of the newly developed IGFBP-rP1 immunoassay indicated a detection limit of 0.7 ug/L, a dynamic range of 3.13-100 ug/L, and intra- and inter-assay coefficients of variation of 2.5-6.8 and 3.1-6.4% at 24-85 ug/L. In random human adult sera (n=41), the median IGFBP-rP1 concentration was 21.0 ug/L, and values did not correlate with serum levels of IGF-I, IGF-II or IGFBP-3. The monoclonal anti-IGFBP-rP1 antibodies also readily detected IGFBP-rP1 expression in human tissue sections, with preferential expression of IGFBP-rP1 in the microvascular endothelium associated with tumorigenesis. These findings support a role for the IGFBP-rPs in vascular biology and suggest that they may be involved in the process of neoangiogenesis in malignancy. Development of highly specific and sensitive assays for IGFBP-rP2/CTGF should allow further evaluation of this hypothesis.

In further studies on the expression of IGFBP-rP2 in cancer, its expression was evaluated in 12 sporadic hepatoblstomas (Reference 6; Von Horn, *et al*, INTERNATIONAL JOURNAL OF MOLECULAR MEDICINE, 9:645-649, 2002). The expression profiles for the IGFBP-rPs were found to be disturbed. In the case of IGFBP-rP2, three tumors had increased gene expression, with one sample having greatly enhanced expression.

Limitations of investigations relevant to Task 1: In addition to generating anti-IGFBP-rP2 polyclonal antibodies, for the studies described above, we also produced monoclonal antibodies, in an effort to enhance specificity. The monoclonal antibodies generated, however, proved upon screening to not have the requisite specificity and sensitivity, and proved to be of less use than the polyclonal antibodies. While polyclonal antibodies were highly useful for western immunoblotting and ELISA studies (see above), attempts to employ these reagents in immunohistochemical analysis of tissue sections proved unsuccessful. In parallel with these efforts, we were successful in generating monoclonal antibodies against recombinant IGFBP-rP1 (see above), and to employ both our polyclonal and monoclonal anti-IGFBP-rP1 antibodies in immunohistochemical analysis of normal and cancerous prostatic tissue (Reference 7; Lopez-Bermejo, *et al*, JOURNAL OF CLINICAL ENDOCRINOLOGY AND METABOLISM 88:3401-3408, 2003.

Task 2: Determine the transcriptional, translational and post-translational regulation of IGFBP-rP2 (months 1-24):

We analyzed the regulation of IGFBP-rP2 expression in prostate cells by employing reagents known to inhibit growth in prostate cancer cells, such as transforming growth factor-ß (TGFß) and retinoic acid (RA), as well as IGF-I and related growth factors (Reference 2; Lopez-Bermejo, *et al*, ENDOCRINOLOGY 141:4072-4080, 2000). Employing our panel of prostate cell lines, we first demonstrated that HPEC was the most sensitive of all the cells tested to TGFß1 and IGF-I treatment. At TGFß1 concentrations as low as 5 ng/ml, proliferation of HPEC was inhibited 70%, compared to untreated control cells, and this inhibition correlated with increased IGFBP-rP2 expression at both the mRNA and protein levels. IGF-I, at concentrations of 100 ng/ml, which stimulates HPEC growth in all cell passage numbers, dramatically inhibited IGFBP-rP2 expression, often by 90%. As a comparison, IGFBP-rP1 expression remained unchanged during these manipulations. RA, like TGFß1, up-regulated IGFBP-rP2 expression. These results strongly suggest that IGFBP-rP2 plays a role in the regulation of prostate cell proliferation in response to a variety of growth factors. The effects of these growth factors on prostate cancer cells (i.e., stimulation by IGF-I and inhibition by TGFß1) were more modest, than in normal HPEC. Nevertheless, the observed effects upon IGFBP-rP2 followed the same trends as observed in HPEC.

We were also able to demonstrate that TGFß1 regulated IGFBP-rP2 expression in human dermal fibroblast cells, as do advanced glycosylation end-products (AGE)-BSA

(Reference 4; Twigg, *et al*, ENDOCRINOLOGY 142:1760-1769, 2001). AGE treatment of primary cultures of nonfetal human dermal fibroblasts in confluent monolayers increased IGFBP-rP2 steady-state mRNA levels in a time- and dose-dependent manner. These findings link AGE and IGFBP-rP2 in profibrotic and proangiogenic roles, a finding of potential relevance to both the complications of diabetes and the growth of human cancers. We further demonstrated that the induction of fibronectin by AGE is partially mediated by the AGE-induced up-regulation of cell-derived IGFBP-rP2/CTGF (Reference 5; Twigg, *et al*, ENDOCRINOLOGY 143:1260-1269, 2002.

The effect of sodium butyrate (NaB), a potent inhibitor of cancer cell growth, on the regulation of IGFBP-rP2 expression was correlated with the inhibitory effects of NaB in a variety of cancer cell lines (Reference 3; Tsubaki, *et al*, JOURNAL OF ENDOCRINOLOGY 169:97-110, 2001). NaB specifically up-regulated the expression of IGFBP-3 and IGFBP-rP2, with parallel results observed on Northern and protein blots. NaB was found to uniformly suppress DNA synthesis in both cancerous and non-cancerous cells and up-regulate IGFBP-3 and IGFBP-rP2 mRNA and protein levels. In prostate cancer cell lines, a cell growth inhibitory NaB concentration of 10 nM, which up-regulates, IGFBP-3, also up-regulated IGFBP-rP2expression in PC-3 cells, but not in LNCaP cells. Proteolysis of IGFBP-rP2 was not found to be a significant factor, either under basal conditions, or following treatment with TGFß, RA, or IGF-I.

Limitations of investigations relevant to Task 2: Given the modest effects observed with TGFß1 and RA on prostate cancer cells, studies employing IGFBP-rP2 antisense oligo-deoxynucleotides were not completed, and are deemed by us to be, at this point, a relatively low priority. Other than this, all aspects of Task 2 were completed.

Task 3: Determine the mechanism by which IGFBP-rP2 regulates prostatic growth:

A role for IGFBP-rP2 in regulation of cell growth was first ascertained in fibroblasts, where the addition of recombinant IGFBP-rP2 resulted in increased expression of fibronectin mRNA (Reference 5; Twigg, *et al*, ENDOCRINOLOGY 143:1260-1269, 2002). The similar addition of exogenous C-terminal FLAG-tagged IGFBP-rP2 to prostate cells did not demonstrate consistent inhibition of cell proliferation, suggesting that either our FLAG-tagged IGFBP-rP2 preparation was less active than untagged IGFBP-rP2, or that, in prostate cancer cells, IGFBP-rP2 may need to act in concert with other regulated factors to promote inhibition of cell growth. On the other hand, we have recently demonstrated that at least one of our IGFBP-rP2 polyclonal antibodies possesses neutralizing properties, and, in our fibroblast model, have shown that the addition of the IgG-purified fraction of the anti-IGFBP-rP2 antibody abrogated AGE-BSA induction of fibronectin mRNA. Use of such antibodies may prove to be an alternative method to the use of antisense ODNs for determining the role of IGFBP-rP2 in growth inhibition.

To address the possibility that our FLAG-tagged IGFBP-rP2 preparation may be less biologically active than non-tagged, heparin-column purified IGFBP-rP2, we generated fresh preparations of both forms of IGFBP-rP2 protein in a baculovirus system, and

purified the protein either via anti-FLAG-agarose column or heparin columns. Further, we elected to test our prepapartions in the cell model system of NIH3T3 cells with an overexpressed IGF-I receptor (IGFIR) (see figures 1-6 included in appendix). Since we had previously demonstrated that IGFBP-rP2 had the capability to bind IGFs with low affinity in *in vitro* assays (Kim, *et al*, PNAS 94:12981-12986, 1997), we reasoned that the NIH3T3:IGFIR would permit us to determine whether recombinant IGFBP-rP2 is capable of exerting IGF-dependent biological effects (as proposed in Task 3). Our results demonstrated that: a) IGFBP-rP2, whether FLAG-tagged, non-tagged-heparin column-purified, or anti-IGFBP-rP2 antibody column-purified, appeared to potentiate and sustain IGF-stimulated IGFIR signaling; b) potentiation effects of IGFBP-rP2 required preincubation of IGFBP-rP2 and IGF; IGFBP-rP2 alone had no effect on IGFIR signaling, and preincubation of cells with IGFBP-rP2 prior to the addition of IGFs did not enhance IGFIR signaling; and c) potentiation effects appear to be IGF-I-specific, as no potentiation of insulin, IGF-II or EGF signaling pathways was observed.

Studies are currently in progress to determine if prostate cell lines (M12 and DU145) stably transfected with IGFBP-rP2, will demonstrate alteration of cell growth. Otherwise, Task 3 has been completed.

KEY RESEARCH ACCOMPLISHMENTS OVER LAST 12 MONTHS:

1. Characterization of IGFBP-rP2 expression in normal and malignant prostatic tissue
2. Characterization of molecular regulation of IGFBP-rP2 by known pro-apoptotoic, profibrotic and proangiogenic factors
3. Characterization of IGFBP-rP expression in hepatoblastoma
4. Development of highly sensitive and specific monoclonal and polyclonal antibodies for IGFBP-rP1 and IGFBP-rP2
5. Development of specific immunoassay for IGFBP-rP1; identification of IGFBP-rP1 in human cancer blood vessels

REPORTABLE OUTCOMES:

1. Vorwerk P, Hohmann B, Oh Y, Rosenfeld RG, Symko RM: Binding properties of insulin-like growth factor binding protein-3 (IGFBP-3), IGFBP-3 N- and C-terminal fragments, and structurally related proteins mac25 and connective tissue growth factor measured using a biosensor. Endocrinology 143:1677-1685, 2002
2. Lopez-Bermejo A, Buckway CK, Devi GR, Hwa V, Plymate SR, Oh Y, Rosenfeld RG: Characterization of inulin-like growth factor binding protein-related proteins (IGFBP-rPs) 1, 2, and 3 in human prostate epithelial cells: potential roles for IGFBP-rP1 and 2 in senescence of the prostatic epithelium. Endocrinology 141:4072-4080, 2000
3. Tsubaki J, Choi W-K, Ingermann AR, Twigg SM, Kim H-S, Rosenfeld RG, Oh Y: Effects of sodium butyrate on expression of members of the IGF-binding protein superfamily in human mammary epithelial cells. J Endocrinol 169:97-110, 2001
4. Twigg SM, Chen MM, Joly AH, Chakrapani SD, Tsubaki J, Kim H-S, Oh Y, Rosenfeld RG: Advanced glycosylation end products up-regulate connective tissue growth factor (insulin-like growth factor-binding protein-related protein 2) in human fibroblasts: a potential mechanism for expansion of extracellular matrix in diabetes mellitus. Endocrinology 142:1760-1769, 2001
5. Twigg SM, Joly AH, Chen MM, Tsubaki J, Kim H-S, Hwa V, Oh Y, Rosenfeld RG: Connective tissue growth factor/IGFBP-rP2 is a mediator in the induction of fibronectin by advanced glycosylation end-products in human dermal fibroblasts. Endocrinology 143:1260-1269, 2002
6. Von Horn H, Hwa V, Rosenfeld RG, Hall K, The BT, Tally M, Ekstrom TJ, Gray SG: Altered expression of low-affinity insulin-like growth factor binding protein related proteins in hepatoblastoma. Int J Mol Med 9:645-649, 2002
7. Lopez-Bermejo A, Khosravi J, Corless CL, Krishna RG, Diamandi A, Bodani U, Kofoed EM, Graham DL, Hwa V, Rosenfeld RG: Generation of anti-insulin-like growth factor binding protein-related protein 1 (IGFBP-rP1/MAC25) monoclonal antibodies and immunoassay; quantification of IGFBP-rP1 in human serum and distribution in human fluids and tissues. J Clin Endocrinol Metab 88:3401-3408, 2003

CONCLUSIONS:

The low-affinity IGFBP-related proteins appear to have important IGF-independent actions in the regulation of normal and malignant cell growth. Studies from our laboratory over the last three years have demonstrated an important role for these factors in senescence, tumor suppression, fibrosis and angiogenesis. Studies of gene expression and protein synthesis have implicated these factors as biologically relevant to cancer. The development of highly specific and sensitive antibodies should permit further delineation of their roles.

"So what": The entire GH-IGF axis has been the subject of increased interest from the perspective of longevity and cancer. In addition to the actions of IGFs and IGFBPs under *in vitro* conditions, a variety of epidemiological studies have served to underscore the relevance of these factors to human biology and tumor suppression. The low-affinity IGFBP-related proteins appear to share with several of the high-affinity IGFBPs, the ability to suppress cancer growth through IGF-independent means. Further studies are clearly warranted in delineating the relative contributions of each component of this complex growth axis.

APPENDICES: attached figures and manuscripts.

Figure 1A

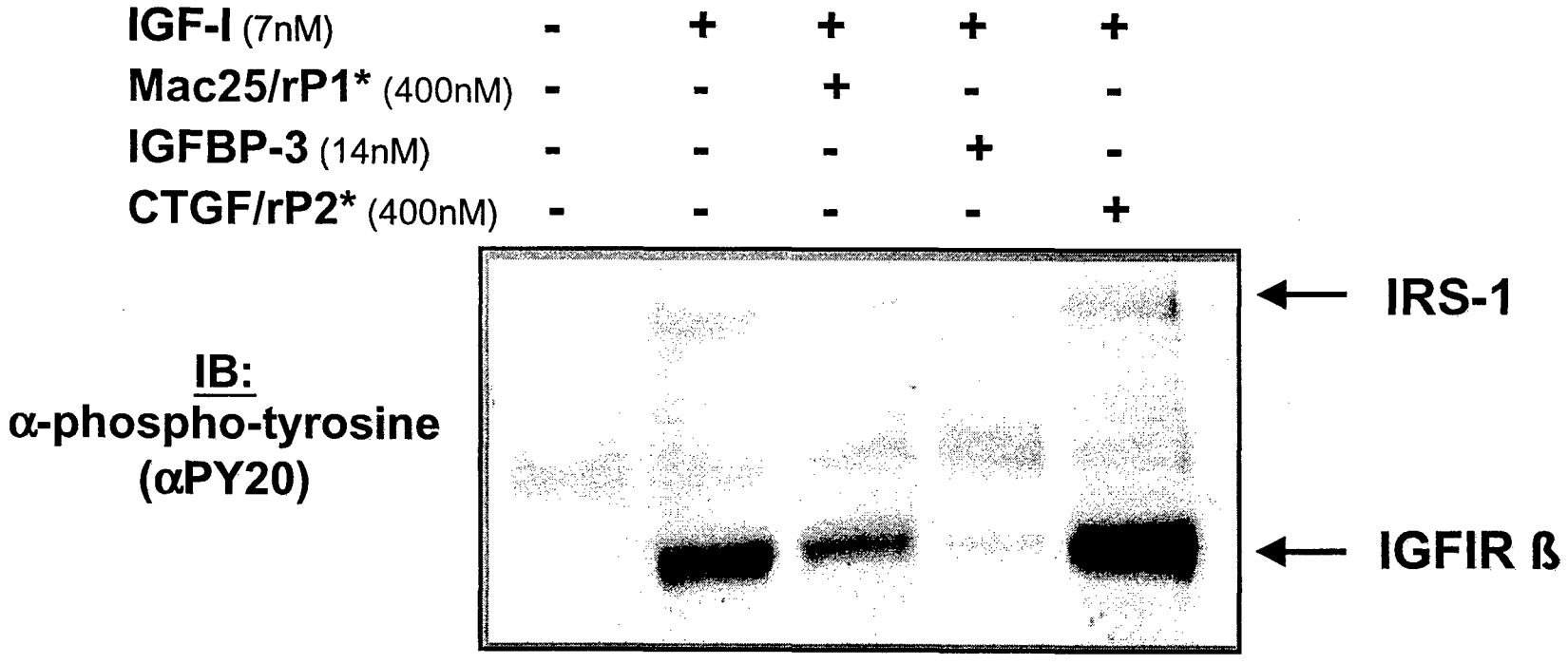
IGF-I (7nM) - + + + +
Mac25/rP1* (400nM) - - + - -
IGFBP-3 (14nM) - - - + -
CTGF/rP2* (400nM) - - - - +
IB:
α-phospho-tyrosine
(αPY20)
IRS-1
IGFIR ß

Figure 1B

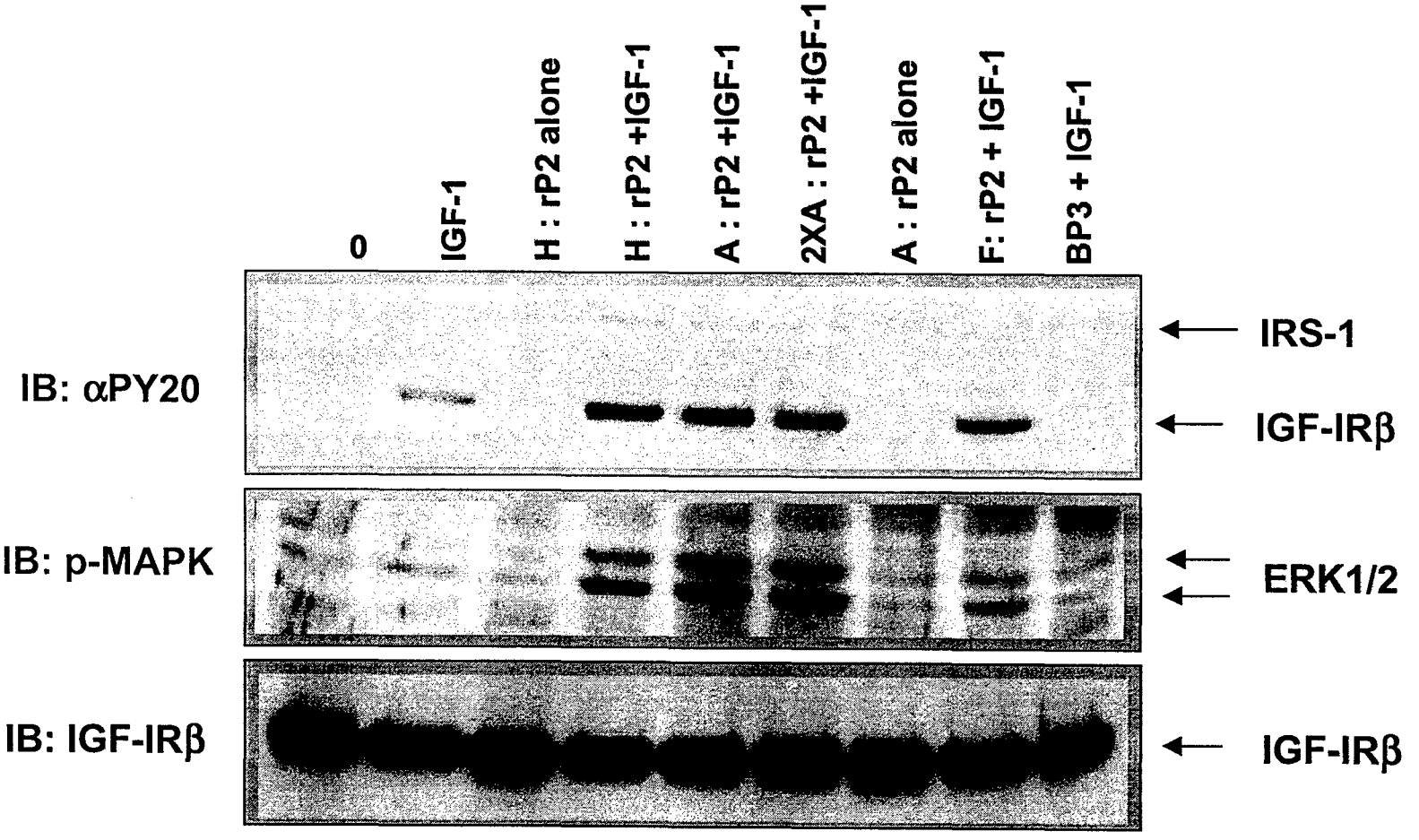

H = Heparin purified rP2
A = rP2 antibody column purified rP2
F = Flag-tagged M2 column purified rP2

Figure 2

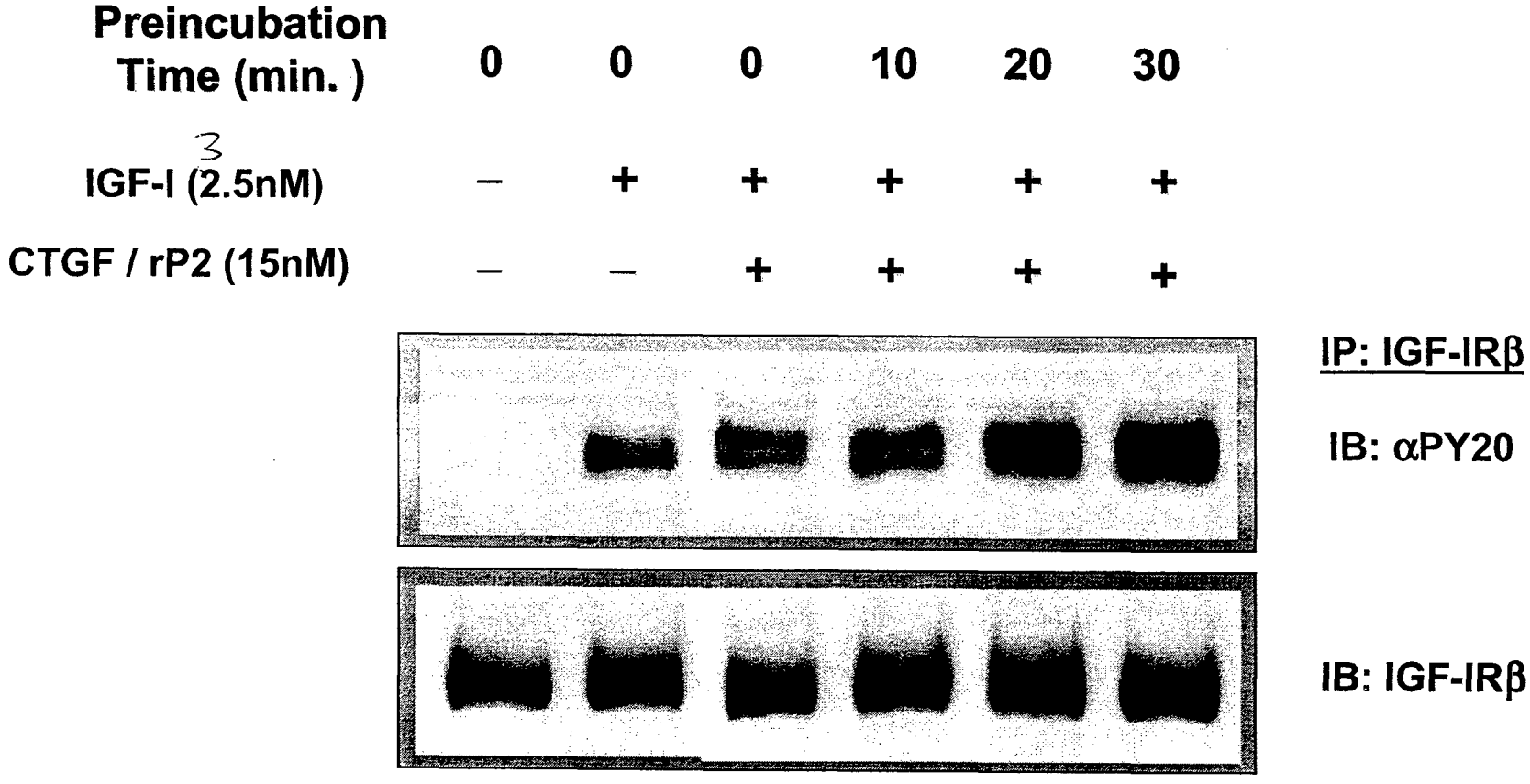
Preincubation Time (min.)
0 0 0 10 20 30
IGF-I (2.5nM)
– + + + + +
CTGF / rP2 (15nM)
– – + + + +
IP: IGF-IRβ
IB: αPY20
IB: IGF-IRβ

Figure 3A & B

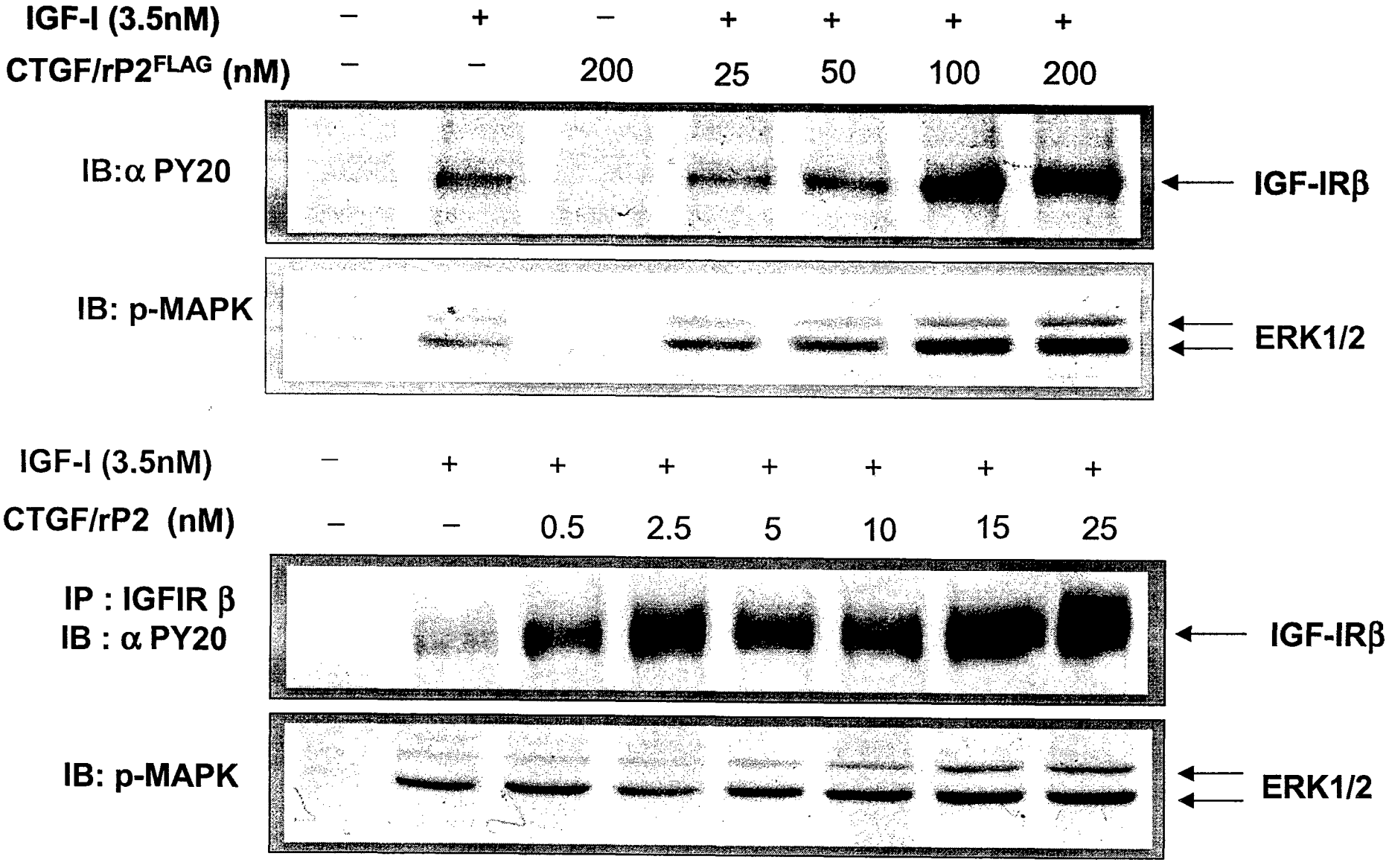
IGF-I (3.5nM) – + – + + + +
CTGF/rP2FLAG (nM) – – 200 25 50 100 200
IB:α PY20
IGF-IRβ
IB: p-MAPK
ERK1/2
IGF-I (3.5nM) – + + + + + + +
CTGF/rP2 (nM) – – 0.5 2.5 5 10 15 25
IP : IGFIR β
IB : α PY20
IGF-IRβ
IB: p-MAPK
ERK1/2

Figure 4

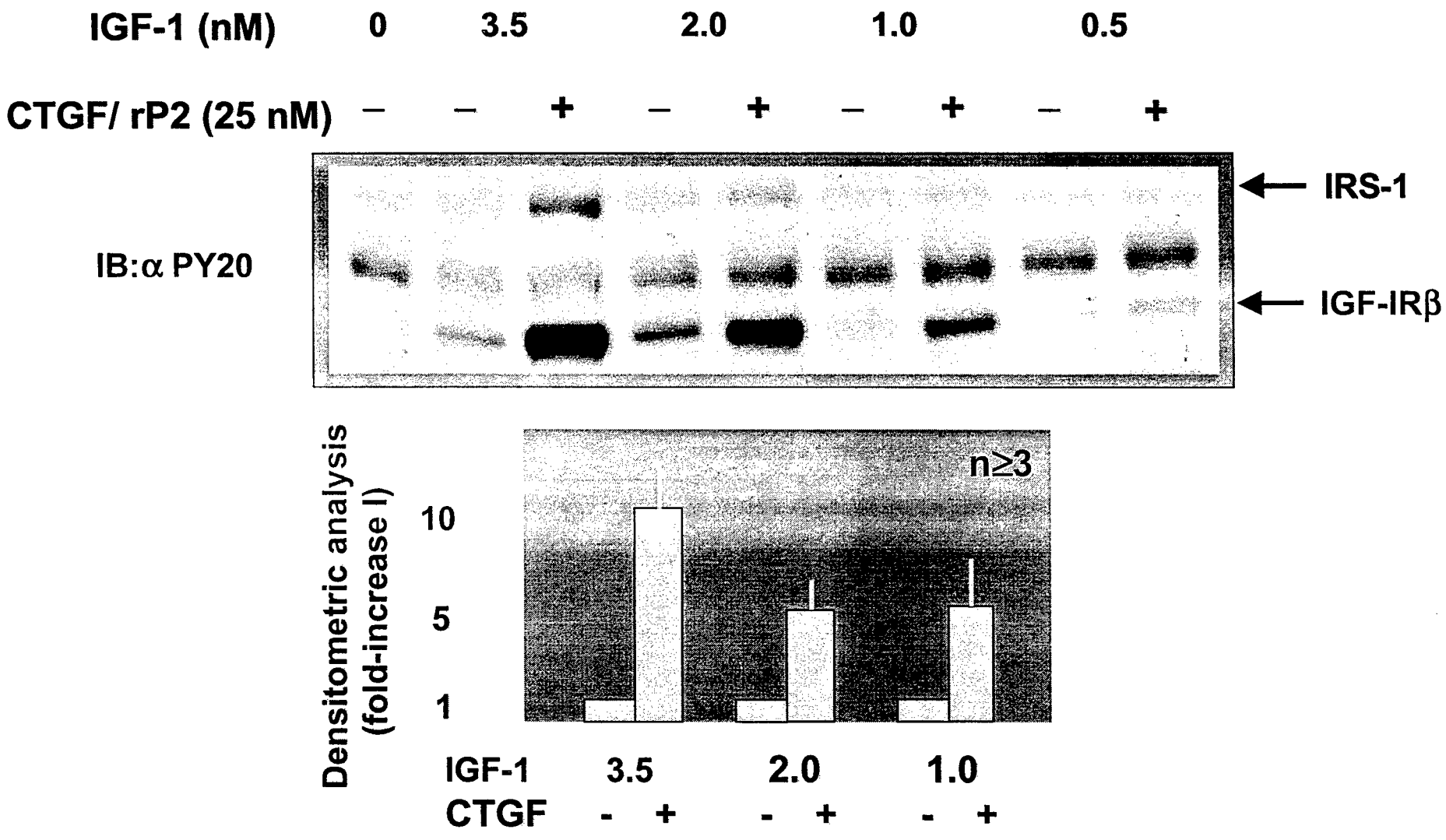
IGF-1 (nM) 0 3.5 2.0 1.0 0.5
CTGF/ rP2 (25 nM) – – + – + – + – +
IB:α PY20
IRS-1
IGF-IRβ
Densitometric analysis (fold-increase I)
10
5
1
n≥3
IGF-1 3.5 2.0 1.0
CTGF - + - + - +

Figure 5

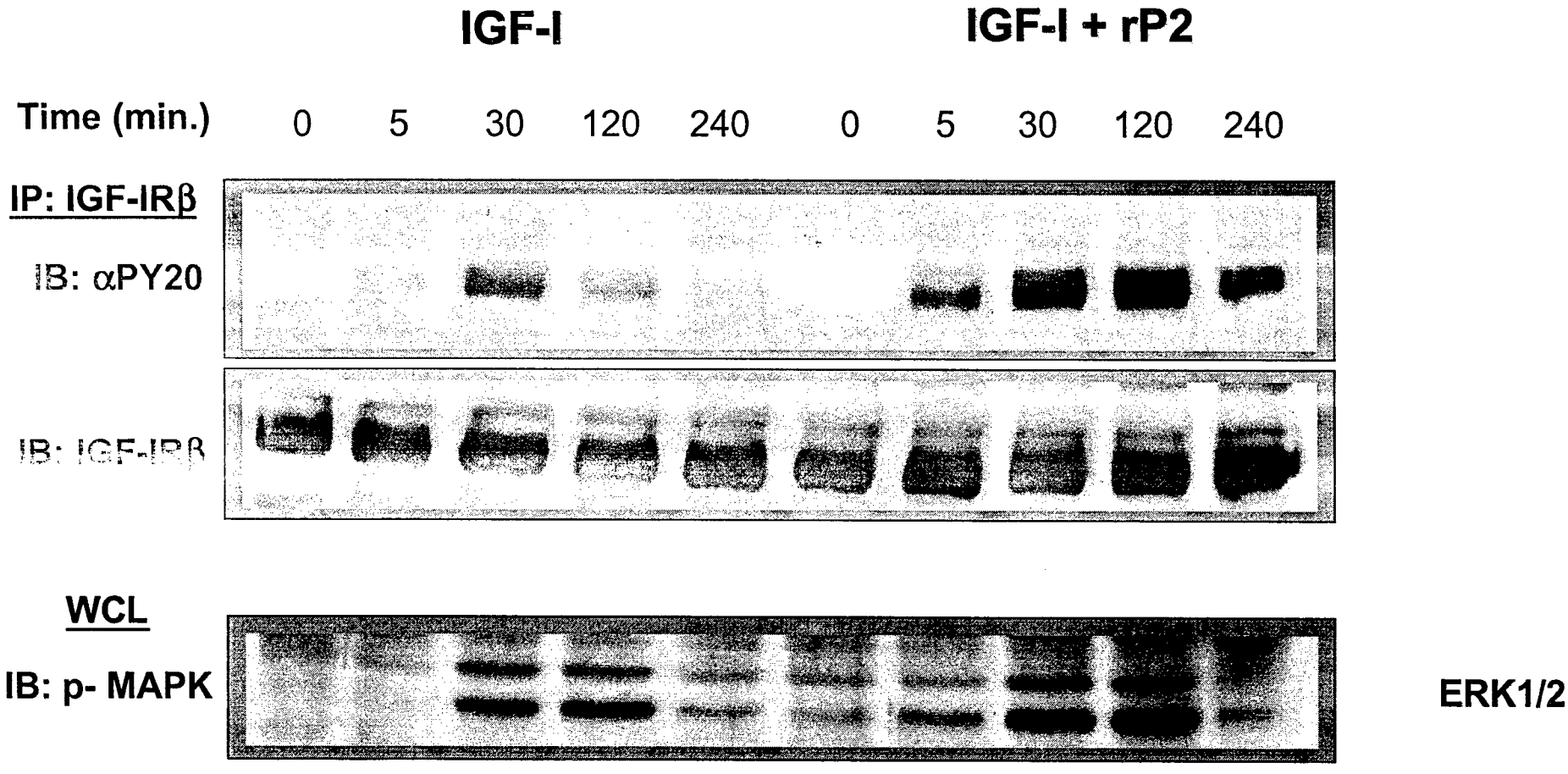
IGF-I
IGF-I + rP2
Time (min.)
0
5
30
120
240
0
5
30
120
240
IP: IGF-IRβ
IB: αPY20
IB: IGF-IRβ
WCL
IB: p- MAPK
ERK1/2

Figure 6

A. NIH3T3:IGFIR

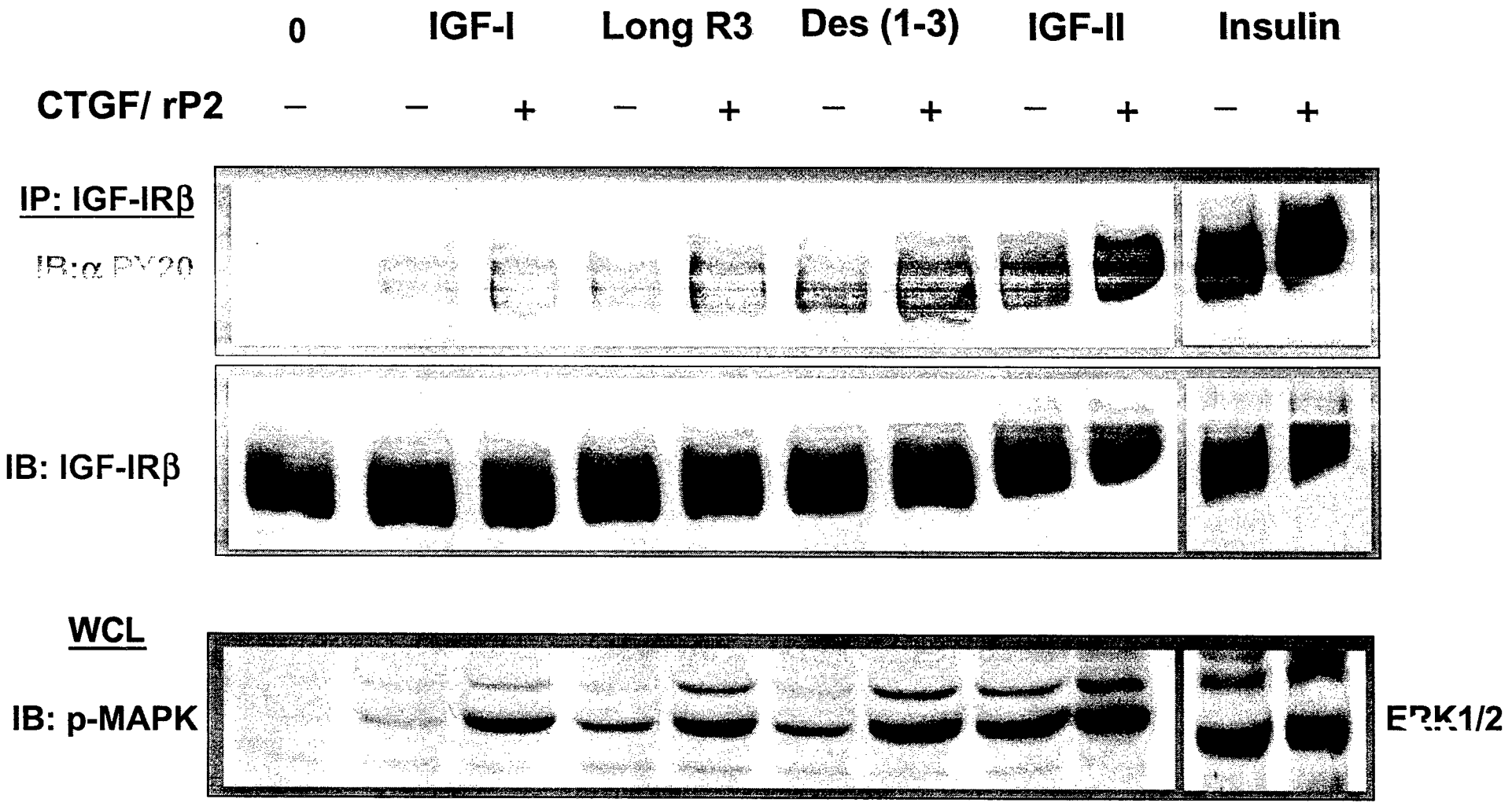

0013-7227/02/$15.00/0
Printed in U.S.A.

Endocrinology 143(5):1677–1685

Binding Properties of Insulin-Like Growth Factor Binding Protein-3 (IGFBP-3), IGFBP-3 N- and C-Terminal Fragments, and Structurally Related Proteins mac25 and Connective Tissue Growth Factor Measured Using a Biosensor

PETER VORWERK, BIANKA HOHMANN, YOUNGMAN OH, RON G. ROSENFELD, AND RONALD M. SHYMKO

Department of Pediatric Oncology, Otto von Guericke University (P.V., B.H.), Magdeburg 39112, Germany; Department of Pediatrics, Oregon Health Sciences University (Y.O., R.G.R.), Portland, Oregon 97201; and Department of Scientific Computing, Novo Nordisk A/S (R.M.S.), Måløv DK-2760, Denmark

We measured the binding of IGF-I and IGF-II to recombinant human N-terminal [residues 1–97; recombinant human IGF-binding protein-3$^{1-97}$ (rhIGFBP-3$^{1-97}$)] and C-terminal (residues 98–264; rhIGFBP-3$^{98-264}$) IGFBP-3 fragments and compared it with IGF binding to intact IGFBP-3 using biosensor analysis. Experiments were carried out in different configurations, either with binding protein or fragment immobilized or with IGF immobilized. These experiments showed that IGF-I and IGF-II bind to IGFBP-3 with affinities of 4–5 × 10^9 M^{-1} and similar binding kinetics. The affinities of both rhIGFBP-3$^{1-97}$ and rhIGFBP-3$^{98-264}$ for IGF proteins were approximately 3 orders of magnitude less than that of full-length IGFBP-3. These results further support the concept that high affinity binding of IGF to IGF-binding proteins results from a two-site interaction of IGF with both the N- and C-terminal regions of the binding protein.

Binding of insulin to IGFBP-3 and its N- and C-terminal fragments and of IGF-I and IGF-II to the structurally related proteins mac25 and connective tissue growth factor was also investigated. Weak insulin binding to full-length IGFBP-3 could be demonstrated in a few experiments, but we found that binding of IGF-I, IGF-II, and insulin to mac25 or connective tissue growth factor was below the detection limit of the biosensor instrument. (*Endocrinology* 143: 1677–1685, 2002)

IGF BINDING PROTEINS (IGFBPs) are important regulators of IGF action that act by modulating IGF binding to its receptors. Initially identified as carriers for IGFs in a variety of biological fluids, their presumed function is to protect IGF peptides from degradation and clearance, increase the half-life of IGFs, and deliver them to appropriate tissue receptors (1). A number of IGFBP fragments have been identified in different biological fluids, and a variety of specific and nonspecific proteases for IGFBPs have been described (2, 3). The concept of IGFBPs as simple carrier proteins has been complicated by the discovery of multiple IGF-independent actions of IGFBPs and the identification of a number of cDNAs encoding proteins that bind IGF with substantially lower affinities than IGFBPs (4). The N-terminal regions of these proteins are structurally homologous to the IGFBPs, with conservation of the cysteine residues and a common N-terminal motif, GCGCCXXC (1). This observation initially suggested an IGFBP superfamily consisting of the classical high affinity IGFBPs and a group of low affinity IGFBP-related proteins, later identified as mac25, CTGF, and others (1, 4).

IGFBP-3 is the major serum IGFBP and transports 70–90% of the circulating IGFs (5). In target cell systems it inhibits IGF actions, but also, under specific conditions, potentiates IGF action or exerts IGF-independent effects (5, 6). Proteolysis of IGFBP-3 was initially demonstrated in human pregnancy serum, in which circulating IGFBP-3 was found primarily in low mol wt forms (7, 8). The proteolytic fragments were shown to bind IGF with lower affinities, thereby increasing availability of IGF to target receptors. Subsequent studies in different biological fluids demonstrated that limited proteolysis is not restricted to IGFBP-3, but also occurs in other IGFBP-species, IGFBP-1 through -5 (2, 3). As for IGFBP-3, the resulting fragments have a decreased affinity for IGFs and, therefore, more easily release IGF to the target receptors. Furthermore, various IGFBP fragments are capable of direct stimulatory or inhibitory action at the target cells (9–13).

All members of the proposed IGFBP superfamily preserve the N-terminal cysteine-rich domain, including the IGFBP motif GCGCCXXC, but vary in the intermediate region and C-terminal domain of the protein. Only the high affinity IGFBPs also share homology in the cysteine-rich C-terminal domain, which has led to the hypothesis that the conserved N-terminal domain contains the main IGF-binding activity, forming, together with the C-terminal conserved region, the high affinity IGF-binding activity in IGFBPs (1, 13–15). With the expression and purification of a variety of recombinant IGFBPs, structurally related proteins mac25 and CTGF, and well defined fragments or mutants, our understanding of structure-function relationships of the members of the pro-

Abbreviations: CTGF, Connective tissue growth factor; IGFBP, IGF binding protein; rhIGFBP-3$^{1-97}$, recombinant human IGF binding protein-3$^{1-97}$; R_{max}, amount of analyte bound at saturation in RU; RU, resonance units.

posed IGFBP superfamily has improved (12, 13, 15–25). However, exact measurement of the binding properties of these various proteins, and especially their proteolytic fragments, has proved difficult. Different methods have been used to estimate the binding affinities: conventional binding assays using radiolabeled IGFs, affinity cross-linking with radiolabeled ligands, gel filtration or Western ligand blots using radiolabeled or biotinylated ligands (12–14, 17, 20, 21, 26–32). However, it has been difficult to determine accurate affinities of IGFs for IGFBPs using those assays due to several limiting factors, such as the quality of labeled ligands and proteins, the effect of labeling iodine on affinity, and the limitation of the measurable range of the binding affinity.

In recent years biosensor instruments using surface plasmon resonance technology have been increasingly used to study biomolecular interactions. We (33–35) and others (15, 36–39) have used this technology to study IGFBP interaction with IGFs or their analogs. In the present study our goal was to make a detailed analysis, using a BIACORE biosensor instrument (Biacore AB, Uppsala, Sweden), of the binding of IGF-I and IGF-II to recombinant IGFBP-3 and fragments of this molecule and also to the structurally related proteins mac25 and CTGF.

Materials and Methods

Equipment and reagents

Experiments were performed on an upgraded BIACORE 1000 instrument (Biacore AB). CM5 certified sensor chips, surfactant P20, and the amine coupling kit (*N*-hydroxysuccinimide, *N*-ethyl-*N*′-(3-diethylaminopropyl)carbodiimide, and ethanolamine hydrochloride) were also obtained from Biacore AB. Recombinant human nonglycosylated IGFBP-3 (rhIGFBP-3) produced in *Escherichia coli* was a gift from Protegen (Mountain View, CA). N- and C-terminal recombinant fragments, rhIGFBP-3^{1-97} and rhIGFBP-3^{98-264} as well as structurally related proteins mac25 and CTGF were synthesized by use of a baculovirus expression system in insect cells that synthesize the correct proteins, as previously described in detail (20, 32, 40). The recombinant proteins possess the expected structure based upon purity and size characterized by silver staining and Western immunoblot and appropriate size shifting in Western immunoblot under reducing conditions, indicating the presence of S-S bonds in the proteins. IGF-I and IGF-II were purchased from GroPep Pty. Ltd. (Adelaide, SA, Australia) and the biotinylation of IGF-I was performed according to the method of Fowlkes (30).

Immobilization of peptides on the sensor chip

All immobilizations were carried out at 25 C using an amine coupling procedure (33) with a constant flow rate of 5 μl/min. A more thorough description of the immobilization procedure can be found elsewhere (41). Equal volumes of 0.1 M *N*-hydroxysuccinimide and 0.1 M *N*-ethyl-*N*′-(3-diethylaminopropyl)carbodiimide were mixed by the BIACORE system's robotics and injected over the surface of the sensor chip to activate the carboxymethylated dextran. For coupling to the sensor chip, peptides were injected over the activated surface in a 10-mM sodium acetate solution. A solution of 1 M ethanolamine was then passed over the surface to deactivate the remaining active carboxyl groups and to wash out nonspecifically bound protein.

Combinations of peptide concentration, pH during coupling, activation time, and coupling time, respectively, giving a stable surface with satisfactory amounts of the coupled peptide, were as follows: rhIGFBP-3: 10 μg/ml, pH 4.5, 3 min, 7 min; rhIGFBP-3^{98-264}: 2 μg/ml, pH 4.5, 7 min, 7 min; rhIGFBP-3^{1-97}: 20 μg/ml, pH 4.0, 10 min, 10 min; IGF-I: 4 μg/ml, pH 4.5, 7 min, 7 min; and IGF-II: 1 μg/ml, pH 4.0, 7 min, 7 min. All ethanolamine deactivation steps were run for 7 min. Immediately after the immobilization procedure, HBS buffer (10 mM HEPES; 150 mM NaCl; 3.4 mM EDTA; and 0.005% P20, pH 7.4) was flowed over the sensor chip surface for a minimum of 2 h to allow the surface to stabilize.

Quality control of immobilized surfaces

In repeated experiments for each peptide, concentration and coupling time were varied to give a range of immobilized peptide coupled to the sensor chip, to check for possible mass transport effects, which are expected to be most pronounced at high immobilization levels and high binding affinities (42, 43), and also to control for dependence of fitted binding parameters or of apparent stoichiometry of binding on immobilization level. We calculate the apparent stoichiometry as the ratio of the maximum achievable analyte bound, measured in the instrument's standard resonance units (RU), to the theoretical maximum, where the theoretical maximum is defined as: immobilized RU × molecular weight (analyte)/molecular weight (immobilized peptide), where immobilized RU is the amount of peptide immobilized on the sensor chip, also expressed in RU. The apparent stoichiometry gives a good indication of the degree of inactivation of protein due to immobilization and the steric hindrance of binding due to overcrowding of immobilized molecules on the surface. Immobilization levels in our experiments were kept low both to give as high apparent stoichiometries as possible and to reduce steric hindrance effects. Typical apparent stoichiometries for immobilized rhIGFBP-3 were 0.8–0.9, whereas those for immobilized IGF-I were about 25% and even lower for IGF-II. Note that a low apparent stoichiometry will still give accurate binding results if the immobilized molecules are all either fully active or fully inactive.

Mass transport effects (42, 43) were observed when measuring binding of rhIGFBP-3 to immobilized IGF-I or IGF-II, and these effects could not be fully eliminated even at the high flow rates (50 μl/min) used in our experiments. Mass transport effects were not apparent for any of the other tested molecules. In the case of rhIGFBP-3 binding to immobilized IGF-I, analysis of sensorgram data using models including or lacking mass transport effects showed only minor differences in estimated binding parameters. These differences were especially minimal in global analyses (*i.e.* simultaneous analysis of multiple sensorgrams at different analyte concentrations) (44, 45). None of the experiments showed a systematic change in binding parameters with immobilization level.

Kinetic assays on the BIACORE

All experiments were carried out at 25 C, with a constant flow rate of 50 μl/min HBS buffer. This high flow rate was chosen to minimize mass transport effects (46). Purified analyte was diluted to various concentrations in HBS buffer using the system robotics, and the solution was injected over the peptides coupled to the chip surface for 5 min (association phase), followed by 10-min flow of HBS buffer alone (dissociation phase). In most experiments the binding phases were preceded by a 10-min wash with HBS buffer alone to allow the surface to equilibrate with the buffer. Bound analyte was removed from the coupled peptide by flowing a solution of 100 mM HCl over the surface for 3 min. This treatment regenerated the surfaces efficiently without any apparent damage. We observed, however, that IGF-I surfaces immobilized at very low levels tended to be somewhat unstable. In these cases the surface was regenerated using 50 mM HCl to minimize any damaging effects of the regeneration procedure.

In most experiments, a standard intermediate concentration of analyte was first injected over the surface to provide a reference sensorgram. Then a series of varying concentrations of analyte was injected, followed by a second reference injection, a repeat of the concentration series, and a final reference injection. With this procedure the immobilized surface could be monitored for loss of activity, and test results checked for reproducibility.

Solution affinity assays

Solution affinity assays are designed to measure the equilibrium affinity of two molecules in solution, using the BIACORE instrument as a probe to measure the free concentration of one of the molecules (47). In these experiments rhIGFBP-3 or one of its N- or C-terminal fragments was immobilized on a sensor chip to provide an active surface for measuring the free concentration of IGF-I or IGF-II in a mixture of IGF and binding protein flowing over the surface. The surface was calibrated by flowing IGF at different (free) concentrations over the surface, recording a sensorgram for each concentration. Mixtures of IGF and binding protein or fragment at various concentrations were flowed over the

same surface, and the calibration curve was used to estimate the free IGF remaining in solution for each of the mixed samples. The equilibrium affinity constant, K_a, was calculated using this estimate plus the known total concentrations of IGF and binding protein, assuming a one-site binding model.

Data analysis

Kinetic analyses were carried out using the BIAEvaluation 3.0 program (Biacore AB), assuming a one-site binding model. If the surface was judged stable by inspection of the repeated series of injected analyte concentrations, all sensorgrams in an experiment were analyzed simultaneously (global analysis). If a surface showed some instability, sensorgrams were analyzed individually, and the results pooled. In all cases, special attention was paid to the fitted R_{max}, which gives the amount of analyte bound at saturation and is a therefore a measure of the apparent stoichiometry of binding. We have observed that even a visually good fit of a binding model to sensorgram data sometimes gives an unreasonable value of R_{max}, especially when analyzing single sensorgrams. Binding parameter estimates were rejected in such cases.

Model fitting was first done allowing the BIAEvaluation program to estimate the bulk refractive index effect for each sensorgram. Sensorgrams were then inspected visually to obtain another estimate of these values based on the step up in the sensorgram at the start of the association phase and the step down at the start of the dissociation phase (33). If the fitted estimates did not correspond to the visual estimates, the fitted estimates were rejected, and the fit was redone with the refractive index values fixed using the visual estimates. In a few experiments the surface baseline signal (that is, the signal seen when buffer alone flows over the surface) drifted slowly downward through time (baseline drift), evident in the 10-min preassociation wash and at the end of the dissociation phase. In these cases, the downward drift rate was estimated by fitting a straight line to the 10-min wash, and the sensorgram was corrected for this drift during the fitting.

Results

Binding of IGF-I and IGF-II to rhIGFBP-3 and its N- and C-terminal fragments

With the BIACORE instrument, a binding reaction can be measured with either of the reacting pair immobilized, and the other injected over the immobilized surface. In this study we attempted to measure all binding reactions in both orientations, which would be expected to give comparable results if the experimental conditions are suitable.

Figure 1 shows the binding of IGF-I to rhIGFBP-3 with either rhIGFBP-3 immobilized (412 RU; Fig. 1A) or IGF-I immobilized (256 RU; Fig. 1B). These sensorgrams show the typical protocol used in these studies: a 10-min wash to allow the surface to equilibrate with the buffer, followed by a 10-min association phase and a 10-min dissociation phase. The short downward spikes seen in the sensorgrams are disturbances resulting from opening and closing of valves in the BIACORE instrument's flow system. A sharp rise in signal at the beginning of the association phase and a corresponding sharp drop at the beginning of the dissociation phase are due to a small refractive index difference between buffer alone and buffer containing the analyte protein.

In Fig. 1, A and B, the concentration of analyte was 20 nM. The difference in maximum analyte bound (75 RU IGF-I *vs.* 200 RU rhIGFBP-3) is due to the difference in mol wt. The linearity of the initial portion of the association phase of the sensorgram in Fig. 1B indicates the presence of mass transport effects. However, analyses of these experiments with or without including mass transport in the model gave comparable results, which were also in agreement with results

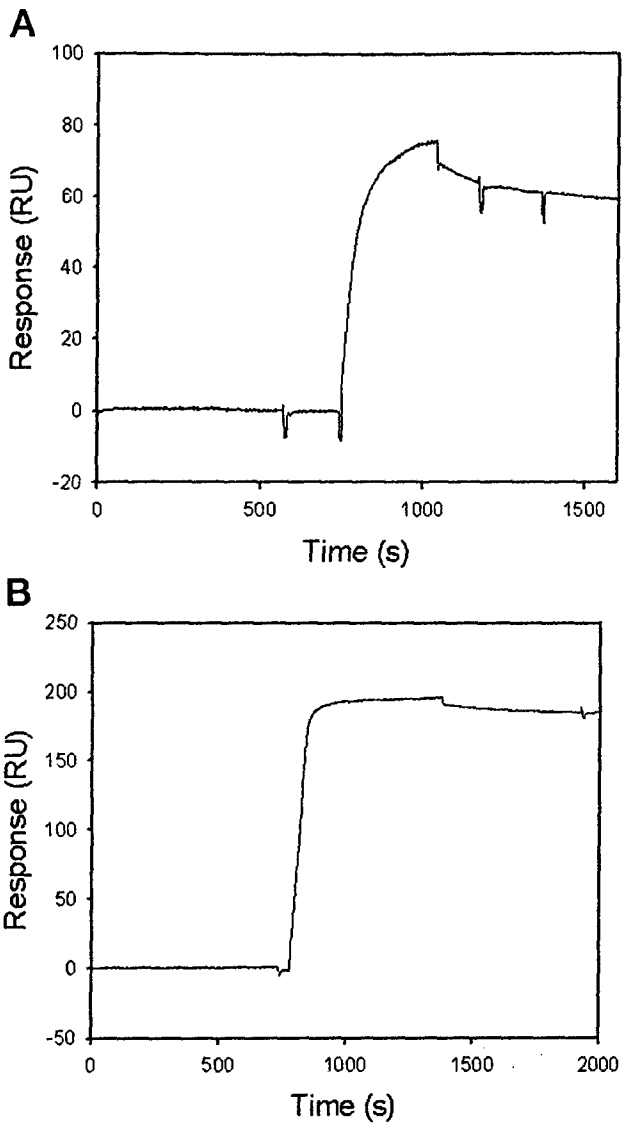

FIG. 1. A, IGF-I (20 nM) binding to immobilized full-length rhIGFBP-3 (412 RU). HBS buffer was flowed over the surface for 12 min, followed by 5 min of association and 10 min of dissociation of IGF-I. B, Full-length rhIGFBP-3 (20 nM) binding to immobilized IGF-I (256 RU).

obtained with rhIGFBP-3 immobilized and IGF-I as analyte (*e.g.* Fig. 1A).

Figure 2 shows the results of similar experiments using the binding protein fragments rhIGFBP-3^{1-97} and rhIGFBP-3^{98-264}. For each of the fragments, the shapes of the sensorgrams were similar whether the fragment or IGF-I was immobilized. The rhIGFBP-3^{1-97} and rhIGFBP-3^{98-264} sensorgrams had different general shapes because both the kinetic association and dissociation constants were slower for rhIGFBP-3^{98-264} than for rhIGFBP-3^{1-97} (see Table 1), although these differences were not statistically significant over the entire set of experiments. Note that there was a downward or upward drift in signal during the initial wash stage in the experiments with binding protein fragments immobilized. This was a general observation during these studies; that is, sensor chip surfaces immobilized with binding protein fragment tend to

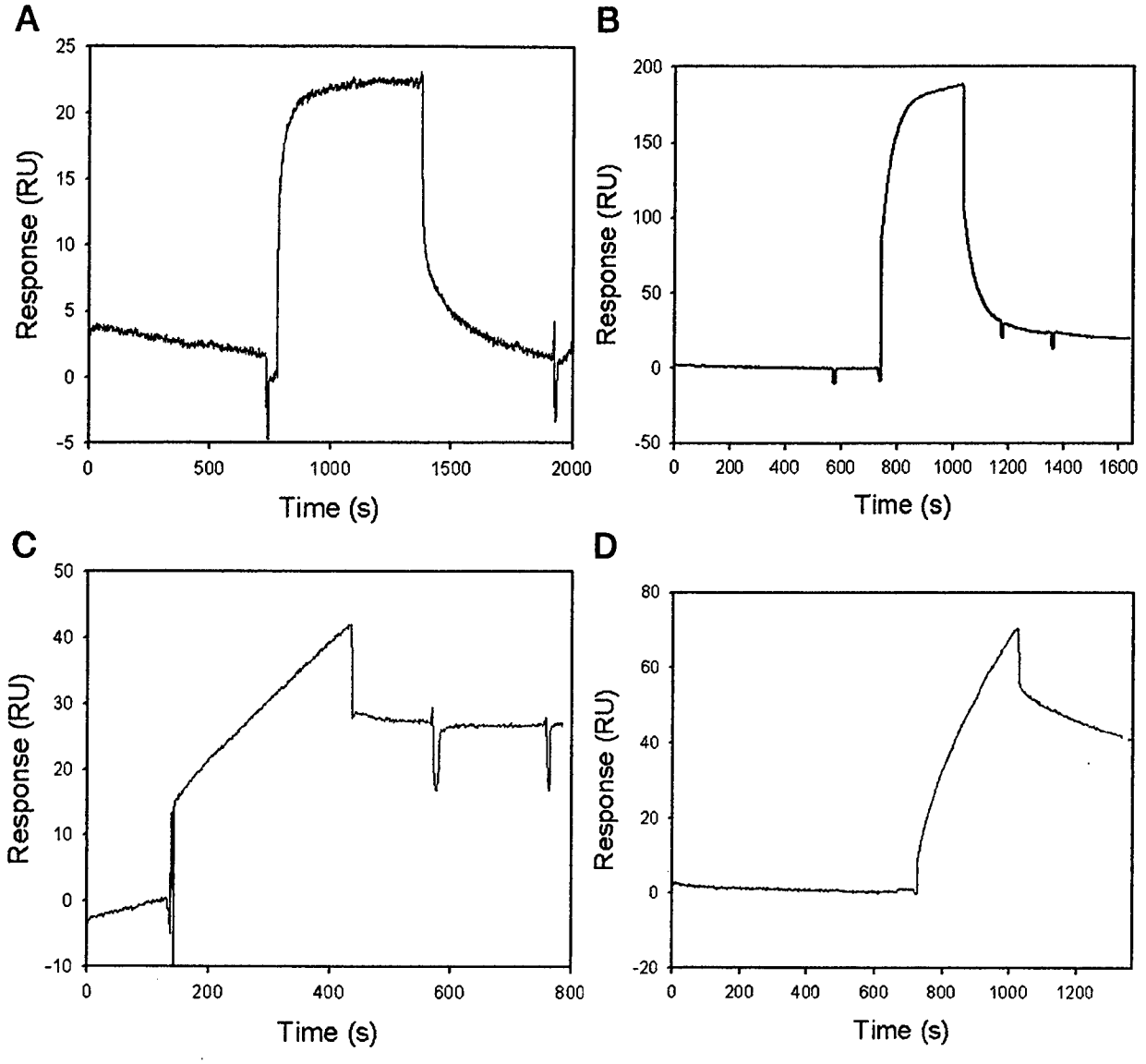

FIG. 2. A, IGF-I (1000 nM) binding to immobilized rhIGFBP-3^{1-97} (1245 RU). B, rhIGFBP-3^{1-97} (200 nM) binding to immobilized IGF-I (532 RU). C, IGF-I (100 nM) binding to immobilized rhIGFBP-3^{98-264} (2253 RU). D, rhIGFBP-3^{98-264} (1000 nM) binding to immobilized IGF-I (191 RU).

be more unstable than those immobilized with full-length rhIGFBP-3, or with IGF-I.

In Fig. 3 is shown a comparison of the measured binding affinity for IGF-I binding to full-length rhIGFBP-3 or to the binding protein fragments, either with binding protein immobilized or with IGF-I immobilized. The data are plotted with a logarithmic ordinate, and the results show that the affinity of IGF-I for either rhIGFBP-3^{1-97} or rhIGFBP-3^{98-264} is approximately 1000-fold lower than the affinity for full-length rhIGFBP-3. Although the mean affinity for rhIGFBP-3^{1-97} measured in these experiments was higher than that for rhIGFBP-3^{98-264}, the differences were not statistically significant. All differences between full-length rhIGFBP-3 and the fragments were significant.

Figure 3 also shows that experiments in either immobilization orientation give similar measured affinities. However, because of apparent self-aggregation of rhIGFBP-3 and the C-terminal fragment (see *Discussion*), the results with IGF-I immobilized on the sensor chip were considered less reliable.

Whenever possible, binding parameter estimates were obtained from global fitting to multiple sensorgrams at different analyte concentrations. An example of such an experiment is shown in Fig. 4. In this experiment rhIGFBP-3 was immobilized at 726 RU, and IGF-I at concentrations from 0.5–50 nM was flowed over the immobilized surface. Because of the high affinity of IGF-I for rhIGFBP-3, binding is affected by mass transport limitation, which is most pronounced at lower analyte concentrations. The entire set of sensorgram data was fitted using a model that includes mass transport effects, and for comparison was refitted using an ordinary one-site (Langmuir) binding model. For this experiment, the computed binding affinities for the two models were 5.6×10^9 and 5.8×10^9 M^{-1}, respectively. The respective kinetic association constants were 8.3×10^5 and 6.4×10^5 $M^{-1}s^{-1}$, and the dissociation constants were 1.4×10^{-4} and 1.2×10^{-4}

TABLE 1. 1 IGF-I and IGF-II binding to immobilized binding protein or fragments

A) K_a values: units = 1/M, errors are SEs			
	rhIGFBP-3	rhIGFBP-3^{1-97}	rhIGFBP-3^{98-264}
IGF-I	$4.13 \pm 0.71 \times 10^9$	$6.14 \pm 1.98 \times 10^6$	$1.80 \pm 0.84 \times 10^6$
IGF-II	$4.68 \pm 0.83 \times 10^9$	$5.89 \pm 1.09 \times 10^6$	$1.01 \pm 0.89 \times 10^7$
B) K_a values: units = 1/M.s, errors are SEs			
	rhIGFBP-3	rhIGFBP-3^{1-97}	rhIGFBP-3^{98-264}
IGF-I	$7.87 \pm 1.00 \times 10^5$	$3.22 \pm 1.11 \times 10^4$	$2.54 \pm 2.15 \times 10^3$
IGF-II	$7.63 \pm 1.60 \times 10^5$	$3.63 \pm 2.67 \times 10^4$	$2.17 \pm 1.61 \times 10^4$
C) K_d values: units = 1/s, errors are SEs			
	rhIGFBP-3	rhIGFBP-3^{1-97}	rhIGFBP-3^{98-264}
IGF-I	$2.09 \pm 0.35 \times 10^{-4}$	$5.55 \pm 1.40 \times 10^{-3}$	$1.09 \pm 0.69 \times 10^{-3}$(NS)
IGF-II	$1.78 \pm 0.53 \times 10^{-4}$	$5.48 \pm 3.52 \times 10^{-3}$(NS)	$3.18 \pm 1.19 \times 10^{-3}$

Binding parameters (±SE) for IGF-I and IGF-II binding to immobilized rhIGFBP-3, rhIGFBP-3^{1-97}, and rhIGFBP-3^{98-264}. A), Equilibrium affinity, K_a (M^{-1}). B), Kinetic association constant, K_a (M^{-1}/s^{-1}). C), Kinetic dissociation constant, K_d (S^{-1}). Differences between the two fragments are not significant. Differences between rhIGFBP-3 and the fragments are significant, except for those with NS in *parentheses*.

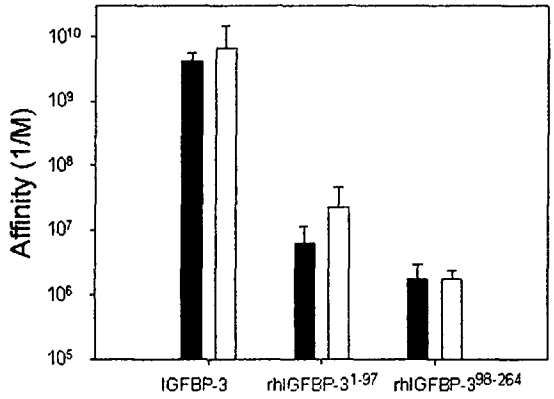

FIG. 3. Comparison of measured IGF-I binding affinities in opposite immobilization orientations. ■, Binding protein or fragment immobilized, IGF-I in the flow-through buffer; □, IGF-I immobilized, binding protein or fragment in the flow-through buffer. *Error bars* show SDs. All differences between parameters for rhIGFBP-3 and those for the fragments are statistically significant, but differences between the two fragments are not.

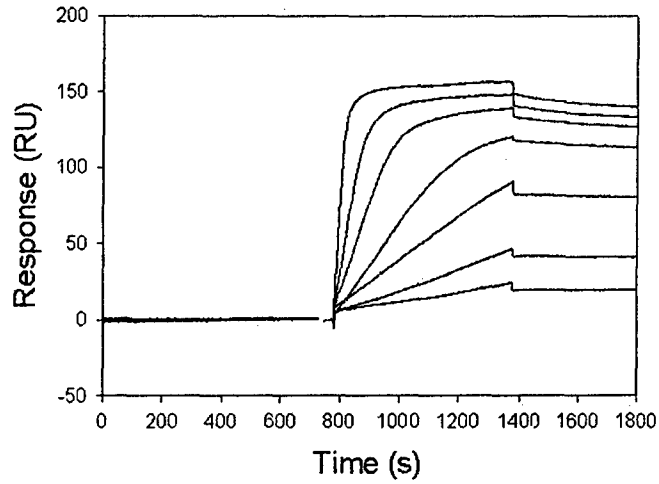

FIG. 4. Example of a dataset used for global binding analysis: IGF-I (*bottom* to *top curves*, 0.5, 1, 2, 5, 10, 20, and 50 nM) binding to immobilized full-length rhIGFBP-3 (726 RU). The linearity of the early part of the association phases, most pronounced at low concentrations, indicates mass transport limitation.

s^{-1}. Other global experiments also showed a close correspondence between the results using the two different models, indicating that the estimated binding parameters, especially the equilibrium constants, are not especially sensitive to mass transport effects when global fitting is used.

Binding of IGF-II or biotinylated IGF-I to rhIGFBP-3 and its fragments

All of the above experiments were repeated using IGF-II instead of IGF-I. In all experiments the sensorgrams for IGF-II were visually very similar to those for IGF-I, and calculated binding parameters were also similar. Figure 5 shows sensorgrams for IGF-I and IGF-II as well as a biotin-labeled IGF-I, all at 50 nM, binding to the same immobilized rhIGFBP-3 surface. These sensorgrams were taken from a larger experiment designed for global analysis. The top two sensorgrams are those for IGF-I and IGF-II. Note that in the association phase the IGF-I signal is higher than that for IGF-II, which is due solely to a slightly higher refractive index of the IGF-I-containing buffer. In the dissociation phase, where both surfaces are exposed to the same buffer, the IGF-II signal is slightly higher, indicating a higher affinity than for IGF-I. The affinities for IGF-I and IGF-II in this experiment, calculated by global analysis, were 2.1×10^9 and 3.0×10^9 M^{-1}, respectively.

Table 1 gives the summary of the calculated binding parameters for IGF-I and IGF-II binding to immobilized rhIGFBP-3 or its N- or C-terminal fragments. The table only includes results from experiments using immobilized binding protein and fragments, as the experiments with the immobilized IGFs were judged to be less reliable, primarily due to possible self-association of binding proteins (see *Discussion*). None of the parameter differences between the two binding protein fragments was statistically significant. All differences between full-length rhIGFBP-3 and the fragments were significant, except for those indicated.

In this experiment we also tested the binding of biotin-labeled IGF-I to immobilized rhIGFBP-3. The lowest of the curves in Fig. 5 shows the binding of biotin-IGF-I to

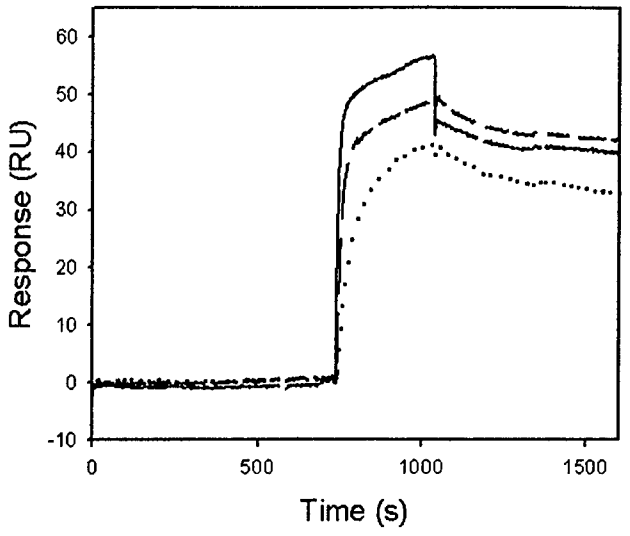

FIG. 5. Sensorgrams for IGF-I, IGF-II, and biotinylated IGF-I, all at 50 nM, binding to immobilized full-length rhIGFBP-3 (158 RU). *Solid line*, IGF-I; *dashed line*, IGF-II; *dotted line*, biotinylated IGF-I. The IGF-I curve is higher than that for IGF-II in the association phase because of a difference in refractive index of the two solutions. In the dissociation phase, where the flow-through buffers are identical, the IGF-II curve is higher, indicating that more IGF-II than IGF-I was bound to the surface.

rhIGFBP-3. In this experiment, using global analysis, the affinity of biotin-IGF-I was calculated to be 1.1×10^9 M^{-1}.

Binding of human insulin to rhIGFBP-3 and its N- and C-terminal fragments

In this study we tested the binding of human insulin to rhIGFBP-3 and its fragments, with either binding protein or insulin immobilized on the sensor chip. In most experiments the observed binding was very weak or absent in either configuration, and reasonable estimates of binding parameters could not be made, nor could comparisons be made of the relative affinities of insulin binding to full-length rhIGFBP-3 or its fragments. Apparent binding was observed in a few experiments, and by comparing this binding with control runs using IGF-I, we could estimate equilibrium K_a values less than 10^6 M^{-1}. Figure 6A shows an example of the weak binding of human insulin (2 μM) to immobilized rhIGFBP-3. For this sensorgram, the equilibrium K_a was estimated to be less than 10^5 M^{-1}, assuming that insulin binds with the same stoichiometry as IGF-I.

Binding of IGF-I and IGF-II to mac25 and CTGF

We also tested the binding of IGF-I, IGF-II, and human insulin to mac25 and CTGF. In no case could we unambiguously demonstrate binding of IGF or insulin molecules to these proteins. Figure 6, B and C, shows examples of tests of mac25 and CTGF binding to immobilized IGF-I.

Self-association of IGFBP and its fragments

Most of our experiments using immobilized IGFs gave consistent results, with calculated binding parameters very similar to those for the experiments with IGFBP immobilized (see Fig. 3). However, because of potential inaccuracies in binding parameter determinations due to the two-dimensional geometry of binding, we also attempted to measure equilibrium binding affinities using solution affinity assays on the BIACORE. In an example of one such experiment, IGF-I at 20 nM was incubated with varying concentrations (2–200 nM) of rhIGFBP-3 for 15–20 min at 25 C, after which the solution was passed over an rhIGFBP-3-immobilized sensor chip to record a sensorgram. Because rhIGFBP-3 in solution should compete for free IGF-I, the binding of IGF-I to the immobilized rhIGFBP-3 was expected to decrease at higher rhIGFBP-3 concentrations. Instead, the signal increased at higher concentrations. The most straightforward interpretation of this was that the rhIGFBP-3 was itself binding to the rhIGFBP-3 immobilized surface, and therefore solution assays could not be performed in this system.

We then investigated directly the binding of rhIGFBP-3 and its fragments to each other. Figure 7 shows an example of binding of rhIGFBP-3 or rhIGFBP-3^{98-264} to a surface immobilized with rhIGFBP-3^{98-264}, in which binding is clearly evident. From experiments using all combinations of immobilized and solution proteins, we observed that rhIGFBP-3 and rhIGFBP-3^{98-264} bind weakly to themselves and to each other (apparent K_a, $\sim 8–30 \times 10^6$ M^{-1}; that is, more than 100-fold lower affinity than that of IGF-I for rhIGFBP-3), whereas rhIGFBP-3^{1-97} binds very weakly or not at all to itself and to the other proteins (K_a, $\sim 0–3 \times 10^6$ M^{-1}). Because rhIGFBP-3 and rhIGFBP-3^{98-264} would be expected to also aggregate in the flow-through solution in these assays, these results are approximate.

Discussion

If the N- and C-terminal regions of IGFBP-3 combine to form a high affinity binding site for IGF molecules (1, 14, 15), one would expect that the N- or C-terminal fragments of IGFBP-3 might individually bind IGF-I or IGF-II, but with lower affinity than the full-length binding protein. The binding regions on the two fragments could combine to form a single larger high affinity site or could interact with two separate regions on the IGF molecule to result in high affinity binding. This last mechanism has been suggested, for example, for insulin binding to the insulin receptor (48, 49). Our results here show that IGF-I and IGF-II bind the N- and C-terminal recombinant fragments rhIGFBP-3^{1-97} and rhIGFBP-3^{98-264} with affinities approximately 1000-fold lower than that of the IGFs for full-length rhIGFBP-3. These results are consistent with the idea that the combination of the two sites results in high affinity binding, but do not distinguish whether there is a single high affinity binding site or two separate sites.

The functional significance of different glycosylation forms of recombinant human IGFBP-3 was studied by Firth *et al.* (18). It could be shown that different glycosylation patterns (*e.g.* fully glycosylated *vs.* nonglycosylated IGFBP-3) do not alter IGF binding to the binding protein in Western ligand blots. Therefore, the difference in binding affinity of nonglycosylated *Escherichia coli*-expressed IGFBP-3 and baculovirus-expressed glycosylated IGFBP-3 fragments is not expected to be due to their glycosylation status.

Recently, Galanis *et al.* (38), using a BIACORE instrument,

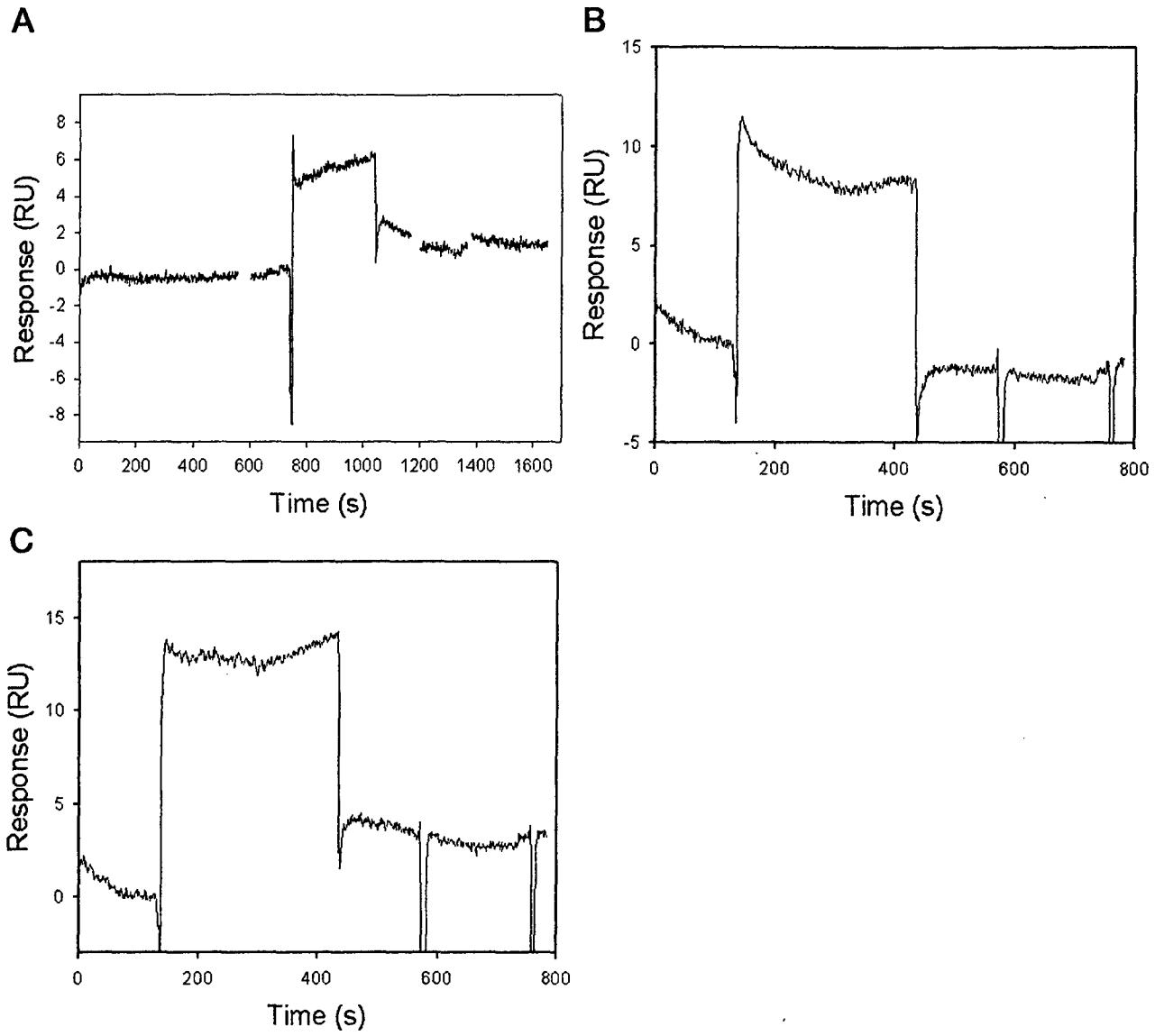

FIG. 6. A, Interaction of human insulin (2000 nM) with full-length rhIGFBP-3 (412 RU). The rising association phase and falling dissociation phase indicate apparent binding, but with very low affinity, and near the detection limit of the instrument. Interaction of mac25 (B) and CTGF (C) with immobilized IGF-I (532 RU). Binding is below the detection limit of the instrument.

measured equilibrium affinities of 1.03×10^7 and 6.16×10^7 M^{-1} for IGF-I and IGF-II binding, respectively, to an N-terminal IGFBP-3^{1-88} fragment, compared with our measurements of about 0.6×10^7 M^{-1} for both IGF-I and IGF-II. Interestingly, they found that the 1–88 N-terminal fragment could not be immobilized using the amine coupling method, and that a 165–264 C-terminal fragment could be immobilized, but was inactive in BIACORE assays. In contrast, both our 1–97 N-terminal and 98–264 C-terminal fragments could be immobilized and retained activity, and both were also active in binding to immobilized IGF-I.

Our measurements of the binding of IGF-I and IGF-II to full-length rhIGFBP-3 indicate equilibrium affinities in the range of $4–5 \times 10^9$ M^{-1}. These estimates are lower than those measured using ^{125}I-labeled IGFs, where affinities between 8×10^9 and 152×10^9 M^{-1} have been reported (quoted and summarized in Ref. 36). We had observed a similar difference in an earlier study of IGF analog binding to IGFBP-3 (33), but it is not clear whether this is due to the different conditions of binding, for example, changes in the ligand due to immobilization or the two-dimensional binding geometry, or to differences in analytical methods.

Wong *et al.* (36), using a BIACORE instrument, calculated an affinity of 18.4×10^9 M^{-1} for IGF-I binding to hrIGFBP-3. These results are apparently the average of separate analyses of individual sensorgrams, whereas our results for IGF-I binding to immobilized rhIGFBP-3 are derived from global analyses (44, 45) (see Fig. 4), in which a binding model is fitted simultaneously to multiple sensorgrams at different analyte concentrations. Global analyses should be more accurate, because they assume a common value in all sensorgrams for R_{max}, the maximum analyte bound at saturation, whereas analyses of single sensorgrams from the same experiment can yield different apparent values of R_{max}, which is unrealistic.

Galanis *et al.* (38) also determined a high affinity (1×10^{11}

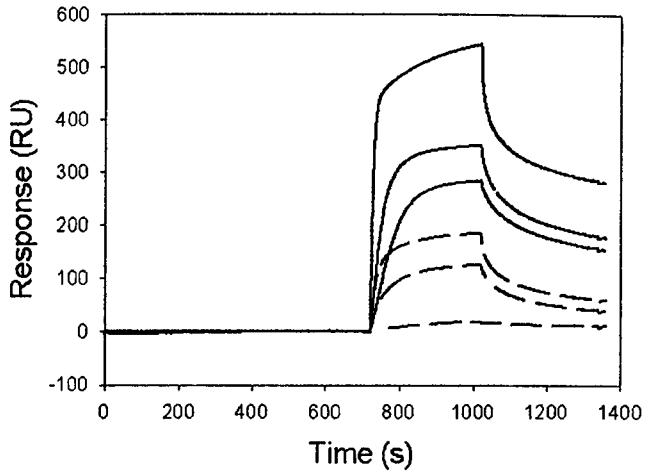

FIG. 7. Interaction of full-length rhIGFBP-3 and rhIGFBP-3^{98-264} with immobilized rhIGFBP-3^{98-264} (2307 RU). *Solid lines*, rhIGFBP-3 (*bottom* to *top*, 50, 200, and 500 nM); *dashed lines*, rhIGFBP-3^{98-264} (*bottom* to *top*, 50, 200, and 500 nM).

M^{-1}) for full-length IGFBP-3 binding to immobilized IGF-I, compared with our estimate of 7×10^9 M^{-1} under similar conditions. Their high affinity was primarily due to a very low kinetic k_d (1×10^{-6} s^{-1} compared with 3×10^{-4} s^{-1} in our experiments). One possible explanation for the difference is that Galanis *et al.* (38) conducted their assays at a flow rate of 5 μl/min, whereas ours were performed at 50 μl/min. It is well known (50, 51) that for high affinity interactions such as that between IGF-I and IGFBP-3, there can be significant rebinding of analyte during the dissociation phase, especially at low flow rates, leading to erroneously low dissociation rates and higher affinities. In tests of IGF-I binding to rhIGFBP-3 using flow rates of 5–10 μl/min and low analyte concentrations, we observed that analyses of individual sensorgrams often yielded unreasonably high R_{max} values, low k_d, and apparent affinities well over 10^{11} M^{-1}. Hence, all of our later experiments were performed at high flow rates, and global analyses were used to minimize this type of error.

Her, and in our previous study (33), our data show that IGF-II binds rhIGFBP-3 with a similar, perhaps slightly higher, affinity than does IGF-I, which was also observed in other studies in the literature (52). Our measurements of binding of biotinylated IGF-I to rhIGFBP-3 using global analysis show that k_a is reduced by a factor of 3, and k_d is increased by a factor of 1.4 relative to nonbiotinylated IGF-I. This results in a 4-fold reduction in the apparent equilibrium affinity of biotinylated IGF-I relative to nonbiotinylated IGF-I. These are relatively small differences, indicating that biotinylation of IGF-I does not greatly interfere with its binding to IGFBPs. It is of note that labeling with iodine resulted in an affinity change of labeled IGFs to IGFBP-3 (53). Thus, the biotinylated IGF-I could be a better alternative to [^{125}I]IGF-I in experiments requiring labeled hormone.

We attempted to measure equilibrium binding affinities using a solution binding assay (47) to minimize errors in kinetic determinations due to the two-dimensional binding geometry in the BIACORE instrument, for example, from mass transport limitation or steric hindrance (46). However, we observed that rhIGFBP-3 and rhIGFBP-3^{98-264} self-aggregate, making solution assays impossible and raising questions about the accuracy of binding results obtained using binding proteins in the flow solution and immobilized IGFs. With increasing binding protein concentration, self-aggregation should increase both in solution and on the sensor chip surface, introducing errors in the binding analysis. Therefore, results using immobilized binding proteins, for example, as shown in Table 1, should be more reliable than those using immobilized IGFs (36, 38) unless binding protein concentrations are kept well below the K_d for self-aggregation ($\sim 10^{-7}$ M by our estimates).

On the basis of evidence that activation of the insulin receptor is inhibited by IGFBPs, and that mac25 is able to bind insulin (13), we tested the binding of human insulin to rhIGFBP-3 and to recombinant mac25 and CTGF molecules using the BIACORE instrument. We also tested insulin binding to the IGFBP recombinant fragments rhIGFBP-3^{1-97} and rhIGFBP$^{98-264}$. Most experiments could not confirm binding, but in a few experiments the binding of insulin to rhIGFBP-3 was detectable, indicating that insulin may bind IGFBP-3 with low affinity, as we had previously observed (33). We could not detect binding of insulin to the IGFBP-related proteins, or to the rhIGFBP-3 fragments, in these biosensor assays.

We tested the binding of IGF-I and IGF-II to the mac25 and CTGF molecules, with either these molecules or the IGF molecules immobilized, at analyte concentrations up to 500 nM. In no case could we detect binding using the biosensor instrument. These results were unexpected in light of the evidence for binding of both IGF-I and insulin to the binding protein molecules from studies using radiolabeled IGF molecules (13, 20). However, as binding affinities less than about 10^5 or 10^6 M^{-1} are difficult to detect using the biosensor, we cannot rule out that there is weak binding below the detection limit of the instrument. There is an indication from affinity cross-linking studies that IGF-I binding affinity for mac25 may be higher than these values (13, 40) so it remains to be determined whether our inability to detect binding on the biosensor instrument is because of differences in binding conditions or because cross-linking experiments are, in fact, measuring extremely low binding affinities.

Acknowledgments

Received August 30, 2001. Accepted January 2, 2002.

Address all correspondence and requests for reprints to: Dr. Peter Vorwerk, M.D., Department of Pediatric Oncology, Otto von Guericke University, Emanuel Larisch Weg 17-19, D-39112 Magdeburg, Germany. E-mail: peter.vorwerk@medizin.uni-magdeburg.de.

This work was supported by NIH Grants CA-58110 and DK-51513 (to R.G.R.), American Cancer Society Grant RPG-99-103-01-TBE, Department of the Army Grant DAMD 17-00-1-0042 (to Y.O.), and a grant from the Ministry of Culture of Saxonia-Anhalt, Germany (003VE1998; to P.V.).

References

1. **Rosenfeld RG, Hwa V, Wilson L, Lopez-Bermejo A, Buckway C, Burren C, Choi WK, Devi G, Ingermann A, Graham D, Minniti G, Spagnoli A, Oh Y** 1999 The insulin-like growth factor binding protein superfamily: new perspectives. Pediatrics 104:1018–1021
2. **Binoux M, Lalou C, Mohseni-Zadeh S** 1999 Biological actions of proteolytic fragments of the IGF binding proteins. In: Rosenfeld RG, Roberts Jr CT, eds. The IGF-system, molecular biology, physiology, and clinical applications. Totowa: Humana Press; 281–313
3. **Maile LA, Holly JM** 1999 Insulin-like growth factor binding protein (IGFBP) proteolysis: occurrence, identification, role and regulation. Growth Horm IGF Res 9:85–95
4. **Oh Y, Rosenfeld RG** 1999 IGF-independent actions of the IGF binding proteins. In: Rosenfeld RG, Roberts Jr CT, eds. The IGF-system, molecular biology, physiology, and clinical applications. Totowa: Humana Press; 257–272

5. **Jones JI, Clemmons DR** 1995 Insulin-like growth factors and their binding proteins: biological actions. Endocr Rev 16:3–34
6. **Oh Y, Muller HL, Lamson G, Rosenfeld RG** 1993 Insulin-like growth factor (IGF)-independent action of IGF-binding protein-3 in Hs578T human breast cancer cells. Cell surface binding and growth inhibition. J Biol Chem 268:14964–14971
7. **Hossenlopp P, Segovia B, Lassarre C, Roghani M, Bredon M, Binoux M** 1990 Evidence of enzymatic degradation of insulin-like growth factor-binding proteins in the 150K complex during pregnancy. J Clin Endocrinol Metab 71:797–805
8. **Giudice LC, Farrell EM, Pham H, Lamson G, Rosenfeld RG** 1990 Insulin-like growth factor binding proteins in maternal serum throughout gestation and in the puerperium: effects of a pregnancy-associated serum protease activity. J Clin Endocrinol Metab 71:806–816
9. **Andress DL, Birnbaum RS** 1992 Human osteoblast-derived insulin-like growth factor (IGF) binding protein-5 stimulates osteoblast mitogenesis and potentiates IGF action. J Biol Chem 267:22467–22472
10. **Lalou C, Lassarre C, Binoux M** 1996 A proteolytic fragment of insulin-like growth factor (IGF) binding protein-3 that fails to bind IGFs inhibits the mitogenic effects of IGF- I and insulin. Endocrinology 137:3206–3212
11. **Angelloz-Nicoud P, Lalou C, Binoux M** 1998 Prostate carcinoma (PC-3) cell proliferation is stimulated by the 22–25-kDa proteolytic fragment (1–160) and inhibited by the 16-kDa fragment (1–95) of recombinant human insulin-like growth factor binding protein-3. Growth Horm IGF Res 8:71–75
12. **Vorwerk P, Yamanaka Y, Spagnoli A, Oh Y, Rosenfeld RG** 1998 Insulin and IGF binding by IGFBP-3 fragments derived from proteolysis, baculovirus expression and normal human urine. J Clin Endocrinol Metab 83:1392–1395
13. **Yamanaka Y, Wilson EM, Rosenfeld RG, Oh Y** 1997 Inhibition of insulin receptor activation by insulin-like growth factor binding proteins. J Biol Chem 272:30729–30734
14. **Spencer EM, Chan K** 1995 A 3-dimensional model for the insulin-like growth factor binding proteins (IGFBPs); supporting evidence using the structural determinants of the IGF binding site on IGFBP-3. Prog Growth Factor Res 6:209–214
15. **Carrick FE, Forbes BE, Wallace JC** 1999 Recreating a high affinity insulin-like growth factor binding protein using discrete N- and C-terminal fragments. Growth Horm IGF Res 9:317–318
16. **Vorwerk P, Oh Y, Lee PD, Khare A, Rosenfeld RG** 1997 Synthesis of IGFBP-3 fragments in a baculovirus system and characterization of monoclonal anti-IGFBP-3 antibodies. J Clin Endocrinol Metab 82:2368–2370
17. **Yang DH, Kim HS, Wilson EM, Rosenfeld RG, Oh Y** 1998 Identification of glycosylated 38-kDa connective tissue growth factor (IGFBP-related protein 2) and proteolytic fragments in human biological fluids, and up-regulation of IGFBP-rP2 expression by TGF-β in Hs578T human breast cancer cells. J Clin Endocrinol Metab 83:2593–2596
18. **Firth SM, Baxter RC** 1999 Characterisation of recombinant glycosylation variants of insulin-like growth factor binding protein-3. J Endocrinol 160:379–387
19. **Firth SM, Ganeshprasad U, Baxter RC** 1998 Structural determinants of ligand and cell surface binding of insulin- like growth factor-binding protein-3. J Biol Chem 273:2631–2638
20. **Kim HS, Nagalla SR, Oh Y, Wilson E, Roberts Jr CT, Rosenfeld RG** 1997 Identification of a family of low-affinity insulin-like growth factor binding proteins (IGFBPs): characterization of connective tissue growth factor as a member of the IGFBP superfamily. Proc Natl Acad Sci USA 94:12981–12986
21. **Burren CP, Wilson EM, Hwa V, Oh Y, Rosenfeld RG** 1999 Binding properties and distribution of insulin-like growth factor binding protein-related protein 3 (IGFBP-rP3/NovH), an additional member of the IGFBP superfamily. J Clin Endocrinol Metab 84:1096–1103
22. **Forbes BE, Turner D, Hodge SJ, McNeil KA, Forsberg G, Wallace JC** 1998 Localization of an insulin-like growth factor (IGF) binding site of bovine IGF binding protein-2 using disulfide mapping and deletion mutation analysis of the C-terminal domain. J Biol Chem 273:4647–4652
23. **Sommer A, Maack CA, Spratt SK, Mascarenhas D, Tressel TJ, Rhodes ET, Lee R, Roumas M, Tatsuno GP, Flynn JA, Gerber N, Taylor J, Cudny H, Nanncy L, Hunt TK, Spencer EM** 1991 Molecular genetics and actions of recombinant insulin-like growth factor binding protein-3. In: Spencer EM, ed. Modern concepts of insulin-like growth factors. Amsterdam: Elsevier; 715–728
24. **Spencer EM, Steenfos H, Strathearn M, Spratt SK, Hunt TK** 1989 Molecular biology and physiology of the insulin-like growth factor binding protein 3, the acid-stable unit of the 150k serum insulin-like growth factor binding komplex. In: Drop SL, Hintz RL, eds. Insulin-like growth factor binding proteins. Amsterdam: Elsevier; 73–79
25. **Chernausek SD, Smith CE, Duffin KL, Busby WH, Wright G, Clemmons DR** 1995 Proteolytic cleavage of insulin-like growth factor binding protein 4 (IGFBP-4). Localization of cleavage site to non-homologous region of native IGFBP-4. J Biol Chem 270:11377–11382
26. **Kiefer MC, Schmid C, Waldvogel M, Schlapfer I, Futo E, Masiarz FR, Green K, Barr PJ, Zapf J** 1992 Characterization of recombinant human insulin-like growth factor binding proteins 4, 5, and 6 produced in yeast. J Biol Chem 267:12692–12699
27. **Bach LA, Hsieh S, Sakano K, Fujiwara H, Perdue JF, Rechler MM** 1993 Binding of mutants of human insulin-like growth factor II to insulin-like growth factor binding proteins 1–6. J Biol Chem 268:9246–9254
28. **Clemmons DR, Dehoff ML, Busby WH, Bayne ML, Cascieri MA** 1992 Competition for binding to insulin-like growth factor (IGF) binding protein-2, 3, 4, and 5 by the IGFs and IGF analogs. Endocrinology 131:890–895
29. **Oh Y, Muller HL, Lee DY, Fielder PJ, Rosenfeld RG** 1993 Characterization of the affinities of insulin-like growth factor (IGF)-binding proteins 1–4 for IGF-I, IGF-II, IGF-I/insulin hybrid, and IGF-I analogs. Endocrinology 132:1337–1344
30. **Fowlkes JL, Serra D** 1996 A rapid, non-radioactive method for the detection of insulin-like growth factor binding proteins by Western ligand blotting. Endocrinology 137:5751–5754
31. **Op De Beeck L, Verlooy JE, Van Buul-Offers SC, Du CM** 1997 Detection of serum insulin-like growth factor binding proteins on western ligand blots by biotinylated IGF and enhanced chemiluminescence. J Endocrinol 154:R1–R5
32. **Devi GR, Yang DH, Rosenfeld RG, Oh Y** 2000 Differential effects of insulin-like growth factor (IGF)-binding protein-3 and its proteolytic fragments on ligand binding, cell surface association, and IGF-I receptor signaling. Endocrinology 141:4171–4179
33. **Heding A, Gill R, Ogawa Y, De Meyts P, Shymko RM** 1996 Biosensor measurement of the binding of insulin-like growth factors I and II and their analogues to the insulin-like growth factor-binding protein-3. J Biol Chem 271:13948–13952
34. **Shymko RM, Hohmann B, Vorwerk P** 1999 Biosensor analysis of insulin-like growth factor/insulin-like growth factor binding protein interactions. Growth Horm IGF Res 9:323
35. **Vorwerk P, Hohmann B, Oh Y, Rosenfeld RG, Shymko RM** 1999 Biosensor measurement of IGF-binding to N- and C-terminal recombinant human IGFBP-3 fragments. Growth Horm IGF Res 9:363
36. **Wong MS, Fong CC, Yang M** 1999 Biosensor measurement of the interaction kinetics between insulin-like growth factors and their binding proteins. Biochim Biophys Acta 1432:293–301
37. **Marinaro JA, Jamieson GP, Hogarth PM, Bach LA** 1999 Differential dissociation kinetics explain the binding preference of insulin-like growth factor binding protein-6 for insulin-like growth factor-II over insulin-like growth factor-I. FEBS Lett 450:240–244
38. **Galanis M, Firth SM, Bond J, Nathanielsz A, Kortt AA, Hudson PJ, Baxter RC** 2001 Ligand-binding characteristics of recombinant amino- and carboxyl-terminal fragments of human insulin-like growth factor-binding protein-3. J Endocrinol 169:123–133
39. **Kalus W, Zweckstetter M, Renner C, Sanchez Y, Georgescu J, Grol M, Demuth D, Schumacher R, Dony C, Lang K, Holak TA** 1998 Structure of the IGF-binding domain of the insulin-like growth factor-binding protein-5 (IGFBP-5): implications for IGF and IGF-I receptor interactions. EMBO J 17:6558–6572
40. **Oh Y, Nagalla SR, Yamanaka Y, Kim HS, Wilson E, Rosenfeld RG** 1996 Synthesis and characterization of insulin-like growth factor-binding protein (IGFBP)-7. Recombinant human mac25 protein specifically binds IGF-I and -II. J Biol Chem 271:30322–30325
41. **Johnsson B, Lofas S, Lindquist G** 1991 Immobilization of proteins to a carboxymethyldextran-modified gold surface for biospecific interaction analysis in surface plasmon resonance sensors. Anal Biochem 198:268–277
42. **Schuck P** 1996 Kinetics of ligand binding to receptor immobilized in a polymer matrix, as detected with an evanescent wave biosensor. I. A computer simulation of the influence of mass transport. Biophys J 70:1230–1249
43. **Myszka DG** 1997 Kinetic analysis of macromolecular interactions using surface plasmon resonance biosensors. Curr Opin Biotechnol 8:50–57
44. **Schuck P** 1997 Reliable determination of binding affinity and kinetics using surface plasmon resonance biosensors. Curr Opin Biotechnol 8:498–502
45. **Karlsson R, Falt A** 1997 Experimental-design for kinetic-analysis of protein-protein interactions with surface-plasmon resonance biosensors. J Immunol Methods 200:121–133
46. **Schuck P** 1997 Use of surface plasmon resonance to probe the equilibrium and dynamic aspects of interactions between biological macromolecules. Annu Rev Biophys Biomol Struct 26:541–566
47. **Karlsson R, Kullman-Magnusson M, Hamalainen MD, Remaeus A, Andersson K, Borg P, Gyzander E, Deinum J** 2000 Biosensor analysis of drug-target interactions: direct and competitive binding assays for investigation of interactions between thrombin and thrombin inhibitors. Anal Biochem 278:1–13
48. **Schäffer L** 1994 A model for insulin binding to the insulin receptor. Eur J Biochem 221:1127–1132
49. **De Meyts P, Ursø B, Christoffersen CT, Shymko RM** 1995 Mechanism of insulin and IGF-I receptor activation and signal transduction specificity. Receptor dimer cross-linking, bell-shaped curves, and sustained versus transient signaling. Ann NY Acad Sci 766:388–401
50. **Glaser RW** 1993 Antigen-antibody binding and mass transport by convection and diffusion to a surface: a two-dimensional computer model of binding and dissociation kinetics. Anal Biochem 213:152–161
51. **Schuck P, Minton AP** 1996 Analysis of mass transport-limited binding-kinetics in evanescent-wave biosensors. Anal Biochem 240:262–272
52. **Martin JL, Baxter RC** 1986 Insulin-like growth factor binding proteins from human plasma. J Biol Chem 261:8754–8760
53. **Suikkari AM, Baxter RC** 1991 Insulin-like growth factor (IGF) binding protein-3 in pregnancy serum binds native IGF-I but not iodo-IGF-I. J Clin Endocrinol Metab 73:1377–1379

0013-7227/00/$03.00/0
Endocrinology

Vol. 141, No. 11
Printed in U.S.A.

Characterization of Insulin-Like Growth Factor-Binding Protein-Related Proteins (IGFBP-rPs) 1, 2, and 3 in Human Prostate Epithelial Cells: Potential Roles for IGFBP-rP1 and 2 in Senescence of the Prostatic Epithelium*

A. LÓPEZ-BERMEJO†, C. K. BUCKWAY, G. R. DEVI, V. HWA, S. R. PLYMATE, Y. OH, AND R. G. ROSENFELD

Department of Pediatrics (A.L.-B., C.K.B., G.R.D., V.H., Y.O., R.G.R.), Oregon Health Sciences University, Portland, Oregon 97201; and Geriatric Research Education and Clinical Center (S.R.P.), Veterans Affairs Health Care System Puget Sound, Seattle/Tacoma, Washington 98493

ABSTRACT

Insulin-like growth factor (IGF)-binding protein (IGFBP)-related proteins (IGFBP-rPs) are newly described cysteine-rich proteins that share significant aminoterminal structural similarity with the conventional IGFBPs and are involved in a diversity of biological functions, including growth regulation. IGFBP-rP1 (MAC25/Angiomodulin/prostacyclin-stimulating factor) is a potential tumor-suppressor gene that is differentially expressed in meningiomas, mammary and prostatic cancers, compared with their malignant counterparts. We have previously shown that IGFBP-rP1 is preferentially produced by primary cultures of human prostate epithelial cells (HPECs) and by poorly tumorigenic P69SV40T cells, compared with the cancerous prostatic LNCaP, DU145, PC-3, and M12 cells. We now show that IGFBP-rP1 increases during senescence of HPEC.

IGFBP-rP2 (also known as connective tissue growth factor), a downstream effector of transforming growth factor (TGF)-β and modulator of growth for both fibroblasts and endothelial cells, was detected in most of the normal and malignant prostatic epithelial cells tested, with a marked up-regulation of IGFBP-rP2 during senescence of HPEC. Moreover, IGFBP-rP2 noticeably increased in response to TGF-β1 and all-*trans* retinoic acid (atRA) in HPEC and PC-3 cells, and it decreased in response to IGF-I in HPEC.

IGFBP-rP3 [nephroblastoma overexpressed (NOV)], the protein product of the NOV protooncogene, was not detected in HPEC but was expressed in the tumorigenic DU145 and PC-3 cells. It was also synthesized by the SV40-T antigen-transformed P69 and malignant M12 cells, where it was down-regulated by atRA.

These observations suggest biological roles of IGFBP-rPs in the human prostate. IGFBP-rP1 and IGFBP-rP2 are likely to negatively regulate growth, because they seem to increase during senescence of the prostate epithelium and in response to growth inhibitors (TGF-β1 and atRA). Although the data collected on IGFBP-rP3 in prostate are modest, its role as a growth stimulator and/or protooncogene is supported by its preferential expression in cancerous cells and its down-regulation by atRA. (*Endocrinology* **141:** 4072–4080, 2000)

THE INSULIN-LIKE growth factor (IGF) system is composed of two ligands (IGF-I and IGF-II), six IGF-binding proteins (IGFBPs -1 to -6), and two receptors (type 1 and type 2 IGF receptors) (1). Recently, the IGFBP family of proteins has been expanded to include additional members that share significant structural similarities, the so-called IGFBP-related proteins (IGFBP-rPs) (2), which not only share the conserved aminoterminal domain of the IGFBPs but also show some degree of affinity for IGFs and insulin.

Abnormalities in the IGF system have been identified in prostate disease, such as prostate hyperplasia and cancer. In this respect, prostate cancer growth seems to be poorly dependent on IGFs, because the type I IGF receptor, which mediates most biological functions of IGF-I and IGF-II, is down-regulated during prostate carcinogenesis (3). Additionally, recent epidemiological studies have shown an increased risk of developing prostatic carcinoma in adult males with high-normal serum concentrations of IGF-I (4).

Despite extensive characterization of the IGFBPs in the human prostate, little is known about their roles in prostate physiology. IGFBP-2 and -4 are known to increase during carcinogenesis of the prostatic epithelium (5, 6), whereas IGFBP-3 is a proteolytic substrate for prostate-specific antigen (7, 8). Recent studies have also shown an increase of several IGFBPs in prostate tissue during involution of the gland in castrated rats and in men taking finasteride (9, 10). These findings suggest that IGFBPs may play a role in apoptosis of prostate cells, either by sequestering IGFs or by direct cellular actions. Our knowledge of the new IGFBP-rPs in the human prostate is only scant at its best.

The IGFBP-rPs are cysteine-rich proteins involved in a diversity of biological functions, including growth regula-

Received April 5, 2000.

Address all correspondence and requests for reprints to: Ron G. Rosenfeld, M.D., Department of Pediatrics, School of Medicine, Oregon Health Sciences University, 3181 SW Sam Jackson Park Road, Portland, Oregon 97201-3098. E-mail: rosenfer@ohsu.edu.

* This work was also supported by NIH Grant DK-52683 and the Veterans Affairs Merit Review Program (to S.R.P.), Grants DAMD17-96-1-6204 and 17-97-1-7204 from the U.S. Army (to Y.O.), and Grants CA-58110 and DK-51513 from the NIH and DAMD 17-00-1-0042 from the U.S. Army (to R.G.R.).

† Supported by a Fellow Research Funding Grant from Eli Lilly & Co. Also, a recipient of Grants 97/5309 and 98/9198 from the Fondo de Investigación Sanitaria, Spain.

tion. IGFBP-rP1 was originally cloned from leptomeningial cells and was termed meningioma-associated complementary DNA (cDNA) (MAC25) (11). This protein has also been reported as tumor-derived adhesion factor (TAF, recently renamed Angiomodulin) (12, 13), prostacyclin-stimulating factor (14), and T1A12 (15). In the human prostate, we have also recently described preferential expression of IGFBP-rP1 in normal human prostate cells and tissues, compared with their malignant counterparts, and we have shown that this protein is up-regulated by transforming growth factor (TGF)-β1 and all-*trans* retinoic acid (atRA) in prostate epithelial cells (16).

IGFBP-rP2 [also known as connective tissue growth factor (CTGF)] was initially isolated from human umbilical endothelial cells and shown to be mitogenic and chemotactic for fibroblasts (17). IGFBP-rP2 belongs to the CCN [for CYR61, CTGF, and nephroblastoma overexpressed (NOV)] family of cysteine-rich proteins involved in a diversity of cellular functions, such as mitogenesis, differentiation, survival, adhesion, migration, and regulation of matrix gene expression (18). IGFBP-rP2 is also a major downstream effector of TGF-β in fibroblasts, where it was evidenced that TGF-β controls IGFBP-rP2 expression via a novel response element in the IGFBP-rP2 gene (19). To date, however, no studies have been reported on the role of IGFBP-rP2 in prostate biology and/or carcinogenesis.

IGFBP-rP3 (also known as NOV) was first recognized as an aberrantly expressed gene in avian nephroblastoma and later shown to be also overexpressed in the human homologue Wilms tumor (20, 21). In the human prostate, it has been reported that NOV is differentially expressed in PC-3 cells, compared with other cancerous and normal cells in culture, but the significance of this finding is unknown (22).

We now report that prostate epithelial cells, in culture, express not only IGFBP-rP1 and 3, but also IGFBP-rP2, and that these proteins are responsive to growth regulators. Interestingly, IGFBP-rP1 and 2 also increase during senescence of normal prostate epithelial cells, thus supporting growth-regulatory roles of these proteins in the prostatic epithelium.

Materials and Methods

Materials

Epidermal growth factor (EGF), dexamethasone, atRA, and the additive ITS (insulin, transferrin, selenium) were purchased from Sigma (St. Louis, MO). PrEBM human prostate epithelial cell (HPEC) media was obtained from Clonetics (San Diego, CA). RPMI (1640 media) was obtained from Life Technologies (Grand Island, NY). IGF-I and TGF-β1 were both purchased from Austral Biologicals (San Ramon, CA). FBS was obtained from HyClone Laboratories, Inc. (Logan, UT). [^{3}H]methylthymidine was purchased from NEN Life Science Products (Boston, MA), and MTS assay kit (CellTiter 96 AQueous One Solution Cell Proliferation Assay) was obtained from Promega Corp. Corporation (Madison, WI). Nitrocellulose and electrophoresis reagents were purchased from Bio-Rad Laboratories, Inc. (Hercules, CA); nylon membranes (Genescreen) were obtained from NEN Life Science Products. Horseradish peroxidase-linked donkey antirabbit and sheep antimouse IgG antibodies and enhanced chemiluminescence detection reagents were purchased from Amersham Pharmacia Biotech (Arlington Heights, IL). HPEC cells were purchased from Clonetics. LNCaP, DU145, and PC-3 cells were obtained from American Type Culture Collection (Manassas, VA). P69SV40T (P69) and M12 prostate epithelial cells were previously described (23). Polyclonal antibodies against IGFBP-rP1, IGFBP-rP2, and IGFBP-rP3 were generated in rabbits, as previously described (24–26). Monoclonal IgG antibody against p16^{INK4a} (13251A) was purchased from Phar-Mingen (San Diego, CA).

Cell culture

Figure 1 summarizes the cell lines employed in these studies. HPEC cells were maintained in PrEBM media supplemented with the following: bovine pituitary extract (BPE), insulin, hydrocortisone, GA-1000, retinoic acid, transferrin, levothyroxine, epinephrine, and human EGF. HPECs were subcultured as recommended by the manufacturer. When they reached 80% confluence, all growth factors were withdrawn, except for BPE, for 12 h. Medium was changed again to PrEBM plus BPE for cell proliferation and growth factor regulation studies.

P69 and its M12 subline were grown in RPMI media supplemented with 10 ng/ml EGF, 0.1 μM dexamethasone, 5 μg/ml insulin, 5 μg/ml transferrin, and 5 ng/ml selenium. LNCaP, DU145, and PC-3 cells were maintained in RPMI enriched with 10% FBS. All cultures used were mycoplasma-free, as determined by the Mycoplasma PCR Primer Set (Stratagene, La Jolla, CA) and were grown at 37 C under 5% CO_2.

Cellular proliferation assays

Cells were seeded at a density of 1×10^4 cells per well, in 48-well plates (Falcon, Becton Dickinson and Co. Labware, Franklin Lakes, NJ), in 500 μl of either rich defined medium or 10% FBS-enriched medium, depending on the cell line. When 80% confluence was reached, the medium was changed to either basal medium or serum free medium for 12 h and then treated with various doses of TGF-β1 (0–5 ng/ml), atRA (0.001–1 μM), or IGF-I (0–100 ng/ml) in 250 μl of the same serum-free medium for 48 h. [^{3}H]thymidine (0.4 μCi/ml) was added for the last 24 h (HPEC and PC-3 cells) or for the last 6 h (P69 and M12 cells). After labeling, the cell layers were washed twice with PBS and incubated with 10% trichloroacetic acid (TCA) at −20 C for 15 min, followed by another wash with 10% TCA before the cells were lysed with 0.25 N sodium hydroxide, and the precipitated material was read by means of an LS 6500 Scintillation Counter (Beckman Coulter, Inc., Fullerton, CA).

Cell proliferation was also tested by MTS assay kit, according to the manufacturer's instructions. Cells were incubated for the last 2 h of treatment, in the presence of the MTS reagent, and absorbance was measured at $A_{490\ nm}$.

Growth factor regulation studies

Cells were seeded at a density of 10×10^4 cells per well, in 60-mm tissue culture dishes, and grown to 80% confluence. Treatments with TGF-β1 (0–5 ng/ml), atRA (0.001–1 μM), or IGF-I (0–100 ng/ml) were also done under serum-free conditions, for 48 h, after which conditioned media, total cell lysates, and total cytoplasmic RNA were collected for Western immunoblots (see *Western immunoblot analyses*) and Northern blots (see *RNA analyses*) studies.

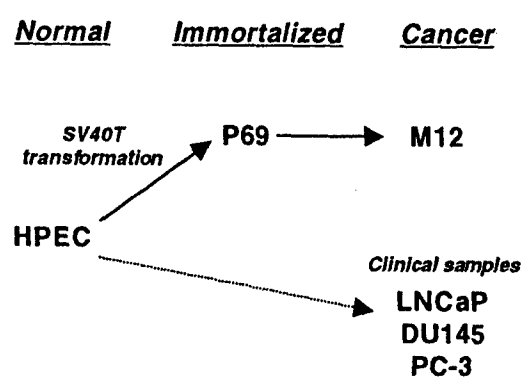

FIG. 1. Prostate epithelial cells studied. Primary cultures of normal HPEC were transformed with the SV40-T antigen to obtain the P69 cell line with low tumorigenic potential. M12 cells, originated after several passages of P69 cells in athymic mice, are, however, highly tumorigenic and metastatic. The well-established androgen-dependent (LNCaP) and androgen-independent (DU145 and PC-3) cells lines, derived from clinical samples, were also studied.

Western immunoblot analyses

Conditioned media and total cell lysates, using RIPA buffer [150 mM NaCl, 20 mM HEPES (pH 7.4), 1% (vol/vol) Triton X-100, 1% (wt/vol) sodium deoxycholate, 0.1% (wt/vol) SDS, and Mini EDTA-free protease inhibitors (Roche Molecular Biochemicals, Laval, Québec, Canada)], from both treated and untreated (control) cells, were normalized for protein concentration, using a DC protein assay (Bio-Rad Laboratories, Inc.). Equal amounts of total protein per sample were dissolved in nondenaturing SDS sample buffer [0.5 M Tris (pH 6.8), 1% SDS, 10% glycerol, and bromphenol blue] and boiled for 5 min. Samples were electrophoresed on 15% SDS-polyacrylamide gels, then electroblotted onto nitrocellulose, and membranes blocked with 4% milk-TBS-T [Tris-buffered saline-Tween-20 (0.1%)] for 1 h at 22 C. Western blots were incubated with IGFBP-rP1, -rP2, or -rP3 antisera at a 1:3000 dilution and with $p16^{INK4a}$ IgG antibody at a dilution of 1:500 (1 μg/ml) in TBS-T overnight at 4 C. Blots were washed with TBS-T and then incubated for 1 h at 22 C with a 1:3000 dilution of horseradish peroxidase-linked antirabbit or antimouse IgG secondary antibodies. Proteins of interest were detected with ECL chemiluminescence reagents, according to the manufacturer's protocol.

RNA analyses

Total cytoplasmic RNA was isolated from cells, by use of RNeasy (QIAGEN, Inc., Chatsworth, CA). Twenty micrograms of each RNA preparation were electrophoresed on a 1.2% agarose-2.2 M formaldehyde gel, transferred overnight onto a nylon membrane (GeneScreen), using 10 × SSC as the transfer solution, and cross-linked to the membrane by UV irradiation in a Stratalinker 1800 (Stratagene). The Northern blots were then probed with an EcoRI/Xho fragment of IGFBP-rP1 (27), or a BamHI/Xho fragment of IGFBP-rP2 (28), which were radiolabeled (1×10^9 dpm/μg) with [α-^{32}P]deoxycycidine triphosphate (NEN Life Science Products-DuPont; SA, 3000 Ci/mmol) using a random priming kit (Prime-a-Gene, Promega Corp.). Northern blots were hybridized overnight at 65 C in hybridization buffer (Rapid-Hyb, Amersham Pharmacia Biotech), according to the manufacturer's instructions. Blots were then washed for 15 min in 2 × SSC/0.1% SDS at 22 C, followed by two more stringent washes in 0.2 × SSC/0.1% SDS at 65 C for 15 min. Blots were exposed to Kodak Biomax film (Eastman Kodak Co., Rochester, NY) for 12 to 48 h at −70 C, using one intensifying screen. Membranes were then reprobed with 18S ribosomal RNA, which acted as a loading control for the RNA samples. An image analyzer (GS-700) equipped with MultiAnalyst version 1.0.2 Software (Bio-Rad Laboratories, Inc.) was used to quantify the resulting bands.

RT-PCR

RT-PCR was performed using 5′-CGCGAATTCGCCATGCAGAGT-GTGCAGAGCACG-3′ and 5′-GGGGCTCGAGTTACATTTTCCCTCT-GGTAGTC-3′ primers specific for IGFBP-rP3. One microgram of total RNA from each cell line was reversed transcribed in a vol of 20 μl, by use of Reverse Transcription System Kit (Promega Corp.), following the manufacturer's instructions. The reaction was performed at 42 C for 15 min, denatured at 99 C for 5 min, and placed on ice. One microliter of the mixture and 50 pmol of 5′ and 3′ primers were employed in PCR amplification reactions using Advantage GC cDNA PCR Kit (CLONTECH Laboratories, Inc., Palo Alto, CA). Amplification of the cDNA was carried out with 25 cycles of denaturing at 94 C for 1 min, annealing at 55 C for 1 min, and extension at 72 C for 2 min. One negative and one positive control were included in all reactions.

Statistical analyses

All experiments were performed at least twice. Statistical analyses were performed by a two-tail Student's *t* test, assuming unequal variances, using Excel Data Analysis Software (Microsoft Corp., Redmond, WA). Data are expressed as means ± SE. $P < 0.05$ was considered significant.

Results

Expression of IGFBP-rP1, 2, and 3 in HPECs

In agreement with previous observations (16), IGFBP-rP1 messenger RNA (mRNA) was detected by Northern blot analysis in the P69/M12 lineage and in primary cultures of prostate epithelial cells, with a parallel detection of IGFBP-rP1 in conditioned media from these cultures (Fig. 2). In the malignant LNCaP, DU145, and PC-3 cells, IGFBP-rP1 mRNA was undetectable by Northern blot, and an immunoreactive band was only present in cell lysates but not in conditioned media from these cells.

IGFBP-rP2 mRNA was detectable in all but one cell line as a single 2.4-kb band, consistent with the molecular size observed in most studies (29). IGFBP-rP2 protein was present in conditioned media and in cell lysates from these cultures. In contrast to IGFBP-rP1, both normal and malignant prostate epithelial cells express similar amounts of IGFBP-rP2 (Fig. 2).

IGFBP-rP3 message was evaluated by RT-PCR in only a limited number of cell lines but was identifiable in P69, M12, LNCaP, and PC-3 cells. IGFBP-rP3 protein was undetectable in conditioned media from HPEC, compared with readily detectable levels in the immortalized P69 cell line and malignant M12, DU145, and PC-3 cells (Fig. 2).

Expression of IGFBP-rP1 and 2 during senescence of HPEC

HPEC cells have a limited life span, with no more than 30 population doublings before they enter replicative senescence (corresponding to our 9th culture passage). Thus, early passages of HPEC (<4th) are highly replicative cells (duplication time for 4th passage is approximately 2 days), whereas senescent cells (>9th passage) are unable to replicate, and they die over time (Fig. 3).

Interestingly, both IGFBP-rP1 and 2 were up-regulated on increasing passage of these cells, with concentrations of both mRNA and secreted protein more than 5-fold higher at late passages, compared with early passages (Fig. 4, A and B).

In support of an increase of these proteins during senescence of HPEC, we also investigated the concentrations of cell-cycle inhibitors that are known to be modified during cellular senescence, such as $p21^{WAF1}$ and $p16^{INK4a}$ (30). In agreement with a previous report in primary cultures of prostate epithelial cells (31), $p21^{WAF1}$ was barely identifiable in our cell lysate preparations, either at early or at late passages (data not shown); whereas a marked up-regulation of $p16^{INK4a}$ at late, low-replicative passages was evidenced (6-fold increase, compared with early passages), paralleling the increases in IGFBP-rP1 and -rP2 (Fig. 4C).

IGFBP-rP2 is responsive to growth regulators in HPECs

Because TGF-β, atRA, and IGF-I are important regulators of prostate epithelial growth and survival (32–34) and because IGFBP-rP2 is tightly regulated by TGF-β in other cellular systems, we wished to investigate the effects of these growth inhibitors (TGF-β and atRA) and growth stimulator (IGF-I) on cell proliferation and IGFBP-rP2 expression in our normal and malignant prostate cells.

Both TGF-β and atRA caused a dose-dependent inhibition

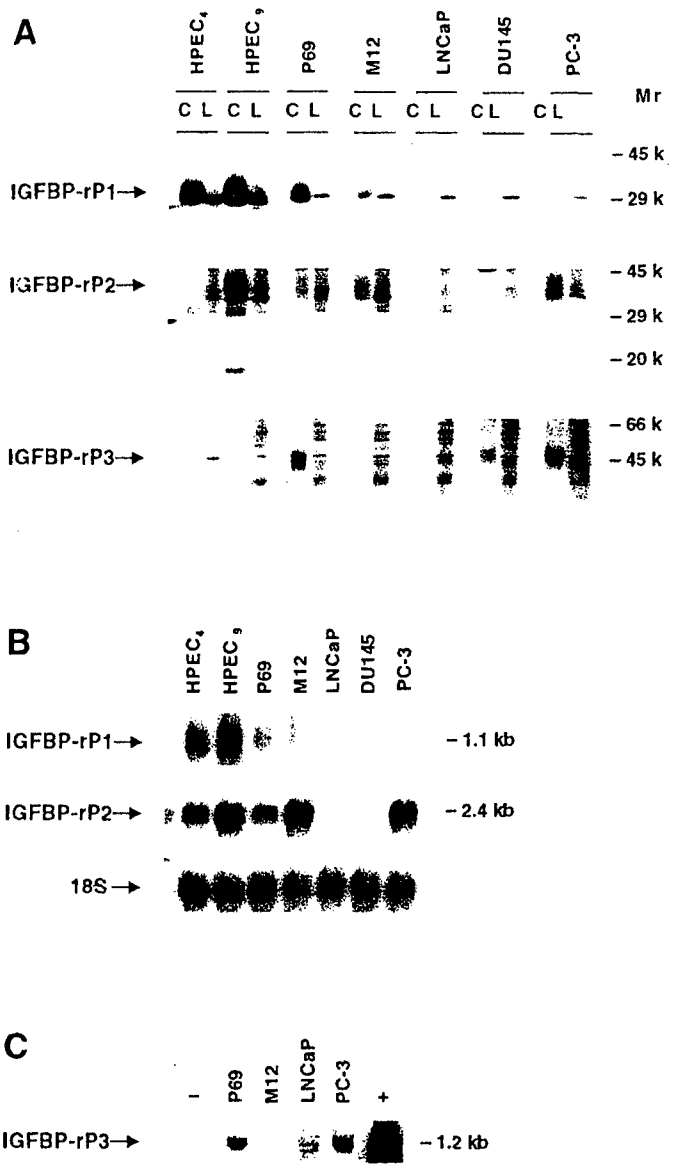

FIG. 2. Expression of IGFBP-rP1, 2, and 3 in HPECs. A, Western immunoblot studies of conditioned media (lane C) and total cell lysates (lane L) from prostate cell lines using polyclonal anti-IGFBP-rP1, 2, and 3 antibodies. Ten micrograms of total protein were loaded per lane; $HPEC_4$: 4th passage (highly-replicative cells); $HPEC_9$: 9th passage (senescent cells). IGFBP-rP1 is highly expressed in normal prostate epithelial cells with low or undetectable concentrations in the malignant M12, LNCaP, DU145, and PC-3 (to avoid oversaturation of the film, only 5 μg of total protein for HPEC-conditioned media were loaded per lane on the IGFBP-rP1 immunoblot). In contrast to IGFBP-rP1, IGFBP-rP3 is undetectable in HPEC but expressed in the immortalized P69 and malignant M12, DU145, and PC-3 cells. IGFBP-rP2 was expressed in both normal and malignant cells. B, Northern blot analyses of prostate cells using [^{32}P] radiolabeled IGFBP-rP1 and 2 probes. Twenty micrograms of total RNA were loaded per lane. Concentrations of 18S ribosomal RNA are shown as an internal control for loading. C, RT-PCR study of IGFBP-rP3 expression in human prostate cells. One microgram of total RNA from each cell line was reversed transcribed, followed by 25 cycles of cDNA amplification. A negative control (−) and a positive control (+) (IGFBP-rP3 cDNA) were included in the PCR step and are shown here. Note that only a limited number of cell lines were studied and that IGFBP-rP3 mRNA was detectable in all of the cultures tested.

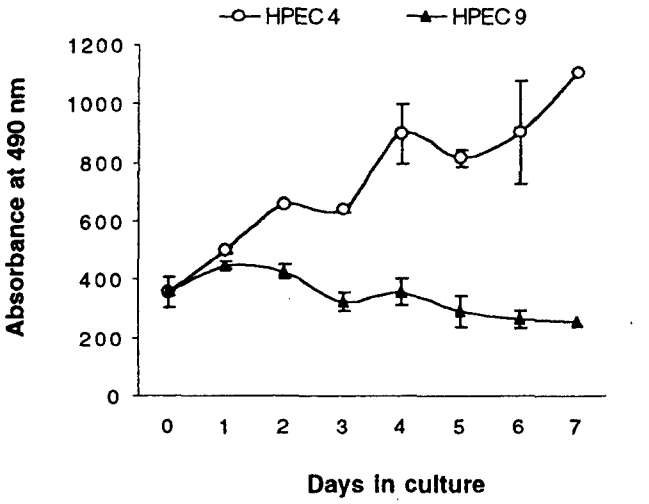

FIG. 3. Growth rates of early and late passages of HPEC. Eight hundred cells of an early passage (4th) and of a late passage (9th) were seeded in 500 μl of rich media per well (48-well plate). At the time points indicated, cell proliferation was investigated, by MTS assay, in triplicate wells. Early passages of HPEC are highly replicative cells with an approximate duplication time of 2 days, whereas late HPEC passages fail to replicate *in vitro*, and die over time. Results are expressed as means ± SE of two independent experiments. The lag phase observed at days 3 and 5 is accounted for by a change in the growth medium.

of cellular growth in the normal HPEC (early replicative passages) cultured for 48 h under serum-free conditions, whereas only TGF-β was inhibitory for the malignant PC-3 cells (Fig. 5). Paralleling the inhibition of proliferation of HPEC by TGF-β and atRA, there was a dose-dependent increase in the concentrations of both IGFBP-rP2 protein and steady-state mRNA. A maximum protein response equivalent to a 6-fold increase over the nontreated cells was observed at a dose of TGF-β1 of 5 ng/ml, whereas 1 μM atRA caused an increase of IGFBP-rP2 protein of about 4-fold over basal levels (Fig. 6A). Similar changes were also observed in the concentrations of IGFBP-rP2 steady-state mRNA (Fig. 6B).

Because IGFBP-rP1 protein and mRNA increase also during senescence of HPEC, we investigated whether IGFBP-rP1 was similarly regulated by these growth regulators. In contrast to IGFBP-rP2, the concentrations of both IGFBP-rP1 protein and steady-state mRNA in HPEC did not change in response to TGF-β treatment. In response to atRA treatment, a 2-fold increase of secreted IGFBP-rP1 protein was detected, although no changes in IGFBP-rP1 mRNA were observed (Figs. 6, A and B).

The effects of IGF-I were also tested in the normal HPEC (late, presenescent passages), where it exerted clear mitogenic actions (Fig. 5A). Importantly, IGFBP-rP2 was also regulated by IGF-I in HPEC, both at the protein and at the mRNA level, with a 90% reduction of both secreted protein and steady-state mRNA, upon treatment with IGF-I at a dose of 100 ng/ml (Fig. 6, C and D). In contrast to IGFBP-rP2, neither IGFBP-rP1 protein nor its mRNA experienced significant changes in response to IGF-I treatment in HPEC (Figs. 6, C and D).

In PC-3 cells, only the effects of TGF-β and atRA on IGFBP-

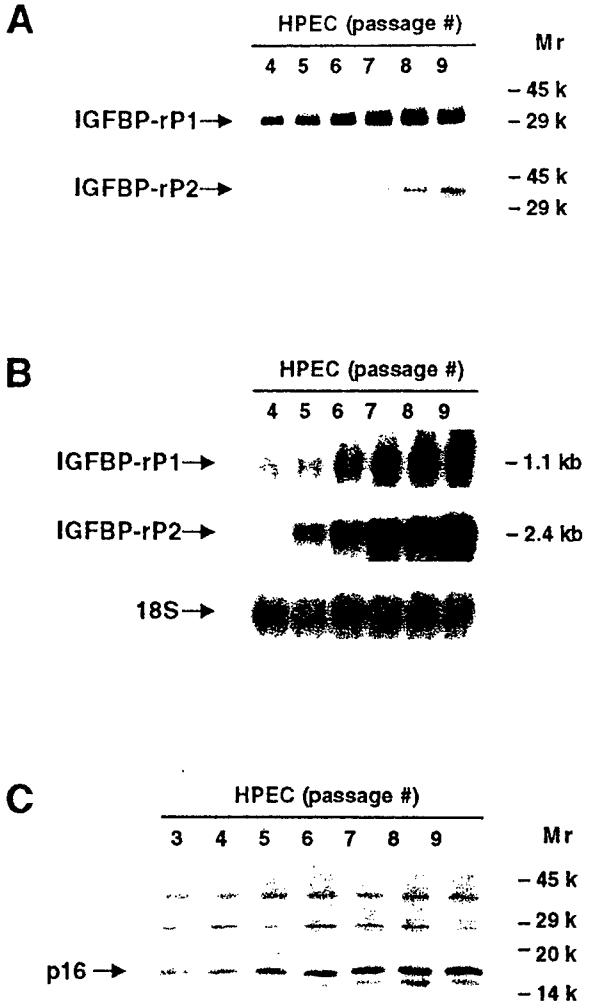

FIG. 4. Expression of IGFBP-rP1 and 2 during serial passages of HPEC. A, Western immunoblot studies of conditioned media from HPEC using polyclonal anti-IGFBP-rP1 and 2 antibodies. Three micrograms of total protein were loaded per lane. Both IGFBP-rP1 and 2 concentrations, in conditioned media, increased approximately 6-fold at late, low-replicative passages, compared with early ones. B, Northern blot analyses of same serial passages of HPEC using [^{32}P] radiolabeled IGFBP-rP1 and 2 probes. Twenty micrograms of total RNA were loaded per lane. Concentrations of 18S ribosomal RNA are shown as an internal control for loading. C, Western immunoblot studies of total cell lysates from HPEC using monoclonal anti-p16^{INK4a} antibody. Ten micrograms of total protein were loaded per lane. Note a marked up-regulation (~6-fold) of p16^{INK4a} concentrations at late, low-replicative passages, compared with early ones, as part of the senescence process of HPEC cells.

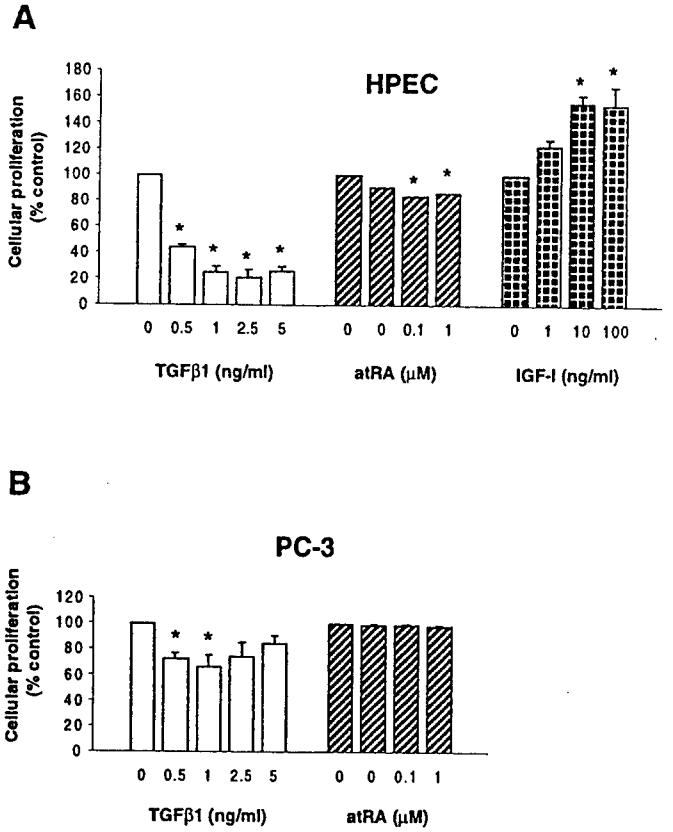

FIG. 5. Effects of growth regulators on cellular proliferation of HPEC and PC-3 cells. A, The growth rates of HPEC cultured with TGF-β, atRA, and IGF-I, for 48 h under serum-free conditions, were investigated by either [^{3}H]thymidine incorporation studies (TGF-β) or by MTS assay (atRA and IGF-I). Both TGF-β and atRA are inhibitory for HPEC, whereas IGF-I is stimulatory for these cells. B, Similarly, the effects of TGF-β and atRA were studied in the malignant PC-3 cells. Only TGF-β was inhibitory for PC-3 cells [atRA did not inhibit the growth of these cells, as judged by either MTS assay or by [^{3}H]thymidine incorporation studies (data not shown)]. Results are expressed as means ± SE of three independent studies for HPEC and two independent studies for PC-3 cells. *Asterisks* indicate statistical significance (compared with control).

rP2 concentrations were studied. TGF-β produced a significant increase (4-fold) in protein levels over nonstimulated values. Similarly, treatment with atRA, under the same experimental conditions, resulted in a 6-fold increase in IGFBP-rP2 concentrations (Fig. 7A). These changes did not, however, follow parallel increases in the concentrations of steady-state mRNA, as the levels of IGFBP-rP2 mRNA did not significantly change on TGF-β treatment and were only increased 2-fold by atRA (Fig. 7B).

In addition, we treated all of the other cell lines with the three above-mentioned growth regulators, but only small responses of IGFBP-rP2 were observed for TGF-β1, atRA, and IGF-I in P69; for TGF-β1 in M12; and for atRA in DU145 cells (data not shown).

IGFBP-rP3 is regulated in HPECs

IGFBP-rP3 has been previously shown to be expressed in prostate epithelial cells, but no regulation has been described, as yet, in these cultures (22). To better understand the role of this protein in the human prostate, we also investigated the effects of TGF-β, atRA, and IGF-I on the expression of IGFBP-rP3 *in vitro*.

IGFBP-rP3 was not produced by normal prostate epithelial cells, nor was it induced by any of the above-mentioned growth regulators in these cells. In the well-established PC-3 (and in DU145) cancer cells, IGFBP-rP3 was readily detected in conditioned media under serum-free incubation, but no significant regulation was observed in these cultures.

In the P69/M12 lineage, both TGF-β and atRA also produced a dose-dependent inhibitory effect on cellular proliferation (Fig. 8). Interestingly, atRA, but not TGF-β, down-

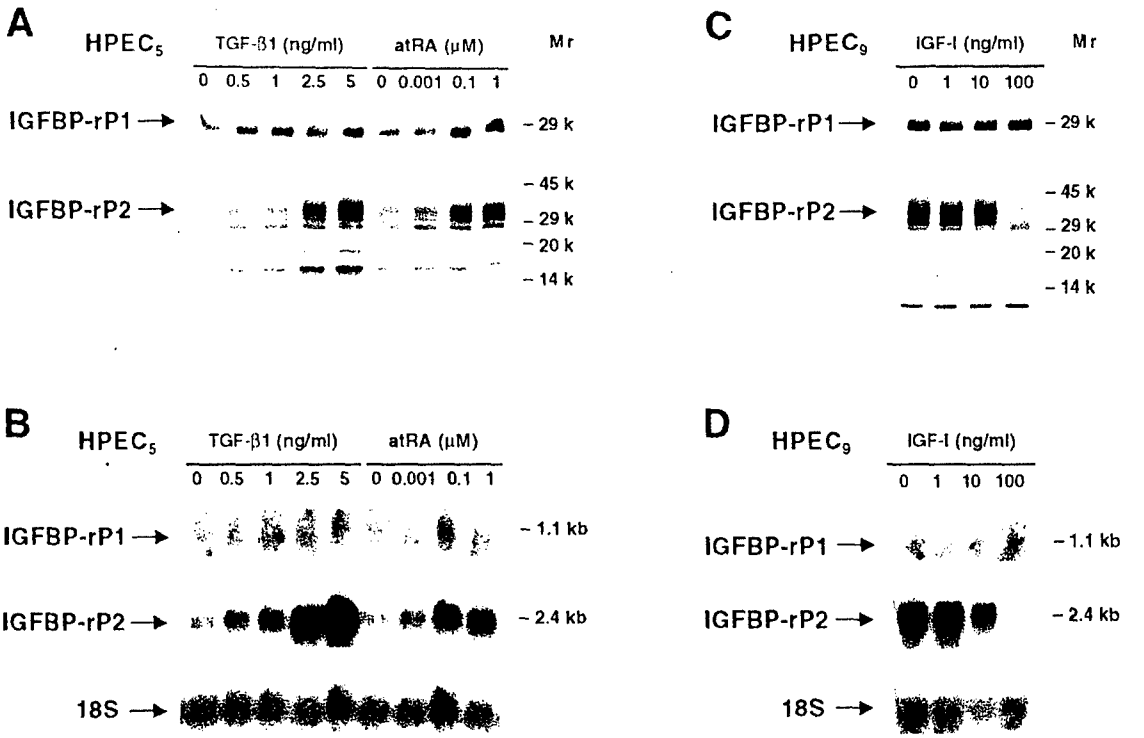

FIG. 6. IGFBP-rP2 is responsive to growth regulators in HPEC. A, Up-regulation of IGFBP-rP2 by the growth inhibitors TGF-β and atRA. Representative Western immunoblot of conditioned media, by HPEC, using polyclonal anti-IGFBP-rP2 antibody. Cells were treated with increasing concentrations of TGF-β1 and atRA, for 48 h, in serum-free conditions. A 4-fold increase or greater was seen with both TGF-β1 and atRA in early, replicative passages of HPEC. IGFBP-rP1 regulation was also studied, but the changes were only modest. B, Northern blot analysis showing similar results for IGFBP-rP1 and -rP2 steady-state mRNA. C, Down-regulation of IGFBP-rP2 by the growth factor IGF-I in HPEC. Representative Western immunoblot of conditioned media, by HPEC, using polyclonal anti-IGFBP-rP2 antibody. Cells were treated with increasing concentrations of IGF-I for 48 h in serum-free conditions. A 90% decrease in IGFBP-rP2 was seen at late passages of IGF-I-treated HPEC. Similar studies with IGFBP-rP1 indicate no regulation by IGF-I in these cells. D, Northern studies of IGF-I regulation of both IGFBP-rP1 and -rP2 in HPEC, showing similar results to those at the protein level.

regulated the concentrations of secreted IGFBP-rP3 in both P69 and M12 cells (4- and 2-fold, respectively; Fig. 9).

The proliferative actions of IGF-I were also investigated in P69 cells. IGF-I was a potent growth stimulator of these cells (Fig. 8A) but had no observable effects on the concentrations of secreted IGFBP-rP3 protein (Fig. 9).

Discussion

Recent studies indicate that both IGFBP-rP1 and IGFBP-rP3 are expressed by the prostate epithelium (16, 22). We now report that prostate cells in culture also synthesize another member of the IGFBP superfamily: IGFBP-rP2. Although the biological functions of these proteins in prostate have yet to be defined, they are likely to play a role in the regulation of proliferation of prostate cells, because they are responsive to growth regulators, and, strikingly, IGFBP-rP1 and 2 expression is significantly increased during senescence of the normal prostate epithelium.

IGFBP-rP1 has been shown to be differentially expressed in normal meningeal, breast, and prostate cells, compared with their malignant counterparts (11, 16, 35). In the prostate, it was suggested that IGFBP-rP1 might have an antiproliferative effect, because it was also up-regulated by the epithelial cell growth inhibitors TGF-β1 and atRA (16). Indeed, a more recent study indicates a possible role of IGFBP-rP1 as a tumor suppressor gene for prostate cancer, because overexpression of this gene in the tumorigenic and metastatic M12 cells caused an antiproliferative effect *in vitro* and *in vivo* (36). More difficult to reconcile, however, is a recent report indicating an up-regulation of IGFBP-rP1 during prostate carcinogenesis (37). Because the results by Degeorges *et al.* are based on immunohistochemistry studies, it is possible that the differences found are attributable to alternative properties or specificity of their antibody; alternatively, different sources of prostatic epithelial cells may vary in these properties.

Further evidence supporting the role of IGFBP-rP1 as a tumor suppressor gene relates to its up-regulation during senescence of normal epithelial cells. Swisshelm *et al.* (35) have described an enhanced expression of IGFBP-rP1 in senescent human mammary epithelial cells, indicating a possible involvement of this protein in the cell-cycle mechanisms leading to cellular senescence.

HPEC, similarly to human mammary epithelial cells, have a limited life span, undergoing senescence after a limited number of population doublings. Besides a failure to replicate *in vitro*, senescent HPECs exhibit phenotypic changes, as they become larger and flattened, and induce β-galactosidase activity (data not shown). Consistent with this, a marked up-regulation of the cell-cycle inhibitor $p16^{INK4a}$ was observed at late passages of HPEC, a phenomenon that has been recently reported in these cells (31). Our results are, thus, in

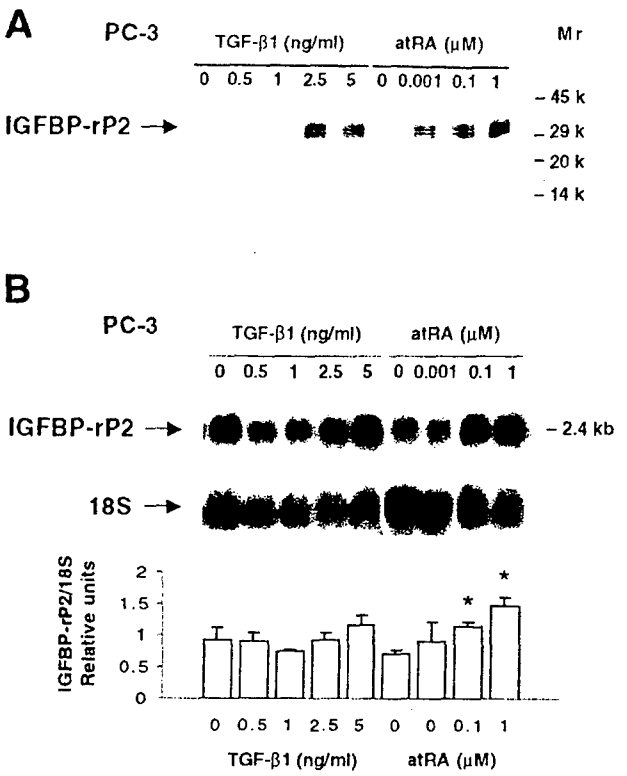

FIG. 7. IGFBP-rP2 is responsive to growth regulators in PC-3. A, Up-regulation of IGFBP-rP2 by the growth inhibitors TGF-β and atRA. Representative Western immunoblot of conditioned media by PC-3 using polyclonal anti-IGFBP-rP2 antibody. Cells were treated with increasing concentrations of TGF-β1 and atRA, for 48 h, in serum-free conditions. A 4-fold increase or greater was seen with both TGF-β1 and atRA in PC-3. B, Northern blot analysis for IGFBP-rP2 indicates only modest increases at the mRNA levels that were statistically different for atRA (graph shows the means ± SE of two independent experiments). *Asterisks* indicate statistical significance (compared with control).

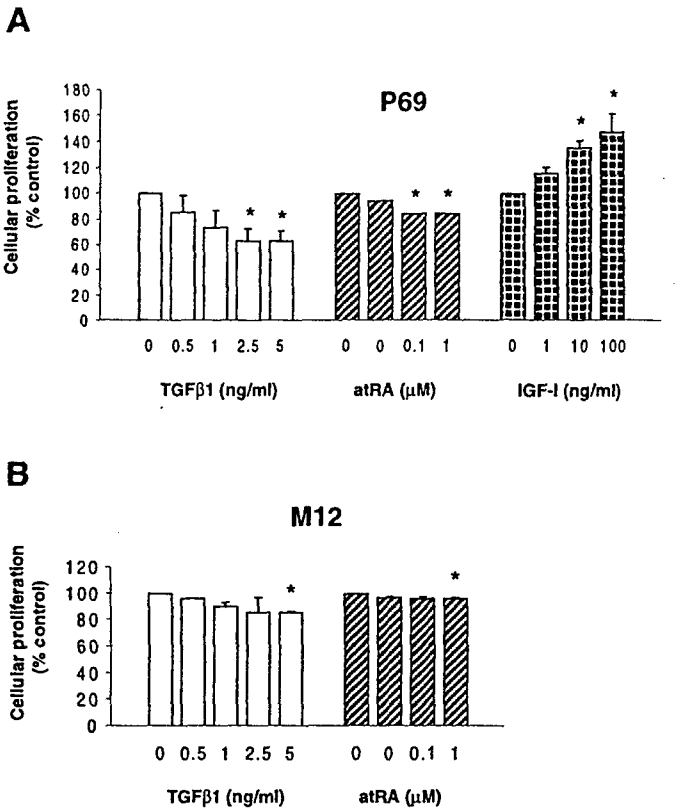

FIG. 8. Effects of growth regulators on cellular proliferation of P69 and M12 cells. A, The growth rates of P69 cultured with TGF-β, atRA, and IGF-I, for 48 h, under serum-free conditions, were investigated by either [^{3}H]thymidine incorporation studies (TGF-β) or by MTS assay (atRA and IGF-I). Both TGF-β and atRA are inhibitory, whereas IGF-I is stimulatory for P69 cells. B, Similarly, the effects of TGF-β and atRA were studied in the malignant M12 cells. Both TGF-β and atRA were inhibitory for M12 cells. Results are expressed as means ± SE of three independent studies for P69 cells and two independent studies for M12 cells. *Asterisks* indicate statistical significance (compared with control).

agreement with observations in human mammary cells, in that the concentrations of both IGFBP-rP1 mRNA and protein were markedly enhanced during replicative senescence of normal prostate epithelial cells. Thus, although the precise role of IGFBP-rP1 in the human prostate has, as yet, to be clarified, our results support the hypothesis that IGFBP-rP1 is a tumor suppressor gene and/or senescence factor.

Several lines of investigation also support roles of IGFBP-rP2 in growth regulation and tumorigenesis. IGFBP-rP2 mediates most of the biological actions of TGF-β in fibroblasts where a novel TGF-β response element in the IGFBP-rP2 promoter has been found (19). Additionally, IGFBP-rP2 is a growth factor for endothelial cells (29, 38). Supporting its role in tumorigenesis, IGFBP-rP2 was expressed by a chondrosarcoma-derived chondrocytic cell line and a fibrosarcoma cell line *in vitro* (29, 39) and has been found in the stromal component of breast and pancreatic cancer and desmoplastic melanomas (40–42). Additionally, it has been shown that IGFBP-rP2 is up-regulated by TGF-β1 in the breast cancer cell line Hs578T (25) and that IGFBP-rP2 induces apoptosis in the estrogen receptor-positive breast cancer cell line MCF-7 (43). These lines of evidence suggest that IGFBP-rP2 plays also a role in modifying the growth of stroma in desmoplastic tumors and in regulating the growth of breast cancer cells.

In this light, our results indicate that IGFBP-rP2 may also regulate the growth of normal and prostate cancer cells, because it is noticeably up-regulated by growth inhibitory factors, such as TGF-β and atRA, in normal and malignant cells, and down-regulated by growth-promoting factors, such as IGF-I, in HPEC. In the prostate, TGF-β is known to limit the proliferation and survival of the normal epithelium, an effect that is lost in malignant cells largely because of a down-regulation of TGF-β receptors during prostate carcinogenesis (44). Retinoids also exert potent inhibitory properties in the normal prostate and have been shown to be present at lower concentration in prostate cancer tissues (33, 45). Thus, both TGF-β and atRA play major roles in controlling the growth and survival of normal prostate cells and probably also in the development of prostate cancer. IGFs regulate also the proliferation of prostate cells (34). Interestingly, the expression of type I IGF-I receptor, which mediates most of the biological activities of IGFs, in markedly down-regulated during carcinogenesis (3). Thus, IGFs seem to play fundamental roles in the regulation of growth and malignant transformation of normal prostate epithelial cells. Because the above-mentioned growth regulators affected the concen-

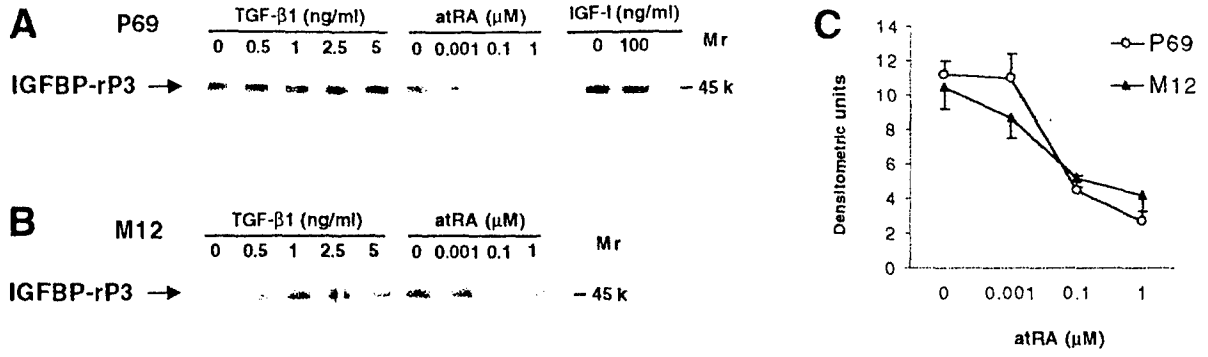

FIG. 9. IGFBP-rP3 is regulated in HPECs: down-regulation of IGFBP-rP3 by the growth inhibitor atRA. Representative Western immunoblots of conditioned media from P69 and M12 cells using polyclonal anti-IGFBP-rP3 antibody. Cells were treated with increasing concentrations of TGF-β, atRA, and IGF-I, for 48 h, in serum-free conditions. Whereas IGFBP-rP3 did not exhibit any regulation by either TGF-β or IGF-I in P69 cells or by TGF-β in M12 cells, both cell lines responded to atRA treatment by decreasing their concentrations of IGFBP-rP3 in conditioned medium. Densitometric analysis of IGFBP-rP3 bands is also shown graphically for atRA (mean ± SE of three independent experiments). All-*trans* RA treatment caused a 4-fold and a 2-fold decrease in the concentrations of IGFBP-rP3 in conditioned media from P69 and M12 cells, respectively.

trations of both IGFBP-rP2 protein and steady-state mRNA in our cultured cells, we speculate that, in the human prostate, IGFBP-rP2 is a downstream effector of growth inhibitors and that IGFBP-rP2 expression must be down-regulated by growth factors to support cell proliferation.

Further observations support the hypothesis that IGFBP-rP2 may act as a growth inhibitor. A striking increase of IGFBP-rP2 was observed during senescence of HPECs, paralleling increases of both IGFBP-rP1 and the cell cycle inhibitor $p16^{INK4a}$. Thus, IGFBP-rP2 could also be a downstream effector in the mechanisms leading to cellular senescence of normal cells. In summary, IGFBP-rP2 is a potential growth inhibitor that is induced during senescence in prostate epithelial cells and can mediate the effects of growth inhibitors on cell-cycle progression and/or apoptosis in normal and malignant prostate.

IGFBP-rP3 is overexpressed in Wilms tumor, showing an inverse correlation with the concentrations of the tumor-suppressor gene WT1(21), which suggests a potential role of this protein as an protooncogene. Supporting this hypothesis is the observation that overexpression of the aminoterminal truncated NOV molecule was also able to transform chicken embryo fibroblasts (20). More recently, NOV has also shown to induce proliferation of mouse fibroblasts *in vitro* and to enhance phosphorylation of a 221-kDa protein, suggesting growth-stimulatory properties of this protein through activation of a still unidentified phosphorylated molecule (46).

In the prostate, data on NOV expression are only modest, with one report showing, by RT-PCR, that NOV mRNA is preferentially expressed in PC-3, compared with other normal and malignant prostatic epithelial cells (22). Our results are consistent with this report, and we have extended these findings by demonstrating that IGFBP-rP3 protein was detectable in the condition medium from PC-3 cells. Moreover, by RT-PCR, we were able to detect IGFBP-rP3 mRNA in the immortalized P69 cells and in the malignant M12 and LNCaP cell lines. IGFBP-rP3 protein was also detected in conditioned media from these cells (except LNCaP cells) and in the conditioned medium from the malignant DU145 cells. However, IGFBP-rP3 expression was not detected in normal HPEC cells. Additionally, IGFBP-rP3 expression was suppressed by the growth-inhibitor atRA in P69 and M12 cells. Thus, IGFBP-rP3 expression in prostatic cells is consistent with its potential role as a protooncogene and/or growth factor.

In summary, we report on the expression and regulation of two additional IGFBP-rPs in prostate cells, IGFBP-rP2 and rP3, with results that support the hypothesis that these proteins, like IGFBP-rP1, are involved in the regulation of prostatic cell growth. IGFBP-rP2 may play a role as a growth inhibitor, because its expression is: 1) enhanced during senescence of normal prostate epithelial cells (in a fashion similar to that of IGFBP-rP1); 2) increased by growth inhibitory factors (TGF-β and atRA); and 3) decreased by IGF-I. Conversely, IGFBP-rP3 may act as a growth stimulator for prostate cells, given its preferential expression in malignant cells and its down-regulation by atRA.

References

1. **Jones JI, Clemmons DR** 1995 Insulin-like growth factors and their binding proteins: biological actions. Endocr Rev 16:3–34
2. **Hwa V, Oh Y, Rosenfeld RG** 1999 The insulin-like growth factor-binding protein (IGFBP) superfamily. Endocr Rev 20:761–787
3. **Tennant MK, Thrasher JB, Twomey PA, Drivdahl RH, Birnbaum RS, Plymate S** 1996 Protein and messenger ribonucleic acid (mRNA) for the type 1 insulin-like growth factor (IGF) receptor is decreased and IGF-II mRNA is increased in human prostate carcinoma compared to benign prostate epithelium. J Clin Endocrinol Metab 81:3774–3782
4. **Chan J, Stampfer M, Giovannucci E, Gann P, Ma J, Wilkinson P, Hennekens C, Pollak M** 1998 Plasma insulin-like growth factor-I and prostate cancer risk: a prospective study. Science 279:563–566
5. **Tennant MK, Thrasher JB, Twomey PA, Birnbaum RS, Plymate SR** 1996 Insulin-like growth factor-binding protein-2 and -3 expression in benign human prostate epithelium, prostate intraepithelial neoplasia, and adenocarcinoma of the prostate. J Clin Endocrinol Metab 81:411–420
6. **Tennant MK, Thrasher JB, Twomey PA, Birnbaum RS, Plymate SR** 1996 Insulin-like growth factor-binding proteins (IGFBP)-4, -5 and -6 in the benign and malignant human prostate: IGFBP-5 messenger ribonucleic acid localization differs from IGFBP-5 protein localization. J Clin Endocrinol Metab 81:3783–3792
7. **Cohen P, Graves HCB, Peehl DM, Kamarei M, Giudice LC, Rosenfeld RG** 1992 Prostate-specific antigen (PSA) is an insulin-like growth factor binding protein-3 protease found in seminal plasma. J Clin Endocrinol Metab 75:1046–1053
8. **Kanety H, Madjar Y, Dagan Y, Levi J, Papa MZ, Pariente C, Goldwasser B, Karasik A** 1993 Serum insulin-like growth factor-binding protein-2 (IGFBP-2) is increased and IGFBP-3 is decreased in patients with prostate cancer: correlations with serum prostate-specific antigen. J Clin Endocrinol Metab 77:229–233
9. **Nickerson T, Pollak M, Huynh H** 1998 Castration-induced apoptosis in the rat ventral prostate is associated with increased expression of genes encoding

insulin-like growth factor binding proteins 2, 3, 4, and 5. Endocrinology 139:807–810
10. **Thomas LN, Wright AS, Lazier CB, Cohen P, Rittmaster RS** 2000 Prostatic involution in men taking finasteride is associated with elevated levels of insulin-like growth factor-binding proteins (IGFBPs)-2, -4, and -5. Prostate 15:203–210
11. **Murphy M, Pykett MJ, Harnish P, Zang KD, George DL** 1993 Identification and characterization of genes differentially expressed in meningiomas. Cell Growth Differ 4:715–722
12. **Akaogi K, Okabe Y, Funahashi K, Yoshitake Y, Nishikawa K, Yasumitsu H, Umeda M, Miyazaki H** 1994 Cell adhesion activity of a 30-kDa major secreted protein from human bladder carcinoma cells. Biochem Biophys Res Commun 198:1046–1053
13. **Akaogi K, Okabe Y, Sato J, Nagashima Y, Yasumitsu H, Sugahara K, Miyazaki K** 1996 Specific accumulation of tumor-derived adhesion factor in tumor blood vessels and in capillary tube-like structures of cultured vascular endothelial cells. Proc Natl Acad Sci USA 93:8384–8389
14. **Yamauchi T, Umeda F, Masakado M, Isaji M, Mizushima S, Nawata H** 1994 Purification and molecular cloning of prostacyclin-stimulating factor from serum-free conditioned medium of human diploid fibroblast cells. Biochem J 303:591–598
15. **Burger A, Zhang X, Li H, Ostrowski JL, Beatty B, Venanzoni M, Papas T, Seth A** 1998 Down-regulation of T1A12/mac25, a novel insulin-like growth factor binding protein related gene, is associated with disease progression in breast carcinomas. Oncogene 16:2459–2467
16. **Hwa V, Tomasini-Sprenger C, López-Bermejo A, Rosenfeld RG, Plymate SR** 1998 Characterization of insulin-like growth factor binding protein-related protein 1 in prostate cells. J Clin Endocrinol Metab 83:4355–4362
17. **Bradham DM, Igarashi A, Potter RL, Grotendorst GR** 1991 Connective tissue growth factor: a cysteine-rich mitogen secreted by human vascular endothelial cells is related to the SRC-induced immediate early gene product CEF-10. J Cell Biol 114:1285–1294
18. **Bork P** 1993 The modular architecture of a new family of growth regulators related to connective tissue growth factor. FEBS Lett 327:125–130
19. **Grotendorst GR, Okochi H, Hayashi N** 1996 A novel transforming growth factor β response element controls the expression of the connective tissue growth factor gene. Cell Growth Differ 7:469–480
20. **Joliot V, Martinerie C, Dambrine G, Plassiart G, Brisac M, Crochet J, Perbal B** 1992 Proviral rearrangements and overexpression of a new cellular gene (NOV) in myeloblastosis-associated virus type 1-induced nephroblastomas. Mol Cell Biol 12:10–21
21. **Martinerie C, Huff V, Joubert I, Badzioch M, Saunders G, Strong L, Perbal B** 1994 Structural analysis of the human NOV proto-oncogene and expression in Wilms tumor. Oncogene 9:2729–2723
22. **Tatoud R, Padilla A, Sethia K, Gibson I,** The novH proto-oncogen mRNA is differentially expressed in human prostate cell lines: a new marker for tumor progression? Program of the 89th Annual Meeting of The American Association for Cancer Research, New Orleans, LA, 1998, p 209 (Abstract)
23. **Plymate SR, Tennant M, Birnbaum RS, Thrasher JB, Chatta G, Ware JL** 1996 The effect on the insulin-like growth factor system in human prostate epithelial cells of immortalization and transformation by simian virus-40 T antigen. J Clin Endocrinol Metab 81:3709–3716
24. **Wilson EM, Oh Y, Rosenfeld RG** 1997 Generation and characterization of an IGFBP-7 antibody: identification of 31kD IGFBP-7 in human biological fluids and Hs578T human breast cancer conditioned media. J Clin Endocrinol Metab 82:1301–1303
25. **Yang D-H, Kim H-S, Wilson EM, Rosenfeld RG, Oh Y** 1998 Identification of glycosylated 38-kDa connective tissue growth factor (IGFBP-related protein 2) and proteolytic fragments in human biological fluids, and up-regulation of IGFBP-rP2 expression by TGF-β in Hs578T human breast cancer cells. J Clin Endocrinol Metab 83:2593–2596
26. **Burren CP, Wilson EM, Hwa V, Oh Y, Rosenfeld RG** 1999 Binding properties and distribution of insulin-like growth factor binding protein-related protein 3 (IGFBP-rP3/NovH), an additional member of the IGFBP superfamily. J Clin Endocrinol Metab 1096–1103
27. **Oh Y, Nagalla SR, Yamanaka Y** 1996 Synthesis and characterization of insulin-like growth factor binding protein-7 (IGFBP-7). J Biol Chem 271:30322–30325
28. **Kim H-S, Nagalla SR, Oh Y** 1997 Identification of a family of low-affinity insulin-like growth factor binding proteins (IGFBPs): characterization of connective tissue growth factor as a member of the IGFBP superfamily. Proc Natl Acad Sci USA 94:12981–12986
29. **Brigstock DR** 1999 The connective-tissue growth factor/cystein-rich 61/nephroblastoma overexpressed (CCN) family. Endocr Rev 20:189–206
30. **Wynford-Thomas D** 1999 Cellular senescence and cancer. J Pathol 187:100–111
31. **Jarrard DF, Sarkar S, Shi Y, Yeager TR, Magrane G, Kinoshita H, Nassif N, Meisner L, Newton MA, Waldman FM, Reznikoff CA** 1999 p16/pRb pathway alterations are required for bypassing senescene in human prostate epithelial cells. Cancer Res 59:2957–2964
32. **Story MT, Hopp KA, Molter M** 1996 Expression of transforming growth factor beta 1 (TGF beta 1), -beta 2, and -beta 3 by cultured human prostate cells. J Cell Physiol 169:97–107
33. **Pasquali D, Rossi V, Prezioso D, Gentile V, Colantuoni V, Lotti T, Bellastella A, Sinisi AA** 1999 Changes in tissue transglutaminase activity and expression during retinoic acid-induced growth arrest and apoptosis in primary cultures of human epithelial prostate cells. J Clin Endocrinol Metab 84:1463–1469
34. **Peehl DM, Cohen P, Rosenfeld RG** 1995 The insulin-like growth factor system in the prostate. World J Urol 13:306–311
35. **Swisshelm K, Ryan K, Tsuchiya K, Sager R** 1995 Enhanced expression of an insulin growth factor-like binding protein (mac25) in senescent human mammary epithelial cells and induced expression with retinoic acid. Proc Natl Acad Sci USA 92:4472–2276
36. **Sprenger CC, Damon SE, Hwa V, Rosenfeld RG, Plymate SR** 1999 Insulin-like growth factor binding protein-related protein 1 (IGFBP-rP1) is a potential tumor suppressor protein for prostate cancer. Cancer Res 59:2370–2375
37. **Degeorges A, Wang F, Frieson Jr HF, Seth A, Chung LWK, Sikes RA** 1999 Human prostate cancer expresses the low affinity insulin-like growth factor binding protein IGFBP-rP1. Cancer Res 59:2787–2790
38. **Lau LF, Lam SC-T** 1999 Minireview: the CCN family of angiogenic regulators: the integrin connection. Exp Cell Res 248:44–57
39. **Nakanishi T, Kimura Y, Tamura T, Ichikawa H, Yamaai Y-I, Sugimoto T, Takigawa M** 1997 Cloning of a mRNA preferentially expressed in chondrocytes by differential display-PCR from a human chondrocytic cell line that is identical with connective tissue growth factor (CTGF)) mRNA. Biochem Biophys Res Commun 234:206–210
40. **Frazier KS, Grotendorst GR** 1997 Expression of connective tissue growth factor mRNA in the fibrous stroma of mammary tumors. Int J Biochem Cell Biol 29:153–161
41. **Kubo M, Kikuchi K, Nashiro K, Kakinuma T, Hayashi N, Nanko H, Tamaki K** 1998 Expression of fibrogenic cytokines in desmoplastic malignant melanoma. Br J Dermatol 139:192–197
42. **Wenger C, Ellenrieder V, Alber B, Lacher U, Menke A, Hameister H, Wilda M, Iwamura T, Beger HG, Adler G, Gress TM** 1999 Expression and differential regulation of connective tissue growth factor in pancreatic cancer cells. Oncogene 28:1073–1080
43. **Hishikawa K, Oemar BS, Tanner FC, Nakaki T, Lüscher TF, Fujii T** 1999 Connective tissue growth factor induces apoptosis in human breast cancer cell line MCF-7. J Biol Chem 274:37461–37466
44. **Lee C, Sintich S, Mathews E, Shah A, Kundu S, Perry K, Cho J, Ilio K, Cronauer M, Janulis L, Sensibar J** 1999 Transforming growth factor-beta in benign and malignant prostate. Prostate 39:285–290
45. **Pasquali D, Thaller C, Eichele G** 1996 Abnormal level of retinoic acid in prostate cancer tissues. J Clin Endocrinol Metab 81:2186–2191
46. **Liu C, Liu X-J, Crowe PS, Kelner GS, Fan J, Barry G, Manu F, Ling N, Souza EBD, Maki RA** 1999 Nephroblastoma overexpressed gene (NOV) codes for a growth factor that induces protein tyrosine phosphorylation. Gene 238: 471–478

Effects of sodium butyrate on expression of members of the IGF-binding protein superfamily in human mammary epithelial cells

J Tsubaki, W-K Choi, A R Ingermann, S M Twigg, H-S Kim, R G Rosenfeld and **Y Oh**

Department of Pediatrics, Oregon Health Sciences University, Portland, Oregon 97201, USA

(Requests for offprints should be addressed to Y Oh, Department of Pediatrics, School of Medicine, NRC 5, Oregon Health Sciences University, 3181 Southwest Sam Jackson Park Road, Portland, Oregon 97201–3042, USA; Email: ohy@ohsu.edu)

Abstract

Dietary factors play an important role in both the development and prevention of human cancers, including breast carcinoma. One dietary micronutrient, sodium butyrate (NaB), is a major end product of dietary starch and fiber, produced naturally during digestion by anaerobic bacteria in the cecum and colon. NaB is a potent growth inhibitor and initiates cell differentiation for many cell types *in vitro*. In this study, we investigated the effects of NaB on three human mammary epithelial cells and regulation of the IGF axis, specifically, IGF-binding protein-3 (IGFBP-3), a known growth regulator in human mammary cells, and IGFBP-related protein 2 (IGFBP-rP2)/connective tissue growth factor.

NaB inhibited DNA synthesis, as measured by [^{3}H]thymidine incorporation, in estrogen-responsive (MCF-7) and estrogen-non-responsive (Hs578T) breast cancer cells, and normal human mammary epithelial cells (HMEC) to a similar degree (up to 90% inhibition at 1–10 mM concentrations). Treatment of cells with NaB induced histone hyperacetylation, suggesting that NaB exerts its biological effects, at least in part, as a histone deacetylase inhibitor in mammary epithelial cells. Treatment of Hs578T cells with NaB caused an induction of apoptotic cell death. NaB treatment resulted in increased levels of $p21^{Waf1/Cip1}$ mRNA and protein in Hs578T cells and distinct upregulation of $p27^{Kip1}$ in HMEC, suggesting that NaB activates different genes involved in cell cycle arrest, depending upon the cell type. In the same context, among the IGFBP superfamily members tested, NaB specifically upregulated the expression of IGFBP-3 and IGFBP-rP2. These two proteins are known to be involved in inhibition of mammary epithelial cell replication. Northern blot analysis showed that NaB treatment at 1–10 mM concentrations caused a dose-dependent stimulation of IGFBP-3 mRNA expression in cancerous cells and IGFBP-rP2 mRNA expression in both cancerous and non-cancerous cells. Protein data from Western ligand blot and immunoblot analyses demonstrated parallel results.

In summary, we have demonstrated that NaB (i) uniformly suppresses DNA synthesis in both cancerous and non-cancerous mammary cells, and (ii) upregulates IGFBP-3 and IGFBP-rP2 mRNA and protein levels in cancerous and non-cancerous mammary cells. These results provide the first demonstration that butyrate regulates the IGFBP system in the human mammary system.

Journal of Endocrinology (2001) **169**, 97–110

Introduction

Butyric acid is a 4-carbon fatty acid which is the major product from microbial fermentation of dietary fibers in the large intestine (Velázquez *et al.* 1997). It is a potent growth inhibitor and initiates cell differentiation in several cell types, including breast cancer cells *in vitro* (Coradini *et al.* 1997, Velázquez *et al.* 1997, Gleave *et al.* 1998, Yamamoto *et al.* 1998). Although the molecular mechanisms by which butyrate exerts its effects are still unclear, it is known to induce a number of alterations within the nucleus, including histone hyperacetylation (de Haan *et al.* 1986, Archer & Hodin 1999).

It has been reported that butyrate, as well as trichostatin A (TSA), a specific histone deacetylase inhibitor (Yoshida *et al.* 1990), modulates specific genes involved in cell cycle regulation and apoptosis. These include the cyclin-dependent kinase (cdk) inhibitor $p21^{Waf1/Cip1}$ (Archer *et al.* 1998), $p16^{INK4}$ (Schwartz *et al.* 1998), $p27^{Kip1}$ (Litvak *et al.* 1998), retinoblastoma protein (Vaziri *et al.* 1998), cyclin D1 (Lallemand *et al.* 1996, Siavoshian *et al.* 1997), Bcl-2 and Bax (Mandal & Kumar 1996, Hague *et al.* 1997). Furthermore, butyrate has also been reported to upregulate the expression of transforming growth factor-β (TGF-β) (Staiano-Coico *et al.* 1990), which is known to be involved in growth suppression of various

0022–0795/01/0169–097

cancer cells, including breast cancer cells (Knabbe *et al.* 1987).

Insulin-like growth factors (IGFs) are potent mitogens for several cell types (Macaulay 1992, Resnicoff *et al.* 1995). The IGF system consists of IGF-I and IGF-II ligands, the transmembrane type I and type II IGF receptors, the IGF-binding proteins (IGFBPs) and IGFBP proteases (Hwa *et al.* 1999). Recently, the concept of the IGFBP superfamily has been proposed (Baxter *et al.* 1998); it consists of high affinity IGF binders (IGFBP-1 to -6) and low affinity IGF binders (IGFBP-related proteins (IGFBP-rPs)). The IGFBPs modulate IGF bioactivity, and bind with differential affinities to IGFs in serum and various biological fluids (Kelley *et al.* 1996, Rajaram *et al.* 1997). In addition, recent evidence suggests that some IGFBPs may have direct receptor-mediated effects independent of IGFs (Oh *et al.* 1993). IGFBP-3, for example, has been demonstrated to be an important mediator of other growth inhibitory agents, such as retinoic acid (Gucev *et al.* 1996), vitamin D (Colston *et al.* 1998), TGF-β (Oh *et al.* 1995, Gucev *et al.* 1996, Rajah *et al.* 1997), anti-estrogens (Huynh *et al.* 1996), tumor necrosis factor-α (Rozen *et al.* 1998) and p53 (Buckbinder *et al.* 1995), independently of the IGF signaling system. Furthermore, the importance of IGF-independent biological effects of the IGFBP superfamily, such as IGFBP-3 (Oh *et al.* 1993), IGFBP-rP1 (Burger *et al.* 1998) and -rP2 (Hishikawa *et al.* 1999) on cell replication has been demonstrated in human breast cancer cell systems.

In this study, we have investigated the effects of sodium butyrate (NaB) on members of the IGFBP superfamily in human mammary epithelial cells, using estrogen-responsive (MCF-7) and estrogen-non-responsive (Hs578T) breast cancer cells, and normal human mammary epithelial (HMEC) cells. We report here that NaB upregulates IGFBP-3 and IGFBP-rP2 mRNA and protein in mammary epithelial cells.

Materials and Methods

Materials

NaB, TSA, BSA and 0·4% trypan blue solution were purchased from Sigma Chemical Co. (St Louis, MO, USA). ^{125}I-labeled IGF-I was kindly provided by Diagnostic Systems Laboratories (Webster, TX, USA). Polyclonal anti-IGFBP-3, anti-IGFBP-rP1, anti-IGFBP-rP2 and anti-HEC1 (specific for both human IGFBP-2 and -3) antisera were generated as previously described (Rosenfeld *et al.* 1990, Oh *et al.* 1993, Wilson *et al.* 1997, Yang *et al.* 1998). Polyclonal anti-IGFBP-5 antibody was purchased from Austral Biologicals (San Ramon, CA, USA). Polyclonal anti-acetyl-lysine, anti-acetylated histone H3 and anti-acetylated histone H4 antibodies were purchased from Upstate Biotechnology (Lake Placid, NY, USA). Polyclonal anti-poly(ADP-ribose)polymerase (PARP) antibody was purchased from Santa Cruz Biotechnology (Santa Cruz, CA, USA). Monoclonal antibodies, anti-p21$^{Waf1/Cip1}$, anti-p16^{INK4} and anti-p27^{Kip1} were purchased from Transducion Laboratories (Lexington, KY, USA), PharMingen (San Diego, CA, USA) and Calbiochem (Cambridge, MA, USA) respectively.

Cell culture

Hs578T estrogen-non-responsive human breast cancer cells and MCF-7 estrogen-responsive human breast cancer cells were purchased from ATCC (Manassas, VA, USA). Both cell lines were maintained in DMEM supplemented with 4·5 g/l glucose, 110 mg/l sodium pyruvate, and 10% fetal bovine serum. HMEC (normal human mammary epithelial cells) were purchased from Clonetics (San Diego, CA, USA), and maintained in mammary epithelium basal medium (MEBM) with growth supplements (bovine pituitary extract (BPE), human epidermal growth factor, insulin, hydrocortisone, gentamicin and amphotericin-B) as directed by the manufacturer.

[^{3}H]thymidine incorporation assay

Cells were seeded into 24-well dishes at 37 °C in 5% CO_2. At 90% confluence, cells were placed in serum-free media for 12 h, then treated as indicated in the text. After 22 h, 0·1 μCi [^{3}H]thymidine (NEN, Boston, MA, USA) in a volume of 25 μl PBS was added to each well, and the plate was incubated for 4 h at 37 °C. Cells were washed with cold PBS twice, treated with 10% trichloroacetic acid (TCA) for 10 min at − 20 °C, washed with 10% TCA followed by 95% ethanol, and lysed with 400 μl 0·25 N NaOH per well. Cell lysates (CL) from each well were transferred to scintillant vials, then 10 ml scintillation fluid with 100 μl 2 N HCl were added to the vials, and the radioactivity was measured in a scintillation counter.

MTS assay

Hs578T cells were seeded into 96-well plates. At 80% confluence, they were incubated for 12 h in serum-free DMEM, then treated with various concentrations of NaB as indicated in the text in serum-free media. After a further incubation of 1–4 days, the MTS reagent (Promega Co., Madison, WI, USA) was added in the ratio recommended by the manufacturer. At 15 min intervals, the absorbance of the formazan product at 490 nm was read with a plate reader (Spectra Shell Reader; SLT Labinstruments GmbH, Austria). On the same plate, cells were dispensed at the differential confluency. These cells were left untreated in serum-free media, and then the MTS reagent was added at the same time as to the butyrate-treated wells. After the reading, cells were trypsinized, then the cell number was counted with a

hemacytometer. Using this method, a linear correlation was obtained between direct cell counts from 1×10^3 to 1×10^4 per well and the absorbance (r=0·85, n=70) (data not shown). The experiment was repeated three times in conditions where the starting untreated control cell number was 8×10^3 per well, and the absorbance at 490 nm read at 45 min after adding the MTS reagent to the wells was ~0·8.

Quantitation of apoptosis

To quantitate apoptotic cell death, the Cell Death Detection ELISA^{PLUS} kit (Roche Molecular Biochemicals, Mannheim, Germany), which measures cytoplasmic histone-bound DNA fragments produced during apoptotic DNA fragmentation, was used (Mandal & Kumar 1996). Hs578T cells were seeded into a 96-well plate at 80% confluence, they were incubated for 12 h in serum-free DMEM, then treated with various concentrations of NaB in serum-free media. After 72 h, cytoplasmic extracts were made from attached cells by adding 100 µl lysis buffer to 5×10^3 cells per well. Supernatant (20 µl from 100 µl) was analyzed in the ELISA, as directed by the manufacturer's protocol. Briefly, the samples were placed into streptavidin-coated multi-well plates, a mixture of anti-histone-biotin and anti-DNA-peroxidase was added and incubated. The ELISA was developed with peroxidase substrate, and the absorbance at 405 nm was measured against 490 nm as a reference wavelength. The experiment was performed from duplicate samples for each data point generated, and was repeated twice independently.

Preparation of conditioned media (CM) and CL

Cells were seeded in 12-well plates. At 95% confluence, they were incubated for 12 h in serum-free DMEM (Hs578T and MCF-7) or supplement-free MEBM with added BPE (HMEC), then treated as indicated in the text in serum- or supplement-free media. CM samples were collected after 72 h and centrifuged at 1000 ***g*** for 10 min to remove debris. The harvested CM from duplicate wells within each experiment were pooled and stored at − 20 °C until assay. Proteins in 40 µl CM per lane were examined by Western immunoblot or Western ligand blot under non-reducing conditions.

CL samples were harvested at 24 h post-treatment by washing with PBS, and then adding 150 µl cold RIPA lysis buffer (20 mM Tris, pH 8·0, 150 mM NaCl, 1% NP-40, 0·5% NaDOC, 0·1% SDS) plus protease inhibitors cocktail (Roche Molecular Biochemicals) directly to each well. Plates were rocked for 30 min at 4 °C, and the lysates were collected and centrifuged at 10 000 ***g*** for 10 min at 4 °C. The supernatants from duplicate wells within each experiment were pooled and stored at − 20 °C until assay. Total protein concentration was determined for each sample using DC Protein Assay Reagent (Bio-Rad, Hercules, CA, USA), and 20 µg total protein per sample were examined by Western immunoblot under reducing conditions.

Western ligand blot analysis

Proteins from CM samples were size-fractionated by 12% SDS-PAGE under non-reducing conditions and electroblotted onto nitrocellulose filters (Hybond; Amersham Pharmacia Biotech, Piscataway, NJ, USA). Filters were washed in 3% NP-40/ddH_2O for 30 min, blocked with 1% BSA/TBS-T (20 mM Tris–HCl, pH 7·6, 150 mM NaCl, 0·1% Tween-20) for 2 h, and incubated overnight with $2·0 \times 10^6$ c.p.m. ^{125}I-labeled IGF-I. The membranes were washed, dried and exposed to film (Kodak BioMax MS, Eastman Kodak Co., Rochester, NY, USA) for 12–18 h.

Western immunoblot analysis

For IGFBP-3, IGFBP-rP1 and IGFBP-rP2 detection, CM samples were separated on non-reducing 12 or 15% SDS-PAGE. For p21$^{Waf1/Cip1}$ detection, CL samples were separated on reducing 15% SDS-PAGE. Proteins were electrotransferred onto nitrocellulose, and membranes were blocked with 5% non-fat dry milk/TBS-T for 1 h at room temperature, then incubated in 1:3000 dilution of primary antibody at 4 °C overnight. Immunoreactive proteins were detected using enhanced chemiluminescence (NEN, Boston, MA, USA).

Total RNA isolation and Northern blot analysis

Cells were grown in 6-well plates until 95% confluent. Cells were then incubated in serum-free media for 12 h, then treated for 18 h in serum- or supplement-free media as indicated in the text. Total RNA was isolated from duplicate wells, using the RNeasy Kit (Qiagen, Valencia, CA, USA), and 5 µg total RNA per sample were separated on a 1% formaldehyde agarose gel and transferred to nylon membranes (GeneScreenPlus; NEN). Membranes were stained with 0·02% methylene blue in 0·3 M NaOAc, pH 5·5, and 18S and 28S rRNA bands were used as internal controls to adjust for sample loading. The blot was then hybridized at 65 °C with full length cDNA probes random-labeled with [^{32}P]dCTP (Prime-It II; Stratagene, Cedar Creek, TX, USA), washed and autoradiographed.

Densitometric analysis

To quantitate the relative induction after Western blot analyses or Northern blot analyses, densitometric measurement was performed by using a GS-700 imaging densitometer with Multi-Analyst software (Bio-Rad).

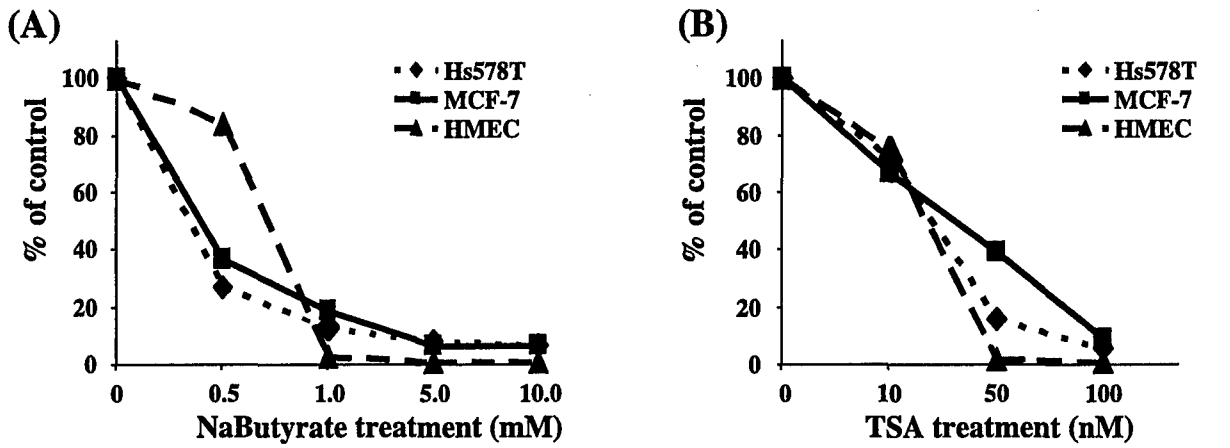

Figure 1 Effect of NaB (A) and TSA (B) on DNA synthesis in Hs578T, MCF-7 and HMEC cells. Serum-starved cells (85–90% confluent) were incubated in basal medium for 22 h in the absence or presence of various concentrations of NaB or TSA as indicated. [^{3}H]Thymidine was added, and the incubation was continued for another 4 h. The incorporation of [^{3}H]thymidine was determined relative to control cells incubated without the addition of these reagents. Results represent the average of two independent experiments each performed in triplicate.

Results

NaB treatment inhibits DNA synthesis and causes histone hyperacetylation in human mammary epithelial cells

Since it has been demonstrated that treatment of NaB resulted in growth inhibition in a variety of cell systems *in vitro*, we first examined the effect of NaB on DNA synthesis in normal (HMEC) and cancerous (Hs578T, MCF-7) human mammary epithelial cells, using the [^{3}H]thymidine incorporation assay. NaB suppressed DNA synthesis in both cancerous and non-cancerous human mammary epithelial cells in a dose-dependent manner, with 90–100% inhibition at NaB concentrations of 5 mM (Fig. 1A). One major function of NaB is inhibition of histone deacetylase activity, resulting in histone hyperacetylation. In order to determine whether NaB-induced inhibition of DNA synthesis might be due to histone hyperacetylation, we treated the cells with TSA, a specific histone deacetylase inhibitor, and compared its effect on DNA synthesis. As shown in Fig. 1B, TSA also suppressed DNA synthesis, with 90–100% inhibition at TSA concentrations of 100 nM in these cells. This suggests that butyrate-induced suppression of DNA synthesis in these human mammary cells may involve histone hyperacetylation, as is shown by Western immunoblot with an anti-acetyl-lysine antibody (Fig. 2). The CL 24 h after treatment with NaB showed an increase of acetylated proteins in a dose-dependent manner, as indicated by the appearance of 11 and 16 kDa bands, which were identified as H4 and H3 histones respectively by Western immunoblot with specific antibodies (data not shown). Histone hyperacetylation was similarly demonstrated by treatment with TSA (Fig. 2). Interestingly, only the 11 kDa band was seen at concentrations over 100 nM.

Effects of NaB on reducing cell number and the induction of apoptosis in human mammary epithelial cells

As NaB inhibits DNA synthesis almost completely by 24 h treatment, cell viability over 4 days after NaB treatment in Hs578T cells was then studied. The MTS assay was used, as described in Materials and Methods, as a marker of relative viable cell number. A progressive reduction in cell number by MTS assay was observed from day 2 onwards using 10 mM NaB, and from day 3 onwards after 5 mM NaB treatment (Fig. 3). In parallel wells, when cell numbers were counted after trypsinizing by direct visualization using a hemacytometer, the attached cell numbers were reduced over the same time course and concentrations of NaB as was detected in the MTS assay above (data not shown). Using trypan blue exclusion during hemacytometer counting, when counted at the same time point, the same number of attached cells were shown to take up trypan blue in the NaB-treated wells compared with the control wells, throughout the full 4 days of the study (data not shown). This trypan blue staining pattern indicates that cell plasma membrane integrity was maintained in the attached cells after NaB treatment compared with the control.

As a reduction in viable cell number by NaB was occurring over time, the possibility that apoptosis was being induced by NaB in the mammary epithelial cells was then addressed. Two independent methods of analysis were used to detect apoptosis: first, nuclear enzyme cleavage, and secondly, DNA fragmentation. The nuclear enzyme PARP is proteolytically cleaved during apoptosis *in vitro* in many cell types, including breast cancer cells (Kaufmann *et al.* 1993). Figure 4A shows Western immunoblots with an anti-PARP antibody after treatment of Hs578T and MCF-7 cells with NaB followed by

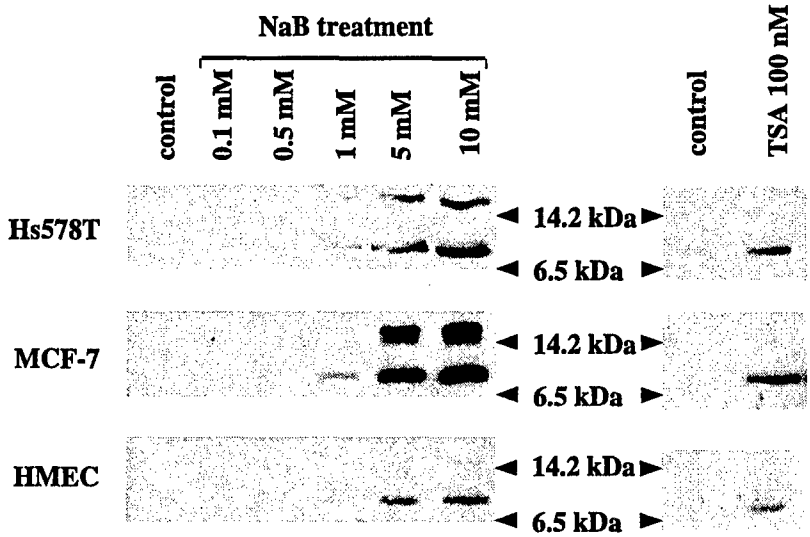

Figure 2 Effect of NaB on protein acetylation. Serum-starved cells were treated for 24 h with various concentrations of NaB as indicated. CL harvested from duplicate wells within each experiment were pooled, and 20 μg protein per lane were loaded onto 15% SDS-PAGE under reducing conditions. Gels were immunoblotted with an anti-acetyl-lysine antibody as described in Materials and Methods. The immunoblots of CL treated with 100 nM TSA are shown on the right. Molecular mass markers are also shown. The results are representative of two independent experiments.

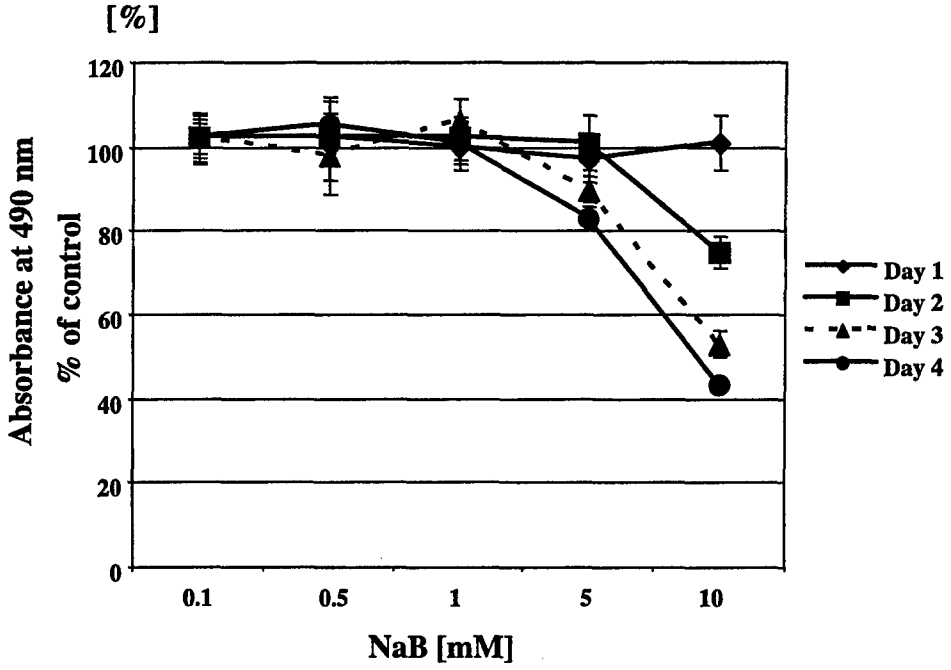

Figure 3 Growth inhibition by NaB. Hs578T cells were seeded into 96-well plates, then serum-starved cells were treated with various concentrations of NaB as indicated. On subsequent days, cell proliferation was measured using the MTS assay. A dose–response effect with added NaB is seen over 4 days. Results are expressed in absorbance readings at 490 nm as percent of the untreated controls ± S.E. (n=16).

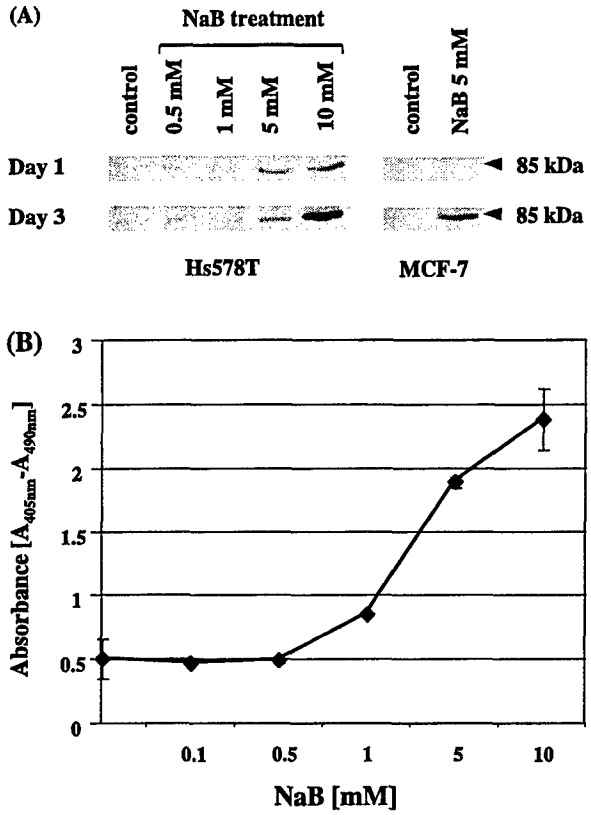

Figure 4 Effect of NaB on apoptosis. (A) Immunoblot analysis of PARP in Hs578T and MCF-7 CL obtained during treatment with NaB (day 1 and day 3). The 85 kDa fragment characteristic of apoptosis is shown. The data shown are representative of two independent experiments. (B) Induction of apoptosis in Hs578T cells treated with increasing doses (0–10 mM) of NaB for 72 h. Cytoplasmic extracts were prepared from attached cells, and apoptotic cell death was quantitated by ELISA measuring cytoplasmic histone-bound DNA complexes characteristic of apoptosis, as described in Materials and Methods. Results are expressed as mean absorbance ± S.D. of two independent experiments performed in duplicate ($n=4$).

analysis of CL. The ~85 kDa carboxy-terminal fragment of PARP detected by Western immunoblotting is indicative of apoptosis occurring in the lysates sampled (Kaufmann *et al.* 1993, Lazebnik *et al.* 1994). In Hs578T cells, some induction of the fragment was already observed by day 1 at concentrations of 5 mM NaB and above, and was more marked in the day 3 lysates, particularly after 10 mM NaB. Detectable increases in the PARP fragment were also seen in the day 3 CL of MCF-7 cells (Fig. 4A).

To verify and more accurately quantitate the apoptosis induced by NaB, an ELISA kit that detects histone-associated DNA fragments (mono- and oligonucleosomes) in the cytoplasmic fraction of CL was used, as described in Materials and Methods. In the Hs578T cytoplasmic extracts from attached cells studied at 3 days post-treatment, NaB induced apoptosis in a dose-dependent manner (Fig. 4B). This sensitive assay demonstrated apoptotic effects initially commencing at 1 mM NaB. Taken together, the two methods of measuring apoptosis show that NaB induces apoptosis in the cells studied, in a more delayed time course compared with the earlier effects on [^{3}H]thymidine incorporation. The apoptosis induced by NaB would be expected to reduce the viable cell number, which was observed, as described earlier.

NaB upregulates expression of $p21^{Waf1/Cip1}$ mRNA and protein levels in human mammary epithelial cells

As the major mechanism for butyrate-induced growth inhibition in various cell systems is known to be through upregulation of cdk inhibitors, in particular $p21^{Waf1/Cip1}$, the induction of $p21^{Waf1/Cip1}$ in mammary epithelial cells was next investigated. Figure 5A is a Northern blot of $p21^{Waf1/Cip1}$ from Hs578T, MCF-7 and HMEC cells treated with or without NaB. $p21^{Waf1/Cip1}$ mRNA expression was upregulated in all three cell lines, and was most marked in Hs578T cells. As shown in Fig. 5B, an upregulation of $p21^{Waf1/Cip1}$ protein levels occurred in these cells, with the greatest increase in $p21^{Waf1/Cip1}$ observed in Hs578T cells, which parallels the mRNA data. As the degree of induction was different between Hs578T cells and the other two cell lines, the NaB effect on cdk inhibitors $p27^{Kip1}$ and $p16^{INK4}$ was further investigated. A distinct upregulation of $p27^{Kip1}$ by NaB treatment (a 2·5-fold increase at 5 mM treatment) was reproducibly seen in HMEC cells, but not in the cancerous cell lines (Fig. 5B). We did not detect $p16^{INK4}$ in Hs578T and MCF-7 cells, and only a slight induction of this protein was seen in HMEC cells. Taken together, these data suggest that differential cdk inhibitors are induced by NaB treatment, in a cell-type-dependent manner.

Butyrate upregulates IGFBP-3 mRNA and protein levels in cancerous, but not in non-cancerous mammary cells

To investigate any correlation between the effect of NaB and the regulation of IGFBP system, we first examined IGFBP-3, a known growth suppressor in human mammary cells. Northern blotting was firstly performed to measure steady-state mRNA levels. Figure 6A shows the time-course effect of NaB treatment on steady-state levels of IGFBP-3 mRNA in Hs578T cells. NaB induced the expression of IGFBP-3 mRNA in a time-dependent manner, with increases first detectable at 6 h after treatment, and with a 2·5-fold increase after treating cells with 5 mM NaB for 24 h, whereas in the non-cancerous HMEC cells, only a slight induction (<1·2-fold) was observed (Fig. 6B). In MCF-7 cells, IGFBP-3 mRNA was not detected in these analyses.

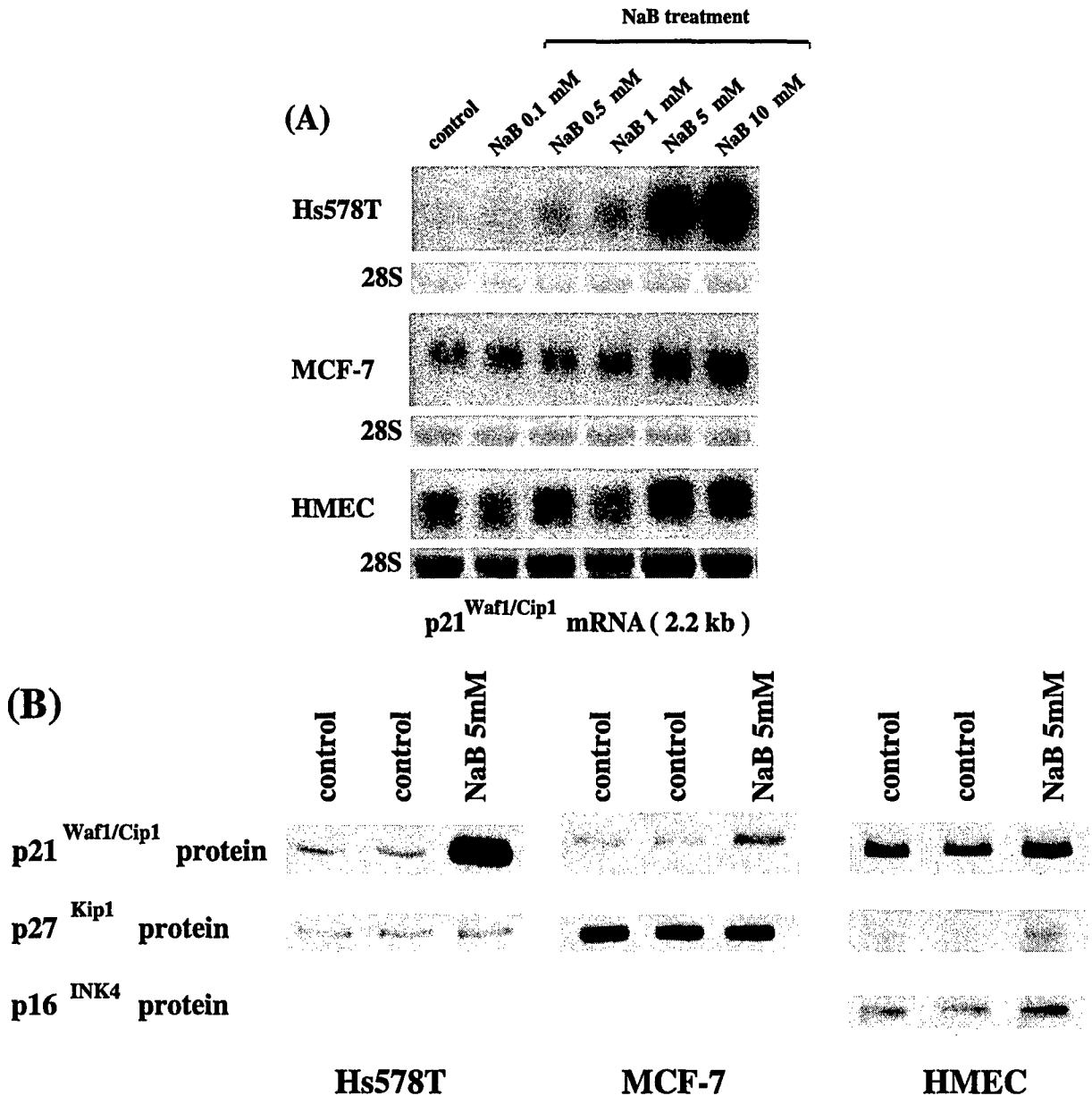

Figure 5 Effect of NaB on expression of $p21^{Waf1/Cip1}$ mRNA (A), and protein of $p21^{Waf1/Cip1}$, $p27^{Kip1}$ and $p16^{INK4}$ (B). (A) Representative Northern blots. Serum-starved cells were treated for 18 h with various concentrations of NaB as indicated. Total RNA was harvested, and 5 μg per lane were electrophoresed. The membrane was probed with labeled cDNA fragments for $p21^{Waf1/Cip1}$. The 28S rRNA is presented as an indicator of loading. The data shown are representative of at least three separate experiments. (B) Representative Western immunoblots. Twenty micrograms total protein from whole CL obtained at 24 h post-treatment per lane were loaded onto 15% SDS-PAGE under reducing conditions, and immunoblotted with anti-$p21^{Waf1/Cip1}$, anti-$p27^{Kip1}$ and anti-$p16^{INK4}$, as indicated in Materials and Methods. Two sets of untreated controls were derived from different wells in the same culture plates. The data shown represent two separate experiments. $p16^{INK4}$ was only detectable in the CL of HMEC cells.

The CM were then examined for changes in IGFBP-3 protein levels after NaB treatment. In order to ascertain a suitable time point to collect CM samples, the time-course induction of media IGFBP-3 protein in Hs578T cells was studied by Western ligand blot analysis, using ^{125}I-labeled IGF-I as the ligand, as described in Materials and Methods. The IGFBP-3 level in the CM was detectably increased at 24 h, even after 1 mM NaB, was further increased at 48 h,

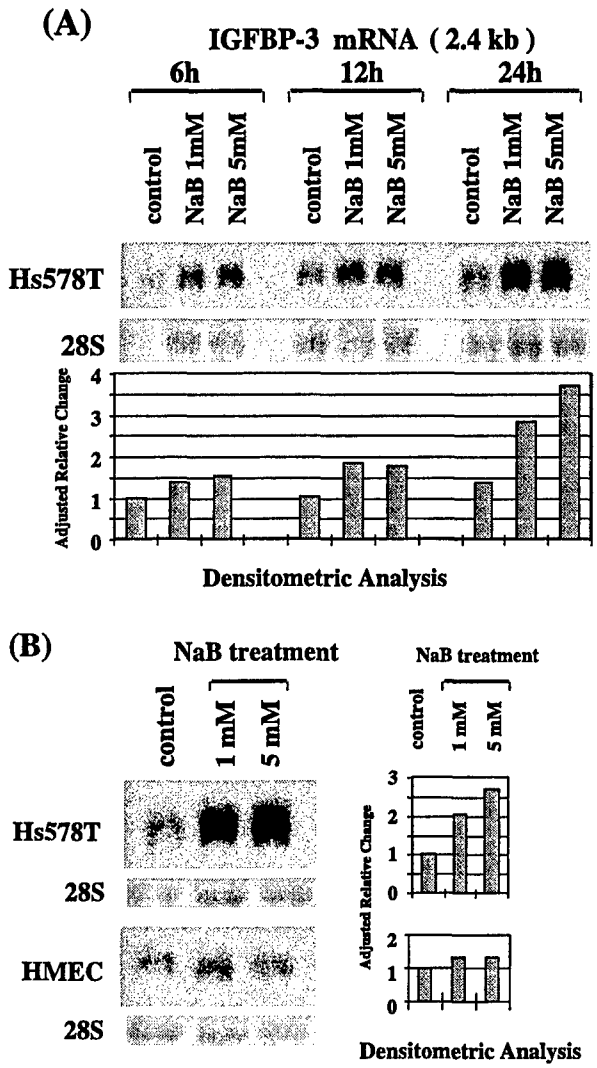

Figure 6 Northern blot analysis of the effect of NaB on the expression of IGFBP-3 mRNA. Total RNA was harvested, and 5 μg per lane were electrophoresed. The membrane was subsequently probed with labeled cDNA fragments of IGFBP-3. (A) Time-course expression of IGFBP-3 mRNA in Hs578T cells. Serum-starved cells were treated for 6, 12 and 24 h, with or without NaB as indicated. (B) Representative Northern blots for IGFBP-3 mRNA expression at 18 h (HMEC) and 24 h (Hs578T) post-treatment. 28S rRNA methylene blue membrane staining is presented as an indicator of equal loading. Densitometric analysis adjusted for 18S and 28S rRNA is also shown. Each result represents at least three independent experiments. In MCF-7 cells, IGFBP-3 mRNA was not detected in 10 μg total RNA.

and peaked at 72 h following NaB treatment (Fig. 7A). Subsequently, CM at 72 h post-treatment were analyzed in further studies. As shown in Fig. 7B, various IGFBPs could be detected by the IGF ligand blot. The identity of these IGFBPs was confirmed by Western immunoblots using IGFBP-3, -2 and -5 specific antibodies, showing the 42–46 kDa doublet bands to be IGFBP-3, the broad 29–36 kDa bands to contain IGFBP-2 and -5, and the 24 kDa band to be IGFBP-4 (data not shown). In HMEC cells, the Western ligand blot did not reveal an IGFBP-5 band, whereas the Western immunoblot with IGFBP-5 antibody revealed a low intensity band of the predicted molecular mass for IGFBP-5 (data not shown) (Adamo *et al.* 1992, Sheikh *et al.* 1992). IGFBP-3 protein levels were upregulated in both Hs578T (2·1-fold over the control) and MCF-7 (12·6-fold over the control) cells, each after 5 mM NaB treatment (Fig. 7B). Further Western immunoblotting analyses demonstrated no detected IGFBP-3 fragments in all samples tested in these cells (data not shown). As the basal level of IGFBP-3 in MCF-7 cells was nearly undetectable, the induction of IGFBP-3 protein by NaB was more conspicuous in this cell line. In contrast, only slight upregulation of IGFBP-3 (<1·5-fold) was observed in HMEC cells, mirroring the mRNA data (shown earlier in Fig. 6B). Levels of IGFBP-2/-5 and -4 showed no significant change up to 10 mM NaB treatment, after accounting for effects of NaB on cell number (not shown). The effect of TSA treatment on IGFBP-3 protein levels by Western ligand blot and immunoblot was also studied. TSA treatment of both Hs578T and MCF-7 cells caused a dose-dependent increase in IGFBP-3 protein levels (not shown), suggesting that NaB-induced upregulation of IGFBP-3 is, at least in part, through histone hyperacetylation. This effect was not seen in the HMEC cells (data not shown).

NaB upregulates IGFBP-rP2 mRNA and protein expression in both cancerous and non-cancerous mammary cells

The induction of the low affinity IGF binders, especially IGFBP-rP2, was then investigated, as this protein also has recently been shown to have a growth suppressive effect in human mammary cells (Hishikawa *et al.* 1999). The effect of NaB treatment on IGFBP-rP2 mRNA expression was potent, particularly in Hs578T cells, where effects occurred with 0·5 mM NaB. As seen in Fig. 8A, a 10-fold induction of IGFBP-rP2 by 5 mM NaB treatment was observed in Hs578T cells, whereas a maximal 2- to 3-fold induction occurred in HMEC cells. IGFBP-rP2 mRNA was not detected in MCF-7 cells.

Western immunoblot analysis against IGFBP-rP2 and -rP1 was then performed. As shown in Fig. 8B, NaB highly upregulated IGFBP-rP2 protein levels in all three cell lines in a dose-dependent manner (>10-fold at 10 mM NaB over the control in all three cell lines). Increases in media IGFBP-rP2 were initially detectable within 24 h, even after only 1 mM NaB (data not shown). In contrast to the effects on IGFBP-rP2, the IGFBP-rP1 band intensity was not increased by NaB treatment. The apparent reduction in IGFBP-rP1 by NaB treatment

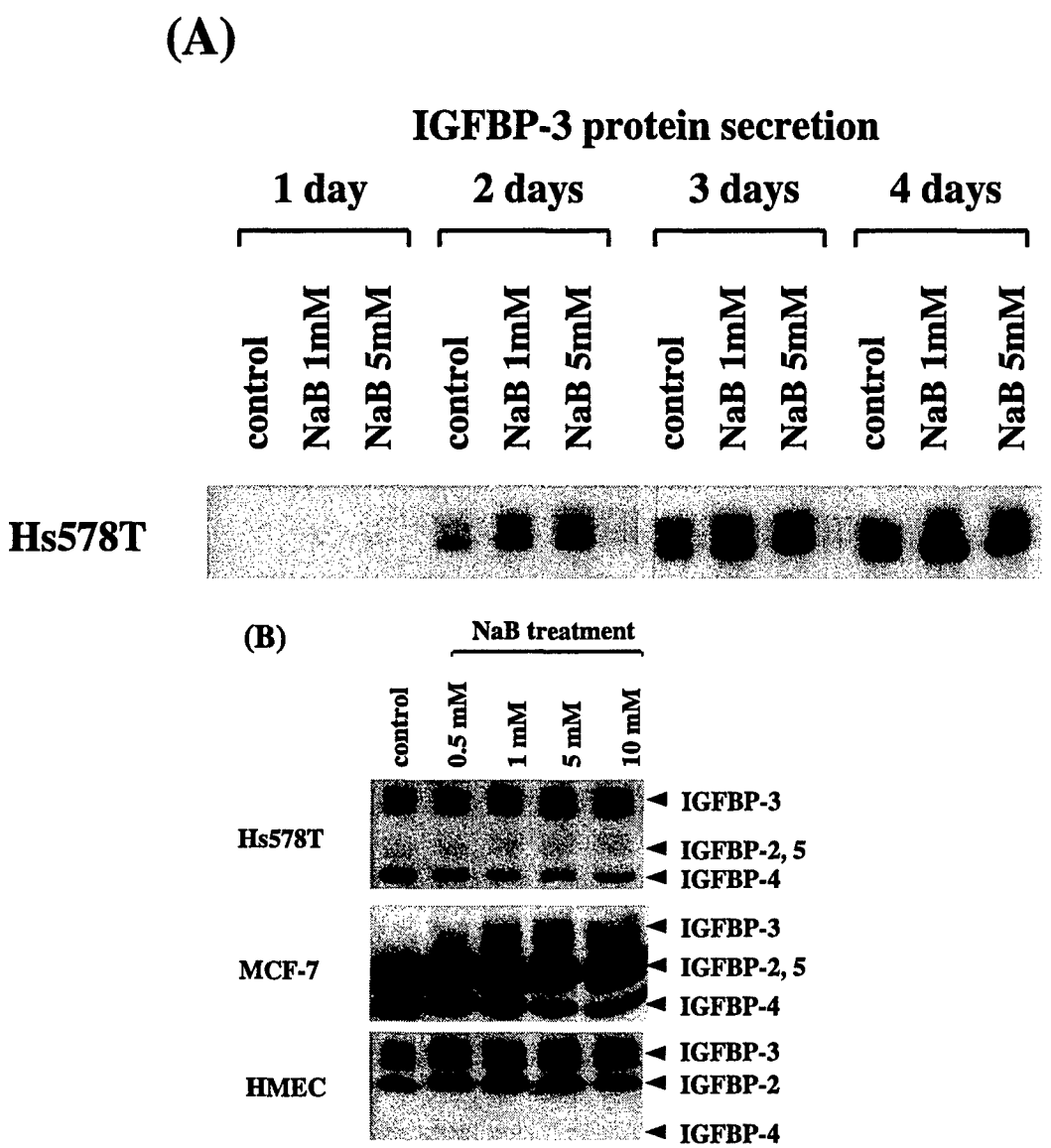

Figure 7 Effect of NaB on IGFBP production in Hs578T, MCF-7 and HMEC cells analyzed by Western ligand blotting. Serum-starved cells were treated with various concentrations of NaB. CM harvested from duplicate wells within each experiment were pooled, size-fractionated using 12% SDS-PAGE under non-reducing conditions, electroblotted onto nitrocellulose membranes, and treated with ^{125}I-labeled IGF-I, as indicated in Materials and Methods. (A) Time-course expression of IGFBP-3 protein in Hs578T cells. Serum-starved cells were treated with or without NaB as indicated and Western ligand blot was performed over 4 days. (B) Representative Western ligand blots using 72 h CM in Hs578T, MCF-7 and HMEC cells. The data shown were derived from at least three independent experiments.

compared with control, especially in Hs578T CM, was 52% on average using densitometric analysis at day 3 after 10 mM NaB. This reduction in IGFBP-rP1 could be fully accounted for by considering the effects of NaB on cell number, as shown earlier in Fig. 3, where 40–50% of the cells are non-viable by this time of NaB treatment compared with control. IGFBP-rP1 was not detected in MCF-7 cells. These results show that IGFBP-rP2 mRNA and protein are specifically induced by NaB in both cancerous and non-cancerous breast epithelial cells.

Discussion

In this study, NaB effects in the human mammary cell system including cancerous and non-cancerous cells, was

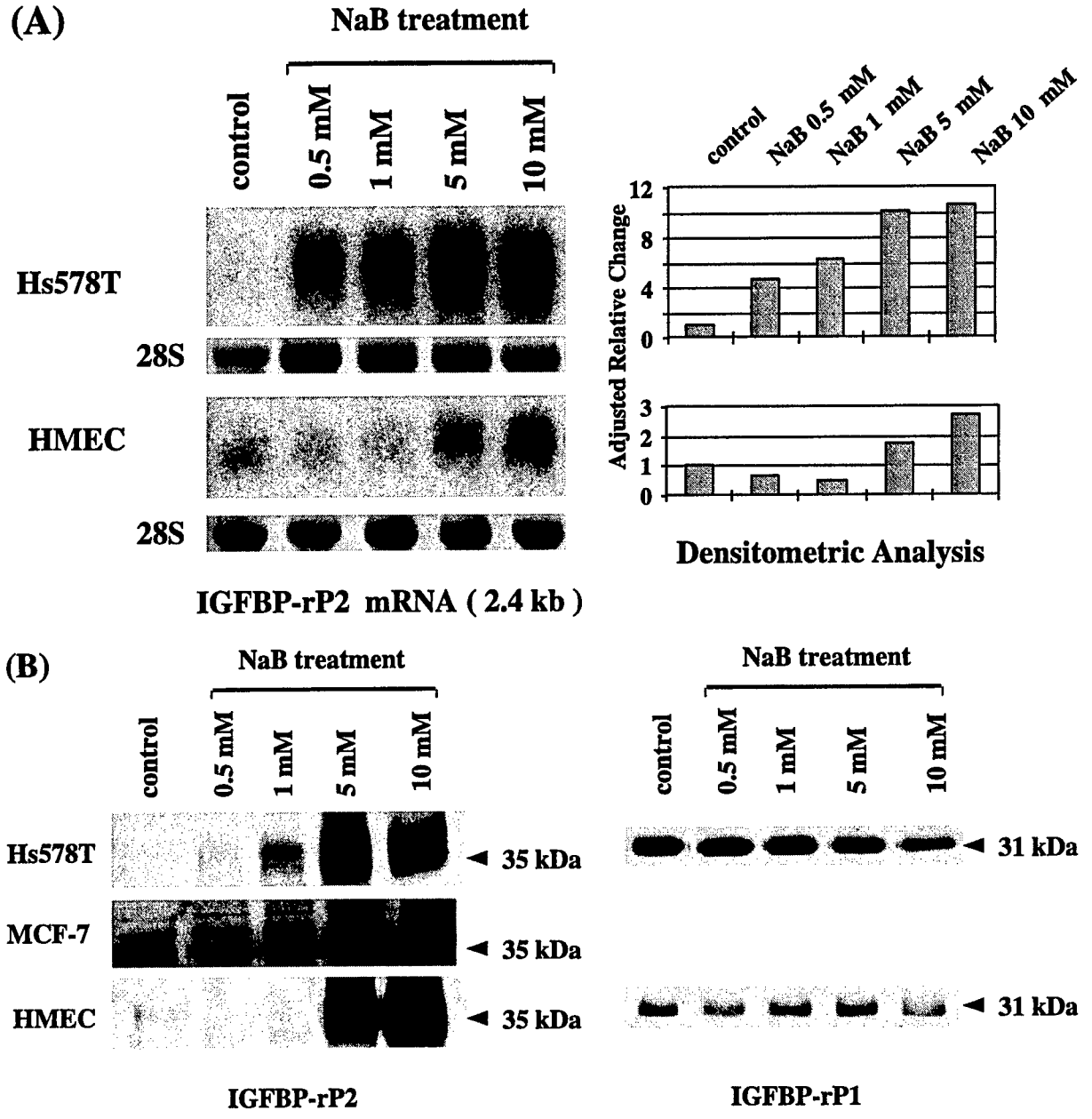

Figure 8 Effect of NaB on (A) IGFBP-rP2 mRNA expression, and (B) IGFBP-rP2 and -rP1 protein expression in Hs578T, MCF-7 and HMEC cells. (A) Representative Northern blots. Total RNA was harvested at 18 h post-treatment, and 5 μg per lane were electrophoresed. The membrane was subsequently probed with labeled cDNA fragments of IGFBP-rP2. 28S rRNA methylene blue membrane staining is presented as an indicator of equal loading. Densitometric analysis adjusted for 18S and 28S rRNA is also shown. Each result represents two independent experiments. In MCF-7 cells, IGFBP-rP2 mRNA was not detected in 10 μg total RNA. (B) Representative Western immunoblot analysis. Serum-starved cells were treated with various concentrations of NaB for 72 h. CM harvested from duplicate wells within each experiment were pooled, size-fractionated using 12% (for IGFBP-rP2) or 15% (for IGFBP-rP1) SDS-PAGE under non-reducing conditions, electroblotted onto nitrocellulose membranes, and treated with appropriate antibodies, as indicated in Materials and Methods. IGFBP-rP1 was not detected in the CM of MCF-7 cells.

investigated, in order to obtain a greater understanding of the cellular mechanism of action of NaB in this cell type. NaB was found to cause an initial inhibition in new DNA synthesis, followed by apoptotic changes, and a reduction in viable cell number. Subsequently, the cdk inhibitors studied showed some cellular specificity in their

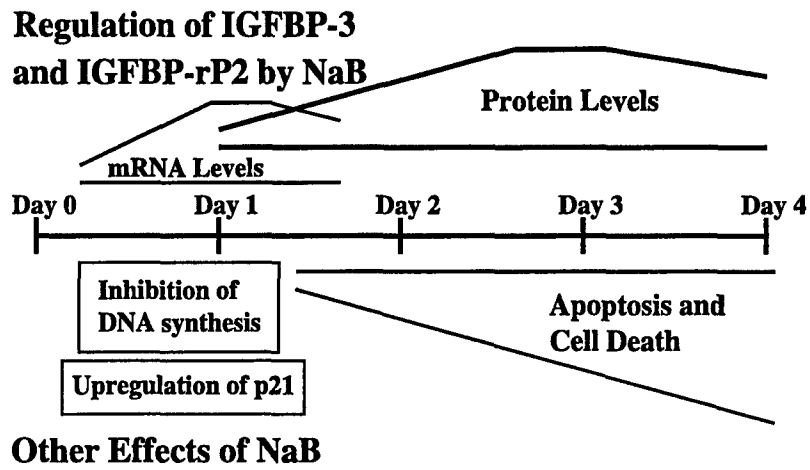

Figure 9 Schematic diagram showing a summary of sequential effects of NaB in Hs578T cells observed in this study. The upregulation of IGFBP-3 and IGFBP-rP2 is shown above the time line and other effects of NaB including cell growth inhibition and cell death are shown below. For further description refer to the discussion in the text.

upregulation by NaB. IGFBP superfamily members known to induce growth inhibition and apoptosis in breast epithelial cells were also upregulated by NaB.

A schematic summary of our observations in Hs578T cells is shown in Fig. 9. We first studied the general effects of NaB on cell growth regulation. Butyrate induces diverse and reversible biological effects on cell differentiation, apoptosis and cell growth *in vitro* (Pouillart 1998). In colonic epithelial cells, butyrate is known to exert paradoxical effects, with induction of proliferation in normal cells and growth inhibition in neoplastic phenotypes (Hassig *et al.* 1997, Archer & Hodin 1999). In the mammary system studied here, butyrate inhibits DNA synthesis in both normal and cancerous cells as measured by [^{3}H]thymidine incorporation at 24 h after treatment. Also, as shown in Fig. 9, after 24 h of NaB treatment at concentrations over 1 mM, cell numbers became reduced in a dose- and time-dependent manner. This reduction in cell number was explained, at least in part, by NaB-induced apoptosis. The observed induction of apoptosis is consistent with previous reports of NaB-induced apoptosis in other cell systems (Hague *et al.* 1993, Carducci *et al.* 1996, Coradini *et al.* 1997). In summary, NaB was found to induce both inhibition of DNA synthesis and programmed cell death, in Hs578T cells.

It is known that butyrate induces a variety of changes within the nucleus (Siavoshian *et al.* 1997, Schwartz *et al.* 1998), including histone hyperacetylation, especially of H3 and H4 (Archer & Hodin 1999), and DNA methylation (de Haan *et al.* 1986). Previous studies indicate that the effect of butyrate and other histone deacetylase inhibitors on cells closely corresponds to the effects of $p21^{Waf1/Cip1}$ expression in the regulation of G1 (Hunter & Pines 1994), S (Ogryzko *et al.* 1997) and G2 (Coradini *et al.* 1997, Lallemand *et al.* 1999) phases of the cell cycle (Hassig *et al.* 1997). The major mechanism for butyrate-induced cell cycle arrest is reported to be through upregulation of $p21^{Waf1/Cip1}$ in various cell systems, including hepatocellular carcinoma cells (Yamamoto *et al.* 1998), colon cancer cells (Nakano *et al.* 1997, Siavoshian *et al.* 1997, Archer *et al.* 1998, Litvak *et al.* 1998), prostate cancer cells (Huang *et al.* 1999) and breast cancer cells (Lallemand *et al.* 1999). In contrast, Vaziri *et al.* (1998) demonstrated $p21^{Waf1/Cip1}$-independent G1 cell cycle arrest by butyrate in 3T3 fibroblasts. In our present studies, the prominent induction of $p21^{Waf1/Cip1}$ was observed in estrogen-non-responsive Hs578T cancer cells, whereas modest induction was observed in estrogen-responsive MCF-7 cancer cells and non-cancerous HMEC cells. Interestingly, butyrate upregulated $p27^{Kip1}$ expression only in HMEC cells. The $p16^{INK4}$ protein was detected only in HMEC cells and no further regulation was observed after butyrate treatment. Taken together, these data imply that the biological function of butyrate is mediated through more than one mechanism, even in butyrate-induced cell cycle arrest, suggesting that butyrate possesses multifunctional mechanisms of action.

This is the first demonstration that butyrate upregulates members of the IGFBP superfamily in human mammary cells. One previous report showed that only IGFBP-2 was upregulated by butyrate in colon cancer cells (Nishimura *et al.* 1998). In contrast, our studies demonstrate that among the six IGFBPs and IGFBP-rP-1 and -2, only IGFBP-3 and IGFBP-rP2 are upregulated by butyrate in cancerous and non-cancerous mammary epithelial cells. Recent evidence has suggested that, in addition to modulating the access of IGFs to their receptors, IGFBP-3 has the ability to suppress proliferation in various cell systems, including

human breast cancer cells, working through IGF-independent mechanisms (Valentinis *et al.* 1995, Oh 1998). Further studies have demonstrated that IGFBP-3 directly induces apoptosis through an IGF-independent pathway in PC-3 human prostatic adenocarcinoma cells (Rajah *et al.* 1997) as well as in other cell systems (Nickerson *et al.* 1997). We, therefore, hypothesized that IGFBP-3 may be a major downstream effector of growth inhibitory and apoptosis-inducing agents.

Indeed, NaB treatment significantly upregulated IGFBP-3 steady-state mRNA and protein levels in a time- and dose-dependent manner in Hs578T and MCF-7 human breast cancer cells, while levels of IGFBP-2 and -4 were unaffected. As summarized in Fig. 9, we observed that the mRNA induction had already started at 6 h after treatment and peaked by 24 h after treatment, while the presence of the protein in CM was barely detectable at the 24 h time point and gradually increased up to day 3. Notably, both the mRNA and protein induction by NaB were detectable earlier than the reduction in cell number and apoptosis, consistent with a specific regulation of these IGFBP superfamily members by NaB rather than effects on these IGFBPs occurring secondary to cell death. In contrast to effects seen in these cancer cell lines, the NaB regulation of IGFBP-3 in normal human mammary epithelial cells was less marked. Additionally, treatment with TSA gave similar results, indicating that histone hyperacetylation may be involved. The differential regulation of IGFBP-3 by NaB in cancerous versus non-cancerous cells may point to an important mechanism for growth inhibition by IGFBP-3 in cancer.

It has been demonstrated that TGF-β, which is a potent growth suppressing factor in human breast cancer cells (Zugmaier *et al.* 1989, Oh *et al.* 1995), induces expression of IGFBP-rP2 mRNA and protein levels (Yang *et al.* 1998). In addition, recent studies have demonstrated that IGFBP-rP2 has a direct apoptotic effect in MCF-7 cells (Hishikawa *et al.* 1999). Our present data show that IGFBP-rP2 was significantly upregulated by NaB treatment in a time- and dose-dependent manner in both cancerous and non-cancerous human mammary epithelial cell lines, suggesting that IGFBP-rP2 may also play a role in the bioactivity of butyrate on cells. In Hs578T cells, the induction of IGFBP-rP2 mRNA was already marked at 0·5 mM, while the protein levels were significantly increased at 5 mM. One potential explanation for this dose discrepancy is that some post-transcriptional modification by NaB of IGFBP-rP2 may also be occurring.

On the basis of this work, it can be speculated that the IGFBP superfamily members, IGFBP-3 and IGFBP-rP2, participate in butyrate-induced sequential cell growth inhibition, particularly in the later event of apoptosis. Detailed studies involving regulation of IGFBP-3 and IGFBP-rP2 bioactivity following butyrate treatment in breast epithelial cells are now required to formally address this issue. It is hoped that exploration of butyrate-induced biological effects subsequent to the cell cycle arrest in this cell system and the investigation of the interaction between butyrate and the IGF axis will lead to a more complete understanding of the complex mechanisms of cell growth control, and to the development of better therapeutic reagents.

Acknowledgements

This research was supported by NIH grants R01 DK51513 (R G R) and CA58110 (R G R), and by US Army grants DAMD17-00-1-0042 (R G R), DAMD17–96–1–6204 (Y O) and DAMD17–96–1–7204 (Y O).

References

Adamo ML, Shao ZM, Lanau F, Chen JC, Clemmons DR, Roberts CT Jr, LeRoith D & Fontana JA 1992 Insulin-like growth factor-I (IGF-I) and retinoic acid modulation of IGF-binding proteins (IGFBPs): IGFBP-2, -3, and -4 gene expression and protein secretion in a breast cancer cell line. *Endocrinology* **131** 1858–1866.

Archer SY & Hodin RA 1999 Histone acetylation and cancer. *Current Opinion in Genetics and Development* **9** 171–174.

Archer SY, Meng S, Shei A & Hodin RA 1998 $p21^{WAF1}$ is required for butyrate-mediated growth inhibition of human colon cancer cells. *PNAS* **95** 6791–6796.

Baxter RC, Binoux MA, Clemmons DR, Conover CA, Drop SL, Holly JM, Mohan S, Oh Y & Rosenfeld RG 1998 Recommendations for nomenclature of the insulin-like growth factor binding protein superfamily. *Journal of Clinical Endocrinology and Metabolism* **83** 3213.

Buckbinder L, Talbott R, Velasco-Miguel S, Takenaka I, Faha B, Seizinger BR & Kley N 1995 Induction of the growth inhibitor IGF-binding protein 3 by p53. *Nature* **377** 646–649.

Burger AM, Zhang X, Li H, Ostrowski JL, Beatty B, Venanzoni M, Papas T & Seth A 1998 Down-regulation of T1A12/mac25, a novel insulin-like growth factor binding protein related gene, is associated with disease progression in breast carcinomas. *Oncogene* **16** 2459–2467.

Carducci MA, Nelson JB, Chan-Tack KM, Ayyagari SR, Sweatt WH, Campbell PA, Nelson WG & Simons JW 1996 Phenylbutyrate induces apoptosis in human prostate cancer and is more potent than phenylacetate. *Clinical Cancer Research* **2** 379–387.

Colston KW, Perks CM, Xie SP & Holly JM 1998 Growth inhibition of both MCF-7 and Hs578T human breast cancer cell lines by vitamin D analogues is associated with increased expression of insulin-like growth factor binding protein-3. *Journal of Molecular Endocrinology* **20** 157–162.

Coradini D, Biffi A, Costa A, Pellizzaro C, Pirronello E & Di Fronzo G 1997 Effect of sodium butyrate on human breast cancer cell lines. *Cell Proliferation* **30** 149–159.

Gleave ME, Sato N, Sadar M, Yago V, Bruchovsky N & Sullivan L 1998 Butyrate analogue, isobutyramide, inhibits tumor growth and time to androgen-independent progression in the human prostate LNCaP tumor model. *Journal of Cellular Biochemistry* **69** 271–281.

Gucev ZS, Oh Y, Kelley KM & Rosenfeld RG 1996 Insulin-like growth factor binding protein 3 mediates retinoic acid- and transforming growth factor β2-induced growth inhibition in human breast cancer cells. *Cancer Research* **56** 1545–1550.

de Haan JB, Gevers W & Parker MI 1986 Effects of sodium butyrate on the synthesis and methylation of DNA in normal cells and their transformed counterparts. *Cancer Research* **46** 713–716.

Hague A, Manning AM, Hanlon KA, Huschtscha LI, Hart D & Paraskeva C 1993 Sodium butyrate induces apoptosis in human colonic tumour cell lines in a p53-independent pathway: implications for the possible role of dietary fibre in the prevention of large-bowel cancer. *International Journal of Cancer* **55** 498–505.

Hague A, Díaz GD, Hicks DJ, Krajewski S, Reed JC & Paraskeva C 1997 bcl-2 and bak may play a pivotal role in sodium butyrate-induced apoptosis in colonic epithelial cells; however overexpression of bcl-2 does not protect against bak-mediated apoptosis. *International Journal of Cancer* **72** 898–905.

Hassig CA, Tong JK & Schreiber SL 1997 Fiber-derived butyrate and the prevention of colon cancer. *Chemistry and Biology* **4** 783–789.

Hishikawa K, Oemar BS, Tanner FC, Nakaki T, Lüscher TF & Fujii T 1999 Connective tissue growth factor induces apoptosis in human breast cancer cell line MCF-7. *Journal of Biological Chemistry* **274** 37461–37466.

Huang H, Reed CP, Zhang JS, Shridhar V, Wang L & Smith DI 1999 Carboxypeptidase A3 (CPA3): a novel gene highly induced by histone deacetylase inhibitors during differentiation of prostate epithelial cancer cells. *Cancer Research* **59** 2981–2988.

Hunter T & Pines J 1994 Cyclins and cancer. II: cyclin D and CDK inhibitors come of age. *Cell* **79** 573–582.

Huynh H, Yang X & Pollak M 1996 Estradiol and antiestrogens regulate a growth inhibitory insulin-like growth factor binding protein 3 autocrine loop in human breast cancer cells. *Journal of Biological Chemistry* **271** 1016–1021.

Hwa V, Oh Y & Rosenfeld RG 1999 Insulin-like growth factor binding proteins: a proposed superfamily. *Acta Paediatrica. Supplement* **428** 37–45.

Kaufmann SH, Desnoyers S, Ottaviano Y, Davidson NE & Poirier GG 1993 Specific proteolytic cleavage of poly (ADP-ribose) polymerase: an early marker of chemotherapy-induced apoptosis. *Cancer Research* **53** 3976–3985.

Kelley KM, Oh Y, Gargosky SE, Gucev Z, Matsumoto T, Hwa V, Ng L, Simpson DM & Rosenfeld RG 1996 Insulin-like growth factor-binding proteins and their regulatory dynamics. *International Journal of Biochemistry and Cell Biology* **28** 619–637.

Knabbe C, Lippman ME, Wakefield LM, Flanders KC, Kasid A, Derynck R & Dickson RB 1987 Evidence that transforming growth factor-β is a hormonally regulated negative growth factor in human breast cancer cells. *Cell* **48** 417–428.

Lallemand F, Courilleau D, Sabbah M, Redeuilh G & Mester J 1996 Direct inhibition of the expression of cyclin D1 gene by sodium butyrate. *Biochemical and Biophysical Research Communications* **229** 163–169.

Lallemand F, Courilleau D, Buquet-Fagot C, Atfi A, Montagne MN & Mester J 1999 Sodium butyrate induces G2 arrest in the human breast cancer cells MDA-MB-231 and renders them competent for DNA rereplication. *Experimental Cell Research* **247** 432–440.

Lazebnik YA, Kaufmann SH, Desnoyers S, Poirier GG & Earnshaw WC 1994 Cleavage of poly (ADP-ribose) polymerase by a proteinase with properties like ICE. *Nature* **371** 346–347.

Litvak DA, Evers M, Hwang KO, Hellmich MR, Ko TC & Townsend CM Jr 1998 Butyrate-induced differentiation of Caco-2 cells is associated with apoptosis and early induction of $p21^{Waf1/Cip1}$ and $p27^{Kip1}$. *Surgery* **124** 161–170.

Macaulay VM 1992 Insulin-like growth factors and cancer. *British Journal of Cancer* **65** 311–320.

Mandal M & Kumar R 1996 Bcl-2 expression regulates sodium butyrate-induced apoptosis in human MCF-7 breast cancer cells. *Cell Growth and Differentiation* **7** 311–318.

Nakano K, Mizuno T, Sowa Y, Orita T, Yoshino T, Okuyama Y, Fujita T, Ohtani-Fujita N, Matsukawa Y, Tokino T, Yamagishi H, Oka T, Nomura H & Sakai T 1997 Butyrate activates the *WAF1/Cip1* gene promoter through Sp1 sites in a p53-negative human colon cancer cell line. *Journal of Biological Chemistry* **272** 22199–22206.

Nickerson T, Huynh H & Pollak M 1997 Insulin-like growth factor binding protein-3 induces apoptosis in MCF7 breast cancer cells. *Biochemical and Biophysical Research Communications* **237** 690–693.

Nishimura A, Fujimoto M, Oguchi S, Fusunyan RD, MacDermott RP & Sanderson IR 1998 Short-chain fatty acids regulate IGF-binding protein secretion by intestinal epithelial cells. *American Journal of Physiology* **275** E55–E63.

Ogryzko VV, Wong P & Howard BH 1997 WAF1 retards S-phase progression primarily by inhibition of cyclin-dependent kinases. *Molecular and Cellular Biology* **17** 4877–4882.

Oh Y 1998 IGF-independent regulation of breast cancer growth by IGF binding proteins. *Breast Cancer Research and Treatment* **47** 283–293.

Oh Y, Müller HL, Lamson G & Rosenfeld RG 1993 Insulin-like growth factor (IGF)- independent action of IGF-binding protein-3 in Hs578T human breast cancer cells. Cell surface binding and growth inhibition. *Journal of Biological Chemistry* **268** 14964–14971.

Oh Y, Müller HL, Ng L & Rosenfeld RG 1995 Transforming growth factor-β-induced cell growth inhibition in human breast cancer cells is mediated through insulin-like growth factor-binding protein-3 action. *Journal of Biological Chemistry* **270** 13589–13592.

Pouillart PR 1998 Role of butyric acid and its derivatives in the treatment of colorectal cancer and hemoglobinopathies. *Life Sciences* **63** 1739–1760.

Rajah R, Valentinis B & Cohen P 1997 Insulin-like growth factor (IGF)-binding protein-3 induces apoptosis and mediates the effects of transforming growth factor-β1 on programmed cell death through a p53- and IGF-independent mechanism. *Journal of Biological Chemistry* **272** 12181–12188.

Rajaram S, Baylink DJ & Mohan S 1997 Insulin-like growth factor-binding proteins in serum and other biological fluids: regulation and functions. *Endocrine Reviews* **18** 801–831.

Resnicoff M, Abraham D, Yutanawiboonchai W, Rotman HL, Kajstura J, Rubin R, Zoltick P & Baserga R 1995 The insulin-like growth factor I receptor protects tumor cells from apoptosis *in vivo*. *Cancer Research* **55** 2463–2469.

Rosenfeld RG, Lamson G, Pham H, Oh Y, Conover C, De Leon DD, Donovan SM, Ocrant I & Giudice L 1990 Insulin-like growth factor binding proteins. *Recent Progress in Hormone Research* **46** 99–159.

Rozen F, Zhang J & Pollak M 1998 Antiproliferative action of tumor necrosis factor-alpha on MCF-7 breast cancer cells is associated with increased insulin-like growth factor binding protein-3 accumulation. *International Journal of Oncology* **13** 865–869.

Schwartz B, Avivi-Green C & Polak-Charcon S 1998 Sodium butyrate induces retinoblastoma protein dephosphorylation, p16 expression and growth arrest of colon cancer cells. *Molecular and Cellular Biochemistry* **188** 21–30.

Sheikh MS, Shao ZM, Clemmons DR, LeRoith D, Roberts CT Jr & Fontana JA 1992 Identification of the insulin-like growth factor binding proteins 5 and 6 (IGFBP-5 and 6) in human breast cancer cells. *Biochemical and Biophysical Research Communications* **183** 1003–1010.

Siavoshian S, Blottiere HM, Cherbut C & Galmiche JP 1997 Butyrate stimulates cyclin D and p21 and inhibits cyclin-dependent kinase 2 expression in HT-29 colonic epithelial cells. *Biochemical and Biophysical Research Communications* **232** 169–172.

Staiano-Coico L, Khandke L, Krane JF, Sharif S, Gottlieb AB, Krueger JG, Heim L, Rigas B & Higgins PJ 1990 TGF-α and TGF-β expression during sodium-n-butyrate-induced differentiation of human keratinocytes: evidence for subpopulation-specific up-regulation of TGF-β mRNA in suprabasal cells. *Experimental Cell Research* **191** 286–291.

Valentinis B, Bhala A, DeAngelis T, Baserga R & Cohen P 1995 The human insulin-like growth factor (IGF) binding protein-3 inhibits the growth of fibroblasts with a targeted disruption of the IGF-I receptor gene. *Molecular Endocrinology* **9** 361–367.

Vaziri C, Stice L & Faller DV 1998 Butyrate-induced G1 arrest results from p21-independent disruption of retinoblastoma protein-mediated signals. *Cell Growth and Differentiation* **9** 465–474.

Velázquez OC, Lederer HM & Rombeau JL 1997 Butyrate and the colonocyte. Production, absorption, metabolism, and therapeutic implication. *Advances in Experimental Medicine and Biology* **427** 123–134.

Wilson EM, Oh Y & Rosenfeld RG 1997 Generation and characterization of IGFBP-7 antibody: identification of 31 kD IGFBP-7 in human biological fluids and Hs578T human breast cancer conditioned media. *Journal of Clinical Endocrinology and Metabolism* **82** 1301–1303.

Yamamoto H, Fujimoto J, Okamoto E, Furuyama J, Tamaoki T & Hashimoto-Tamaoki T 1998 Suppression of growth of hepatocellular carcinoma by sodium butyrate *in vitro* and *in vivo*. *International Journal of Cancer* **76** 897–902.

Yang DH, Kim HS, Wilson EM, Rosenfeld RG & Oh Y 1998 Identification of glycosylated 38-kDa connective tissue growth factor (IGFBP-related protein 2) and proteolytic fragments in human biological fluids, and up-regulation of IGFBP-rP2 expression by TGF-β in Hs578T human breast cancer cells. *Journal of Clinical Endocrinology and Metabolism* **83** 2593–2596.

Yoshida M, Kijima M, Akita M & Beppu T 1990 Potent and specific inhibition of mammalian histone deacetylase both *in vivo* and *in vitro* by trichostatin A. *Journal of Biological Chemistry* **265** 17174–17179.

Zugmaier G, Ennis BW, Deschauer B, Katz D, Knabbe C, Wilding G, Daly P, Lippman ME & Dickson RB 1989 Transforming growth factors type β1 and β2 are equipotent growth inhibitors of human breast cancer cell lines. *Journal of Cellular Physiology* **141** 353–361.

Received 21 November 2000
Accepted 8 December 2000

0013-7227/01/$03.00/0
Endocrinology

Vol. 142, No. 5
Printed in U.S.A.

Advanced Glycosylation End Products Up-Regulate Connective Tissue Growth Factor (Insulin-Like Growth Factor-Binding Protein-Related Protein 2) in Human Fibroblasts: A Potential Mechanism for Expansion of Extracellular Matrix in Diabetes Mellitus*

STEPHEN M. TWIGG, MICHELLE M. CHEN, ALISON H. JOLY, SANJAY D. CHAKRAPANI, JUNKO TSUBAKI, HO-SEONG KIM, YOUNGMAN OH, AND RON G. ROSENFELD

Department of Pediatrics, Oregon Health Sciences University (S.M.T., S.D.C., J.T., H.-S.K., Y.O., R.G.R.), Portland, Oregon 97201; and Cardiorenal Cell Biology, Scios, Inc. (M.M.C., A.H.J.), Sunnyvale, California 94086

ABSTRACT

Expansion of extracellular matrix with fibrosis occurs in many tissues as part of the end-organ complications in diabetes, and advanced glycosylation end products (AGE) are implicated as one causative factor in diabetic tissue fibrosis. Connective tissue growth factor (CTGF), also known as insulin-like growth factor-binding protein-related protein-2 (IGFBP-rP2), is a potent inducer of extracellular matrix synthesis and angiogenesis and is increased in tissues from rodent models of diabetes. The aim of this study was to determine whether CTGF is up-regulated by AGE *in vitro* and to explore the cellular mechanisms involved. AGE treatment of primary cultures of nonfetal human dermal fibroblasts in confluent monolayer increased CTGF steady state messenger RNA (mRNA) levels in a time- and dose-dependent manner. In contrast, mRNAs for other IGFBP superfamily members, IGFBP-rP1 (mac 25) and IGFBP-3, were not up-regulated by AGE. The effect of the AGE BSA reagent on CTGF mRNA was due to nonenzymatic glycosylation of BSA and, using neutralizing antisera to AGE and to the receptor for AGE, termed RAGE, was seen to be due to late products of nonenzymatic glycosylation and was partly mediated by RAGE. Reactive oxygen species as well as endogenous transforming growth factor-β1 could not explain the AGE effect on CTGF mRNA. AGE also increased CTGF protein in the conditioned medium and cell-associated CTGF. Thus, AGE up-regulates the profibrotic and proangiogenic protein CTGF (IGFBP-rP2), a finding that may have significance in the development of diabetic complications. (*Endocrinology* **142:** 1760–1769, 2001)

MULTIPLE MECHANISMS have been described by which chronic hyperglycemia might contribute to the pathological end-organ complications that occur in diabetes mellitus. These include direct effects of elevated glucose on cells, hyperosmolality, oxidant stress, and nonenzymatic glycosylation (1, 2). Advanced glycosylation end products (AGE) are biochemical end products of nonenzymatic glycosylation that are formed irreversibly (3). AGE is elevated in serum (4) and in many tissues in patients with diabetes (5), including skin (6), and has the ability to covalently cross-link and biochemically modify protein structure and affect protein function (7). Additionally, in recent years cell surface receptors for AGE have been identified (8), and postreceptor signaling pathways are being defined (9, 10). Through an AGE receptor-dependent mechanism, AGE induction of cytokines and growth factors has been implicated in contributing to end-organ changes that occur in tissues in patients with diabetes (11–13).

Pathological hallmarks in most tissues where diabetes complications occur include expansion of extracellular matrix (ECM) and angiogenesis (1). The ECM expansion has been proposed to be due to a combination of increased ECM production (14) (15) and biochemically modified matrix, with a reduction in ECM breakdown (16). Connective tissue growth factor (CTGF), also known as insulin-like growth factor (IGF)-binding protein-related protein-2 (IGFBP-rP2) (17), is a potent inducer of ECM in fibroblasts (18, 19) and a potent angiogenic factor (20, 21). A potential role for CTGF in fibrotic disease states is increasingly being described (22–24), suggesting that CTGF may be a mediator of ECM expansion and fibrosis in diabetes. The aim of this study was to determine whether CTGF is up-regulated by AGE and subsequently to explore the cellular mechanism(s) that might be responsible for this effect.

Materials and Methods

Reagents

Polyclonal anti-IGFBP-rP2 (CTGF) antibodies (8799 and 8800) were generated in New Zealand White rabbits, as previously described (25). The anti-AGE antibody, which neutralizes the activity of AGE BSA (26),

Received October 3, 2000.

Address all correspondence and requests for reprints to: Dr. Stephen M. Twigg, Department of Pediatrics, NRC-5, Mark O. Hatfield Research Center, Oregon Health Sciences University, 3181 SW Sam Jackson Park Road, Portland Oregon 97201. E-mail: twiggs@ohsu.edu.

* This work was supported by the National Health and Medical Research Council of Australia (C. J. Martin Postdoctoral Fellowship to S.T.), and the NIH [Summer Student's Scholarship (to S.C.) and Grants CA-58110 and DK-51513 (to R.G.)]. This work was presented in part at the 82nd Annual Meeting of The Endocrine Society, Toronto, Canada, 2000.

was a gift from Dr. H. Miyata, Kissei Pharmaceutical Co. Ltd. (Nagano, Japan). The antihuman polyclonal antibody generated in rabbits against the receptor for AGE (RAGE) was provided as an IgG fraction (gift from Dr. A.M. Schmidt, Columbia University, New York, NY). This antibody inhibits ligand-stimulated activation of RAGE by AGE (27, 28). The transforming growth factor-β1 (TGFβ1) affinity-purified IgG antibody generated in chickens that neutralizes TGFβ1 bioactivity was purchased from R&D Systems, Inc. (Minneapolis, MN). Nonimmune rabbit IgG, D-glucose, glycolaldehyde, BSA (fraction V, fatty acid and endotoxin free), and aminoguanidine were purchased from Sigma (St. Louis, MO). TGFβ1 was purchased from Austral Biologicals (San Ramon, CA).

Intact carboxyl-terminal flag-tagged IGFBP-rP2 (CTGF), used as a standard in the Western immunoblots and in the CTGF enzyme-linked immunosorbent assay (ELISA), was purified from a baculovirus expression system, and pure IGFBP-rP2 (CTGF) protein was quantitated using Coomassie-stained gels with BSA as standard, all as previously described (29). The approximately 14-kDa fragment of IGFBP-rP2 (CTGF), described in Fig. 7A, was purified from a highly proteolyzed preparation of pure IGFBP-rP2 (CTGF) protein, using late-harvested SF-9 insect cell lysates. After initial purification of this preparation by means of flag protein-Sepharose affinity chromatography (29), the fragment was separated from any remaining intact IGFBP-rP2 (CTGF) using a high performance size-fractionation gel permeation column (HR-75, Pharmacia Biotech, Piscataway, NJ) with PBS as buffer, with fast performance liquid chromatography, eluting at 0.5 ml/min with 0.5-ml fractions. Pure, approximately 14-kDa fragment was confirmed by Coomassie staining and Western immunoblot using IGFBP-rP2 (CTGF) primary antibody (not shown).

AGE synthesis

Advanced glycosylation end products were synthesized *in vitro*, following methods previously described (26, 30, 31). BSA (Sigma, RIA grade, fraction V) at 10 mM was coincubated in sterile PBS with either 0.5 M D-glucose for 10 weeks or 25 mM glycolaldehyde for 3 days, each with 1.5 mM phenylmethylsulfonylfluoride under aerobic conditions at 37 C. To generate control BSA for comparison with AGE treatments, tubes were prepared with simultaneous incubations under the same conditions without the addition of the respective reducing sugar or aldehyde. Additionally, in parallel preparations, aminoguandine at 100 mM, as an inhibitor of formation of products of nonenzymatic glycosylation (13), was added to the BSA and glucose. All preparations were extensively dialyzed in PBS, using a low M_r cut-off membrane (6–8 kDa, Spectrapor 1, Spectrum Industries, Los Angeles, CA) (13).

The AGE content in the preparations was assessed by means of fluorescence, SDS-PAGE analysis, and ELISA. The fluorescence content, measured with a fluorescence spectrometer at 390 nm emission after 450 nm excitation in relative fluorescence units per mg BSA, was 11.2 ± 2.5 for control BSA, 67.1 ± 12.5 for AGE BSA from glycolaldehyde, 52.3 ± 6.3 for AGE BSA from glucose, and 9.7 ± 1.2 for aminoguanidine added to BSA and glucose (termed aminoguanidine BSA) (31). By SDS-PAGE analysis under reducing conditions, followed by Coomassie staining, the AGE BSA produced from D-glucose and glycolaldehyde was shown to have high M_r species consistent with the intermolecular cross-linking ability of AGE, as previously described (26). In contrast, the control BSA and aminoguanidine BSA preparations did not have these high M_r forms (data not shown). By competitive ELISA (32), performed by Dr. P. Foiles (Alteon, Inc., Ramsey, NJ), using a synthetic *N*-ε-carboxymethyl lysine (CML) analog as the standard, the CML content of the preparations (picomoles of CML per μg BSA ± 95% confidence interval) was 82 ± 8.5 for AGE BSA from glycolaldehyde and 13 ± 1.4 for AGE BSA from glucose and was undetectable (<1) for control BSA and also undetectable when aminoguanidine at 100 mM was coincubated with BSA and glucose. Unless otherwise indicated in the text, the data described refer to the use of AGE BSA synthesized from glucose.

Cell culture

Primary cell cultures of nonfetal human dermal fibroblasts, CRL-2097 and CRL-1474, were purchased from American Type Culture Collection (Manassas, VA). Cells were maintained in MEM supplemented with 10% FBS and were used in these studies between passages 4 and 12. The human primary cultures of dermal fibroblasts, designated A35 (derived from the forearm of a 70-yr-old male) and A305 (newborn foreskin fibroblasts), were gifts from Dr. S. Goldstein, Memorial Veteran's Hospital (Little Rock, AR). These cells were maintained in DMEM with 15% FBS.

Cell treatment

After trypsinization, cells were grown in 12-well plates for 5 days in their respective media with FBS until they were confluent. For experiments requiring the use of blocking antibodies to RAGE and AGE, cells were grown in 24-well plates under the same conditions. Cells were then incubated in their respective serum-free medium for 16 h and then treated with additions on day 0 under serum-free conditions, using fresh media. Unless otherwise indicated in the text, the conditioned media were not changed after adding the treatments. When cells were transiently treated for 8 h with reagents, they were washed with PBS, and fresh serum-free medium with 0.05% BSA was added. Cell lysates and conditioned media were harvested up to 3 days after treatments. For experiments involving the use of blocking antibodies or antioxidants, cells were preincubated with the antibody or reagent for 2 h under serum-free conditions before adding AGE or control BSA directly to the medium.

Total RNA isolation and analysis by quantitative real-time RT-PCR

Total RNA was isolated from duplicate wells using the RNeasy Mini-kit from QIAGEN (Valencia, CA) and was then analyzed by quantitative real-time PCR using an ABI Prism 7700 Sequence Detection System (PE Applied Biosystems, Foster City, CA). This system is based on the ability of the 5′-nuclease activity of *Taq* polymerase to cleave a nonextendable dual labeled fluorogenic hybridization probe during the extension phase of PCR. The following sequence-specific primers and probes for human CTGF, IGFBP-rP1, IGFBP-3, and 18S ribosomal RNA were designed using Primer Express Software 1.0 (PE Applied Biosystems): for CTGF: forward, 5′-GAGGAAAACATTAAGAAGGGCAAA-3′; reverse, 5′-CGGCACAGGTCTTGATGA-3′; and probe, 5′-6FAM-TTTGAGCTTTCTGGCTGCACCAGTGT-TAMRA-3′; for IGFBP-rP1: forward, 5′-GCGGAAAATGGCAGACAATT-3′; reverse, 5′-CTTGAGGGTTTGGGTTTCCA-3′; and probe, 5′-6FAM-TTCGCTCCATGATGCGTTATCTGGGTAMRA-3′; for IGFBP-3: forward, 5′-AAGGTGGGTAGGCACGTTGTAG-3′; reverse, 5′-ATATCAAAACCCGAATCCACTTTACT-3′; and probe, 5′-6FAM-CAAAGCAATGTCTAGTCCCGGTATGTCCAA-TAMRA-3′; for 18S: forward, 5′-CGGCTACCACATCCAAGGAA-3′; reverse, 5′-GCTGGAATTACCGCGGCT-3′; and probe, 5′-6FAM-TGCTGGCACCAGACTTGCCCTC-TAMRA-3′. Primers were used at a concentration of 200 nM and probes at 100 nM in each reaction. Multiscribe reverse transcriptase and AmpliTaq Gold polymerase (PE Applied Biosystems) were used in all RT-PCR reactions. Each RNA sample was analyzed in triplicate. Relative quantitation of 18S ribosomal RNA and human CTGF, IGFBP-rP1, and IGFBP-3 messenger RNAs (mRNAs) was calculated using the comparative threshold cycle number for each sample fitted to a five-point standard curve (ABI prism 7700 User Bulletin 2, PE Applied Biosystems). The standard curve was constructed using a serial dilution of total RNA extracted from human cardiac fibroblasts that had been treated with TGFβ1 at 1 ng/ml for 24 h. Expression levels were normalized to 18S ribosomal RNA and related to relevant controls, as indicated in the text.

Preparation of conditioned media and cell lysates

Cell lysate samples were harvested after treatment, by washing cells with PBS, then adding 100 μl cold RIPA lysis buffer [20 mM Tris (pH 8.0), 150 mM NaCl, 1% Nonidet P-40, 0.5% sodium deoxycholate, and 0.1% SDS] plus a protease inhibitor cocktail (Roche Molecular Biochemicals, Mannheim, Germany) directly to each well. Plates were rocked for 15 min at 4 C, and lysates were collected and centrifuged at 10,000 × *g* for 10 min at 4 C. The supernatants from duplicate wells within each experiment were pooled and stored at −20 C until analysis. The total protein concentration was determined for each sample by use of the DC Protein Assay reagent (Bio-Rad Laboratories, Inc., Hercules, CA). Then 20 μg total protein were loaded per lane for SDS-PAGE analysis, and 5 μg total protein were added to each ELISA well for CTGF quantitation.

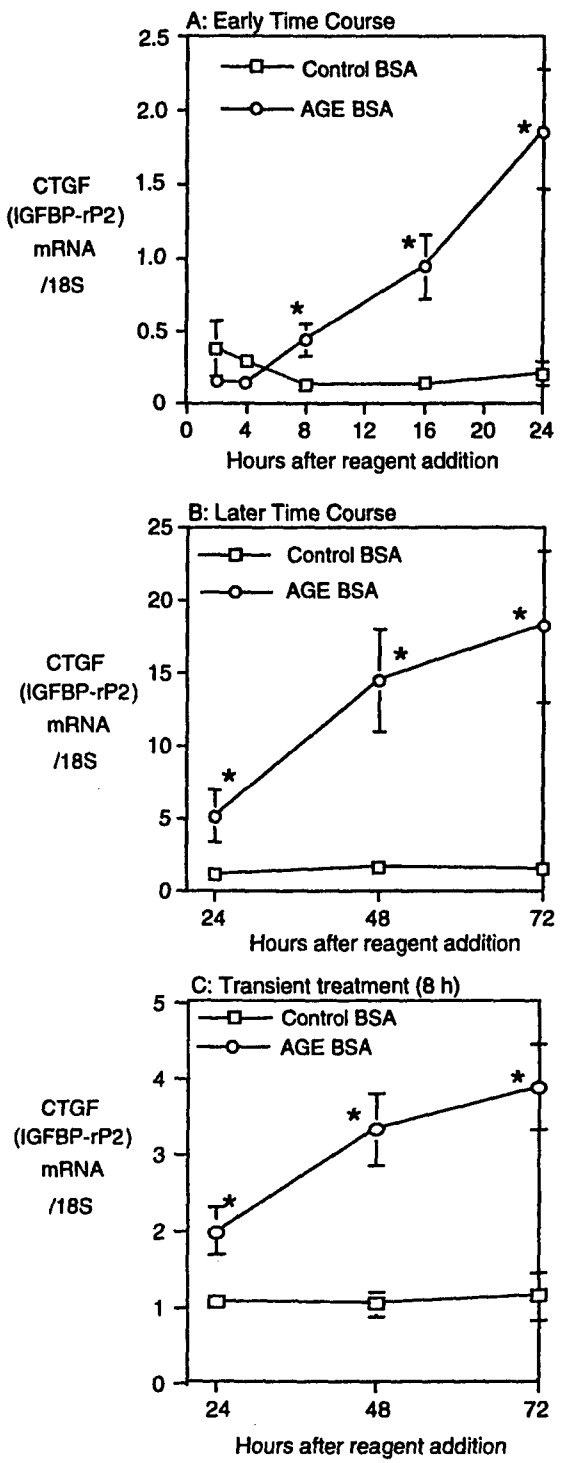

FIG. 1. Time-course induction of CTGF (IGFBP-rP2) mRNA by AGE BSA. Soluble AGE BSA at 100 μg/ml was added to duplicate wells of confluent primary cultures of human fibroblasts (CRL-2097 cells) under serum-free conditions, and total RNA was collected at the time points shown. Control BSA at the same concentration was added to other wells, also in duplicate. CTGF mRNA was then determined by quantitative RT-PCR in triplicate for each sample, as described in *Materials and Methods*. The CTGF mRNA level is expressed in arbitrary units normalized to 18S. A, Time course up to 24 h. B, Time course from 1–3 days. C, Treatment for 8 h only with AGE BSA or control BSA at 100 μg/ml, followed by RNA analysis on days 1–3. Data in A–C are the mean ± 1 SD from three independent experiments. *, $P < 0.05$ *vs.* the respective control BSA.

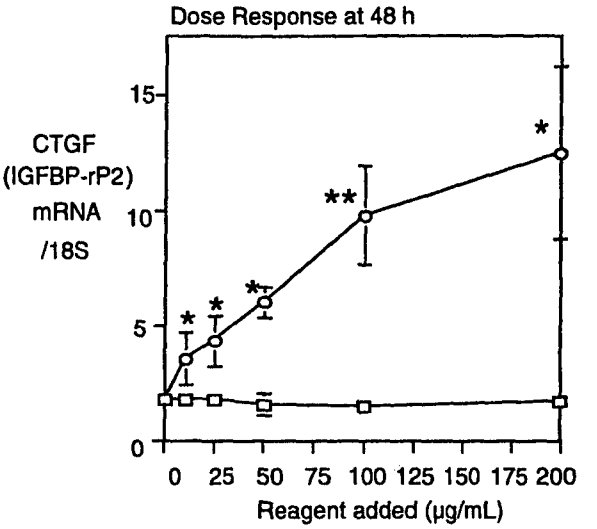

FIG. 2. Dose-dependent induction of CTGF (IGFBP-rP2) mRNA by AGE BSA. Dose response with AGE BSA or control BSA treatment from 0–200 μg/ml added to wells of confluent human fibroblasts (CRL-2097 cells), with RNA collection at 48 h. CTGF mRNA was determined by quantitative RT-PCR in triplicate for each sample, and the CTGF mRNA level is expressed in arbitrary units normalized to 18S. Data are the mean ± 1 SD from three independent experiments. *, $P < 0.05$, **, $P < 0.01$ *vs.* the respective control BSA.

Western immunoblot analysis

Conditioned medium samples were separated on 15% nonreducing SDS-PAGE. Proteins were electrotransferred onto nitrocellulose, and membranes were blocked with 5% nonfat dry milk/TBS with 0.1% (vol/vol) Tween 20 for 1 h at 22 C, then incubated in IGFBP-rP2 (CTGF) antiserum at 1:1000 dilution at 4 C overnight. After incubation of membranes with a horseradish peroxidase (HRP)-labeled secondary antibody for 1 h at 22 C, immunoreactive proteins were detected by use of enhanced chemiluminescence (NEN Life Science Products, Boston, MA).

CTGF (IGFBP-rP2) ELISA

The anti-IGFBP-rP2 (CTGF) antibody (8800) (25) was biotinylated by incubating protein A affinity-purified 8800 (0.8 μg) with 150 μg sulfo-NHS-LC biotin (Pierce Chemical Co., Rockford, IL) for 2 h at 22 C, followed by separation from unreacted biotin through a size-fractionation and desalting column with PBS as buffer according to the manufacturer's instructions. Affinity-purified 8800 antibody (600 ng/well) in 10 mM sodium carbonate, pH 9.6, was adsorbed to 96-well immunoplates (Nalge Nunc International, Rochester, NY) by a 20-h incubation at 4 C. The unbound antibody was removed, and the wells were blocked by incubation with PBS and 0.1% (vol/vol) Triton X-100 (buffer A) containing 10 g/liter BSA for 2 h at 37 C, then washed four times with buffer A. Purified intact recombinant human (rh) IGFBP-rP2 (CTGF) in buffer A and 1 g/liter BSA was used to generate standard curves. Standard and samples (100 μl/well) were incubated in duplicate at 4 C for 20 h. The plate was washed, then incubated with biotinylated IGFBP-rP2 (CTGF) antibody (80 ng/well) for 20 h at 4 C. After washing, the plate was incubated with streptavidin-HRP (1:500) for 30 min at 22 C, followed by substrate [0.1 g/liter 3,3′,5,5′-tetramethylbenzidine in 0.2 M sodium acetate (pH 6) containing 0.06% (wt/wt) H_2O_2] for 30 min at 22 C. The reaction was stopped by the addition of 2 M H_2SO_4, and the absorbance was measured at 450 nm using a microplate reader. The interassay coefficient of variation was 8.1% for the middle concentration (10 ng/well) of rhIGFBP-rP2 (CTGF) standard used. No cross-reactivity was detected with 1 μg/well purified rhIGFBP-3, rhIGFBP-rP1 (mac 25), or rhIGFBP-rP3 (Nov H; not shown).

CTGF (IGFBP-rP2) cell association assay

To determine whether increases in rhIGFBP-rP2 (CTGF) in the whole cell lysates after AGE treatment are due to increases in rhIGFBP-rP2

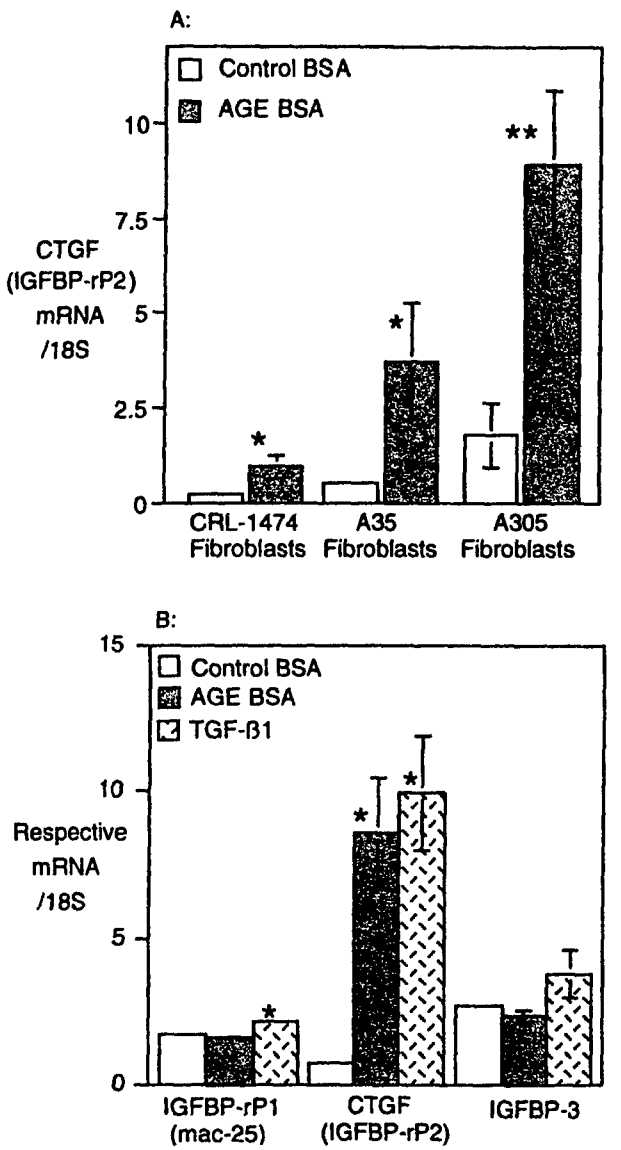

FIG. 3. Generalizability of the AGE BSA effect on CTGF (IGFBP-rP2) mRNA to multiple sources and donors of human skin fibroblasts, and specificity of the effect to CTGF (IGFBP-rP2). A, Soluble AGE BSA or control BSA at 100 μg/ml was added to duplicate wells of confluent primary cultures of human skin fibroblasts from multiple donors under serum-free conditions, and total RNA was collected at the time points shown. IGFBP-rP2 (CTGF) mRNA was then determined by quantitative RT-PCR in triplicate for each sample. The IGFBP-rP2 (CTGF) mRNA level is expressed in arbitrary units, normalized to 18S. The donor age and skin site of the fibroblasts studied are: 7-yr-old male abdomen (CRL-1474 cells), 70-yr-old male forearm (A35), and newborn foreskin (A305). Data are the mean ± 1 SD from three independent experiments. B, Soluble AGE BSA or control BSA at 100 μg/ml or TGFβ1 at 1 ng/ml was added to duplicate wells of confluent primary cultures of human fibroblasts (CRL-2097) under serum-free conditions. Total RNA was collected at 48 h, and CTGF (IGFBP-rP2) mRNA, IGFBP-rP1 (mac-25) mRNA, and IGFBP-3 mRNA levels were determined by quantitative RT-PCR in triplicate for each sample. The mRNA levels are expressed in arbitrary units. Data are the mean ± SD from three independent experiments. *, $P < 0.05$; **, $P < 0.01$ (*vs.* the respective control BSA).

(CTGF) at a cell-associated site either on the cell surface or in the extracellular matrix, rather than intracellularly, 2097 fibroblasts in confluent monolayer were treated under serum-free conditions with AGE or control BSA (each at 100 μg/ml) for 3 days in replicates of four. After washing twice with PBS at 4 C, biotinylated rhIGFBP-rP2 (CTGF) antibody (800 ng/well) together with streptavidin-HRP (1:500) was added for 2 h at 22 C in PBS and 0.1% BSA. In some wells the streptavidin-HRP (1:500) was added in the absence of primary antibody to determine nonspecific binding and endogenous cellular peroxidase activity. After two further (gentle) PBS washes, developing substrate was added, and absorbance was read as described for the IGFBP-rP2 (CTGF) ELISA above.

Densitometric analysis

To quantify the relative induction of CTGF after Western immunoblots, densitometric measurement was performed using GS-700 Imaging Densitometer with Mutli-Analyst Software (Bio-Rad Laboratories, Inc.).

Statistical analysis

Results are expressed as the mean ± SD or the mean ± SEM as indicated in the text. All data were pooled from three or four independent experiments, each performed in triplicate. Differences between groups were assessed using Student's two-tailed paired *t* test in Excel 98 (Microsoft Corp., Redmond, WA). $P < 0.05$ was considered statistically significant.

Results

To determine whether CTGF mRNA steady state levels are up-regulated by AGE in primary cultures of human dermal fibroblasts, confluent monolayers of CRL-2097 fibroblasts were treated with soluble AGE BSA under serum-free conditions. In response to 100 μg/ml AGE BSA, an increase in CTGF mRNA was initially detectable after 8 h of AGE treatment (Fig. 1A), and a progressive increase occurred over the 3-day time course of the study (Fig. 1B). In contrast, no change in CTGF mRNA over time was seen with the same concentration of control BSA (Fig. 1, A and B). These results were confirmed by Northern analysis (not shown). Transient treatment of cells with AGE for 8 h, followed by washing of cells with PBS and replacement with fresh serum-free medium, also caused a progressive increase in CTGF mRNA over subsequent days (Fig. 1C), with a clear persistence of the effect for at least 72 h after AGE addition.

A dose-response study with AGE BSA from 0–200 μg/ml, with continuous AGE treatment and RNA collection at 48 h after initial AGE addition, showed that increases in CTGF mRNA were significant using 10 μg/ml or more AGE BSA, whereas increasing concentrations of control BSA did not produce any change in CTGF mRNA compared with no addition of BSA (Fig. 2).

Primary human skin fibroblasts from other donors were studied to assess whether the changes seen in CTGF mRNA in human foreskin fibroblast CRL-2097 cells are generalizable to human dermal fibroblasts. When these other cells were treated with 100 μg/ml AGE BSA, increases in CTGF mRNA were observed 48 h after treatment, compared with the control BSA, in all of the fibroblast cell lines studied whether they were derived from neonatal foreskin (A305), a child's abdomen (CRL-1474), or the forearm of a mature adult (A35; Fig. 3A).

To address whether the changes seen in CTGF mRNA were relatively specific, other members of the IGFBP superfamily were analyzed in the same cell system. In contrast to the observed regulation of CTGF mRNA by AGE, IGFBP-rP1 (mac 25) mRNA was not up-regulated by AGE BSA (Fig. 3B). IGFBP-3 is the predominant IGFBP present in human fibro-

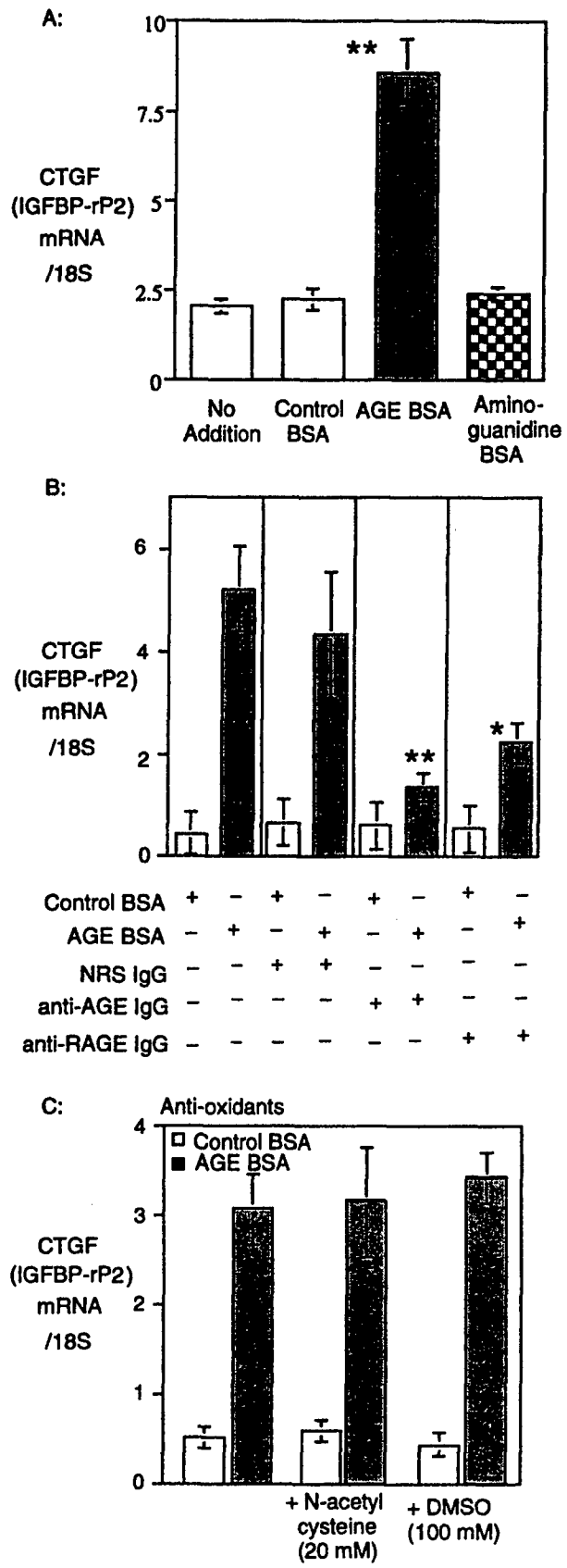

FIG. 4. The AGE effect on CTGF (IGFBP-rP2) occurs through nonenzymatic glycosylation of BSA, is blocked by an anti-AGE-neutralizing antibody, is partially mediated through the AGE receptor, RAGE, and is not inhibited by oxygen free radical scavengers. A, Soluble AGE BSA or control BSA at 100 μg/ml, or no treatment, was added to duplicate wells of confluent primary cultures of human fibroblasts (CRL-2097 cells) under serum-free conditions. In other wells BSA was added that had previously been coincubated with glucose and aminoguanidine before dialysis, as described in *Materials and Methods*. Total RNA was collected at 48 h, and CTGF mRNA was determined by quantitative RT-PCR in triplicate for each sample. The CTGF mRNA level is expressed in arbitrary units. Data are the mean ± 1 SD from three independent experiments. **, $P < 0.01$ *vs.* all other treatments. B, Wells were preincubated with anti-AGE polyclonal neutralizing IgG, anti-RAGE polyclonal neutralizing IgG (each at 100 μg/ml IgG), or 100 μg/ml normal rabbit serum (NRS) IgG for 2 h. Soluble AGE BSA or control BSA at 100 μg/ml was then added to the wells. Total RNA was collected at 48 h, and IGFBP-rP2 (CTGF) mRNA was determined by quantitative RT-PCR in triplicate for each sample. Data are the mean ± 1 SD from four independent experiments. *, $P < 0.05$; **, $P < 0.01$ (*vs.* AGE BSA added alone). C, Duplicate wells of human fibroblasts under serum-free conditions were incubated with serum-free medium alone, 20 mM *N*-acetyl cysteine, or 100 mM dimethylsulfoxide (DMSO) for 2 h. Soluble AGE BSA or control BSA at 100 μg/ml was then added to the wells. Total RNA was collected at 48 h, and CTGF (IGFBP-rP2) mRNA was determined by quantitative RT-PCR in triplicate for each sample. The mRNA levels are expressed in arbitrary units. Data are the mean ± 1 SD from three independent experiments.

blast conditioned medium (33), and its mRNA also was not increased by AGE (Fig. 3B). In comparison with the lack of effect of AGE treatment, TGFβ1 treatment modestly up-regulated IGFBP-rP1, and possibly IGFBP-3 mRNA, at 48 h (Fig. 3B), as previously described (33, 34). Also consistent with previous observations in cultured human fibroblasts (35), a pronounced up-regulation of CTGF mRNA occurred after TGFβ1 addition (Fig. 3B).

Formation of products of nonenzymatic glycosylation was inhibited by the dihydrazine compound, aminoguanidine (13). When cells were treated with BSA that had been coincubated for 10 weeks with both glucose and aminoguanidine as described in *Materials and Methods*, no increase in CTGF mRNA was observed compared with control BSA treatment alone or with serum-free medium without any addition (Fig. 4A). This result confirms that the active component in the AGE reagent used is a product of nonenzymatic glycosylation.

To determine whether early or advanced glycosylation end products are mediating the effect on CTGF in this cell system, cells were preincubated with anti-AGE IgG before addition of the AGE reagent. Using the anti-AGE antibody, the AGE induction of CTGF mRNA was inhibited, on the average, by 86.2% (Fig. 4B). As this antibody is specific to AGE and it does not bind to amadori products (26), which are early products of nonenzymatic glycosylation, these results show that AGE is the active component in the synthesized reagent responsible for increasing CTGF in these studies.

AGE may bind to and activate one or more of the defined cell surface receptors for AGE (8). The AGE receptor subtype, termed RAGE, has recently been shown to be present on the surface of human fibroblasts (27), and in some cell systems the induction of growth factors by AGE has been shown to be mediated by RAGE (36). When cells were preincubated with a blocking antibody of RAGE activation by AGE ligand, the induction of CTGF mRNA by AGE was attenuated by the

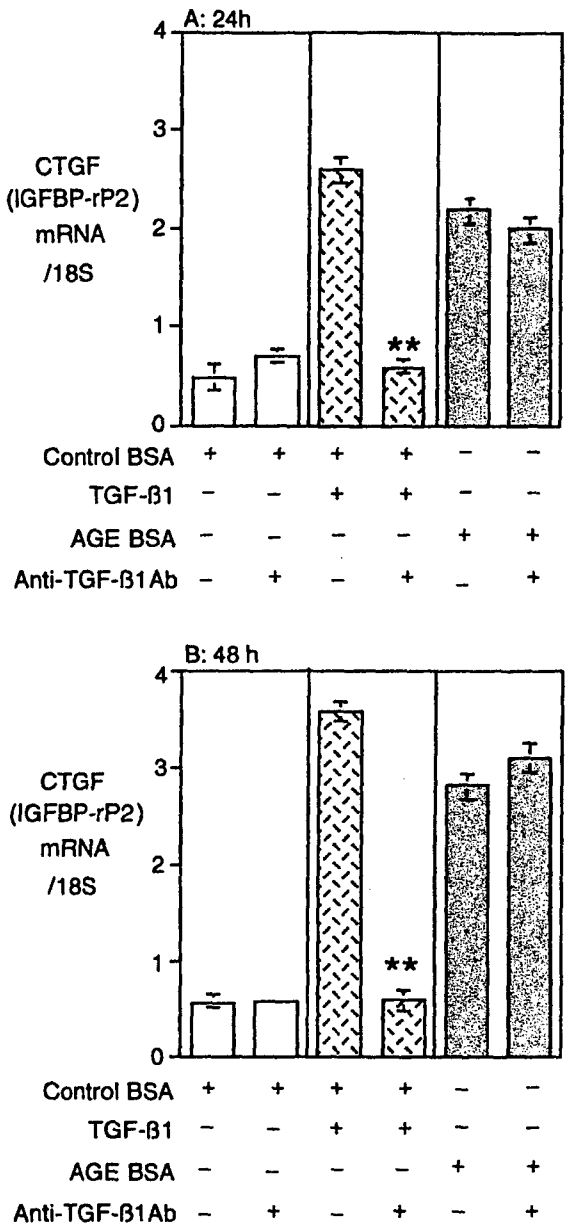

FIG. 5. AGE induction of CTGF (IGFBP-rP2) mRNA is independent of endogenous TGFβ1 activity. Duplicate wells of confluent primary cultures of human fibroblasts (CRL-2097 cells) under serum-free conditions were incubated with AGE BSA or control BSA at 100 μg/ml or with TGFβ1 at 1 ng/ml for 24 h (A) or 48 h (B), and in some wells a chicken antihuman TGFβ1-neutralizing antibody (200 ng/ml) was added simultaneously as indicated. Total RNA was collected at 24 h (A) and 48 h (B), and CTGF mRNA was determined by quantitative RT-PCR in triplicate for each sample. The mRNA levels are expressed in arbitrary units. Data are the mean ± 1 SD from three independent experiments in A and B. **, $P < 0.01$ *vs.* TGFβ1 added without neutralizing antibody.

anti-RAGE IgG by 64.1%, on the average (Fig. 4B). Higher concentrations of anti-RAGE IgG did not have any additional effect (not shown). In contrast, the AGE effect was not significantly inhibited by normal rabbit serum IgG (Fig. 4B). These results show that RAGE is at least partly mediating the AGE induction of CTGF mRNA in the fibroblasts.

As reactive oxygen (RO) species are commonly generated in cells after activation of AGE receptors by its ligand (9, 37), an effect of inhibiting RO species formation during AGE treatment was studied. Preincubation of the fibroblasts with the antioxidants dimethylsulfoxide or *N*-acetyl cysteine, however, did not inhibit the increases in CTGF mRNA (Fig. 4C). These results imply that RO species are unlikely to play a role in the observed AGE effect on CTGF.

A potential role for autocrine TGFβ1 in CTGF mRNA induction by AGE was then examined. TGFβ1 is a potent inducer of CTGF gene expression in this cell system (Fig. 3A), and in addition, AGE may induce TGFβ1 mRNA and protein in some cells (13). Induction of CTGF mRNA by rhTGFβ1 added to the cultured fibroblasts was fully inhibited by a TGFβ1-neutralizing antibody at 24 h (Fig. 5A) and 48 h (Fig. 5B). In contrast, when the same antibody was added under the same conditions in parallel wells, no significant inhibition of the CTGF mRNA increase induced by AGE occurred (Fig. 5, A and B), indicating that the effect of AGE is TGFβ1 independent in this cell system.

The fibroblast cellular protein from CRL-2097 skin fibroblasts was then analyzed to determine whether AGE treatment causes increases in CTGF protein as well as increases in steady state CTGF mRNA levels. By Western immunoblot after SDS-PAGE, using a polyclonal IGFBP-rP2 (CTGF) antiserum (25), CTGF steady state protein levels over days 1–3 in the conditioned medium were increased in response to AGE BSA, compared with control BSA treatment (Fig. 6A). A progressive increase in intact CTGF as well as previously described lower M_r immunoreactive forms, at approximately 14 and 20 kDa (38), occurred (Fig. 6A). High M_r immunoreactive material (>80 kDa) was also more prominent in the AGE-treated medium, which may include CTGF covalently cross-linked by AGE. All of these increases were more marked using AGE BSA synthesized from glycolaldehyde compared with AGE BSA synthesized from glucose (not shown). Using densitometric analysis from three independent experiments, the intact CTGF in the medium was increased by AGE compared with control BSA treatment (mean ± SEM) by 3.6 ± 1.1-fold on day 1, 8.0 ± 1.3-fold on day 2, and 14.5 ± 3.1-fold on day 3 ($P < 0.05$ for all days of AGE treatment compared with control BSA treatment).

As CTGF is an extracellular matrix and cell-associated signaling protein and also exists in cell media (38), analysis of whole cell lysates for CTGF protein after AGE treatment was performed. Western immunoblot analysis of the whole cell lysates after SDS-PAGE showed that intact CTGF was increased by AGE treatment from day 3 compared with control BSA treatment (Fig. 6B). There was no CTGF fragment or high M_r immunoreactive material observed in the lysates (not shown). Densitometric analysis of CTGF from lysates from four independent experiments (mean ± SEM) gave the following results for fold change with AGE treatment compared with control BSA treatment: 0.89 ± 0.33 on day 1, 0.97 ± 0.17 on day 2, and 1.53 ± 0.25 on day 3 ($P < 0.05$ for day 3 only for AGE compared with control BSA on the respective day).

Considering that the increase in CTGF in whole cell lysates on day 3 after AGE treatment was relatively modest, changes in cell lysate CTGF were further determined by a CTGF ELISA, as described in *Materials and Methods*. This assay can measure endogenous intact CTGF, which is present in whole cell lysates, but due to a lack of parallelism with the intact

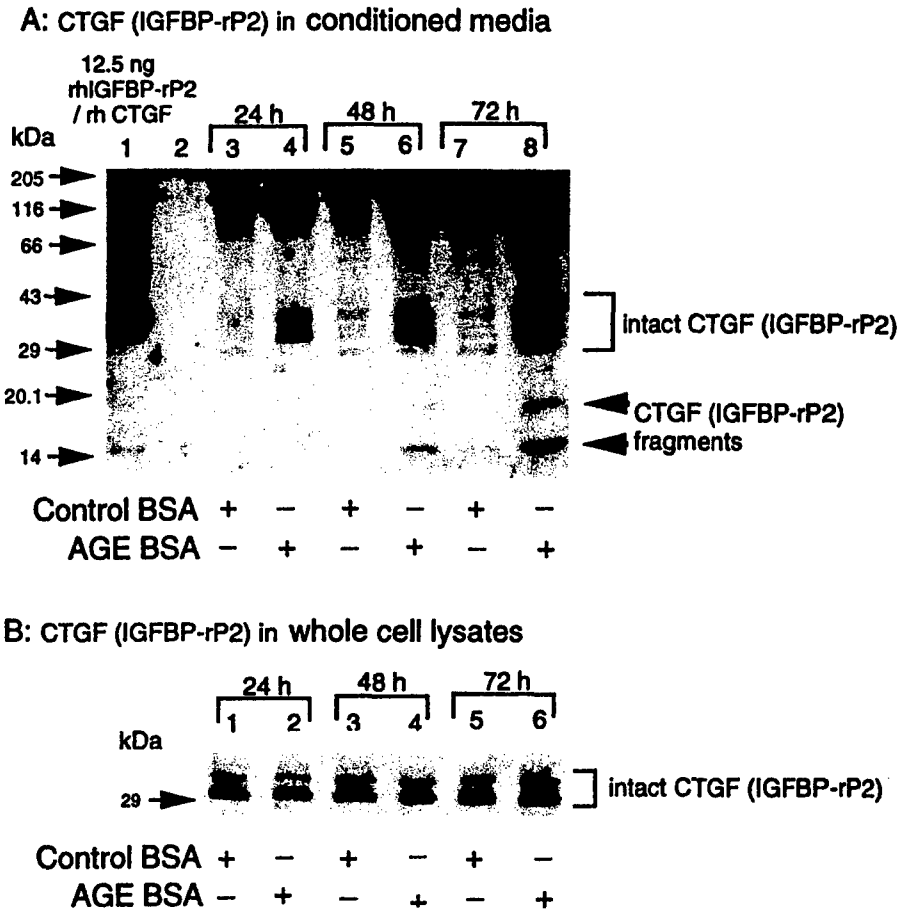

FIG. 6. CTGF (IGFBP-rP2) protein up-regulation by AGE BSA in conditioned media and whole cell lysates. Soluble AGE BSA or the respective control BSA was added to duplicate wells of confluent primary cultures of human fibroblasts (CRL-2097 cells) under serum-free conditions. After 24–72 h, as indicated, conditioned media and whole cell lysates were collected and subjected to SDS-PAGE and then Western immunoblotted using IGFBP-rP2 (CTGF) antiserum, as described in *Materials and Methods*. A, Conditioned medium; lane 2, unconditioned serum-free medium loaded alone. B, Whole cell lysates, with 20 μg total protein loaded in each sample lane. In A and B one representative immunoblot is shown from three and four independent experiments, respectively, with each experiment showing equivalent results.

rhCTGF used as the standard, it cannot be used to accurately measure the 14-kDa CTGF fragment (Fig. 7A), which is present in the fibroblast-conditioned media (Fig. 6A). Consistent with the Western immunoblots of cell lysates (Fig. 6B), the ELISA also showed that AGE treatment reproducibly increased CTGF in the fibroblast whole cell lysates on day 3 (Fig. 7B). Thus, in contrast to the increases in CTGF protein observed in the conditioned media, there was no increase in CTGF protein in the first 2 days after AGE treatment in the whole cell lysates compared with control, and there was only a modest and delayed increase in CTGF in the lysates, which was much less striking than the increases in CTGF protein observed in the conditioned media (Fig. 6A).

To determine whether the increase in CTGF in the whole cell lysates seen by day 3 of AGE treatment was accessible to the extracellular environment, a cell association assay for CTGF was performed, as described in *Materials and Methods*. This assay uses binding of a biotinylated CTGF primary antibody to endogenous CTGF protein, followed by antibody detection using a streptavidin-HRP system. As no plasma membrane-permeabilizing agents were used in the protocol, the specific signal detected by the CTGF primary antibody was due to CTGF present on the cell surface or in the extracellular matrix, rather than CTGF present in an intracellular compartment. As shown in Fig. 7C, at 72 h AGE at 100 μg/ml specifically increased the absorbance signal compared with control ($P < 0.05$ for analysis of combined data from four independent experiments). In parallel wells, under the same conditions of confluent cell monolayers in serum-free media, cell number determined by hemocytometer counting and trypan blue exclusion was not changed by AGE treatment compared with control BSA (not shown). Thus, these results indicate that at 72 h, AGE treatment increases cell-associated CTGF compared with BSA control treatment alone.

Discussion

This study describes the up-regulation of CTGF mRNA and protein by treatment of human skin fibroblasts with advanced glycosylation end products. The effect of AGE on CTGF induction was caused by products of nonenzymatic glycosylation, as coincubation of aminoguanidine, an inhibitor of nonenzymatic glycosylation, with glucose and BSA did not have an effect on CTGF mRNA, nor was an effect seen with increasing control BSA alone. The up-regulation of CTGF in this cell model was mediated by AGE rather than by earlier products of nonenzymatic glycosylation, such as amadori products, as the use of an antibody specific for AGE that does not bind amadori products inhibited the induction of CTGF gene expression. The effect was at least partly mediated through the AGE receptor known as RAGE, as an anti-RAGE antibody significantly attenuated the effect of AGE on CTGF.

The up-regulation of CTGF by AGE appears to be specific for CTGF and is generalizable to skin fibroblasts from dif-

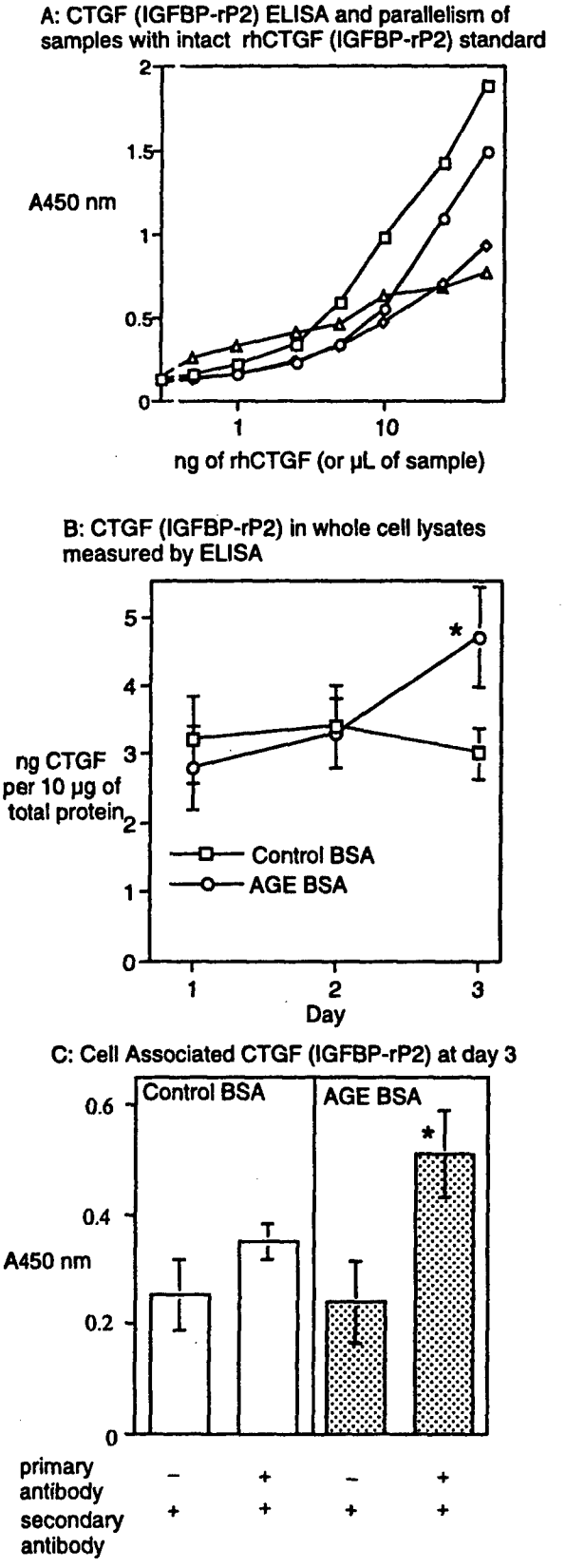

FIG. 7. Whole cell lysate and cell-associated increases in CTGF (IGFBP-rP2) after AGE BSA treatment. A, CTGF (IGFBP-rP2) ELISA as described in *Materials and Methods*, showing the standard curve generated for intact CTGF (IGFBP-rP2; □) compared with the curves generated with a 14-kDa fragment of CTGF (IGFBP-rP2; △), endogenous intact CTGF present in 2097 cell-conditioned medium (◇), and 2097 cell whole cell lysates (○). B, Results of analysis of CTGF in the whole cell lysates by CTGF ELISA after treatment up to 72 h with AGE or control BSA, each at 100 µg/ml. Data are the mean ± 1 SD of four independent experiments. *, $P < 0.05$ *vs.* control BSA on day 3. C, Results showing cell-associated CTGF after AGE treatment compared with control BSA (100 µg/ml) at 72 h, using biotinylated anti-CTGF IgG primary antibody followed by HRP-labeled secondary antibody or the secondary antibody alone, as described in *Materials and Methods*. Data are the mean ± 1 SD of four independent experiments. *, $P < 0.05$ *vs.* all other groups.

fering sources and passage number. In each of the four fibroblast cell lines studied, AGE up-regulated CTGF. In the cell line most extensively studied, CRL-2097, CTGF was regulated by AGE in early passages (passage 4) and also at later passages (passage 12). In contrast to effects on CTGF, the two other members of the IGFBP superfamily that were studied, IGFBP-3 and IGFBP-rP1, were not up-regulated by AGE. Further studies will be required to determine whether AGE affects other members of the CCN (CTGF, Cyrbl, Nov) family.

The concentrations of AGE BSA used in these experiments approximate those used *in vitro* in other studies exploring biological effects of AGE on cells (13, 27). Although there is no universal standard method for measuring specific AGE components at this time, and the AGE antibodies used in assays measuring AGE differ (39), the AGE BSA concentrations studied are in the broad range for AGE concentrations found in diabetic serum (40).

Few AGE components have been defined biochemically to date, and the specific end-product(s) that might be mediating the effect on CTGF was not identified in this work. AGE adducts existing in diabetic tissues that have been shown to signal through AGE receptors include mainly CML (28) and imidazoline-based products (41). Considering that CML adduct is a ligand for RAGE (28), that our AGE reagent contained CML, and that at least part of the AGE effect on CTGF has been shown to be mediated through RAGE, it is plausible that CML adducts are one of the AGE components operative in this study. In the current work, when AGE BSA synthesized from glycolaldehyde was studied in experiments where AGE BSA synthesized from glucose was also used in treatments, each at the same AGE concentration of 100 µg/ml BSA with mRNA measurements over 3 sequential days, the induction of CTGF mRNA by these reagents did not differ (data not shown). As these two AGE reagents contain differing amounts of CML (as described in *Materials and Methods*), the CML adduct cannot be the only explanation for the observed AGE effect on CTGF mRNA in these AGE preparations. Further experiments with pure CML and other pure AGE adducts, when available, will be required to address this issue.

A number of subtypes of cell surface receptor bind AGE specifically and are responsible for mediating multiple cellular effects of AGE (42). These receptors exist in four main classes: RAGE, AGE-R1, AGE-R2, and AGE-R3 (8). In the diabetic environment, the increased AGE present is hypothesized to bind and activate AGE receptors, and in some studies, the induction of growth factors by AGE has been shown to be mediated by AGE receptors, including RAGE (43). Our studies indicate that RAGE is responsible for mediating at least part of the effect of AGE on CTGF mRNA. The

possibility that other AGE receptors might also contribute to these effects is not excluded by this work.

A role for growth factors in contributing to chronic diabetes-related end-organ complications, particularly vascular endothelial growth factor (VEGF), TGFβ1, IGF-I, and platelet-derived growth factor, is under increasing evaluation, and a potential role for CTGF in chronic diabetic complications is emerging. CTGF is a potent profibrotic agent (18, 44), which is reflected in its ability to induce ECM components and increase fibroblast DNA synthesis (18) and to promote angiogenesis (20, 21). CTGF mRNA levels are up-regulated in many chronic disease states where fibrosis is prominent (22–24). Two separate studies involving renal mesangial cells and differing diabetic rat models recently reported that CTGF gene expression (45) as well as protein (46) are increased in mesangial cells after exposure to high glucose and *in vivo* in diabetic rat kidneys. Immunohistochemical studies of kidney tissue in human end-stage renal disease showed increased CTGF protein in diabetic kidneys as well as other nephropathies (47), and CTGF mRNA is markedly increased in advanced atheromatous lesions (48).

This is the first report of CTGF induction by advanced glycosylation end products, and it provides a potentially critical linkage among AGE, growth factors, and fibrosis. AGE induction of growth factors and cytokines has been described for VEGF, TGFβ1, IGF-I and platelet-derived growth factor, TNFα, IL-1β, and IL-6 (3) mainly in various endothelial and mesenchymal cultured cells and in some cases by AGE administration *in vivo* (15). CTGF appears to fit well into this group of proinflammatory and/or profibrotic proteins.

The striking persistent effect over 3 days of AGE on CTGF mRNA even after transient treatment suggests that regulation of CTGF by the AGE reagent tested is complex and may involve multiple interrelated intracellular signals. The cellular mechanism of AGE induction of CTGF mRNA was not defined in this study. RO species were not implicated, because antioxidants were ineffective in inhibiting AGE induction of CTGF. TGFβ1 is a known potent inducer of CTGF gene expression, and CTGF is implicated as a downstream mediator of TGFβ1 effects (49), particularly in fibrosis (44). We were unable to show, however, that TGFβ1 is a mediator in the AGE induction of CTGF. In the current work, both the early time course of initial induction of CTGF mRNA by AGE at 8 h as well as the inability of TGFβ1-neutralizing antibodies to inhibit AGE induction of CTGF suggest that AGE is operating through mechanisms that are independent of TGFβ1. Although studies involving the use of exogenously added neutralizing antibodies have potential limitations in assessing the role of endogenous protein bioactivity, that total TGFβ1 measurements in conditioned media measured by TGFβ1 ELISA (Promega Corp., Madison, WI) in these cells were not increased by AGE compared with control BSA treatment (data not shown) is also supportive that TGFβ1 is not a mediator of AGE induction of CTGF in this work. These results contrast with studies describing TGFβ-dependent effects of glucose on CTGF up-regulation in human mesangial cells (45, 46), but are consistent with other studies showing that various reagents can potently up-regulate CTGF mRNA independently of TGFβ1 (50).

In human fibroblast primary cultures, CTGF exists at very low levels in conditioned medium and is often present in low M_r fragment forms, which may also have bioactivity (38). That intact CTGF was readily detectable in the medium after AGE treatment may be partly related to posttranslational modification of CTGF, with cross-linking of CTGF protein by AGE into a high M_r immunoreactive form and redistribution of CTGF from a cell-associated site into the conditioned medium. In addition to the CTGF increases in the conditioned medium and consistent with the progressive increase in CTGF mRNA after AGE treatment, AGE caused increases in intact CTGF in whole cell lysates at 72 h. Further analysis showed that the CTGF increase in the lysates included protein that was cell associated and in a site accessible to the extracellular environment. To what extent the bioactivity of CTGF protein is affected by its presence in the medium compared with a cell-associated site is an important issue for future study of CTGF bioactivity.

There is a rationale to potentially link AGE effects and diabetic complications with the induction of CTGF in skin and, by association, with pathology in other tissues. A feature commonly present in human diabetes, even in late childhood and adolescence, is skin thickening and contracture (51), termed diabetic sclerosis. This process affects mainly the distal extremities and is characterized by expansion of extracellular matrix, fibroblast proliferation, and angiogenesis (52). The presence of overt diabetic sclerosis of skin is correlated with the presence and future development of end-organ complications, particularly diabetic nephropathy and retinopathy (53). AGE products are increased in human diabetic skin (6), and the levels of AGE in skin also correlate positively with the presence of diabetic microvascular kidney and eye disease (5, 6). That the ability of CTGF to induce fibrosis has been well characterized in skin (18, 44) makes skin fibroblasts a relevant cell model for the current study.

Clearly, *in vivo* and longer term studies are required to substantiate a more definitive role for induction of CTGF by AGE in potentially mediating diabetic fibrotic complications in skin and other organs. Activation of receptors for AGE, particularly RAGE (54), has also been implicated in the pathogenesis of fibrosis that develops in chronic diseases other than diabetes (42, 54, 55). That AGE up-regulates CTGF in nontransformed human fibroblasts suggests that CTGF may be a factor mediating the observed AGE and RAGE effects, which is a hypothesis that requires further testing.

Acknowledgments

We thank Alteon Inc., for measuring the CML adduct concentration in the AGE reagent with their CML ELISA. The generous gifts of anti-AGE antiserum from Dr. Miyata, Kissei Pharmaceutical Co. Ltd. (Hotaka, Japan), and the anti-RAGE antiserum from Dr. Anne-Marie Schmidt, at Columbia University (New York, NY), are gratefully acknowledged.

References

1. **King GL, Wakasaki H** 1999 Theoretical mechanisms by which hyperglycemia and insulin resistance could cause cardiovascular diseases in diabetes. Diabetes Care 22:C31–C37
2. **Nishikawa T, Edelstein D, Du XL, Yamagishi S, Matsumura T, Kaneda Y, Yorek MA, Beebe D, Oates PJ, Hammes HP** 2000 Normalizing mitochondrial superoxide production blocks three pathways of hyperglycaemic damage. Nature 404:787–790
3. **Bierhaus A, Hofmann MA, Ziegler R, Nawroth PP** 1998 AGEs and their interaction with AGE-receptors in vascular disease and diabetes mellitus. I. The AGE concept. Cardiovasc Res 37:586–600
4. **Chiarelli F, de Martino M, Mezzetti A, Catino M, Morgese G, Cuccurullo F, Verrotti A** 1999 Advanced glycation end products in children and adolescents with diabetes: relation to glycemic control and early microvascular complications. J Pediatr 134:486–491

5. **Beisswenger PJ, Makita Z, Curphey TJ, Moore LL, Jean S, Brinck-Johnsen T, Bucala R, Vlassara H** 1995 Formation of immunochemical advanced glycosylation end products precedes and correlates with early manifestations of renal and retinal disease in diabetes. Diabetes 44:824–829
6. **Sell DR, Lapolla A, Odetti P, Fogarty J, Monnier VM** 1992 Pentosidine formation in skin correlates with severity of complications in individuals with long-standing IDDM. Diabetes 41:1286–1292
7. **Vlassara H, Brownlee M, Cerami A** 1986 Nonenzymatic glycosylation: role in the pathogenesis of diabetic complications. Clin Chem 32:B37–B41
8. **Thornalley PJ** 1998 Cell activation by glycated proteins. AGE receptors, receptor recognition factors and functional classification of AGEs. Cell Mol Biol 44:1013–1023
9. **Schmidt AM, Hori O, Brett J, Yan SD, Wautier JL, Stern D** 1994 Cellular receptors for advanced glycation end products. Implications for induction of oxidant stress and cellular dysfunction in the pathogenesis of vascular lesions. Arterioscler Thromb 14:1521–1528
10. **Brownlee M** 2000 Negative consequences of glycation. Metabolism 49:9–13
11. **Vlassara H** 1992 Receptor-mediated interactions of advanced glycosylation end products with cellular components within diabetic tissues. Diabetes [Suppl 2] 41:52–56
12. **Hirata C, Nakano K, Nakamura N, Kitagawa Y, Shigeta H, Hasegawa G, Ogata M, Ikeda T, Sawa H, Nakamura K** 1997 Advanced glycation end products induce expression of vascular endothelial growth factor by retinal Muller cells. Biochem Biophys Res Commun 236:712–715
13. **Pugliese G, Pricci F, Romeo G, Pugliese F, Mene P, Giannini S, Cresci B, Galli G, Rotella CM, Vlassara H** 1997 Upregulation of mesangial growth factor and extracellular matrix synthesis by advanced glycation end products via a receptor-mediated mechanism. Diabetes 46:1881–1887
14. **Striker LJ, Striker GE** 1996 Administration of AGEs in vivo induces extracellular matrix gene expression. Nephrol Dial Transplant 11:62–65
15. **Yang CW, Vlassara H, Peten EP, He CJ, Striker GE, Striker LJ** 1994 Advanced glycation end products up-regulate gene expression found in diabetic glomerular disease. Proc Natl Acad Sci USA 91:9436–9440
16. **Paul RG, Bailey AJ** 1999 The effect of advanced glycation end-product formation upon cell-matrix interactions. Int J Biochem Cell Biol 31:653–660
17. **Baxter RC, Binoux MA, Clemmons DR, Conover CA, Drop SL, Holly JM, Mohan S, Oh Y, Rosenfeld RG** 1998 Recommendations for nomenclature of the insulin-like growth factor binding protein superfamily. Endocrinology 139:4036
18. **Frazier K, Williams S, Kothapalli D, Klapper H, Grotendorst GR** 1996 Stimulation of fibroblast cell growth, matrix production, and granulation tissue formation by connective tissue growth factor. J Invest Dermatol 107:404–411
19. **Grotendorst GR** 1997 Connective tissue growth factor: a mediator of TGF-β action on fibroblasts. Cytokine Growth Factor Rev 8:171–179
20. **Shimo T, Nakanishi T, Kimura Y, Nishida T, Ishizeki K, Matsumura T, Takigawa M** 1998 Inhibition of endogenous expression of connective tissue growth factor by its antisense oligonucleotide and antisense RNA suppresses proliferation and migration of vascular endothelial cells. J Biochem 124:130–140
21. **Babic AM, Chen CC, Lau LF** 1999 Fisp12/mouse connective tissue growth factor mediates endothelial cell adhesion and migration through integrin $\alpha_v\beta_3$, promotes endothelial cell survival, and induces angiogenesis in vivo. Mol Cell Biol 19:2958–2966
22. **Igarashi A, Nashiro K, Kikuchi K, Sato S, Ihn H, Grotendorst GR, Takehara K** 1995 Significant correlation between connective tissue growth factor gene expression and skin sclerosis in tissue sections from patients with systemic sclerosis. J Invest Dermatol 105:280–284
23. **Dammeier J, Brauchle M, Falk W, Grotendorst GR, Werner S** 1998 Connective tissue growth factor: a novel regulator of mucosal repair and fibrosis in inflammatory bowel disease? Int J Biochem Cell Biol 30:909–922
24. **di Mola FF, Friess H, Martignoni ME, Di Sebastiano P, Zimmermann A, Innocenti P, Graber H, Gold LI, Korc M, Buchler MW** 1999 Connective tissue growth factor is a regulator for fibrosis in human chronic pancreatitis. Ann Surg 230:63–71
25. **Yang DH, Kim HS, Wilson EM, Rosenfeld RG, Oh Y** 1998 Identification of glycosylated 38-kDa connective tissue growth factor (IGFBP-related protein 2) and proteolytic fragments in human biological fluids, and up-regulation of IGFBP-rP2 expression by TGF-β in Hs578T human breast cancer cells. J Clin Endocrinol Metab 83:2593–2596
26. **Yamagishi S, Yonekura H, Yamamato Y, Katsuno K, Sato F, Mita I, Ooka H, Satozawa N, Kawakami T, Nomura M** 1997 Advanced glycation end-products driven angiogenesis in vitro: induction of the growth and tube formation of human microvascular endothelial cells through. J Biol Chem 272:8723–8730
27. **Owen Jr WF, Hou FF, Stuart RO, Kay J, Boyce J, Chertow GM, Schmidt AM** 1998 β_2-Microglobulin modified advanced glycation end products modulates collagen synthesis in human fibroblasts. Kidney Int 53:1365–1373
28. **Kislinger T, Fu C, Huber B, Qu W, Taguchi A, Du Yan S, Hofmann M, Yan SF, Pischetsrieder M, Stern D** 1999 $N(\epsilon)$-(Carboxymethyl)lysine adducts of proteins are ligands for receptor for advanced glycation end products that activate cell signaling pathways and modulate gene expression. J Biol Chem 274:31740–31749
29. **Kim HS, Nagalla SR, Oh Y, Wilson E, Roberts Jr CT, Rosenfeld RG** 1997 Identification of a family of low-affinity insulin-like growth factor binding proteins (IGFBPs): characterization of connective tissue growth factor as a member of the IGFBP superfamily. Proc Natl Acad Sci USA 94:12981–12986
30. **Lander HM, Tauras JM, Ogiste JS, Hori O, Moss RA, Schmidt AM** 1997 Activation of the receptor for advanced glycation end products triggers a $p21^{ras}$-dependent mitogen activated protein kinase pathway regulated by oxidant stress. J Biol Chem 272:17810–17814
31. **Lu M, Kuroki M, Amano S, Tolentino M, Keough K, Kim I, Bucala R, Adamis AP** 1998 Advanced glycation end products increase retinal vascular endothelial growth factor expression. J Clin Invest 101:1219–1224
32. **Koschinsky T, He CJ, Mitsuhashi T, Bucala R, Liu C, Buenting C, Heitmann K, Vlassara H** 1997 Orally absorbed reactive glycation products (glycotoxins): an environmental risk factor in diabetic nephropathy. Proc Natl Acad Sci USA 94:6474–6479
33. **Martin JL, Ballesteros M, Baxter RC** 1992 Insulin-like growth factor-I (IGF-I) and transforming growth factor-β1 release IGF-binding protein-3 from human fibroblasts by different mechanisms. Endocrinology 131:1703–1710
34. **Damon SE, Haugk KL, Swisshelm K, Quinn LS** 1997 Developmental regulation of Mac25/insulin-like growth factor-binding protein-7 expression in skeletal myogenesis. Exp Cell Res 237:192–195
35. **Igarashi A, Okochi H, Bradham DM, Grotendorst GR** 1993 Regulation of connective tissue growth factor gene expression in human skin fibroblasts and during wound repair. Mol Biol Cell 4:637–645
36. **Bierhaus A, Illmer T, Kasper M, Luther T, Quehenberger P, Tritschler H, Wahl P, Ziegler R, Muller M, Nawroth PP** 1997 Advanced glycation end product (AGE)-mediated induction of tissue factor in cultured endothelial cells is dependent on RAGE. Circulation 96:2262–2271
37. **Lalla E, Lamster IB, Schmidt AM** 1998 Enhanced interaction of advanced glycation end products with their cellular receptor RAGE: implications for the pathogenesis of accelerated periodontal disease in diabetes. Ann Periodontol 3:13–19
38. **Steffen CL, Ball-Mirth DK, Harding PA, Bhattacharyya N, Pillai S, Brigstock DR** 1998 Characterization of cell-associated and soluble forms of connective tissue growth factor (CTGF) produced by fibroblast cells in vitro. Growth Factors 15:199–213
39. **Munch G, Keis R, Wessels A, Riederer P, Bahner U, Heidland A, Niwa T, Lemke HD, Schinzel R** 1997 Determination of advanced glycation end products in serum by fluorescence spectroscopy and competitive ELISA. Eur J Clin Chem Clin Biochem 35:669–677
40. **Makita Z, Vlassara H, Cerami A, Bucala R** 1992 Immunochemical detection of advanced glycosylation end products *in vivo*. J Biol Chem 267:5133–5138
41. **Al-Abed Y, Bucala R** 2000 Structure of a synthetic glucose derived advanced glycation end product that is immunologically cross-reactive with its naturally occurring counterparts. Bioconjug Chem 11:39–45
42. **Park L, Raman KG, Lee KJ, Lu Y, Ferran Jr LJ, Chow WS, Stern D, Schmidt AM** 1998 Suppression of accelerated diabetic atherosclerosis by the soluble receptor for advanced glycation endproducts. Nat Med 4:1025–1031
43. **Yan SD, Stern D, Schmidt AM** 1997 What's the RAGE? The receptor for advanced glycation end products (RAGE) and the dark side of glucose. Eur J Clin Invest 27:179–181
44. **Duncan MR, Frazier KS, Abramson S, Williams S, Klapper H, Huang X, Grotendorst GR** 1999 Connective tissue growth factor mediates transforming growth factor beta-induced collagen synthesis: down-regulation by cAMP. FASEB J 13:1774–1786
45. **Murphy M, Godson C, Cannon S, Kato S, Mackenzie HS, Martin F, Brady HR** 1999 Suppression subtractive hybridization identifies high glucose levels as a stimulus for expression of connective tissue growth factor and other genes in human mesangial cells. J Biol Chem 274:5830–5834
46. **Riser BL, Denichilo M, Cortes P, Baker C, Grondin JM, Yee J, Narins RG** 2000 Regulation of connective tissue growth factor activity in cultured rat mesangial cells and its expression in experimental diabetic glomerulosclerosis. J Am Soc Nephrol 11:25–38
47. **Ito Y, Aten J, Bende RJ, Oemar BS, Rabelink TJ, Weening JJ, Goldschmeding R** 1998 Expression of connective tissue growth factor in human renal fibrosis. Kidney Int 53:853–861
48. **Oemar BS, Werner A, Garnier JM, Do DD, Godoy N, Nauck M, Marz W, Rupp J, Pech M, Luscher TF** 1997 Human connective tissue growth factor is expressed in advanced atherosclerotic lesions. Circulation 95:831–839
49. **Grotendorst GR, Okochi H, Hayashi N** 1996 A novel transforming growth factor beta response element controls the expression of the connective tissue growth factor gene. Cell Growth Differ 7:469–480
50. **Dammeier J, Beer HD, Brauchle M, Werner S** 1998 Dexamethasone is a novel potent inducer of connective tissue growth factor expression. Implications for glucocorticoid therapy. J Biol Chem 273:18185–18190
51. **Huntley AC** 1989 Cutaneous manifestations of diabetes mellitus. Dermatol Clin 7:531–546
52. **Hanna W, Friesen D, Bombardier C, Gladman D, Hanna A** 1987 Pathologic features of diabetic thick skin. J Am Acad Dermatol 16:546–553
53. **Seibold JR** 1982 Digital sclerosis in children with insulin-dependent diabetes mellitus. Arthritis Rheum 25:1357–1361
54. **Schmidt AM, Yan SD, Wautier JL, Stern D** 1999 Activation of receptor for advanced glycation end products: a mechanism for chronic vascular dysfunction in diabetic vasculopathy and atherosclerosis. Circ Res 84:489–497
55. **Vlassara H, Fuh H, Donnelly T, Cybulsky M** 1995 Advanced glycation endproducts promote adhesion molecule (VCAM-1, ICAM-1) expression and atheroma formation in normal rabbits. Mol Med 1:447–456

517

0013-7227/02/$15.00/0
Printed in U.S.A.

Endocrinology 143(4):1260–1269

Connective Tissue Growth Factor/IGF-Binding Protein-Related Protein-2 Is a Mediator in the Induction of Fibronectin by Advanced Glycosylation End-Products in Human Dermal Fibroblasts

STEPHEN M. TWIGG, ALISON H. JOLY, MICHELLE M. CHEN, JUNKO TSUBAKI, HO-SEONG KIM, VIVIAN HWA, YOUNGMAN OH, AND RON G. ROSENFELD

Department of Pediatrics (S.M.T., J.T., H.-S.K., V.H., Y.O., R.G.R.), Oregon Health Sciences University, Portland, Oregon 97201; and Cardiorenal Cell Biology (A.H.J., M.M.C.), Scios, Inc., Sunnyvale, California 94086

Expansion of extracellular matrix with fibrosis occurs in many tissues, including skin, as part of the end-organ complications in diabetes. Advanced glycosylation end-products (AGEs) have been implicated as a pathogenic factor in diabetic tissue fibrosis. Connective tissue growth factor (CTGF), also known as IGF-binding protein-related protein-2, induces extracellular matrix. We have recently shown that CTGF mRNA and protein are up-regulated by AGE treatment of cultured human dermal fibroblasts. The aim of this study was to determine whether CTGF is an autocrine mediator in the induction of fibronectin (FN) by AGE. Primary cultures of nonfetal human dermal fibroblasts in confluent monolayer were treated with synthesized soluble AGE BSA, 0–200 μg/ml. Analysis of mRNA, by quantitative real-time RT-PCR and conditioned media from treated cultures, showed that FN mRNA was increased by approximately 4-fold at 48 h, and FN protein levels by Western immunoblot and FN ELISA were doubled, compared with control. In the same system, added recombinant human CTGF (0–500 ng/ml) induced FN mRNA and protein levels dose dependently and in a rapid time course. To test whether AGE BSA acts through cell-derived CTGF to induce FN, a CTGF neutralizing antibody was shown to significantly attenuate, but not fully inhibit, the AGE induction of FN mRNA. A pan-specific PKC inhibitor, GF109203X, at 0.2 μM, inhibited the induction of FN mRNA by AGE BSA. Although the same inhibitor did not significantly affect the induction of CTGF mRNA by AGE, it blocked the induction of FN mRNA by recombinant human CTGF. In summary, the induction of FN by AGE is partly mediated by the AGE-induced up-regulation of cell-derived CTGF and is dependent on PKC activity. These results have potential implications for the expansion of extracellular matrix in diabetes mellitus by advanced glycosylation end products. (*Endocrinology* 143: 1260–1269, 2002)

A MECHANISM PROPOSED whereby chronic hyperglycemia contributes to diabetic complications is in the formation of advanced glycosylation end-products (AGEs) (1). AGEs constitute irreversibly formed biochemical end-products of nonenzymatic glycosylation (2) and are elevated in many tissues, including skin (3), in subjects with diabetes (4). One method by which AGEs appear to contribute to pathological end-organ changes that occur in tissues in subjects with diabetes is through the induction of specific cytokines and growth factors, which may act as mediators in causing tissue pathology (5–7).

One hallmark in most tissues in which diabetic complications occur is expansion of extracellular matrix [ECM (8)]. AGEs (7) and increased cellular PKC activity (9) have each been identified as contributors to ECM expansion in diabetes through increased ECM production. An integral component of ECM is the glycoprotein, fibronectin (FN), which acts as a scaffold for collagens, and contributes to an ECM network involved in cell proliferation and migration (10). FN is increased *in vivo* in the ECM expansion that occurs in diabetes (11, 12).

Recently, we have reported that the cytokine, connective tissue growth factor (CTGF), is up-regulated at the mRNA and protein level by AGEs in confluent monolayers of cultured human dermal fibroblasts (13). Also known as IGF-binding protein-related protein-2 [IGFBP-rP2 (14)], CTGF is a potent inducer of ECM, including FN (15), in fibroblasts (16) as well as an angiogenic factor (17, 18). A potential role for CTGF in fibrotic disease states is increasingly being described (19, 20), suggesting that CTGF is a mediator in the ECM expansion and fibrosis occurring in diabetes. To date, the cellular mechanism of action of CTGF in enhancing ECM has been inadequately studied (21).

Because AGEs and CTGF can both up-regulate fibronectin, and AGEs also up-regulate CTGF in human fibroblasts, the aim of this study was to determine whether the induction of FN by AGEs is mediated through up-regulation of endogenous CTGF and to explore the cellular secondary messenger systems involved in mediating this effect on FN expression. Our work shows that CTGF contributes significantly to AGE up-regulation of FN in human dermal fibroblasts, through a PKC-dependent mechanism.

Abbreviations: AGE, Advanced glycosylation end-products; CML, carboxymethyl lysine; CTGF, connective tissue growth factor; ECM, extracellular matrix; FN, fibronectin; IGFBP-rP, insulin-like growth factor binding protein related protein; NRS, normal rabbit serum; rhCTGF, recombinant human connective tissue growth factor.

Materials and Methods

Reagents

The antifibronectin mouse monoclonal antibody against human fibronectin was purchased from Neomarkers Inc. (Union City, CA). Polyclonal anti-IGFBP-rP2 (CTGF) antibody (8800), was generated in New Zealand White rabbits, using full-length human CTGF (IGFBP-rP2) as the immunogen, as previously described (22). The anti-AGE polyclonal antiserum generated in New Zealand White rabbits, which neutralizes the activity of AGE BSA (23), was a generous gift from Dr. Miyata (Kissei Pharmaceutical Co. Ltd., Nagano, Japan). The antisera to human CTGF, and to AGE, as well as nonimmune normal rabbit serum (Sigma, St. Louis, MO) were each affinity purified by protein A affinity chromatography, using protein A-Sepharose (Pharmacia Biotech, Uppsala, Sweden). In each case, the eluted IgG protein was dialyzed against PBS, using a low-molecular-mass-cut-off membrane (Spectrapor 1, 6–8 kDa, Spectrum Industries, Los Angeles, CA), and confirmed to be immunoglobulin by migration characteristics on nonreducing SDS-PAGE, followed by Coomassie staining. The total amount of IgG protein was quantitated using the DC protein assay reagent (Bio-Rad Laboratories, Inc., Hercules, CA) and was further confirmed by spectrophotometer absorbance readings at 280 nm. D-Glucose, BSA (fraction V, fatty acid and endotoxin free), human plasma fibronectin, and aminoguanidine were purchased from Sigma. TGF-β1 was purchased from Austral Biologicals (San Ramon, CA). The pan-specific PKC inhibitor, GF109203X, was purchased from BIOMOL Research Laboratories, Inc. (Plymouth Meeting, PA).

AGE synthesis

Advanced glycosylation end-products were synthesized *in vitro*, following methods previously described (13, 23, 24, 25). BSA (Sigma, RIA grade, fraction V) at 10 mM, was coincubated in sterile PBS with 0.5 M D-glucose for 10 wk, with 1.5 mM phenylmethylsulfonyl fluoride, under aerobic conditions at 37 C. To generate control BSA for comparison with AGE treatments, tubes were prepared with simultaneous incubations under the same conditions without the addition of the D-glucose. Additionally, in parallel preparations, aminoguanidine at 100 mM, as an inhibitor of formation of products of nonenzymatic glycosylation (7), was added to the BSA and glucose. All preparations were extensively dialyzed in PBS, using a low-molecular-mass-cut-off membrane (Spectrapor 1, 6–8 kDa, Spectrum Industries; Ref. 7).

The AGE content in the preparations was assessed by means of fluorescence, SDS-PAGE analysis, and ELISA. The fluorescence content, measured with a fluorescence spectrometer at 390 nm emission after a 450-nm excitation, in relative fluorescence units per milligram of BSA, was 11.2 ± 2.5 for control BSA, 52.3 ± 6.3 for AGE BSA, and 9.7 ± 1.2 for aminoguanidine added to BSA and glucose (termed aminoguanidine BSA) (25). By SDS-PAGE analysis under reducing conditions, followed by Coomassie staining, the AGE BSA produced was shown to have high-molecular-mass species, consistent with the intermolecular cross-linking ability of AGE, as described (23). In contrast, the control BSA and aminoguanidine BSA preparations did not have these high-molecular-mass forms (data not shown). By competitive ELISA [as described in (26)] performed by Dr. P. Foiles (Alteon Inc., Ramsey, NJ), using a synthetic N-ϵ carboxymethyl lysine (CML) analog as the standard, the CML content of the preparations (picomole CML per microgram of BSA ± 95% confidence interval) was: 13 ± 1.4 for AGE BSA from glucose and was undetectable (<1) for control BSA and also undetectable when aminoguanidine at 100 mM was coincubated with BSA and glucose.

Synthesis and purification of recombinant human CTGF

The recombinant human CTGF [rhCTGF (IGFBP-rP2)] protein was produced using a baculovirus expression system (Invitrogen Corp., Carlsbad, CA). The CTGF 1047-bp cDNA open reading frame was cloned from an Hs578T human breast cancer cDNA library and sequenced. The resulting fragment coding for full-length nontagged human CTGF was subcloned into *Bam*HI and *Xho*I sites in the baculovirus recombination vector, pFastBac1 (Life Technologies, Inc., Rockville, MD), and insert presence and orientation were verified by DNA sequencing. Recombinant baculovirus stocks were isolated and produced in increasing titer, as recommended by the supplier of the expression system. The rhCTGF protein was then produced by infecting HIGH Five insect cells with recombinant virus under serum-free conditions and collecting the conditioned media. To purify rhCTGF protein from filtered media, heparin-Sepharose affinity chromatography, using HiTrap columns (Pharmacia Biotech) with a step-up salt gradient in the elution, was employed as previously described (15, 27). Peak fractions containing rhCTGF were determined by Western immunoblotting and CTGF protein was quantitated using Coomassie Blue-stained gels with BSA as standard, as previously described (13, 28).

Cell culture

Primary cell cultures of nonfetal human dermal fibroblasts, CRL-2097, and CRL-1474 were purchased from ATCC (Manassas, VA). Cells were maintained in MEM supplemented with 10% FBS and were used in these studies between passages 4 and 12. The human primary cultures of dermal fibroblasts, designated A35 (derived from the forearm of a 70-yr-old male) and A305 (newborn foreskin fibroblasts) were generous gifts from Dr. S. Goldstein, Memorial Veteran's Hospital (Little Rock, AR). These cells were maintained in DMEM containing 450 mg/dl glucose and 15% FBS.

Cell treatment

After trypsinization, cells were grown in 12-well plates for 5 d in their respective media with FBS until they were confluent. For experiments requiring the use of blocking antibodies to AGE or CTGF, or using control normal rabbit serum IgG, cells were grown in 24-well plates under the same conditions. Cells were then incubated in their respective serum-free media for 16 h and were then treated on d 0 under serum-free conditions using fresh media. Unless otherwise indicated, the conditioned media were not changed after adding the treatments. Cell lysates and conditioned media were harvested up to 3 d after treatments. For experiments involving the use of blocking antibodies or PKC inhibitors, cells were preincubated with the antibody or reagent for 2 h under serum-free conditions before the addition of AGE or control BSA.

Total RNA isolation and analysis by quantitative real-time RT-PCR

Total RNA was isolated from duplicate wells, (RNeasy minikit, QIAGEN, Valencia, CA) and analyzed by quantitative real-time PCR using an ABI Prism 7700 sequence detection system (PE Applied Biosystems, Foster City, CA) as previously described (13, 29). This system is based on the ability of the 5′ nuclease activity of *Taq* polymerase to cleave a nonextendable dual-labeled fluorogenic hybridization probe during the extension phase of PCR. The following sequence specific primers and probes for human CTGF, FN, and 18S rRNA were designed, using Primer Express software 1.0 (PE Applied Biosystems): for FN, forward 5′-TCCTTGCTGGTATCATGGCAG-3′, reverse 5′-AGACCCAGGCTTCTCATACTTGA-3′, and probe 5′-6FAM-CCACGTGCCAGGATTACCGGCTACAT-TAMRA-3′; for CTGF, forward 5′-GAGGAAAACATTAAGAAGGGCAAA-3′, reverse 5′-CGGCACAGGTCTTGATGA-3′, and probe 5′6FAM-TTTGAGCTTTCTGGCTGCACCAGTGT-TAMRA3′; for 18S, forward 5′-CGGCTACCACATCCAAGGAA-3′, reverse 5′-GCTGGAATTACCGCGGCT-3′, and probe 5′-6FAM-TGCTGGCACCAGACTTGCCCTC-TAMRA3′. Primers were used at a concentration of 200 nM and probes at 100 nM in each reaction. Multiscribe reverse transcriptase and Amplitaq gold polymerase (PE Applied Biosystems) were used in all RT-PCR. Each RNA sample was analyzed in triplicate. Relative quantitation of 18S rRNA and human FN and CTGF mRNAs were calculated, using the comparative threshold cycle number for each sample fitted to a five-point standard curve (ABI prism 7700 user bulletin no. 2, PE Applied Biosystems). The standard curve was constructed using a serial dilution of total RNA extracted from human cardiac fibroblasts that had been treated with TGF-β1 at 1 ng/ml for 24 h. Expression levels were normalized to 18S rRNA and related to relevant controls as indicated in the text.

Preparation of conditioned media and cell lysates

Conditioned media were collected after cell treatment and centrifuged at 10,000 × *g* for 10 min at 4 C, and then supernatants from duplicate wells within each experiment were pooled and stored at −20

C until analysis. Cell lysate samples were harvested after treatment by washing cells with PBS and then adding 100 μl cold RIPA lysis buffer (20 mM Tris, pH 8.0, 150 mM NaCl, 1% Nonidet P-40, 0.5% NaDOC, 0.1% SDS) plus a protease inhibitor cocktail (Roche Molecular Biochemicals, Mannheim, Germany) directly to each well. Plates were rocked for 15 min at 4 C, and lysates were collected and centrifuged at 10,000 × *g* for 10 min at 4 C. The supernatants from duplicate wells within each experiment were pooled and stored at −20 C until analysis. Total protein concentration was determined for each sample by use of the DC protein assay reagent (Bio-Rad Laboratories, Inc.). Twenty micrograms of total protein were then loaded per lane for SDS-PAGE analysis.

Western immunoblot analysis

Conditioned media samples were separated on 7.5% nonreducing SDS-PAGE. Proteins were electrotransferred onto nitrocellulose, and membranes were blocked with 5% nonfat dry milk/TBS with 0.1% (vol/vol) Tween 20 for 1 h at 22 C, then incubated overnight, 4 C, in FN antiserum (1:800 dilution; Neomarkers, Inc.). After incubation of membranes with a horseradish peroxidase-labeled secondary antibody for 1 h at 22 C, immunoreactive proteins were detected by use of enhanced chemiluminescence (NEN Life Science Products, Boston, MA).

ELISA for fibronectin

A competitive ELISA was developed based on previously described methods (30). Pure human plasma FN (100 ng/well) in 10 mM sodium carbonate, pH 9.6, was adsorbed to 96-well immunoplates (Nalge Nunc International, Rochester, NY) by a 20-h incubation at 4 C. The wells were then blocked by incubation with PBS, 0.1% (vol/vol) Triton X-100 (buffer A) containing 10 g/liter BSA for 2 h at 37 C, and washed four times with buffer A. Purified human FN in buffer A was used to generate standard curves. Standard and samples (125 μl/tube) were incubated with a limiting amount (1:2500 titer, 0.005 μl/tube) of antifibronectin antibody (Neomarkers, Inc.) at 22 C for 1 h. The plate was then incubated with the FN standards (0–500 ng) and samples (each at 100 μl/well) for 30 min at 22 C. After washing, the plate was incubated with streptavidin horseradish peroxidase at 1:3000 (Sigma) for 30 min at 22 C and, after four more washes in buffer A, with substrate [0.1 g/liter 3,3′,5,5′-tetramethyl benzidine in 0.2 M sodium acetate, pH 6, containing 0.06% (wt/wt) H_2O_2] for 10 min at 22 C. The reaction was stopped by the addition of 2 M H_2SO_4, and the absorbance was measured at 450 nm using a microplate reader. Linearity in the assay was achieved over the range of 15–250 ng/well of FN.

Densitometric analysis

To quantify the relative induction of FN following SDS-PAGE and Western immunoblotting, densitometric measurement was performed using GS-700 imaging densitometer with MultiAnalyst Software (Bio-Rad Laboratories, Inc.).

Statistical analysis

Results are expressed as mean ± SD or mean ± SEM as indicated. Differences between groups were assessed using a two-tailed paired *t* test in Microsoft Corp. (Redmond, WA) Excel 98, where shown. A level of $P < 0.05$ was considered statistically significant.

Results

To determine whether FN mRNA steady-state levels are up-regulated by AGE in primary cultures of human dermal fibroblasts, confluent monolayers of CRL-2097 fibroblasts were treated with soluble AGE BSA under serum-free conditions. In response to 100 μg/ml of AGE BSA, an increase in FN mRNA was observed at 24 h of AGE treatment, and a progressive increase occurred over the 3-d time course of the study (Fig. 1A). In contrast, no change in FN mRNA over time was seen after treatment with the same concentration of control BSA (Fig. 1A). A dose-response study with AGE BSA

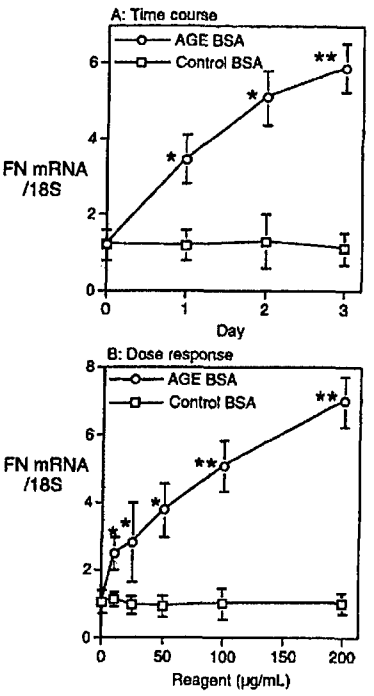

FIG. 1. Time course and dose-response induction of FN mRNA by AGE BSA. Soluble AGE BSA or control BSA was added in fresh media to duplicate wells of confluent primary cultures of human fibroblasts (CRL-2097) under serum-free conditions. Total RNA was collected, and FN mRNA was determined by quantitative RT-PCR in triplicate for each sample, as described in *Materials and Methods*. The FN mRNA level is expressed in arbitrary units normalized to 18S. A, Time course from 1 to 3 d, with AGE BSA or control BSA treatment, each at 100 μg/ml. B, Dose response with AGE BSA or control BSA from 0 to 200 μg/ml added to wells followed by RNA collection at 48 h. The mean of three independent experiments ± 1 SD is shown in A and B. *, $P < 0.05$; **, $P < 0.01$ *vs.* the respective control BSA.

from 0 to 200 μg/ml in 2097 cells, with continuous AGE treatment and RNA collection at 48 h after initial AGE addition, showed that increases in FN mRNA were detectable using 10 μg/ml or greater AGE BSA, but increasing concentrations of control BSA did not show any change in FN mRNA in comparison with no addition (Fig. 1B).

Formation of products of nonenzymatic glycosylation are inhibited by the dihydrazine compound aminoguanidine (7). When cells were treated with BSA that had been coincubated for 10 wk with both glucose and aminoguanidine, as described in *Materials and Methods*, no increase in FN mRNA was observed, compared with control BSA treatment alone or with serum-free media without any addition (Fig. 2A). This result confirms that the active component in the AGE reagent used is a product of nonenzymatic glycosylation. As a positive control reagent in this system for the induction of FN, TGF-β1 (1 ng/ml) was also seen to induce FN mRNA (Fig. 2A).

To determine whether early or advanced glycosylation end-products mediate the effect of the AGE reagent on FN in this cell system, cells were preincubated with anti-AGE IgG before addition of the AGE reagent. Using the anti-AGE antibody, the AGE induction of FN mRNA was inhibited on average by 81% (Fig. 2B). In contrast, normal rabbit serum

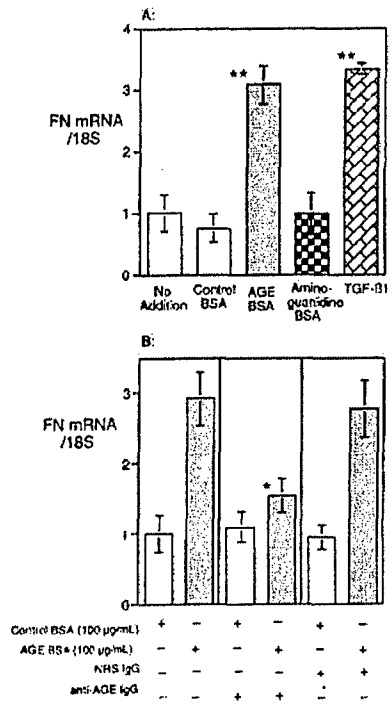

FIG. 2. AGE effect on FN mRNA occurs through nonenzymatic glycosylation of BSA and is blocked by an anti-AGE-neutralizing antibody. A, Soluble AGE BSA or control BSA at 100 μg/ml, or no treatment, was added to duplicate wells of confluent primary cultures of human fibroblasts under serum-free conditions. In other wells BSA that had previously been coincubated with glucose and aminoguanidine before dialysis, termed aminoguanidine BSA, as described in *Materials and Methods*, was added. Treatment with TGF-β1 (1 ng/ml) as a positive control is shown for comparison. Total RNA was collected at 48 h, and FN mRNA was determined by quantitative RT-PCR in triplicate for each sample. The FN mRNA level is expressed in arbitrary units. The mean ± SD of three independent experiments is shown. **, $P < 0.01$ *vs.* no addition, control BSA, and aminoguanidine BSA. In B, wells were preincubated with anti-AGE polyclonal neutralizing IgG, at 100 μg/ml IgG or 100 μg/ml NRS IgG for 2 h. Soluble AGE BSA or control BSA at 100 μg/ml was then added to the wells. Total RNA was collected at 48 h and FN mRNA determined by quantitative RT-PCR in triplicate for each sample. The means ± 1 SD of four independent experiments are shown. *, $P < 0.05$ *vs.* AGE BSA added alone.

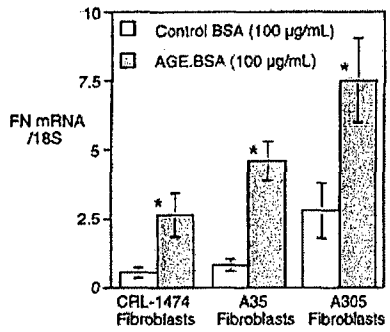

FIG. 3. AGE BSA effects on FN mRNA are observed in human skin fibroblasts. Soluble AGE BSA or control BSA at 100 μg/ml was added to duplicate wells of confluent primary cultures of human skin fibroblasts from multiple donors under serum-free conditions, and total RNA was collected at the time points shown. FN mRNA was then determined by quantitative RT-PCR in triplicate for each sample. The FN mRNA level is expressed in arbitrary units, normalized to 18S. The donor age and skin site of the fibroblasts studied are: 7-yr-old male abdomen (CRL-1474); 70-yr-old male forearm (A35); and newborn foreskin (A305). The means ± 1 SD of three independent experiments are shown.

had no effect (Fig. 2B). Because the anti-AGE antibody is specific for AGE and does not bind to Amadori products (23), which are early products of nonenzymatic glycosylation, these results showed that AGE is the active component in the synthesized reagent responsible for increasing FN in these studies.

To test whether the changes seen in FN mRNA in human foreskin fibroblast CRL-2097 cells after AGE treatment can also be observed in human dermal fibroblasts, primary human skin fibroblasts from other donors were studied. When these other cells were treated with 100 μg/ml of AGE BSA, increases in FN mRNA were observed 48 h after treatment, compared with control BSA, in all of the fibroblast cell lines studied, whether they were derived from neonatal foreskin (A305), a child's abdomen (CRL-1474), or the forearm of a mature adult (A35) (Fig. 3).

The 2097 fibroblasts were used in all subsequent experiments. The addition of pure rhCTGF protein (500 ng/ml) caused an induction of FN mRNA. Up-regulation was observed at 24 h and 48 h after reagent addition (Fig. 4A). In a parallel fashion, CTGF mRNA was autoinduced by rhCTGF treatment (Fig. 4A). Such autoinduction of CTGF mRNA, observed with the addition of recombinant CTGF protein, is consistent with a similar effect of added CTGF protein previously described in cultured rodent renal mesangial cells (27). A dose-response study from 0 to 500 ng/ml rhCTGF showed that statistically significant increases in FN mRNA at 24 h after treatment occurred when 100 ng/ml or more rhCTGF protein was added to the conditioned media (Fig. 4B). In parallel with the induction observed for FN, a dose-response induction of CTGF mRNA by added rhCTGF was also seen with a statistically significant increase occurring from 250 ng/ml added protein (Fig. 4B).

To determine whether AGE and rhCTGF treatment up-regulated FN protein levels, conditioned media were collected and analyzed by Western immunoblots and by FN ELISA. Immunoblot analysis indicated that in the presence of no addition, with serum free media alone, basal levels of FN protein accumulated in the conditioned media (Fig. 5A), a finding that has been observed by others in human fibroblasts (28). After treatment with rhCTGF, increased FN protein, compared with the no addition control, was detected in a time- and dose-dependent manner (Fig. 5, A and B). The addition of control BSA resulted in an accumulation of soluble FN protein (Fig. 5C). Over the 3 d of the study, after treatment of cells with AGE BSA, FN protein levels were further increased above that of the control BSA (Fig. 5C). In whole-cell lysates, an increase in FN protein was also observed after rhCTGF and AGE treatment, compared with either no addition or control BSA (data not shown). Quantitation by FN ELISA confirmed the media Western immunoblot results (Fig. 5, D through E). FN protein in conditioned media after 48 h treatment with 500 ng/ml rhCTGF was approximately 1.6-fold higher than in cells in which serum-free media were added alone (Fig. 5D). Increases in FN media

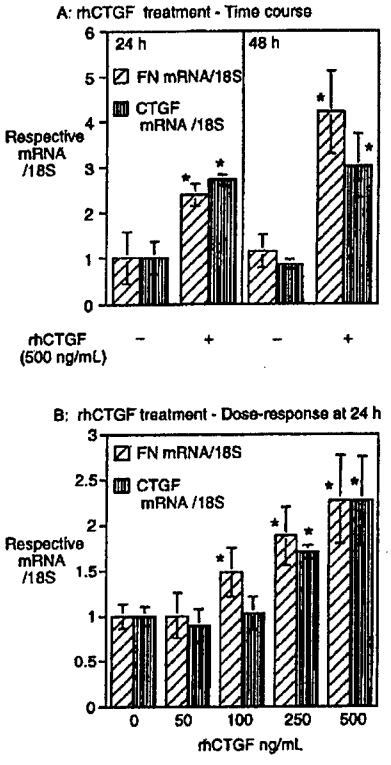

FIG. 4. Induction of FN mRNA and CTGF mRNA autoinduction by soluble rhCTGF. RhCTGF was added to human foreskin fibroblasts (2097 cells) under serum-free conditions. Total RNA was collected and FN mRNA and CTGF mRNA were both analyzed in A and B by quantitative RT-PCR in triplicate for each sample, with correction in each sample for 18S. A, Time course over 2 d, at 500 ng/ml rhCTGF. B, Dose-response induction of FN mRNA and CTGF mRNA using 0–500 ng/ml rhCTGF with isolation of total RNA at 48 h. The means ± 1 SD of four independent experiments are shown in A and B. *, $P < 0.05$ *vs.* no addition on the same curve.

protein by ELISA after AGE treatment peaked at 1.9-fold at 48 h and remained significant at 72 h at 1.4-fold (Fig. 5E). The progressive accumulation of soluble FN protein in the media seen after control BSA addition did not differ statistically from that of the no reagent addition, serum-free control (Fig. 5, D and E). When measured by ELISA in media derived from three independent experiments in which both controls were studied, the FN protein level averaged 2.49 μg/ml at 24 h by no addition and 1.95 μg/ml after control BSA addition and 5.04 μg/ml at 48 h by no addition and 4.11 μg/ml at 48 h after control BSA addition. Thus, after both AGE and CTGF treatment, the increases in FN-soluble protein were increased above the controls, and these increases were somewhat less marked than the observed increases in FN mRNA.

We have recently reported that in the same dermal fibroblast system and under the same cell culture conditions, AGE BSA induces up-regulation of CTGF mRNA and protein (13). Increases in CTGF mRNA were detectable from 8 h onward after AGE addition to the media and became most marked after 72 h of AGE treatment and were seen using 10 μg/ml or more of the AGE BSA (13). Increases in CTGF protein in the conditioned media were detectable within 24 h of AGE treatment and continued to increase for the study duration of 72 h (13).

Based on our present observation that both AGE and rhCTGF up-regulate FN and that AGE increases endogenous CTGF in fibroblasts, we tested whether cell-derived CTGF, in an autocrine manner, is a contributor to the observed increase in FN mRNA following AGE treatment. Using an IgG affinity purified fraction of polyclonal antibody against rhCTGF, the induction of FN at 48 h by exogenously added rhCTGF (250 ng/ml) was fully inhibited (Fig. 6A). In contrast, no inhibition of FN mRNA up-regulation by rhCTGF occurred when the same amount of normal rabbit serum IgG was added exogenously to cells (Fig. 6A). In other experiments, the anti-CTGF antibody inhibited rhCTGF-induced increases in FN mRNA after 24 h of rhCTGF treatment (data not shown). In addition, the autoinduction of CTGF mRNA by rhCTGF, described in Fig. 4, was fully blocked by the CTGF antibody (data not shown). These results confirm that the anti-CTGF antibody specifically neutralizes the bioactivity of CTGF in this system.

The ability of the CTGF-neutralizing antibody to block AGE induction of FN mRNA was then assessed. When the CTGF antibody was added before AGE treatment of cells, the induction of FN mRNA at 48 h by AGE, was attenuated by about 42%, compared with no IgG addition (Fig. 6A). In contrast to the effect of the anti-CTGF IgG, the same amount of normal rabbit serum IgG had no obvious effects (Fig. 6A). A longer-term protocol to 96 h was then performed, with the anti-CTGF IgG or normal rabbit serum IgG also added at 48 h (Fig. 6B). These studies showed that anti-CTGF IgG abrogated the induction of FN mRNA by AGE by about 82% at 96 h, compared with the effect of normal rabbit serum IgG (Fig. 6B). Higher concentrations of CTGF antibody and more frequent treatments did not produce any greater inhibitory effect on AGE induction of FN (data not shown). These data show that endogenous CTGF contributes to the induction of FN by AGE in this cell system.

Recent studies have implicated PKC in the induction of FN in a diabetic environment (12, 31). Because AGE can regulate PKC isoforms in some systems (32), we tested whether PKC activity might be involved in the induction of FN by AGE and/or by rhCTGF. Cells were preincubated with a PKC inhibitor for 2 h, followed by addition of reagent (rhCTGF or AGE), and total RNA was collected at 48 h. Preincubation of cell monolayers with the pan-specific PKC inhibitor GF109203X at 0.2 μM caused an inhibition of AGE induction of FN mRNA by about 72% (Fig. 7A). In contrast, there was no statistically significant inhibition of CTGF mRNA induction by AGE (Fig. 7B). In a similar manner, preincubation of cells with GF109203X reduced rhCTGF induction of FN mRNA to basal levels (Fig. 7C). Autoinduction of CTGF mRNA by rhCTGF, however, was not significantly inhibited by preincubation with GF109203X (Fig. 7D). The effects of GF109203X were observed at relatively low concentrations (0.2 μM), consistent with specificity of this inhibitor for PKC isoforms (33). In addition, no significant effects on basal (unstimulated) FN mRNA were observed, suggesting that the PKC blocker was specifically inhibiting the activity of these reagents on FN mRNA induction (Fig. 7, A and C). No further specific inhibitory effects on FN mRNA or CTGF mRNA were seen with higher concentrations (up to 5 μM) of GF109203X (data not shown). These results indicate that in

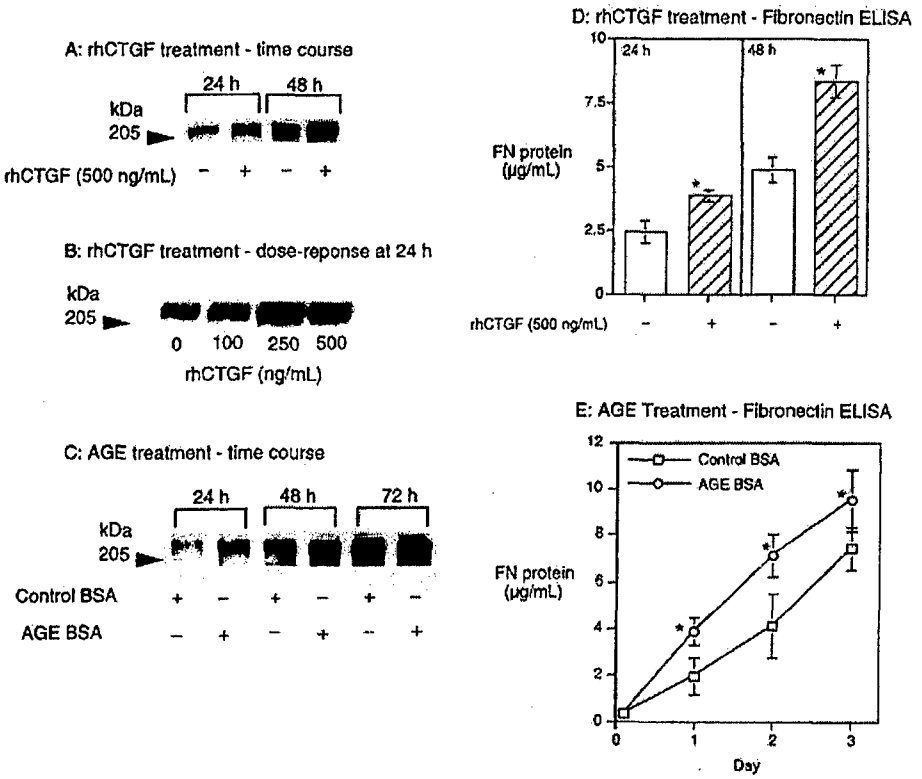

FIG. 5. Increases in FN protein in conditioned media by AGE and rhCTGF. Duplicate wells of confluent primary cultures of human fibroblasts (CRL-2097) under serum-free conditions were incubated with rhCTGF (500 ng/ml) for 24–48 h (A) and increasing amounts of rhCTGF (0–500 ng/ml) for 24 h (B). Conditioned media were analyzed for FN immunoreactivity by Western immunoblot after SDS-PAGE under reducing conditions. C, Cells cultured as in A were treated with AGE BSA or control BSA at 100 µg/ml for 24–72 h, and then FN immunoreactivity was detected in the conditioned media by Western immunoblot. For A–C, molecular mass markers are shown to the left of the figure, and representative immunoblots are shown from three experiments, each showing equivalent results. D, Media levels of FN measured by FN ELISA, as described in *Materials and Methods*, after treatment of cells with rhCTGF for 24 and 48 h, compared with no addition. *, $P < 0.05$ *vs.* no addition on the respective day. E, Media levels of FN measured by FN ELISA, after treatment of cells with AGE BSA or control BSA each for 24–72 h. *, $P < 0.05$ for AGE BSA *vs.* control BSA on the respective day. For D and E, data shown are means ± 1 SD from three independent experiments.

this cell system, cellular PKC activity is required for optimal induction of FN mRNA by both AGE and rhCTGF but not for the induction of CTGF mRNA by either AGE or rhCTGF.

Discussion

This study describes the stimulation of FN mRNA and protein following treatment of human skin fibroblasts with advanced glycosylation end-products and with rhCTGF and the demonstration that CTGF contributes to AGE up-regulation of FN mRNA. The effect of the synthesized AGE reagent on FN mRNA induction was seen to be caused by products of nonenzymatic glycosylation because coincubation of aminoguanidine, an inhibitor of nonenzymatic glycosylation, with glucose and BSA did not affect FN mRNA, and no effect was seen with control BSA alone. The up-regulation of FN mRNA in this cell model by the synthesized AGE reagent was mediated by AGE rather than by earlier products of nonenzymatic glycosylation, such as Amadori products, because the use of an antibody specific for AGE, which does not bind Amadori products, inhibited the AGE induction of FN gene expression. The increase in soluble FN protein in this system by AGE and rhCTGF were greater than the accumulation of FN protein over time, which was seen in the presence of either no addition or after the addition of control BSA.

The up-regulation of FN by AGE is generalizable to skin fibroblasts from differing sources and passage number. In each of the four fibroblast cell lines studied, AGE up-regulated FN. In the cell line most extensively studied, CRL-2097, FN was regulated by AGE in early passages (passage 4) and also at later passage (passage 12). The concentrations of AGE BSA used in these experiments approximate those used *in vitro* in other studies exploring biological effects of AGE on cells (7, 34). In addition to AGE BSA synthesized from glucose, we have also synthesized AGE BSA from glycolaldehyde as substrate (13) and have confirmed that AGE synthesized from glycolaldehyde also induces FN mRNA (data not shown). BSA was used as the protein for synthesizing AGE adduct because it is highly purified and delipidated and has commonly been used in AGE experiments by others (23–25). We have not yet studied other proteins made from AGE, such as AGE synthesized using extracellular matrix proteins. Few AGE components have to date been defined biochemically, and the specific glycosylation end-product(s) that might be mediating the effect on FN were not identified in this work.

Recent studies using AGE in human dermal fibroblasts have focused on AGE effects on type 1 collagen, rather then FN. These reports have shown that in contrast to the observed up-regulation of FN by AGE BSA in the current work, type 1 collagen mRNA and protein synthesis were inhibited by soluble AGE BSA treatment (35). This prior report and the current work are not inconsistent because regulation of FN and type 1 collagen gene transcription differs. Specifically, epidermal growth factor receptor activation, which was shown to mediate AGE inhibition of type 1 collagen gene expression in the previous work (35), is known to have a role in positively regulating FN transcriptional activity in fibroblasts (36, 37). What role the epidermal growth factor receptor may play in AGE up-regulation of FN, possibly in cooperation with CTGF, is an important topic to address in future studies.

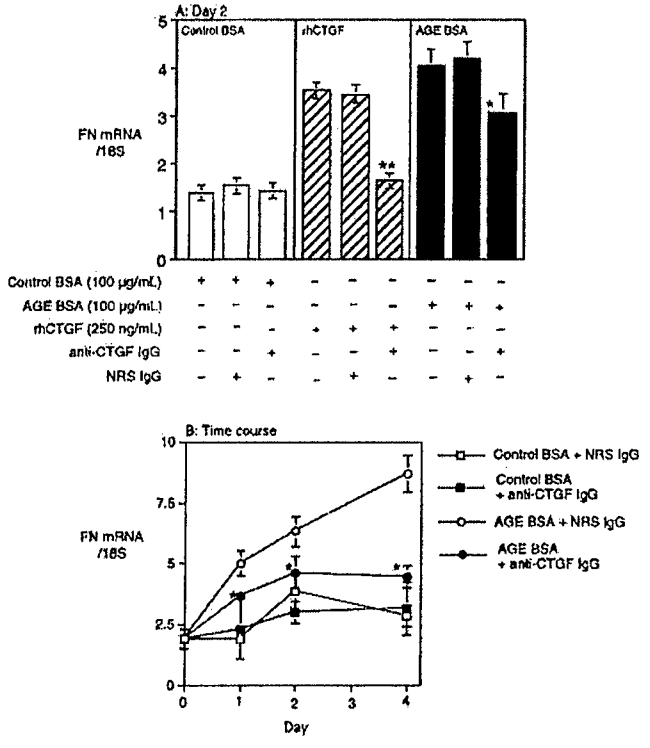

FIG. 6. AGE induction of FN mRNA is partly mediated by endogenous CTGF. A, Duplicate wells of confluent primary cultures of human fibroblasts (CRL-2097) under serum-free conditions were preincubated with anti-CTGF IgG (40 µg/ml), NRS-derived IgG (40 µg/ml), or no IgG. Then AGE BSA or control BSA each at 100 µg/ml or rhCTGF (250 ng/ml) was added. Total RNA was collected 48 h later and FN mRNA analyzed by real-time quantitative RT-PCR. The mRNA levels are expressed in arbitrary units. The means ± 1 SD of four independent experiments are shown. **, $P < 0.01$ for rhCTGF with no IgG addition *, $P < 0.05$ *vs.* AGE BSA with no IgG addition. B, The same protocol was followed as in A, except that a further addition of anti-CTGF IgG or NRS IgG, each at 40 µg/ml, was made to the media bathing the cells, followed by RNA collection at 96 h and analysis for FN mRNA. Results are the means ± 1 SD from two independent experiments. *, $P < 0.05$; **, $P < 0.01$ for AGE BSA with anti-CTGF IgG preincubation *vs.* AGE BSA with preincubation of NRS IgG, on the respective day.

CTGF is known to induce FN and to be profibrotic (16). The concentrations of soluble CTGF recombinant protein required in this cell system to induce FN mRNA and protein, at and above 100 ng/ml of rhCTGF, appear higher than others have employed in human fibroblasts (15). It is possible that the purified rhCTGF used in the current study is somewhat less bioactive than endogenous CTGF protein and that used by other groups and/or that quantitation of the purified protein differs between groups. Nonetheless, the current work shows that added CTGF induces FN mRNA and protein in this cell system. That the anti-CTGF IgG specifically and completely blocked FN induction by rhCTGF indicates that this antibody is efficient at blocking CTGF effects on the fibroblast cells. This same antibody was then seen to significantly attenuate AGE induction of FN in a specific manner.

This is the first study demonstrating that CTGF is a mediator in the induction of ECM by AGE, and it provides a potentially important link among AGE, growth factors, and fibrosis. The CTGF neutralizing antibody studies do not implicate CTGF as the only mediator of AGE induction of FN: that AGE induction of FN was only partially inhibited by CTGF-neutralizing IgG also implicates CTGF-independent pathways in AGE-induced increases in FN. We have previously reported that in the same system, a TGF-β1 neutralizing antibody did not inhibit the induction of AGE by CTGF and that total TGF-β1 levels were not detectably increased over the time course of the study (13). These results suggest that TGF-β1 is not involved in the role played by CTGF in contributing to the AGE induction of fibronectin in this cell system. Up-regulation of CTGF in tissues in rodent models of diabetic nephropathy has recently been reported (27, 38). Although AGE has been shown to up-regulate FN *in vivo* (12), AGE as a reagent has not yet been reported *in vivo* to induce CTGF mRNA or protein. In contrast to our experimental model, AGE appears to accumulate slowly *in vivo*, particularly in long-lived proteins (1, 2), and *in vivo* studies are now required to further substantiate a role for CTGF in mediating diabetic and, specifically, AGE-related ECM expansion.

Up-regulation of PKC activity and PKC isoforms in a diabetic environment has been shown *in vitro* and *in vivo* in cells and in tissues that are susceptible to diabetic complications (31), and inhibition of PKC activity may attenuate chronic diabetes-related events (12). Although effects on PKC activity have been well described for high extracellular D-glucose (9) and early products of nonenzymatic glycosylation (39, 40), only recently has AGE been implicated in up-regulating PKC activity (32) and potentially using PKC pathways in inducing diabetic complications (41), indicating that the pathological effects of AGE and PKC on tissues may be interrelated at the level of induction of PKC by AGE. In addition, PKC pathways have been shown to regulate FN induction in various cell types, including human fibroblasts (30). The PKC inhibitor concentrations of GF109203X used in the current work (0.2 µM) are consistent with the published amounts required for specifically blocking PKC activity of both conventional and novel PKC isoforms (33). Although the isoform(s) of PKC that is mediating the effect of AGE on FN remains to be described, this study demonstrates a link between AGE and PKC in human dermal fibroblasts, two major proposed mechanisms involved in the pathogenesis of diabetic complications.

The intracellular second messenger systems mediating the up-regulation of ECM by CTGF have been studied to a limited extent only. Inhibition of the induction of type 1 collagen by cAMP in human dermal fibroblasts has been described without evidence of regulation by cellular PKC activity (42). Second messenger systems affecting the previously observed up-regulation of FN mRNA by rhCTGF in human fibroblasts (15) have not been reported before this work. The current studies show that the induction of FN mRNA by rhCTGF is fully blocked by a pan-specific PKC inhibitor in this cell system. These data using the PKC inhibitor do not indicate the number of cellular signaling intermediates involved and the sequence of the effect. Further work is needed to better define the second messenger pathways involved, and the specific PKC isoform(s) mediating the effect is also part of an ongoing study. CTGF cellular signaling in fibroblast cells has

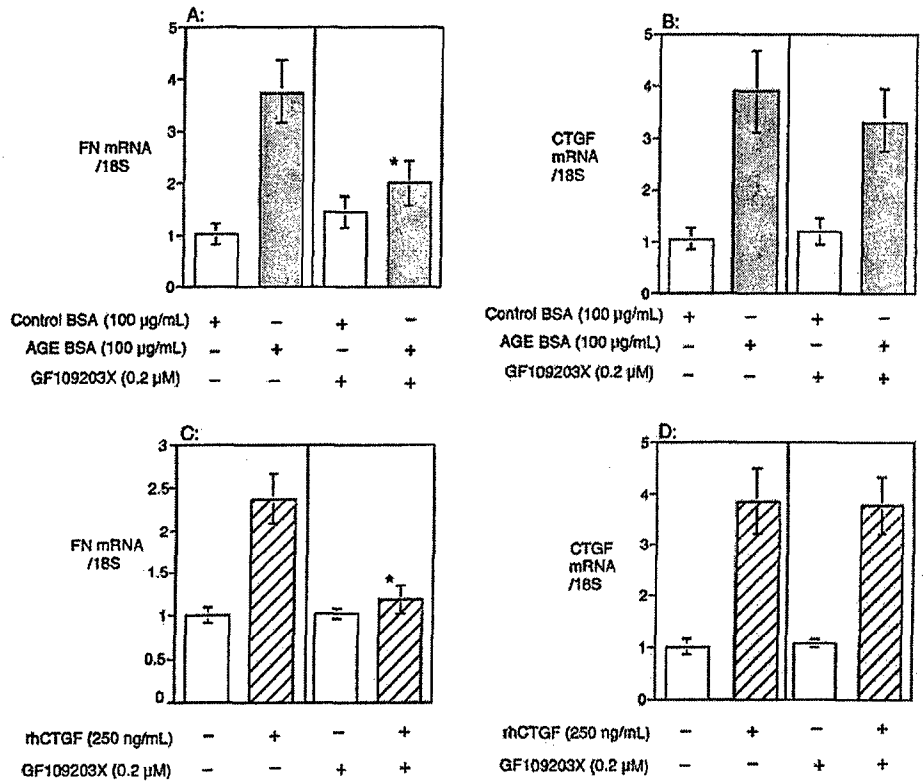

FIG. 7. FN mRNA up-regulation by AGE BSA and by rhCTGF is blocked by the pan-specific PKC inhibitor, GF109203X. A, Duplicate wells of confluent primary cultures of human fibroblasts (CRL-2097) under serum free conditions were preincubated for 2 h in the presence or absence of the PKC inhibitor GF109203X (0.2 μM). Then AGE or control BSA (each at 100 μg/ml) in A and B or rhCTGF (250 ng/ml) in C and D was added, and RNA was collected at 48 h. FN mRNA in A and C and CTGF mRNA in B and D, each analyzed by real-time quantitative RT-PCR and corrected for 18S are shown. For A–D, the means ± 1 SD of three independent experiments are shown. *, $P < 0.05$ *vs.* same reagent addition but with no addition of GF109203X.

been linked to CTGF-induced activation of cell surface receptors, such as the platelet-derived growth factor receptor (43) and, when in solid phase, the integrin receptor, $\alpha_6\beta_1$ (44). Which of these receptors, if any, is involved in FN up-regulation by CTGF, through a PKC-dependent mechanism, will require further study.

Recently, PKC activity has been shown to regulate CTGF mRNA in fibroblasts. A previous report showed that blocking conventional and novel PKC isoform activity in combination by using GF109203X and other PKC inhibitors, or PKC depletors, caused an induction of CTGF mRNA under conditions of high FCS in the conditioned media (45). The FCS content likely contributed to prominent basal PKC activity and the detection of the inhibition of CTGF gene expression by basal PKC activity (46). That only a slight and nonsignificant induction of CTGF mRNA was observed by GF109203X in the current study in the basal state (Fig. 7) may reflect low cellular PKC activity in these serum-deprived cells. Low PKC activity under serum-free conditions has been observed previously by other groups (47). As well as having no significant effect in the basal state, GF109203X also did not significantly affect the autoinduction of CTGF mRNA by rhCTGF in the current work (Fig. 7D).

The finding that CTGF is a mediator in AGE induction of FN *in vitro* may have relevance in diabetic complications. Based on previous work, there is a rationale to potentially link AGE effects and diabetic complications with the induction of CTGF and ECM in skin and, by association, with pathology in other tissues. A feature commonly present in human diabetes is skin thickening and contracture, termed diabetic sclerosis. This affects mainly the distal extremities and is characterized by expansion of extracellular matrix, fibroblast proliferation, and angiogenesis (48). The presence of overt diabetic sclerosis of skin is correlated with the presence and future development of other end-organ complications (49). AGE products are increased in human diabetic skin (3) as is FN (50, 51), and the levels of AGE in skin also correlate positively with the presence of diabetic microvascular kidney and eye disease (3, 4). That the ability of CTGF to induce fibrosis has been well characterized in skin (15, 42) makes skin fibroblasts a relevant cell model for the current study.

Our work provides potential links in diabetic complications characterized by ECM expansion. Interactions between AGE effects and PKC activity have been described, and AGE induced up-regulation of the profibrotic agent CTGF, which itself contributes to AGE-induced ECM expansion through a PKC-dependent mechanism, has been observed. This work contributes toward further understanding mechanisms involved in the development of chronic diabetes complications, particularly those characterized by ECM expansion and fibrosis.

Acknowledgments

We thank Alteon, Inc. (Ramsey, NJ) for measuring the CML adduct concentration in the AGE reagent by their CML ELISA. The generous gift of the anti-AGE antiserum from Dr. Miyata at Kissei Pharmaceutical Co. Ltd. (Hotaka, Japan) is gratefully acknowledged.

Received August 27, 2001. Accepted December 12, 2001.

Address all correspondence and requests for reprints to: Stephen M. Twigg, Kolling Institute of Medical Research, Royal North Shore Hos-

pital, Pacific Highway, St. Leonards, New South Wales 2065, Australia. E-mail: stwigg@med.usyd.edu.au.

This work was supported by National Health and Medical Research Council of Australia (S.M.T., C. J. Martin Postdoctoral Fellowship); NIH Grants CA-58110 and DK-51513 and U.S. Army Medical Research Grant DAMD 17-00-1-0042 (to R.G.R.); and American Cancer Society Grant RPG-99-103-01-TBE (to Y.O.).

References

1. **Friedman EA** 1999 Advanced glycosylated end products and hyperglycemia in the pathogenesis of diabetic complications. Diabetes Care 22(Suppl 2): B65–B71
2. **Bierhaus A, Hofmann MA, Ziegler R, Nawroth PP** 1998 AGEs and their interaction with AGE-receptors in vascular disease and diabetes mellitus. I. The AGE concept. Cardiovasc Res 37:586–600
3. **Sell DR, Lapolla A, Odetti P, Fogarty J, Monnier VM** 1992 Pentosidine formation in skin correlates with severity of complications in individuals with long-standing IDDM. Diabetes 41:1286–1292
4. **Beisswenger PJ, Makita Z, Curphey TJ, Moore LL, Jean S, Brinck-Johnsen T, Bucala R, Vlassara H** 1995 Formation of immunochemical advanced glycosylation end products precedes and correlates with early manifestations of renal and retinal disease in diabetes. Diabetes 44:824–829
5. **Vlassara H** 1992 Receptor-mediated interactions of advanced glycosylation end products with cellular components within diabetic tissues. Diabetes 41(Suppl 2):52–56
6. **Hirata C, Nakano K, Nakamura N, Kitagawa Y, Shigeta H, Hasegawa G, Ogata M, Ikeda T, Sawa H, Nakamura K, Ienaga K, Obayashi H, Kondo M** 1997 Advanced glycation end products induce expression of vascular endothelial growth factor by retinal Muller cells. Biochem Biophys Res Commun 236:712–715
7. **Pugliese G, Pricci F, Romeo G, Pugliese F, Mene P, Giannini S, Cresci B, Galli G, Rotella CM, Vlassara H, Di Mario U** 1997 Upregulation of mesangial growth factor and extracellular matrix synthesis by advanced glycation end products via a receptor-mediated mechanism. Diabetes 46:1881–1887
8. **King GL, Wakasaki H** 1999 Theoretical mechanisms by which hyperglycemia and insulin resistance could cause cardiovascular diseases in diabetes. Diabetes Care 22:C31–C37
9. **Koya D, King GL** 1998 Protein kinase C activation and the development of diabetic complications. Diabetes 47:859–866
10. **Hynes RO** 1986 Fibronectins. Sci Am 254:42–51
11. **Asselot C, Labat-Robert J, Kern P** 1989 Heparin fragments regulate collagen phenotype and fibronectin synthesis in the skin of genetically diabetic mice. Biochem Pharmacol 38:895–899
12. **Koya D, Haneda M, Nakagawa H, Isshiki K, Sato H, Maeda S, Sugimoto T, Yasuda H, Kashiwagi A, Ways DK, King GL, Kikkawa R** 2000 Amelioration of accelerated diabetic mesangial expansion by treatment with a PKCβ inhibitor in diabetic *db/db* mice, a rodent model for type 2 diabetes. FASEB J 14:439–447
13. **Twigg SM, Chen MM, Joly AH, Chakrapani SD, Tsubaki J, Kim H-S, Oh Y, Rosenfeld RG** 2001 Advanced glycosylation end-products up-regulate connective tissue growth factor (IGFBP-rP2) in human fibroblasts: a potential mechanism for expansion of extracellular matrix in diabetes mellitus. Endocrinology 142:1760–1769
14. **Baxter RC, Binoux MA, Clemmons DR, Conover CA, Drop SL, Holly JM, Mohan S, Oh Y, Rosenfeld RG** 1998 Recommendations for nomenclature of the insulin-like growth factor binding protein superfamily. Endocrinology 139:4036
15. **Frazier K, Williams S, Kothapalli D, Klapper H, Grotendorst GR** 1996 Stimulation of fibroblast cell growth, matrix production, and granulation tissue formation by connective tissue growth factor. J Invest Dermatol 107:404–411
16. **Grotendorst GR** 1997 Connective tissue growth factor: a mediator of TGF-β action on fibroblasts. Cytokine Growth Factor Rev 8:171–179
17. **Shimo T, Nakanishi T, Kimura Y, Nishida T, Ishizeki K, Matsumura T, Takigawa M** 1998 Inhibition of endogenous expression of connective tissue growth factor by its antisense oligonucleotide and antisense RNA suppresses proliferation and migration of vascular endothelial cells. J Biochem (Tokyo) 124:130–140
18. **Babic AM, Chen CC, Lau LF** 1999 Fisp12/mouse connective tissue growth factor mediates endothelial cell adhesion and migration through integrin αvβ3, promotes endothelial cell survival, and induces angiogenesis *in vivo*. Mol Cell Biol 19:2958–2966
19. **Igarashi A, Nashiro K, Kikuchi K, Sato S, Ihn H, Grotendorst GR, Takehara K** 1995 Significant correlation between connective tissue growth factor gene expression and skin sclerosis in tissue sections from patients with systemic sclerosis. J Invest Dermatol 105:280–284
20. **Dammeier J, Brauchle M, Falk W, Grotendorst GR, Werner S** 1998 Connective tissue growth factor: a novel regulator of mucosal repair and fibrosis in inflammatory bowel disease? Int J Biochem Cell Biol 30:909–922
21. **Gupta S, Clarkson MR, Duggan J, Brady HR** 2000 Connective tissue growth factor: potential role in glomerulosclerosis and tubulointerstitial fibrosis. Kidney Int 58:1389–1399
22. **Yang DH, Kim HS, Wilson EM, Rosenfeld RG, Oh Y** 1998 Identification of glycosylated 38-kDa connective tissue growth factor (IGFBP-related protein 2) and proteolytic fragments in human biological fluids, and up-regulation of IGFBP-rP2 expression by TGF-β in Hs578T human breast cancer cells. J Clin Endocrinol Metab 83:2593–2596
23. **Yamagishi S, Yonekura H, Yamamato Y, Katsuno K, Sato F, Mita I, Ooka H, Satozawa N, Kawakami T, Nomura M, Yamamato H** 1997 Advanced glycation end-products driven angiogenesis *in vitro*: induction of the growth and tube formation of human microvascular endothelial cells through. J Biol Chem 272:8723–8730
24. **Lander HM, Tauras JM, Ogiste JS, Hori O, Moss RA, Schmidt AM** 1997 Activation of the receptor for advanced glycation end products triggers a $p21^{ras}$-dependent mitogen activated protein kinase pathway regulated by oxidant stress. J Biol Chem 272:17810–17814
25. **Lu M, Kuroki M, Amano S, Tolentino M, Keough K, Kim I, Bucala R, Adamis AP** 1998 Advanced glycation end products increase retinal vascular endothelial growth factor expression. J Clin Invest 101:1219–1224
26. **Koschinsky T, He CJ, Mitsuhashi T, Bucala R, Liu C, Buenting C, Heitmann K, Vlassara H** 1997 Orally absorbed reactive glycation products (glycotoxins): an environmental risk factor in diabetic nephropathy. Proc Natl Acad Sci USA 94:6474–6479
27. **Riser BL, Denichilo M, Cortes P, Baker C, Grondin JM, Yee J, Narins RG** 2000 Regulation of connective tissue growth factor activity in cultured rat mesangial cells and its expression in experimental diabetic glomerulosclerosis. J Am Soc Nephrol 11:25–38
28. **Kim HS, Nagalla SR, Oh Y, Wilson E, Roberts Jr CT, Rosenfeld RG** 1997 Identification of a family of low-affinity insulin-like growth factor binding proteins (IGFBPs): characterization of connective tissue growth factor as a member of the IGFBP superfamily. Proc Natl Acad Sci USA 94:12981–12986
29. **Chen MM, Lam A, Abraham JA, Schreiner GF, Joly AH** 2000 CTGF expression is induced by TGF-β in cardiac fibroblasts and cardiac myocytes: a potential role in heart fibrosis. J Mol Cell Cardiol 32:1805–1819
30. **Lee BH, Park RW, Choi JY, Ryoo HM, Sohn KY, Kim IS** 1996 Stimulation of fibronectin synthesis through the protein kinase C signalling pathway in normal and transformed human lung fibroblasts. Biochem Mol Biol Int 39: 895–904
31. **Ha H, Kim KH** 1999 Pathogenesis of diabetic nephropathy: the role of oxidative stress and protein kinase C. Diabetes Res Clin Pract 45:147–151
32. **Scivittaro V, Ganz MB, Weiss MF** 2000 AGEs induce oxidative stress and activate protein kinase C-β(II) in neonatal mesangial cells. Am J Physiol Renal Physiol 278:F676–F683
33. **Toullec D, Pianetti P, Coste H, Bellevergue P, Grand-Perret T, Ajakane M, Baudet V, Boissin P, Boursier E, Loriolle F, Duhamel L, Charon D, Kirilovsky J** 1991 The bisindolylmaleimide GF 109203X is a potent and selective inhibitor of protein kinase C. J Biol Chem 266:15771–15781
34. **Owen Jr WF, Hou FF, Stuart RO, Kay J, Boyce J, Chertow GM, Schmidt AM** 1998 β2-microglobulin modified advanced glycation end products modulates collagen synthesis in human fibroblasts. Kidney Int 53:1365–1373
35. **Kislinger T, Fu C, Huber B, Qu W, Taguchi A, Du Yan S, Hofmann M, Yan SF, Pischetsrieder M, Stern D, Schmidt AM** 1999 N(ε)-(carboxymethyl)lysine adducts of proteins are ligands for receptor for advanced glycation end products that activate cell signaling pathways and modulate gene expression. J Biol Chem 274:31740–31749
36. **Umezawa K, Sugata D, Yamashita K, Johtoh N, Shibuya M** 1992 Inhibition of epidermal growth factor receptor functions by tyrosine kinase inhibitors in NIH3T3 cells. FEBS Lett 314:289–292
37. **Gleave ME, Hsieh JT, Wu HC, Hong SJ, Zhau HE, Guthrie PD, Chung LW** 1993 Epidermal growth factor receptor-mediated autocrine and paracrine stimulation of human transitional cell carcinoma. Cancer Res 53:5300–5307
38. **Murphy M, Godson C, Cannon S, Kato S, Mackenzie HS, Martin F, Brady HR** 1999 Suppression subtractive hybridization identifies high glucose levels as a stimulus for expression of connective tissue growth factor and other genes in human mesangial cells. J Biol Chem 274:5830–5834
39. **Cohen MP, Ziyadeh FN, Lautenslager GT, Cohen JA, Shearman CW** 1999 Glycated albumin stimulation of PKC-β activity is linked to increased collagen IV in mesangial cells. Am J Physiol 276:F684–F690
40. **Chen S, Cohen MP, Ziyadeh FN** 2000 Amadori-glycated albumin in diabetic nephropathy: pathophysiologic connections. Kidney Int 58:40–44
41. **Iwashima Y, Eto M, Horiuchi S, Sano H** 1999 Advanced glycation end product-induced peroxisome proliferator-activated receptor γ gene expression in the cultured mesangial cells. Biochem Biophys Res Commun 264:441–448
42. **Duncan MR, Frazier KS, Abramson S, Williams S, Klapper H, Huang X, Grotendorst GR** 1999 Connective tissue growth factor mediates transforming growth factor β-induced collagen synthesis: down-regulation by cAMP. FASEB J 13:1774–1786
43. **Bradham DM, Igarashi A, Potter RL, Grotendorst GR** 1991 Connective tissue growth factor: a cysteine-rich mitogen secreted by human vascular endothelial cells is related to the SRC-induced immediate early gene product CEF-10. J Cell Biol 114:1285–1294
44. **Chen CC, Chen N, Lau LF** 2001 The angiogenic factors Cyr61 and CTGF induce

adhesive signaling in primary human skin fibroblasts. J Biol Chem 276:10443–10452
45. **Fan WH, Karnovsky MJ** 2000 Activation of protein kinase C inhibits the expression of connective tissue growth factor. Biochem Biophys Res Commun 275:312–321
46. **Bi N, Mamrack MD** 1994 PMA inhibits the growth of human fibroblasts after the induction of immediate-early genes. Exp Cell Res 212:105–112
47. **Hasan NM, Adams GE, Joiner MC** 1999 Effect of serum starvation on expression and phosphorylation of PKC-α and p53 in V79 cells: implications for cell death. Int J Cancer 80:400–405
48. **Hanna W, Friesen D, Bombardier C, Gladman D, Hanna A** 1987 Pathologic features of diabetic thick skin. J Am Acad Dermatol 16:546–553
49. **Seibold JR** 1982 Digital sclerosis in children with insulin-dependent diabetes mellitus. Arthritis Rheum 25:1357–1361
50. **Leutenegger M, Birembaut P, Poynard JP, Eschard JP, Ricard Y, Caron Y, Robert L, Szendroi M, Labat-Robert J** 1983 Distribution of fibronectin in diabetic skin. Pathol Biol (Paris) 31:45–48
51. **Labat-Robert J, Kern P, Robert L** 1991 Modifications of the biosynthesis of type-I and type-III collagens and fibronectin during diabetes and atherosclerosis. Z Gerontol 24:66–69

Erratum

In the article by Dennis D. Rasmussen *et al.* (*Endocrinology* **140**:1009–1012, 1999), part of Table 1 appeared incorrectly. The values in the row beginning with T3 actually correspond to T4, and the values in the row beginning with T4 correspond with T3. The correct table appears below. *The authors regret the error.*

Table 1. Effect of aging and melatonin treatment on hormones involved with energy regulation and body composition

Hormone	Units	Young	Middle Age Control	Middle Age Melatonin
Leptin	ng/ml	3.48 ± 0.27	8.28 ± 1.48[b]	3.27 ± 0.45
Insulin	ng/ml	2.75 ± 0.25	3.48 ± 0.53	2.57 ± 0.25
Testosterone	ng/ml	1.95 ± 0.26	0.67 ± 0.08[a]	0.68 ± 0.23[a]
Corticosterone	ng/ml	26.6 ± 11.5	12.2 ± 3.8	20.7 ± 7.0
T4	ng/ml	56.1 ± 2.1	36.0 ± 3.4[a]	36.3 ± 2.9[a]
T3	ng/ml	0.87 ± 0.11	0.93 ± 0.04	0.99 ± 0.03
IGF-1	μg/ml	1.82 ± 0.05	1.66 ± 0.04[a]	1.55 ± 0.04[a]

Data represent the mean ± SEM of 8 rats/group. [a] $P < 0.05$ *vs.* Young. [b] $P < 0.05$ *vs.* Young and *vs.* Melatonin.

INTERNATIONAL JOURNAL OF MOLECULAR MEDICINE 9: 645-649, 2002

Altered expression of low affinity insulin-like growth factor binding protein related proteins in hepatoblastoma

HENRIK VON HORN[1,2], VIVIAN HWA[3], RON G. ROSENFELD[3], KERSTIN HALL[2], BIN TEAN TEH[4], MICHAEL TALLY[2], TOMAS. J. EKSTRÖM[1] and STEVEN G. GRAY[1,4]

[1]Laboratory for Molecular Development and Tumour Biology Experimental Alcohol and Drug Addiction Section, Department of Clinical Neuroscience, Karolinska Institute, CMM, L8:01, S-171 76 Stockholm; [2]Endocrinology and Diabetes Unit, Department of Molecular Medicine, Karolinska Hospital, S-171 76 Stockholm, Sweden; [3]Department of Pediatrics, Oregon Health Sciences University, Portland, OR 97201; [4]Van Andel Research Institute, 333 Bostwick Ne, Grand Rapids, MI 49503, USA

Received January 30, 2002; Accepted February 27, 2002

Abstract. Hepatoblastoma is a poorly understood rare pediatric liver tumour. We have previously shown that the IGF-axis is seriously disrupted in this tumour type. With the recent discovery that several other proteins also have the potential to bind to IGFs called insulin-like growth factor binding protein related proteins (IGFBP-rPs), we undertook an examination of several such genes in a series of hepatoblastomas with matched normal liver tissue. The expression profiles obtained reveal that the expression of these genes are also disturbed in these tumours, and may have implications for our understanding of the IGF-axis and its importance in this disease.

Introduction

Hepatoblastoma is a rare pediatric liver disease with an incidence of between 0.5-1.5 per million children (1). Most hepatoblastomas are sporadic, but some familial inherited disorders, most notably Beckwith-Wiedemann (BWS), and familial adenomatous polyposis (FAP), are associated with an increased risk for developing hepatoblastomas. Pre-operative chemotherapy regimes have proven to be extremely successful for treating this disease, but an understanding of the molecular processes behind the development of hepatoblastoma has lagged.

Gene expression studies have revealed that several genes show altered expression in hepatoblastomas. These include genes involved with modifying chromatin, cell growth and cell cycle control (2,3). We have previously shown that the insulin-like growth factor axis is greatly altered in hepatoblastoma not only at the level of the growth factors themselves but also to their receptors and binding proteins (4,5). Because the IGF-axis plays an important role in many diverse cellular functions including the promotion of cell growth and cell survival, such alterations may be critical to this tumour type.

Recently an increasing number of proteins have been identified to have the ability to bind to the insulin-like growth factors albeit with low affinity. This has led to them being called insulin-like growth factor binding related proteins or IGFBP-rPs, although some controversy exists as to them being renamed. While the concept of an IGFBP superfamily with shared N-terminal domain is incontrovertible, the role of these proteins in modulating IGF action is still uncertain (6,7). These include the proteins CTGF, NovH and TAF all of which have been shown to have altered expression in cancer (6).

Because these genes may have functional roles with regard to the IGF-axis and have been shown to have altered expression in various cancers we sought to examine their expression in series of hepatoblastoma for which matched normal liver was available and in which the IGF-axis has been shown to be altered, in an attempt to assess whether their expression may also be altered as a consequence of the tumour.

Materials and methods

Samples. Twelve sporadic hepatoblastomas were examined in this study. For eight of these, matched normal liver tissue was available. All of the tumours with the exception of cases 6 and 7 were freeze-sectioned into 1 mm portions interrupted by 5 µm sections. The 1-mm sections were used for RNA isolation, while the interrupted thin sections were prepared for histopathological evaluation. These samples were fixed in formalin, stained and processed with hematoxylin and eosin in the usual manner. The results of this evaluation are presented in Table I, along with particulars for each sample. Human fetal livers (14- and 18-week) were obtained from therapeutic terminations, with the permission of the local ethics committee. Due to the nature of such procedures, limited amounts of tisuue were obtained, and where available the mRNA was included in the analyses.

Correspondence to: Dr Steven Gray, Van Andel Research Institute, 333 Bostwick NE, Grand Rapids, MI 49503, USA
E-mail: steven.gray@vai.org

Key words: hepatoblastoma, insulin-like growth factor binding protein related protein, gene expression

Table I. Clinical data for the tumour samples used in the study.

Case no.	Age at diagnosis (months)	Sex	Histology	Pre-operative chemotherapy
1	6	M	Epithelial	No
2	19	M	Epithelial	Yes
3	19	M	Epithelial	Yes
4	22	M	Epithelial/ mesenchymal	Yes
5	54	M	Epithelial	Yes
6	2	M	Fetal	No
7	12	F	Fetal	Yes
8	36	M	Not available	Yes
9	11	F	Fetal	No
10	13	M	Fetal	No
11	8	F	Epithelial/ mesenchymal	No
12	18	M	Not available	Yes

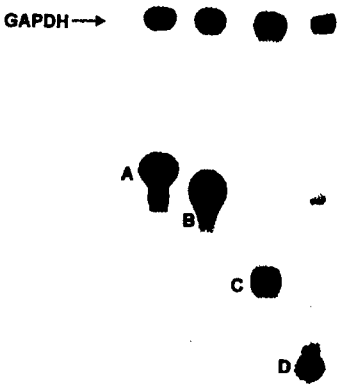

Figure 1. RNase protection analysis. Representative results for each gene examined in the hepatoblastomas. *GAPDH* was used as an internal control in each sample for use in the quantitation of gene expression. *GAPDH* is indicated with an arrow. Letters indicate the protected band for each gene as follows: A, *IGFBP-rP1*; B, *IGFBP-rP2*; C, *IGFBP-rP4*; D, *IGFBP-rP5*.

Nucleic acid isolation. Total RNA was prepared as described previously (8).

Preparation of probe and RNase protection analysis. T3, T7 and Sp6 RNA polymerases (Invitrogen) were used to make antisense RNA probes from the following templates according to the protocol provided in the RPA II kit (Ambion). When incorporating radioactivity into the probe, radioactive ^{32}P-UTP with a specific activity of 800 Ci/mmol was used. Cold UTP was added such that final UTP specific-activity was 80 Ci/mmol for the *GAPDH* probe and 400 Ci/mmol for the others.

The probes used in this study were prepared as follows: To measure *IGFBP-rP1* (*Mac25/TAF/PSF*) expression, a *Sma*I/*Kpn*I fragment from the full length cDNA contained in pcDNA3.1 (9), was blunted and subcloned into the *Eco*RV site of pBluescript II SK (-) (Stratagene). When linearised with *Hin*dIII a probe of 320 bases could be generated using T3 RNA polymerase of which 210 bases hybridize to *IGFBP-rP1* specific transcripts.

IGFBP-rP2 (*CTGF*) expression was measured using a 217 bp *Sma*I fragment from the full length *IGFBP-rP2* (pFastBac1 IGFBPrP2) (10) cloned into the *Eco*RV site of pBluescript II SK (-). Following linearization with *Eco*RI, a probe of 237 bases could be generated with T7 of which 217 bases hybridize to *IGFBP-rP2* mRNA and protect from RNase.

A template for *IGFBP-rP4* (*Cyr61*) was generated by cloning a 214 bp *Sma*I/*Pst*I fragment of the full length cDNA from a pBK-CMV plasmid containing the full length Cyr61 mRNA (generous gift from Dr P. Berta) (11) into pBluescript II SK (-). Following linearization with *Eco*RI a probe of 305 bases could be generated with T3 RNA polymerase of which 214 bases hybridize specifically to *IGFBP-rP4* specific mRNA transcripts.

IGFBP-rP5 (*L56/HtraA*) expression was measured by cloning a 186 bp *Ava*II fragment from a pUC19 plasmid containing the full length cDNA (kind gift of Dr B. Treub) (12) into the *Sma*I site of pGem3Zf(+) (Promega). Following linearization with *Eco*RI a probe of approximately 255 bases could be generated with SP6 of which 186 bases hybridize specifically to *IGFBP-rP5* mRNA transcripts.

All of the plasmids described above were sequenced, in order to ensure that the fragment cloned corresponded to the gene under examination. Sequencing was carried out with T7 Sequenase according to the manufacturer's instructions (United States Biochemical). RNase protection was carried out according to the protocol given with the RPA II kit.

Analysis of expression. Quantification of the RPA results was obtained using phosphorimager analysis (BAS-1000, Fuji Photo Film Co., Ltd) with *GAPDH* mRNA levels utilized as the internal control in each case. The values for the gene under scrutiny were normalised to the internal control.

Results

RNase protection analysis. Following sectioning and histopathological examination (Table I), total RNA was isolated and gene expression was measured using RNase protection analysis. A representative image of the results obtained for each gene examined is shown in Fig. 1. The results of each analysis are described in more detail in the following sections.

Expression of IGFBP-rP1 (Mac25/TAF/PSF) in hepatoblastoma. We examined the mRNA expression levels of *IGFBP-rP1* in a series of matched hepatoblastomas and the corresponding normal liver tissue from patients between the ages of 2 and 54 months. Included in the analysis were some hepatoblastomas with no counterpart normal tissues and fetal liver samples. The results of this analysis are shown in Fig. 2. In four of the eight matched tumours expression of this gene was downregulated when compared to their matched normal counterparts. In the unmatched sample tumours, two had expression which was below the average normal liver values.

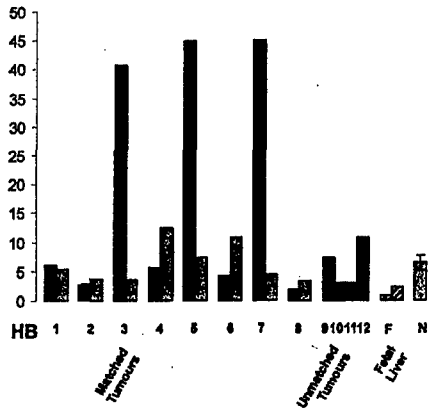

Figure 2. RNase protection analysis of *IGFBP-rP1* expression. Analysis of total *IGFBP-rP1* transcripts in hepatoblastomas. *GAPDH* expression is used as the internal control for quantification purposes. In all the following figures the Y-axis units represent the values for each gene divided by the value obtained for the housekeeping gene *GAPDH* (in this case: *IGFBP-rP1/GAPDH*) as determined by phosphorimager analysis and following the adjustments as described in Materials and methods. The mean ± standard error of the mean was also calculated for the normal liver (N), and graphed along with the individual samples. Matched tumours are those samples for which normal liver was taken from the same individual at time of surgery. Unmatched tumours are those samples for which normal liver tissue was unavailable. Fetal livers were included to compare against normal liver and tumour expression.

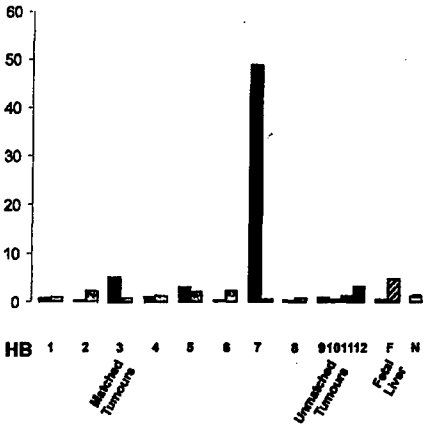

Figure 3. RNase protection analysis of *IGFBP-rP2* expression. Using RNase protection analysis *IGFBP-rP2* transcripts were quantified and graphed as described in Fig. 2.

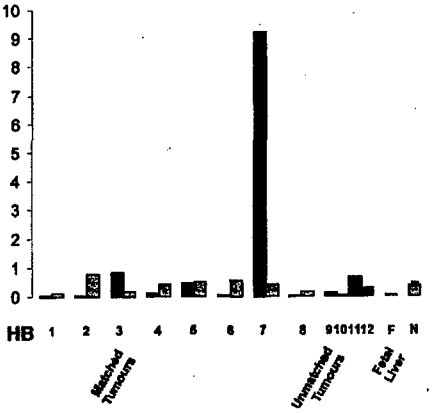

Figure 4. RNase protection analysis of *IGFBP-rP4* expression. Quantification of *IGFBP-rP4* transcripts in hepatoblastomas. Following quantification, the results were graphed as described in Fig. 2.

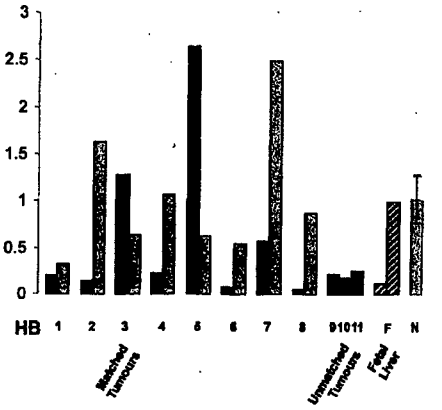

Figure 5. RNase protection analysis of *IGFBP-rP5* expression. Quantification of *IGFBP-rP5* transcripts in hepatoblastomas. Following RNase protection analysis, the results were quantified and graphed as described in Fig. 2.

downregulated in the tumours. Thus, 6 out of 12 (50%) tumours showed downregulated expression of this gene. However, in cases 3, 5 and 7 (25% of the tumours) *IGFBP-rP1* was greatly upregulated in these tumours.

Expression of IGFBP-rP2 (CTGF) in hepatoblastoma. Next we examined the expression of *IGFBP-rP2* in these samples. One tumour (case 7) showed greatly increased expression over its corresponding normal liver (Fig. 3). Two other samples (cases 3 and 5) showed slightly elevated levels of expression. Including the unmatched tumours, four samples (33%) have upregulated expression of *IGFBP-rP2*. In the matched tumours, downregulated expression of this gene was observed in three tumours (cases 2, 6 and 8). One of the unmatched tumours also showed decresaed expression of this gene and two samples had unaltered expression.

Expression of IGFBP-rP4 (Cyr61) in hepatoblastoma. When *IGFBP-rP4* expression was examined most of the tumours were observed to have reduced levels of expression of this gene in comparison with their matched normal liver (Fig. 4). The exceptions to this were cases 3 and 7 which showed upregulated expression. Of these, case 7 had greatly increased expression of *IGFBP-rP4*. In the unmatched samples two samples showed lower levels of expression than the average

Table II. Expression patterns of the IGFB-rPs in hepatoblastomas.[a]

Case no.	*IGFBP-rP1*	*IGFBP-rP2*	*IGFBP-rP4*	*IGFBP-rP5*
1	N/↑	N	↓	↓
2	↓	↓	↓	↓
3	↑	↑	↑	↑
4	↓	↓/N	↓	↓
5	↑	↑/N	↓/N	↑
6	↓	↓	↓	↓
7	↑	↑	↑	↓
8	↓	↓	↓	↓
9	N	↓/N	↓	↓
10	↓	↓	↓	↓
11	↓	N	↑/N	↓
12	↑	↑	N	n.d.

[a]↑, increased expression; ↓, decreased expression; N, normal expression; N/↑, normal or slightly increased expression; N/↓, normal or slightly decreased expression; n.d., not determined.

normal liver value. Overall, 7 of 12 (58%) samples of the hepatoblastomas showed downregulated expression of this gene.

Expression of IGFBP-rP5 (HTRA/L56) in hepatoblastoma. The levels of mRNA transcripts for *IGFBP-rP5* were then measured in these samples. In almost all cases expression of this gene was downregulated in the matched tumour samples compared to their normal liver counterparts (Fig. 5). Two samples, cases 3 and 5 showed an increased level of expression of *IGFBP-rP5*. All of the unmatched tumours had levels of expression below that of average normal liver. If these are taken into account, 9 out of 11 (82%) hepatoblastomas had downregulated expression of *IGFBP-rP5*.

Discussion

In the present study we have examined the mRNA expression of four genes whose products have recently been identified as having the ability to bind IGFs at low affinity in a series of hepatoblastomas in relation to their matched normal tissues (summarized in Table II). Previously we have reported that many members of the IGF-axis have altered expression in these samples including the IGFs which may therefore lead to increased mitogenic signalling within their surroundings (2,4). IGFBPs are critical regulators of IGF activity, and by binding to IGFs they form biologically inactive complexes which in addition to increasing the half-life of the growth factor, also modulate the binding of the IGFs to their cognate receptors (6). Thus, the newly identified IGFBP-rPs may also prove to have important roles in regulating IGF signalling in addition to their other roles (6,7).

IGFBP-rP1 has been shown to be a potential tumour suppressor (6) and decreased expression of this gene has been observed in higher stage breast cancer (13). In addition, downregulation of this gene by methylation has been shown to be important for tumorigenesis in a mouse model of liver cancer (14). As such, the decreased expression of this gene in some of our samples may reflect the loss of tumour suppressive capability, or it may indicate that increased methylation of this gene may be occurring in those samples. Cases 3, 5 and 7 however have greatly increased expression of this gene, and this may indicate an attempt to regulate or suppress the tumour.

IGFBP-rP2 or CTGF is a major mitogenic factor for connective tissue cells. It has also been shown to be specifically expressed in the maligant lymphoblasts of patients with acute lymphoblastic leukemia (15). In our samples three tumours have increased expression of this gene, with one sample in particular (case 7), having greatly enhanced expression, and may therefore lead to increased mitogenic signalling in these particular tumours.

IGFBP-rP4 (*Cyr61*) has also been implicated in cancer where it has been shown to be downregulated in prostate cancer (16). However overexpression of this gene in a xenograft model appears to promote tumour growth (17). In our analysis of hepatoblastomas, one sample (case 7) has a very high overexpression of this gene compared to its matched normal liver, and this may be a reflection of increased growth potential in this tumour. However, five of the samples also showed reduced expression of this gene in a manner similar to that observed for prostate cancer (16).

IGFBP-rP5 (L56/HtrA) is an interesting protein because it has serine protease activity. One feature of the IGF-axis is that the IGFBPs themselves are regulated in part by the actions of serine proteases. The cleavage of such binding proteins could therefore increase the availability of free IGFs, leading to increased mitogenic signalling. *IGFBP-rP5* has been shown to be able to cleave IGFBP-5 and as such overexpression of this gene may enhance the mitogenic signalling by IGFs in the vicinity of the tumour (6). In our samples two hepatoblastomas (cases 3 and 5) showed elevated expression of this serine protease. However, in most cases the expression of this gene is reduced, and this may signal an attempt by the tumours to limit the mitogenic signalling in their vicinity. It is interesting to note that the same samples which show elevated IGFBP-rP5 also have a concommitant overexpression of IGFBP-5 indicating that the regulation of IGFBP-5 may be linked to IGFBP-rP5 activity (18).

In conclusion, the data presented indicate that in hepatoblastomas, the IGF-axis is seriously disturbed, extending even to the members of the low affinity insulin-like growth factor binding protein related proteins, confirming the importance of this axis in the pathogenesis of this disease.

Acknowledgements

This work was supported by grants from The Children's Cancer Foundation of Sweden and The Swedish Cancer Foundation to T. Ekström, and by The Swedish Research Council grant no. 72X-13143 to M. Tally. The authors would like to thank Drs B. Treub and P. Berta for their generous gifts of cDNA clones for *IGFBP-rP4* and *IGFBP-rP5*.

References

1. Perilongo G and Shafford EA: Liver tumours. Eur J Cancer 35: 953-958, 1999.
2. Gray SG, Hartmann W, Eriksson T, *et al:* Expression of genes involved with cell cycle control, cell growth and chromatin modification are altered in hepatoblastomas. Int J Mol Med 6: 161-169, 2000.
3. Iolascon A, Giordani L, Moretti A, Basso G, Borriello A and Della Ragione F: Analysis of CDKN2A, CDKN2B, CDKN2C, and cyclin Ds gene status in hepatoblastoma. Hepatology 27: 989-995, 1998.
4. Gray SG, Eriksson T, Ekström C, *et al:* Altered expression of members of the IGF-axis in hepatoblastomas. Br J Cancer 82: 1561-1567, 2000.
5. Li X, Adam G, Cui H, Sandstedt B, Ohlsson R and Ekström TJ: Expression, promoter usage and parental imprinting status of insulin-like growth factor II (IGF2) in human hepatoblastoma: uncoupling of IGF2 and H19 imprinting. Oncogene 11: 221-229, 1995.
6. Hwa V, Oh Y and Rosenfeld RG: The insulin-like growth factor-binding protein (IGFBP) superfamily. Endocrine Rev 20: 761-787, 1999.
7. Grotendorst GR, Lau LF and Perbal B: CCN proteins are distinct from and should not be considered members of the insulin-like growth factor-binding protein superfamily. Endocrinology 141: 2254-2256, 2000.
8. Chomczynski P and Sacchi N: Single-step method of RNA isolation by acid guanidinium thiocyanate-phenol-chloroform extraction. Anal Biochem 162: 156-159, 1987.
9. Sprenger CC, Damon SE, Hwa V, Rosenfeld RG and Plymate SR: Insulin-like growth factor binding protein-related protein 1 (IGFBP-rP1) is a potential tumor suppressor protein for prostate cancer. Cancer Res 59: 2370-2375, 1999.
10. Kim HS, Nagalla SR, Oh Y, Wilson E, Roberts CT Jr and Rosenfeld RG: Identification of a family of low-affinity insulin-like growth factor binding proteins (IGFBPs): characterization of connective tissue growth factor as a member of the IGFBP superfamily. Proc Natl Acad Sci USA 94: 12981-12986, 1997.
11. Jay P, Berge-Lefranc JL, Marsollier C, Mejean C, Taviaux S and Berta P: The human growth factor-inducible immediate early gene, CYR61, maps to chromosome 1p. Oncogene 14: 1753-1757, 1997.
12. Zumbrunn J and Trueb B: Primary structure of a putative serine protease specific for IGF-binding proteins. FEBS Lett 398: 187-192, 1996.
13. Landberg G, Ostlund H, Nielsen NH, *et al:* Downregulation of the potential suppressor gene IGFBP-rP1 in human breast cancer is associated with inactivation of the retinoblastoma protein, cyclin E overexpression and increased proliferation in estrogen receptor negative tumors. Oncogene 20: 3497-3505, 2001.
14. Komatsu S, Okazaki Y, Tateno M, *et al:* Methylation and down-regulated expression of mac25/insulin-like growth factor binding protein-7 is associated with liver tumorigenesis in SV40T/t antigen transgenic mice, screened by restriction landmark genomic scanning for methylation (RLGS-M). Biochem Biophys Res Commun 267: 109-117, 2000.
15. Vorwerk P, Wex H, Hohmann B, Oh Y, Rosenfeld RG and Mittler U: CTGF (IGFBP-rP2) is specifically expressed in malignant lymphoblasts of patients with acute lymphoblastic leukaemia (ALL). Br J Cancer 83: 756-760, 2000.
16. Pilarsky CP, Schmidt U, Eissrich C, *et al:* Expression of the extracellular matrix signaling molecule Cyr61 is downregulated in prostate cancer. Prostate 36: 85-91, 1998.
17. Babic AM, Kireeva ML, Kolesnikova TV and Lau LF: CYR61, a product of a growth factor-inducible immediate early gene, promotes angiogenesis and tumor growth. Proc Natl Acad Sci USA 95: 6355-6360, 1998.
18. Von Horn H, Tally M, Hall K, Eriksson T, Ekström TJ and Gray SG: Expression levels of insulin-like growth factor binding proteins and insulin receptor isoforms in hepatoblastomas. Cancer Lett 162: 253-260, 2001.

536

0021-972X/03/$15.00/0
Printed in U.S.A.

The Journal of Clinical Endocrinology & Metabolism 88(7):3401–3408

doi: 10.1210/jc.2002-021315

Generation of Anti-Insulin-Like Growth Factor-Binding Protein-Related Protein 1 (IGFBP-rP1/MAC25) Monoclonal Antibodies and Immunoassay: Quantification of IGFBP-rP1 in Human Serum and Distribution in Human Fluids and Tissues

ABEL LÓPEZ-BERMEJO, JAVAD KHOSRAVI, CHRISTOPHER L. CORLESS, RADHA G. KRISHNA, ANASTASIA DIAMANDI, UMESH BODANI, ERIC M. KOFOED, DONNA L. GRAHAM, VIVIAN HWA, AND RON G. ROSENFELD

Departments of Pediatrics (A.L.-B., E.M.K., D.L.G., V.H., R.G.R.) and Pathology (C.L.C.), Oregon Health Sciences University, Portland, Oregon 97201; Department of Laboratory Medicine and Pathobiology (J.K.), Mount Sinai Hospital, Toronto M5G IX5, Canada; Diagnostic System Laboratories (J.K., A.D.), Toronto, Canada; and Diagnostic System Laboratories (R.G.K., U.B.), Webster, Texas 77598

The IGF-binding protein (IGFBP)-related proteins (rPs) are a group of recently described cysteine-rich proteins that share significant amino-terminal structural similarity with the conventional IGFBPs. IGFBP-rP1 (also known as MAC25/angiomodulin/prostacyclin-stimulating factor and T1A12), regulates cellular proliferation, adhesion, and angiogenesis and stimulates prostacyclin synthesis. We characterized new monoclonal antibodies generated against IGFBP-rP1 and have used them to study the distribution of IGFBP-rP1 in human biological fluids and tissues. Additionally, we have developed a noncompetitive sandwich-type immunoassay to quantitate the concentrations of IGFBP-rP1 in human serum. IGFBP-rP1 was readily detectable in serum, urine, amniotic fluid, and cerebrospinal fluid by immunoblot analysis. Evaluation of the newly developed immunoassay demonstrated acceptable analytical performance, with a detection limit of 0.7 μg/liter, a dynamic range of 3.1–100 μg/liter, and intra- and interassay coefficients of variation of 2.5–6.8% and 3.1–6.4% at approximately 24–85 ng/ml IGFBP-rP-1, respectively. No significant cross-reactivity with IGFBP-1–6 was observed. In random normal human adult sera (n = 37), the median IGFBP-rP1 was 21.0 μg/liter, and values did not correlate with levels of IGF-I (r = 0.085, P = 0.61), IGF-II (r = 0.051, P = 0.75), or IGFBP-3 (r = 0.061, P = 0.74). The monoclonal anti-IGFBP-rP1 antibodies also readily detected IGFBP-rP1 expression in human tissue sections, with preferential expression of IGFBP-rP1 in the microvascular endothelium associated with tumorigenesis. In summary, using newly developed IGFBP-rP1 monoclonal antibodies, we confirm the presence of IGFBP-rP1 in the major human body fluids, provide quantitative normative data on the concentrations of IGFBP-rP1 in human serum, and show preferential expression of IGFBP-rP1 in the microvascular endothelium associated with tumorigenesis. The use of these novel IGFBP-rP1 detection tools should prove useful in the elucidation of the biological role(s) of this protein. (*J Clin Endocrinol Metab* 88: 3401–3408, 2003)

THE IGF SYSTEM comprises two ligands, IGF-I and IGF-II, six IGF-binding proteins (IGFBPs), IGFBP-1 to -6, and two receptors, type 1 and type 2 IGF receptors (1). Recently the IGFBP family has been expanded to include the IGFBP-related proteins (IGFBP-rPs), which share significant structural similarities with the IGFBPs (2, 3). Thus, the IGFBP superfamily includes the six conventional IGFBPs, which have high affinity for IGFs, and at least 10 IGFBP-rPs, which not only share the conserved amino-terminal domain of the IGFBPs but also show some degree of affinity for IGFs and insulin in several, but not all, assay systems (4–7).

The IGFBP-rPs are a group of cysteine-rich proteins that control diverse cellular functions, such as cellular growth, cellular adhesion and migration, and synthesis of extracellular matrix. In addition, these proteins are involved in biological processes that include development and differentiation, reproduction, angiogenesis, wound repair, inflammation, fibrosis, and tumorigenesis (3).

IGFBP-rP1 was initially identified as a gene differentially expressed in normal leptomeningeal and mammary epithelial cells, compared with their counterpart tumor cells, and named meningioma-associated cDNA (MAC25) (8). The expressed protein was independently purified as a tumor-derived adhesion factor (later renamed angiomodulin) (5, 9) and as a prostacyclin-stimulating factor (10). It has additionally been reported as T1A12, a gene down-regulated in breast carcinomas (11).

Although the biological roles of IGFBP-rP1 have not been clearly established, there is a growing body of evidence that suggests that it may act as a tumor suppressor gene. IGFBP-rP1 is preferentially expressed in normal (*vs.* neoplastic) meningeal, mammary, and prostatic cells (8, 12, 13); it is up-regulated during senescence of mammary and prostatic cells (14, 15); loss of heterozygosity of the IGFBP-rP1 locus has been observed in 50% of cancerous breast tissues in one

Abbreviations: AF, Amniotic fluid; CCN, connective tissue growth factor/Cyr61/Nov; CSF, cerebrospinal fluid; CTGF, connective tissue growth factor; HRP, horseradish peroxidase; IGFBP, IGF-binding protein; IGFBP-rP, IGF-binding protein-related protein; rh, recombinant human; WIB, Western immunoblot.

study (11); and IGFBP-rP1 shows growth inhibitory effects when overexpressed in prostate cancer cells (16, 17) or breast cancer cells (18).

In addition, IGFBP-rP1 may have an important role in vascular biology. It has been detected in tube-like structures *in vitro* (19) and high endothelial cells (20, 21) and is preferentially localized in the basement membrane of neocapillaries, like those seen in tumor tissues (5, 22, 23). Furthermore, analysis of genes differentially expressed in endothelial cells indicates that IGFBP-rP1 expression is up-regulated in tumor-derived endothelium (24). A role for IGFBP-rP1 in vascular biology emerges from demonstrations that IGFBP-rP1 is capable of stimulating the synthesis of the vasodilator prostacyclin in cultured endothelial cells and may, therefore, be involved in maintaining the permeability of newly synthesized capillaries (10).

We recently generated and characterized a polyclonal anti-IGFBP-rP1 antibody and identified IGFBP-rP1 in conditioned media from cultured human mammary and prostatic cells and in human biological fluids (12, 25). In this report, we further characterize the presence of IGFBP-rP1 in human biological fluids using anti-IGFBP-rP1 monoclonal antibodies. In addition, we provide quantitative data on serum IGFBP-rP1 using a newly developed IGFBP-rP1 immunoassay and examine the distribution of IGFBP-rP1 protein in human tissues.

Materials and Methods

Materials

HPLC-purified IGFBP-1 from human amniotic fluid was kindly provided by Dr. D. R. Powell (Baylor College of Medicine, Houston, TX); rhIGFBP-2, -4, -5, and -6 were purchased from Austral Biologicals (San Ramon, CA); rhIGFBP-3, a nonglycosylated 29-kDa core protein expressed in *Escherichia coli* was a generous gift from Celtrix, Inc. (Santa Clara, CA). C-terminally^{FLAG}-tagged rhIGFBP-rP1, CTGF, and NovH were expressed in a baculovirus system as previously reported (2, 4, 26). Baculovirus-generated nontagged rhIGFBP-rP1 protein was purified over SP Sepharose (Sigma Chemical Co., St. Louis, MO) column equilibrated in MES buffer [50 mM *N*-morpholino-ethenesulfonic acid (pH 6.0), 2 mM EDTA, and 1 mM phenylmethylsulfonyl fluoride]. IGFBP-rP1 protein retained on the column was eluted with an NaCl gradient [0.2–1.0 M in 2-(*N*-morpholine) ethane sulfonic acid buffer]. Fractions containing recombinant human (rh)IGFBP-rP1 were pooled and dialyzed against PBS. Analysis for protein purity and quantitation was as previously described (4). ^{125}I-IGF-I and ^{125}I-IGF-II were gifts from Diagnostic Systems Laboratories (Diagnostic Systems Laboratories, Webster, TX).

Nitrocellulose and electrophoresis reagents were purchased from Bio-Rad Laboratories, Inc. (Hercules, CA). Polyclonal antibodies against IGFBP-rP1^{FLAG}, CTGF^{FLAG}, and NovH^{FLAG} were generated in rabbits, as previously described (2, 25, 26). The IgG fractions were purified by a protein A affinity column (Amersham, Arlington Heights, IL). Monoclonal antibodies against IGFBP-rP1 (designated no. 1 through 11) were produced against the baculovirus-generated rhIGFBP-rP1^{FLAG} described above. Horseradish peroxidase (HRP)-linked donkey antirabbit and sheep antimouse IgG antibodies and enhanced chemiluminescence detection reagents were purchased from Amersham.

Human biological fluids were obtained as anonymous samples from the Oregon Health Sciences University Central Laboratory and were residuals from routine clinical test samples. They were from apparently healthy adult subjects (*i.e.* with no known acute or chronic diseases); for cerebrospinal fluid (CSF), samples from both apparently healthy adult and pediatric subjects were analyzed. Additional serum and urine samples were collected from apparently healthy adult volunteers. The protocol was approved by the hospital Institutional Review Board, and informed consent was obtained from the healthy adult volunteers.

Adult serum samples included in the analysis were from 18 women, aged 25–76 yr and 19 men, aged 25–67 yr. On collection, blood samples were allowed to clot, then separated; after clinical testing, the residuals were used for these studies within 48 h of collection. Spot urine samples were from 20 women, aged 18–78 yr, and 10 men, aged 28–81 yr, collected after the first morning void. Urinalysis abnormalities excluded samples to be further tested for IGFBP-rP1. Samples were stored at −80 C after centrifugation to discard the cellular pellet. Residuals samples of amniotic fluid were from normal pregnancies between 15 and 20 wk gestation and were stored, after centrifugation, at −80 C until use. Residual samples from normal CSF (two women, four men, two boys, age range for the whole group: 4–88 yr) were also stored at −80 C until use. Urine, amniotic fluid (AF), and CSF were screened for IGFBP-rP1 within 2 months of collection.

Generation of monoclonal anti-IGFBP-rP1 antibodies

Five 10-wk-old Balb/c mice (Charles River, NC) were immunized with 50 μg/ml baculovirus-generated rhIGFBP-rP1^{FLAG} protein with Freund's complete adjuvant (ICN Biomedicals Inc., Aurora, OH). Three boosters (30 μg rhIGFBP-rP1^{FLAG} with Freund's incomplete adjuvant) were given at 30-d intervals. Two of the mice with high titers of antibodies against rhIGFBP-rP1^{FLAG} were identified and were subsequently used for hybridoma generation. A third booster (75 μg rhIGFBP-rP1^{FLAG}) was administered to the selected mice, and fusion was performed according to Lane (27).

The resulting hybridomas were screened as follows: IgG from hybridomal cell culture supernatants was captured on goat antimouse IgG-coated plates (DSL). After 2 h, the plates were washed three times with PBS-Tween 20 (0.01 M), and further incubated with 100 μl biotinylated IGFBP-rP1^{FLAG} protein (200 ng/ml in PBS-Tween with 1% BSA and 1% goat serum). After washing with PBS-Tween, the plates were incubated with avidin-HRPO (Zymed Laboratories Inc., South San Francisco, CA) for 30 min, and the signal was developed with TMB (Life Technologies Inc., Grand Island, NY). To obtain pure clones, limiting dilution to 1 cell/well was performed for all positive hybridoma colonies and the resultant monoclonals confirmed by plate assays. The 11 clones are designated no. 1 to 11 in this report and represent the following isolated clones: 1, 1B4A; 2, 1B4B; 3, 1B4C; 4, 1D1A; 5, 1D1B; 6, 2A2A; 7, 2A2B; 8, 2C4A; 9, 2C4B; 10, 2C4C; and 11, 2C5.

Immunoadsorption of IGFBP-rP1 polyclonal antibody

Aliquots of the IGFBP-rP1 polyclonal antiserum were incubated overnight at 4 C with either rhIGFBP-rP1^{FLAG} at a ratio of 15 μg/μl of antiserum (subsequently designated preadsorbed fraction) or buffer alone (immune fraction). To remove the rhIGFBP-rP1/anti-IGFBP-rP1 immune complexes, equal volumes of anti-FLAG M2 agarose beads (Sigma) were added to the aliquots above, and samples were incubated for another hour at 4 C. Samples were pelleted (5 min, at 12,000 g) and supernatants collected and frozen for subsequent Western immunoblot (WIB) studies.

WIB studies

For the initial characterization of the IGFBP-rP1 monoclonal antibodies, conditioned medium from normal human prostate epithelial cells, which are known to secrete large amounts of IGFBP-rP1 protein (12), was used as the source of endogenous IGFBP-rP1. Equal amounts of total protein per lane were dissolved in nondenaturing SDS sample buffer [0.5 mol/liter Tris (pH 6.8), 1% SDS, 10% glycerol, and bromphenol blue] and boiled for 5 min. Samples were electrophoresed on 15% SDS-polyacrylamide gels, electroblotted onto nitrocellulose, and membranes blocked with 4% milk-TBS-T [Tris-buffered saline-Tween-20 (0.1%)] for 1 h at 22 C. Western blots were incubated with IGFBP-rP1 polyclonal antiserum (IgG fraction, 6 μg/μl) at a 1:3000 dilution or with IGFBP-rP1 monoclonal antibodies (IgG fraction, 1 μg/μl) at a dilution of 1:2000 in TBS-T overnight at 4 C. Membranes were washed with TBS-T and incubated for 1 h at 22 C with a 1:3000 dilution of HRP-linked antirabbit or antimouse IgG secondary antibodies. Proteins of interest were detected with enhanced chemiluminescence reagents, according to the manufacturer's protocol.

For the characterization of IGFBP-rP1 in human biological fluids, representative samples from healthy human subjects were prepared

similarly and resolved on 15% SDS-polyacrylamide gels. Normal human serum was concentrated 10-fold using a heparin affinity column (Amersham) before these studies. Immunoblotting of nitrocellulose membranes involved: 1) both the immune and the preadsorbed fractions of the IGFBP-rP1 antiserum, and 2) anti-IGFBP-rP1 monoclonal antibody no. 5 and/or 10.

Western ligand blotting

Equimolar amounts of IGFBPs and IGFBP-rPs were resuspended in SDS sample buffer and resolved on 15% SDS-polyacrylamide gels. Separated proteins were electroblotted onto nitrocellulose membranes. Membranes were rinsed in 3% IGEPAL (Sigma) in TBS-T for 30 min at 22 C, blocked with 1% BSA IGEPAL (Sigma) in TBS-T for 1 h at 22 C and incubated with 2×10^6 cpm of a mixture of ^{125}I-IGF and ^{125}I-IGF-II in 1% BSA/TBS-T overnight at 4 C. Membranes were washed, dried, and exposed to Biomax film (Eastman Kodak Co., Rochester, NY).

IGFBP-rP1 ELISA development

Anti-IGFBP-rP1 monoclonal antibodies were employed to construct a noncompetitive sandwich-type immunoassay (see below). The antibody selection was based on extensive pair-wise evaluations in both one-step (equilibrium) and two-step (sequential) immunoreaction formats. Using this protocol, combinations of the 11 different anti-IGFBP-rP1 monoclonal antibodies were analyzed. The protocol optimization was based on the initial evaluation of a number of factors that could potentially affect detection limit, dynamic range, precision, and delayed sample addition (28). Antibody combinations demonstrating favorable analytical performances were further assessed for accuracy and comparative IGFBP-rP1 determinations. The sources of the raw materials and composition of the various buffers employed have been previously described (29, 30).

IGFBP-rP1 antibody coating to microtiter wells was performed at a concentration of 0.25–20 mg/liter by using previously published methods (29, 30). The IGFBP-rP1 detection antibodies were coupled to HRP as previously described (29). IGFBP-rP1 calibrators were prepared by appropriately diluting the recombinant IGFBP-rP1 in a protein-based buffer matrix [0.05 mol/liter sodium phosphate (pH 7.4), 9 g/liter NaCl, 6 g/liter BSA, and 0.5% Proclin 300]. The preparation was stable for at least 5 d at 4 C and more than 6 months at −70 C.

IGFBP-rP1 ELISA protocol

Calibrators or samples (0.020 ml) were added in duplicate to the precoated wells, followed by addition (0.1 ml) of the detection antibody-HRP conjugate (diluted in the assay buffer to approximately 0.1–0.25 mg/liter) and 4 h of incubation at room temperature with continuous shaking. The wells were washed five times and incubated with 0.1 ml/well of the TMB/H_2O_2 substrate solution for 10 min. Stopping solution (0.1 ml) was then added and absorbance measured by dual-wavelength measurement at 450 nm with background wavelength correction set at 620 nm. Absorbance measurements and ELISA data analysis were performed with the Labsystems Multiskan Multisoft microplate reader (Labsystems, Helsinki, Finland).

The best performances were obtained with a coating antibody concentration of 10 mg/liter (1000 ng/0.1 ml/well), a detection antibody concentration of approximately 0.1–0.25 mg/liter (10–25 ng/0.1 ml per well), a sample size of 0.02 ml, and a 4-h one-step (equilibrium) ELISA configuration. With this protocol, the differences in assay results caused by 1- to 20-min delay between addition of the same samples into the coated wells was less than 10%.

IGFBP-rP1 ELISA validation procedures

The lower limit of detection (sensitivity) was determined by interpolating the mean plus 2 SD of 12 replicate measurements of the zero calibrator. The intraassay coefficients of variation were determined by replicate analysis (n = 12) of four samples at IGFBP-rP1 concentrations of approximately 10–50 μg/liter in one run and interassay coefficients of variation by duplicate measurement of the samples in 12 separate assays. Recovery was assessed by adding 25 μl recombinant IGFBP-rP1 diluted in the standard matrix to 225 μl of three sera and analyzing the spiked and unspiked samples. Percent recovery was determined by comparison of the amount of added IGFBP-rP1 with the amount measured after subtracting the endogenous IGFBP-rP1 levels. Linearity was tested by analyzing three serum samples serially diluted (2- to 8-fold) in the zero calibrator of the assay.

The standard range and performance characteristics of IGFBP-rP1 are summarized in Table 1. Analysis of IGFBP-1, IGFBP-2, IGFBP-4–6 (up to 500 μg/liter) and IGFBP-3 (up to 5 mg/liter) did not show any cross-reactivity or interference. There was no cross-reactivity with IGF-I or IGF-II (up to 600 μg/liter) added to the assay zero standard followed by IGFBP-rP-1 analysis (data not shown).

Immunohistochemistry

Anonymous samples of normal and neoplastic human tissues were provided by the Cancer Pathology Shared Resource of the Oregon Cancer Center. These samples had been collected in the fresh state shortly after surgical resection and either snap frozen in optimal cutting temperature embedding compound, using a dry-ice/pentane slurry, or fixed in 10% buffered formalin. The fixed tissues were processed and embedded in paraffin using standard techniques.

Five-micrometer sections of the frozen samples were prepared in a cryostat, placed on Fisherbrand Plus slides (Fisher Scientific, Pittsburgh, PA) and allowed to air dry for 15 min at room temperature. Dried slides were wrapped in cellophane and stored at −80 C. The cryostat sections were allowed to warm to room temperature and then fixed for 10 min in freshly prepared 1% paraformaldehyde/PBS. Five-micrometer sections of the paraffin-embedded tissues were cut on a microtome and placed on Fisherbrand Plus slides. The slides were deparaffinized through xylenes and alcohol and then placed in TBS buffer for use in immunohistochemistry.

Immunohistochemistry was performed using an automated immunostainer (DAKO Corp., Carpinteria, CA), with all steps carried out at room temperature. Antibodies were diluted in a buffer containing 1% BSA, 0.1% Tween 20, 0.1% sodium azide in PBS. TBS was used for all wash steps. Following a 10-min incubation in dilution buffer, primary antibody (IgG fractions of anti-IGFBP-rP1 polyclonal or the anti-IGFBP-rP1 monoclonal antibodies) was added at a concentration of 1 μg/ml for 45 min, followed by washing and application of the secondary antibody. The secondary antibody (at a 1:400 dilution) was either biotinylated goat antirabbit or biotinylated horse antimouse (Vector Laboratories, Burlingame, CA). After 30-min incubation with the secondary antibody, the samples were treated with quench buffer (methanol/6% H_2O_2), washed, and bound antibodies were detected using the Vectastain Elite ABC kit (Vector Laboratories) as per the manufacturer's recommendations. Premixed DAB solution (DAKO) was used in the final reaction (10 min). Slides were counterstained with hematoxylin before dehydration and coverslipping.

Results

Characterization of IGFBP-rP1 monoclonal antibodies

Anti-IGFBP-rP1 monoclonal antibodies (IgG fractions) were initially screened by WIB for their ability to recognize rhIGFBP-rP1^{FLAG} protein. As shown in Fig. 1A, baculovirus-generated rhIGFBP-rP1^{FLAG} protein was detected by both the panel of monoclonal antibodies (no. 1 through 10) and the polyclonal anti-IGFBP-rP1 antibody. Anti-IGFBP-rP1 monoclonal antibody no. 11 was significantly less potent in rec-

TABLE 1. IGFBP-rP1 ELISA validation data

Assay parameters	Performance characteristics
Detection limit (ug/liter)	0.7 ug/liter
Standard range (ug/liter)	3.1–100
Intra-assay CV (%)	2.5–6.8
Inter-assay CV (%)	3.1–6.4
Recovery of added IGFBP-rP1 (%)	106 ± 10%
Recovery after dilution (%)	108 ± 8.6%

CV, Coefficient of variation.

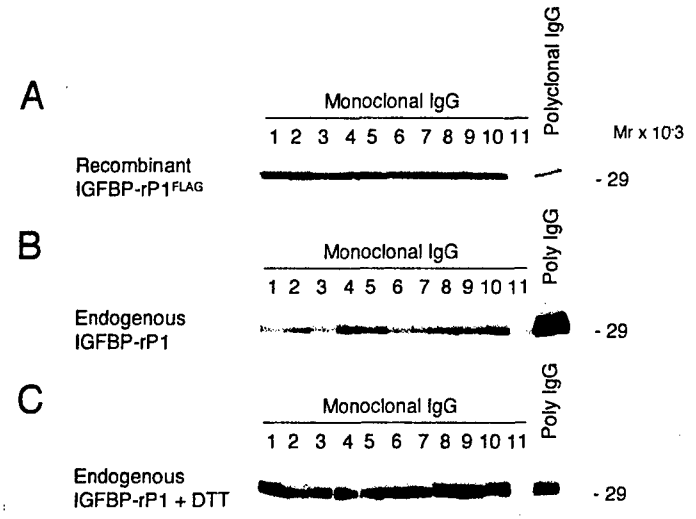

FIG. 1. Characterization of anti-IGFBP-rP1 monoclonal antibodies. Immunoreactivity of 11 anti-IGFBP-rP1 monoclonal antibodies was compared with our polyclonal anti-IGFBP-rP1 antibody (25). A, WIB using rhIGFBP-rP1^{FLAG} and the IgG fractions of these antibodies. B, WIB using conditioned media from normal prostate epithelial cells, which are known to secrete large amounts of IGFBP-rP1 (15). C, Same as in B, except a reducing agent (dithiothreitol) was added to the conditioned media before gel electrophoresis.

ognizing the recombinant protein. We next examined the ability of these antibodies to identify human nonrecombinant (endogenous) IGFBP-rP1. As shown in Fig. 1B, all 11 anti-IGFBP-rP1 monoclonal antibodies and the polyclonal anti-IGFBP-rP1 antibody recognized the secreted IGFBP-rP1 in conditioned medium from normal human prostate epithelial cells (15). Although the sensitivity of the monoclonal antibodies for endogenous IGFBP-rP1 appeared to be lower than that of the polyclonal antibody, the sensitivity of the antibodies for human endogenous IGFBP-rP1 was comparable when electrophoresis was performed under reducing conditions (Fig. 1C).

IGFBP-rP1 is structurally related to the conventional IGFBPs as well as to other members of the IGFBP superfamily (3), like connective tissue growth factor (CTGF) (31) and NovH (32), both members of the CTGF/Cyr61/Nov (CCN) family. To confirm the specificity of the anti-IGFBP-rP1 monoclonal antibodies, equimolar amounts of the six IGFBPs (IGFBP-1 through 6), rhIGFBP-rP1^{FLAG}, CTGF^{FLAG} (2) and NovH^{FLAG} (26) were electrophoresed and immunoblotted with two representative anti-IGFBP-rP1 monoclonal antibodies (no. 5 and 10). Neither of these antibodies cross-reacted significantly with CTGF^{FLAG}, NovH^{FLAG}, or any of the IGFBPs (Fig. 2A). The presence of these proteins was demonstrated by immunoblotting the same membranes with anti-CTGF and anti-NovH antibodies (data not shown) and by Western ligand blotting with ^{125}I-IGF-I and ^{125}I-IGF-II for the IGFBPs (Fig. 2B).

Characterization of IGFBP-rP1 in normal human biological fluids by WIB

Once the sensitivity and specificity of the anti-IGFBP-rP1 monoclonal antibodies were demonstrated, we investigated the presence of IGFBP-rP1 in the major human body fluids, such as serum, urine, AF, and CSF using these antibodies. In pooled normal human serum from healthy adults, both the polyclonal anti-IGFBP-rP1 antibody and the panel of monoclonal antibodies recognized an approximately 31-kDa protein that ran at slightly higher molecular mass than the baculovirus-generated rhIGFBP-rP1^{FLAG}. Furthermore, the specificity of this band was demonstrated by immunoblotting with an rhIGFBP-rP1^{FLAG} preadsorbed fraction of the polyclonal antibody (Fig. 3A). Similarly, distinct and specific IGFBP-rP1 bands were detected by both the polyclonal anti-IGFBP-rP1 antibody and monoclonal anti-IGFBP-rP1 antibodies in pooled normal human urine, AF, and CSF from healthy adults (Fig. 3B). The lower sensitivity of the monoclonals can be attributed to the fact that nonreducing conditions were employed for these WIB analyses because, as demonstrated above (see Fig. 1), reducing conditions en-

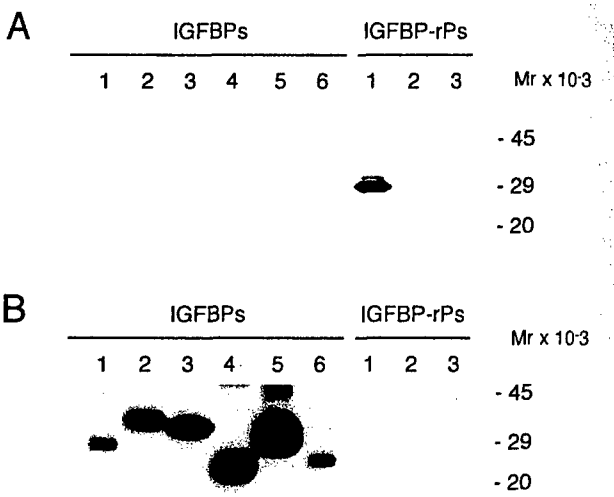

FIG. 2. Specificity of anti-IGFBP-rP1 monoclonal antibodies. Monoclonal anti-IGFBP-rP1 antibody (no. 5) was tested against equimolar amounts of IGFBPs (IGFBP-1 through 6) and rhIGFBP-rP1^{FLAG}, CTGF^{FLAG} (2), NovH^{FLAG} (26). Note that rhIGFBP-3 is *Escherichia coli* expressed and nonglycosylated, with a molecular mass of 29 kDa. Identical results were obtained with monoclonal anti-IGFBP-rP1 no. 10 (data not shown). A, WIB. B, Western ligand blot. The WIB in A was incubated with [^{125}]IGF-I and [^{125}]IGF-II (ligand blot) to confirm the presence of the six IGFBPs.

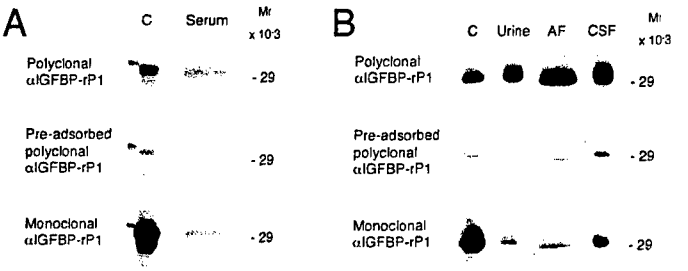

FIG. 3. WIB studies of IGFBP-rP1 in human body fluids. A, Two-microliter aliquots of 10-fold heparin affinity column-concentrated normal human serum were electrophoresed in triplicate and immunoblotted with polyclonal anti-IGFBP-rP1 antibody, rhIGFBP-rP1^{FLAG}-preadsorbed fraction of anti-IGFBP-rP1 polyclonal antibody, or a representative monoclonal antibody (no. 5 and/or 10). Baculovirus-generated rhIGFBP-rP1 (100 ng) was run as control ("C"). B, Similar WIB studies were carried out with human urine (50 μl), AF (20 μl), CSF (50 μl), and rhIGFBP-rP1 (100 ng) as control ("C").

hance the affinity of the monoclonals for endogenous IGFBP-rP1.

Quantification of IGFBP-rP1 in normal human serum by ELISA

An IGFBP-rP1 noncompetitive sandwich-type immunoassay (see *Materials and Methods*) was developed to analyze individual human serum samples. The IGFBP-rP1 ELISA standard curve for the assay is shown in Fig. 4.

In normal human adult sera (n = 37), the median IGFBP-rP1 was 21.0 μg/liter (Table 2). The values did not correlate with IGF-I (r = 0.085, $P = 0.61$), IGF-II (r = 0.051, $P = 0.75$), or IGFBP-3 (r = 0.061, $P = 0.74$) levels. A sexual dimorphism in circulating IGFBP-rP1 was evident, with higher IGFBP-rP1 concentrations in male subjects (26.3 ± 6.8, n = 19 *vs.* 19.8 ± 9.2, n = 18; $P = 0.01$). In matched samples from normal adult males and females (n = 13), median IGFBP-rP1 levels were similar in serum, plasma-EDTA, and plasma-heparin (ANOVA $P = 0.768$) and were 20.8, 19.9, and 22.0 ng/ml, respectively. The anti-IGFBP-rP1 antibodies also immunodetected circulating IGFBP-rP1 in other mammals (*e.g.* pigs and cows) but not rodents (data not shown). IGFBP-rP1 in the matched samples, in fetal bovine serum, as well as the recombinant (nontagged) form, was stable at 4 C for at least 4 d.

Distribution of IGFBP-rP1 in human tissues

Immunostaining of human tissues with IGFBP-rP1 antibodies generated against a decapeptide in the C terminus of IGFBP-rP1 has been reported by Akaogi *et al.* (5) and more recently by Degeorges *et al.* (33). With our panel of characterized antibodies, the tissue distribution of IGFBP-rP1 in cryostat sections of normal and malignant human tissues was analyzed.

To ascertain the specificity of the immunostaining, parallel tissue sections (Fig. 5, A and B, lung squamous carcinoma tissue) were initially prepared with both the polyclonal anti-IGFBP-rP1 antibody and antibody preadsorbed with rhIGFBP-rP1^{FLAG}. Figure 5A shows typical positive immunostaining (*arrows*), which was reduced to background with the preadsorbed fraction of the polyclonal antibody (Fig. 5B, *arrows*). Identical patterns of staining were observed in these sections with the monoclonal anti-IGFBP-rP1 antibodies (Fig. 5C, lung squamous carcinoma tissue).

In normal tissues (prostate, breast, and colon), immunoreactivity was weak and limited to small blood vessels (Fig. 5D, normal prostate). Diffuse staining of the stroma was also observed. The immunostaining was, however, notably enhanced in the endothelial cells of the microvasculature of most of the human cancer tissues examined (lung, prostate, colon), using either the polyclonal or the monoclonal anti-IGFBP-rP1 antibodies (Figs. 5, A, C, E, and F).

Immunohistochemical analysis of IGFBP-rP1 expression was extended to include paraffin-embedded tissue sections (data not shown). Unlike frozen tissue sections, only the monoclonal anti-IGFBP-rP1 antibodies were capable of detecting IGFBP-rP1 expression, but the overall signal was less robust than that detected in frozen tissue sections. The pattern of staining, however, remained the same, with immunostaining predominantly identified in vascular endothelium, particularly in the microvasculature of tumor tissues.

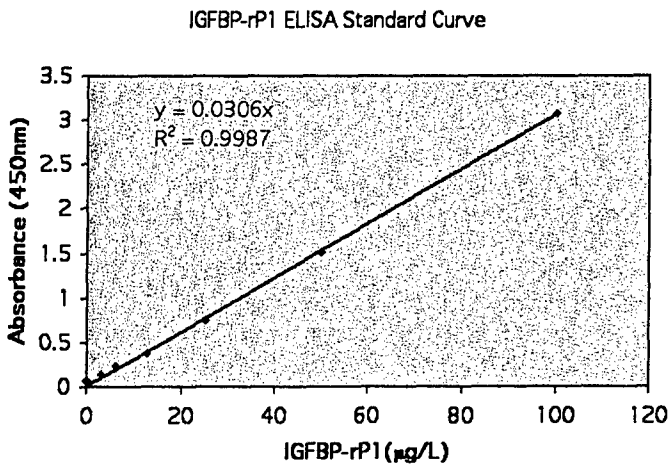

FIG. 4. IGFBP-rP1 ELISA standard curve. Linearity of the curve is as indicated (R2).

TABLE 2. IGFBP-rP1 levels in human body fluids

Sample	Mean	Median	SD	Range	n
Serum					
All	23.1	21.0	8.6	9.9–40	37
Male	26.3	27.3	6.8	15.6–37.9	19
Female	19.8	17.5	9.2	9.9–40.0	18

Discussion

The biological roles of IGFBP-rP1 have been evaluated in numerous studies and include diverse actions, such as tumor suppression (8, 11, 12, 14, 16, 34), stimulation of prostacyclin synthesis (10), and involvement in angiogenesis (5, 19, 24).

We previously characterized a polyclonal anti-IGFBP-rP1 antibody and identified IGFBP-rP1 in conditioned media from cultured human cells as well as in human biological fluids (25). Here we extend these studies with the characterization of new anti-IGFBP-rP1 monoclonal antibodies to study the distribution of IGFBP-rP1 in human biological fluids and tissues. These monoclonal antibodies, like the polyclonal antibody, do not cross-react with the six conventional IGFBP proteins or proteins of the CCN family. All 11 of the monoclonal antibodies specifically recognize the approximately 31-kDa secreted IGFBP-rP1 protein in conditioned medium from cultured human cells.

Here we also show for the first time quantitative data on serum IGFBP-rP1 in humans and indicate a dimorphic distribution of circulating IGFBP-rP1, with higher concentrations of IGFBP-rP1 in males. Because IGFBP-rP1 could be down-regulated by estrogens, according to one report (8), a plausible mechanism for the lower concentrations of circulating IGFBP-rP1 in females could be its tonic inhibition by estrogens. Although the assay was not developed to quantitate IGFBP-rP1 in other body fluids, the assay readily detected IGFBP-rP1 in human urine, AF, and CSF (data not shown), consistent with the findings obtained by immuno-

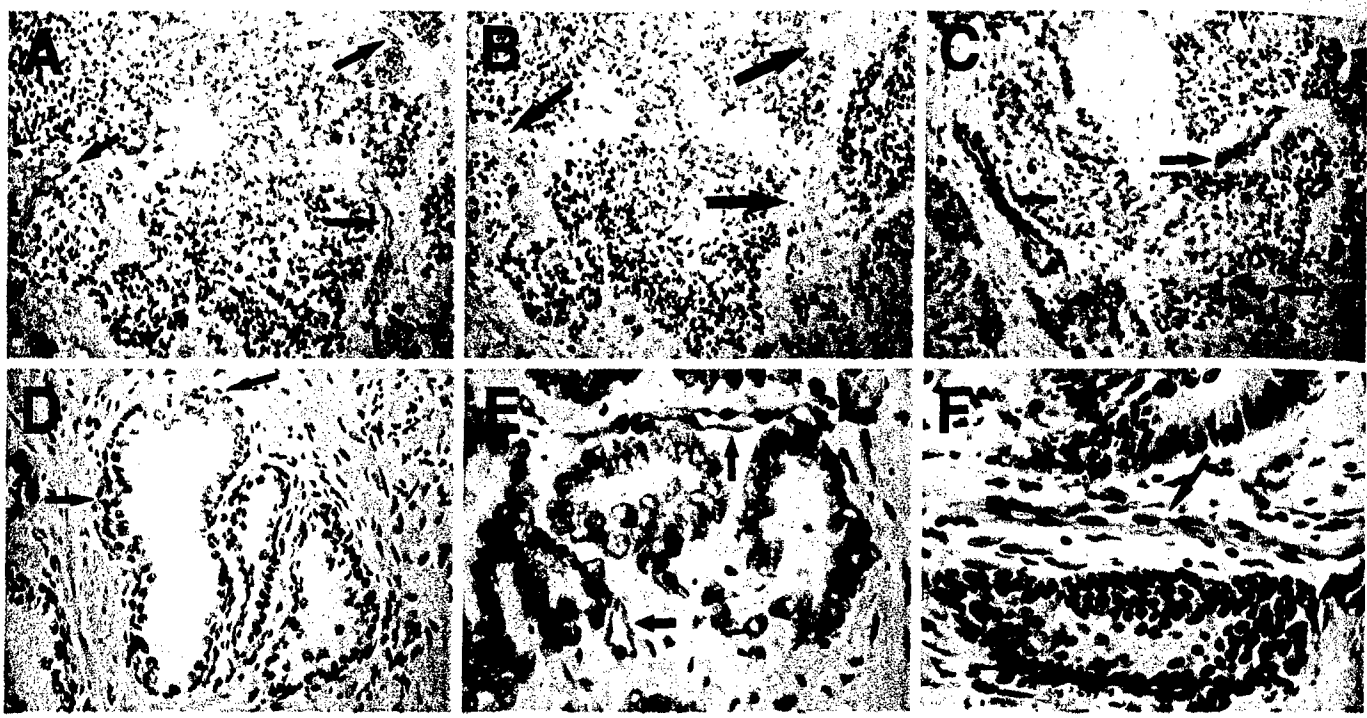

FIG. 5. Immunohistochemical analyses of IGFBP-rP1 in normal and malignant human tissues. Cryostat sections of various human tissues were fixed on slides and immunohistochemistry analysis performed using either the polyclonal or representative monoclonal antibodies (no. 5 and/or 10). Representative sections are as shown. *Arrows* indicate regions of specific immunostaining. A, Lung squamous carcinoma immunostained with the IgG fraction of anti-IGFBP-rP1 polyclonal antibody (αIGFBP-rP1 polyclonal). B, Parallel section of A immunostained with the preadsorbed fraction of αIGFBP-rP1 polyclonal antibody. C, Lung squamous carcinoma immunostained with the IgG fraction of anti-IGFBP-rP1 monoclonal antibody no. 10. Identical results were obtained with monoclonal antibody no. 5 (data not shown). D, Normal prostatic tissue immunostained with αIGFBP-rP1 polyclonal. E, Prostate cancer stained with αIGFBP-rP1 monoclonal no. 10. F, Colon cancer stained with polyclonal αIGFBP-rP1 antibody. Magnification, ×200 (A–D) and ×400 (E and F).

blot analysis. Further investigations are warranted to evaluate the clinical significance of these observations.

Both the polyclonal and the panel of monoclonal anti-IGFBP-rP1 antibodies were capable of detecting IGFBP-rP1 in major human body fluids, such as serum, urine, AF, and CSF. Interestingly, the IGFBP-rP1 protein detected in most of these samples (with the exception of amniotic fluid) appeared to be of a slightly higher molecular mass than the rhIGFBP-rP1^{FLAG} protein (Fig. 3). This observation may be accounted for by differences in glycosylation or other post-translational modifications between the baculovirus-generated recombinant protein and human IGFBP-rP1 detected in body fluids. These observations are consistent with the molecular weight of IGFBP-rP1 protein detected in the conditioned media of mammalian cells (12, 15, 25).

To further characterize IGFBP-rP1 protein expression *in vivo*, we used the panel of anti-IGFBP-rP1 antibodies to evaluate IGFBP-rP1 distribution in tissues. For both the polyclonal and panel of monoclonal antibodies, frozen tissue sections were superior to paraffin-embedded sections for immunodetection. Identical patterns of staining in the frozen tissues were observed with polyclonal and monoclonal antibodies, and the staining appears to be specific because preclearing of the relevant IgG fraction with rhIGFBP-rP1^{FLAG} protein abrogated the signals. Most striking was that the distribution of IGFBP-rP1 was predominantly among endothelial cells of tumor tissues, with reduced, but detectable, signals in endothelial cells of normal tissues and in the stroma of all tissues examined. Similar observations were made with the paraffin-embedded tissue sections.

Our findings concur, in part, with other reports of the IGFBP-rP1 distribution in human tissues (5, 11, 33, 35). In these previous studies, the tissue sections examined were all paraffin embedded, and immunohistochemical analysis employed an incompletely characterized monoclonal antibody (5) or a polyclonal antibody (11, 33, 35) generated against a decapeptide in the C terminus of IGFBP-rP1 and, therefore, of uncertain specificity. The latter polyclonal antibody (11) recognized only the reduced approximately 37-kDa form of IGFBP-rP1 protein (33). Because our polyclonal and monoclonal antibodies were generated against intact IGFBP-rP1 protein, the patterns and sensitivity of staining might be expected to differ from that of other laboratories. Nevertheless, Akaogi *et al.* (5) detected tumor-derived adhesion factor (IGFBP-rP1) immunoreactivity in the vascular membrane of small blood vessels as well as capillaries of diverse cancer tissues but not those associated with normal tissues. Degeorges *et al.* (33), in contrast, did observe immunostaining of normal endothelial cells, but intense immunoreactivity was associated predominantly with supporting cells of peripheral nerves and stromal cells of numerous tissues.

The implication from this present study (and others) is that not only do endothelial cells express IGFBP-rP1 protein but also expression is considerably higher in endothelial cells

associated with cancers. Intriguingly, a recent comparative study profiling gene expression in endothelium derived from normal and tumor tissue supports these observations (24). Analysis by serial analysis of gene expression determined that IGFBP-rP1 was the pan endothelial marker most abundantly expressed in endothelial cells and there was a 2-fold increase in gene expression in malignant tissues (24). These observations support an important role of IGFBP-rP1 in vascular biology and, as first proposed by Akaogi *et al.* (5), suggest that IGFBP-rP1 may be involved in the process of neoangiogenesis in malignancy. Furthermore, because IGFBP-rP1 appears to induce prostacyclin synthesis in endothelial cells (10), IGFBP-rP1 may also have roles in noncancerous human vascular diseases, such as atherosclerosis and hypertension. The new tools presented here should, therefore, prove useful in dissecting out the involvement of this protein in vascular function of normal and malignant tissues.

Other than endothelial cells, IGFBP-rP1 was detected rarely in epithelial cells in our immunohistochemical analysis of IGFBP-rP1 distribution. This was somewhat unexpected because we previously demonstrated that epithelial cells, at least *in vitro*, do express IGFBP-rP1 protein, and *in situ* hybridization studies of normal prostate tissues indicate IGFBP-rP1 mRNA in glandular epithelium that surrounds the lumen (12, 15). The apparent contradiction could be due to the sensitivity of antibodies. Akaogi *et al.* (5), similarly, did not detect immunostaining of epithelial cells with their antibody. However, the polyclonal antibody raised against the C-terminal region of IGFBP-rP1 was reactive to the luminal epithelial cell of normal lobules and ducts of breast tissues (11); the tumor epithelial cells of prostate tissue (35); and ciliated cells of bronchial, epididymal, and fallopian epithelia (33). Thus, the variations in the immunoreactivity of tissues and cell types in each study clearly depend on the source of antibodies and, most likely, also on the method of tissue preparation and processing.

Existing data on IGFBP-rP1 indicate that its role in cancer remains to be defined. Based on recent serial analysis of gene expression analysis (24) and immunohistochemical studies, including the present report, IGFBP-rP1 is implicated in the neovascularization process so critical for tumor growth. This contrasts with a growing body of evidence that suggests IGFBP-rP1 is a potential tumor suppressor gene. In a number of cancers, such as breast (8, 11, 13, 18), meningiomas (8), prostate cancer (12), and liver tumorigenesis (36), IGFBP-rP1 expression was down-regulated, although expression appeared to be up-regulated in carcinogenesis of colon mucosa (23, 37). Interestingly, IGFBP-rP1 is associated with a 50% loss of heterozygosity (LOH) in breast cancer (11). Furthermore, overexpression of IGFBP-rP1 in a prostate cancer cell line was shown to dramatically reduce tumorigenic potential of the cell line (16, 17), and exogenous addition of the protein to cancer cell lines appeared to inhibit cell growth (38). Taken altogether, these observations suggest that although IGFBP-rP1 is clearly important in tumorigenesis, its specific role(s) is still unclear, and most likely depends on a number of factors, including the tissue and cell type under study, the sensitivity, and specificity of reagents used as well as the techniques employed.

In summary, using a panel of newly developed IGFBP-rP1 monoclonal antibodies and an immunoassay, we demonstrate that IGFBP-rP1 is detectable in serum and other biological fluids and provide quantitative data on the concentrations of IGFBP-rP1 in human serum. We also have shown distribution of IGFBP-rP1 in human normal and cancerous tissues. IGFBP-rP1 appears to be involved in vascular biology, possibly in the process of neoangiogenesis that occurs in tumor tissues. The use of these novel IGFBP-rP1 detection tools should prove useful in the elucidation of the biological role of this IGFBP related protein.

Acknowledgments

Received August 16, 2002. Accepted March 24, 2003.

Address all correspondence and requests for reprints to: Ron G. Rosenfeld, M.D., Department of Pediatrics-CDRCP, Oregon Health Sciences University, 707 SW Gaines Road, Portland, Oregon 97201. E-mail: rosenfer@ohsu.edu.

This work was supported by NIH Grant CA58110 and DMD17-00-1-0042. A.L.-B. is supported by a Fellow Research Funding Grant from Eli Lilly & Co. and is also a recipient of Grants 97/5309 and 98/9198 from the Fondo de Investigacion Sanitaria, Spain.

References

1. **Jones JI, Clemmons DR** 1995 Insulin-like growth factors and their binding proteins: biological actions. Endocr Rev 16:3–34
2. **Kim HS, Nagalla SR, Oh Y, Wilson E, Roberts Jr CT, Rosenfeld RG** 1997 Identification of a family of low-affinity insulin-like growth factor binding proteins (IGFBPs): characterization of connective tissue growth factor as a member of the IGFBP superfamily. Proc Natl Acad Sci USA 94:12981–12986
3. **Hwa V, Oh Y, Rosenfeld RG** 1999 The insulin-like factor binding protein (IGFBP) superfamily. Endocr Rev 20:761–787
4. **Oh Y, Nagalla SR, Yamanaka Y, Kim HS, Wilson E, Rosenfeld RG** 1996 Synthesis and characterization of insulin-like growth factor-binding protein (IGFBP)-7. Recombinant human mac25 protein specifically binds IGF-I and -II. J Biol Chem 271:30322–30325
5. **Akaogi K, Okabe Y, Sato J, Nagashima Y, Yasumitsu H, Sugahara K, Miyazaki K** 1996 Specific accumulation of tumor-derived adhesion factor in tumor blood vessels and in capillary tube-like structures of cultured vascular endothelial cells. Proc Natl Acad Sci USA 93:8384–8389
6. **Yamanaka Y, Wilson EM, Rosenfeld RG, Oh Y** 1997 Inhibition of insulin receptor activation by insulin-like growth factor binding proteins. J Biol Chem 272:30729–30734
7. **Vorwerk P, Hohmann B, Oh Y, Rosenfeld RG, Shymko RM** 2002 Binding properties of insulin-like growth factor binding protein-3 (IGFBP-3), IGFBP-3 N- and C-terminal fragments, and structurally related proteins mac25 and connective tissue growth factor measured using a biosensor. Endocrinology 143:1677–1685
8. **Murphy M, Pykett MJ, Harnish P, Zang KD, George DL** 1993 Identification and characterization of genes differentially expressed in Meningiomas. Cell Growth Differ 4:715–722
9. **Akaogi K, Okabe Y, Funahashi K, Yoshitake Y, Nishikawa K, Yasunitsu H, Umeda M, Miyazaki K** 1994 Cell adhesion activity of a 30-kDa major secreted protein from human bladder carcinoma cells. Biochem Biophys Res Commun 198:1046–1053
10. **Yamauchi T, Umeda F, Masakado M, Isaji M, Mizushima S, Nawata H** 1994 Purification and molecular cloning of prostacyclin-stimulating factor from serum-free conditioned medium of human diploid fibroblast cells. Biochem J 303:591–598
11. **Burger AM, Zhang X, Li H, Ostrowski JL, Beatty B, Venanzoni M, Papas T, Seth A** 1998 Down-regulation of T1A12/mac25, a novel insulin-like growth factor binding protein related gene, is associated with disease progression in breast carcinomas. Oncogene 16:2459–2467
12. **Hwa V, Tomasini-Sprenger C, Bermejo AL, Rosenfeld RG, Plymate SR** 1998 Characterization of insulin-like growth factor-binding protein-related protein-1 in prostate cells. J Clin Endocrinol Metab 83:4355–4362
13. **Landberg G, Ostlund H, Nielsen NH, Roos G, Emdin S, Burger AM, Seth A** 2001 Downregulation of the potential suppressor gene IGFBP-rP1 in human breast cancer is associated with inactivation of the retinoblastoma protein, cyclin E overexpression and increased proliferation in estrogen receptor negative tumors. Oncogene 20:3497–3505
14. **Swisshelm K, Ryan K, Tsuchiya K, Sager R** 1995 Enhanced expression of an insulin growth factor-like binding protein (mac25) in senescent human mam-

mary epithelial cells and induced expression with retinoic acid. Proc Natl Acad Sci USA 92:4472–4476

15. **Lopez-Bermejo A, Buckway CK, Devi GR, Hwa V, Plymate SR, Oh Y, Rosenfeld RG** 2000 Characterization of insulin-like growth factor-binding protein-related proteins (IGFBP-rPs) 1, 2, and 3 in human prostate epithelial cells: potential roles for IGFBP-rP1 and 2 in senescence of the prostatic epithelium. Endocrinology 141:4072–4080
16. **Sprenger CC, Damon SE, Hwa V, Rosenfeld RG, Plymate SR** 1999 Insulin-like growth factor binding protein-related protein 1 (IGFBP-rP1) is a potential tumor suppressor protein for prostate cancer. Cancer Res 59:2370–2375
17. **Sprenger CC, Vail ME, Evans K, Simurdak J, Plymate SR** 2002 Over-expression of insulin-like growth factor binding protein-related protein-1(IGFBP-rP1/mac25) in the M12 prostate cancer cell line alters tumor growth by a delay in G1 and cyclin A associated apoptosis. Oncogene 21:140–147
18. **Wilson HM, Birnbaum RS, Poot M, Quinn LS, Swisshelm K** 2002 Insulin-like growth factor binding protein-related protein 1 inhibits proliferation of MCF-7 breast cancer cells via a senescence-like mechanism. Cell Growth Differ 13: 205–213
19. **Kishibe J, Yamada S, Okada Y, Sato J, Ito A, Miyazaki K, Sugahara K** 2000 Structural requirements of heparan sulfate for the binding to the tumor-derived adhesion factor/angiomodulin that induces cord-like structures to ECV-304 human carcinoma cells. J Biol Chem 275:15321–15329
20. **Girard JP, Baekkevold ES, Yamanaka T, Haraldsen G, Brandtzaeg P, Amalric F** 1999 Heterogeneity of endothelial cells: the specialized phenotype of human high endothelial venules characterized by suppression subtractive hybridization. Am J Pathol 155:2043–2055
21. **Izawa D, Tanaka T, Saito K, Ogihara H, Usui T, Kawamoto S, Matsubara K, Okubo K, Miyasaka M** 1999 Expression profile of active genes in mouse lymph node high endothelial cells. Int Immunol 11:1989–1998
22. **Sato J, Hasegawa S, Akaogi K, Yasumitsu H, Yamada S, Sugahara K, Miyazaki K** 1999 Identification of cell-binding site of angiomodulin (AGM/TAF/Mac25) that interacts with heparan sulfates on cell surface. J Cell Biochem 75:187–195
23. **Adachi Y, Itoh F, Yamamoto H, Arimura Y, Kikkawa-Okabe Y, Miyazaki K, Carbone DP, Imai K** 2001 Expression of angiomodulin (tumor-derived adhesion factor/mac25) in invading tumor cells correlates with poor prognosis in human colorectal cancer. Int J Cancer 95:216–222
24. **St. Croix B, Rago C, Velculescu V, Traverso G, Romans KE, Montgomery E, Lal A, Riggins GJ, Lengauer C, Vogelstein B, Kinzler KW** 2000 Genes expressed in human tumor endothelium. Science 289:1197–1202
25. **Wilson EM, Oh Y, Rosenfeld RG** 1997 Generation and characterization of an IGFBP-7 antibody: identification of 31kD IGFBP-7 in human biological fluids and Hs578T human breast cancer conditioned media. J Clin Endocrinol Metab 82:1301–1303
26. **Burren CP, Wilson EM, Hwa V, Oh Y, Rosenfeld RG** 1999 Binding properties and distribution of insulin-like growth factor binding protein-related protein 3 (IGFBP-rP3/NovH), an additional member of the IGFBP superfamily. J Clin Endocrinol Metab 84:1096–1103
27. **Lane RD** 1985 A short-duration polyethylene glycol fusion technique for increasing production of monoclonal antibody-secreting hybridomas. J Immunol Methods 81:223–228
28. **Khosravi MJ, Diamandi A, Mistry J** 1997 Immunoassay of insulin-like growth factor binding protein-1. Clin Chem 43:532–532
29. **Khosravi MJ, Diamandi A, Mistry J** 1995 Ultrasensitive immunoassay for prostate-specific antigen based on conventional colorimetric detection. Clin Biochem 28:407–414
30. **Khosravi MJ, Diamandi A, Mistry J, Lee PDK** 1996 A non-competitive ELISA for human serum insulin-like growth factor-1. Clin Chem 42:1147–1154
31. **Bradham DM, Igarashi A, Potter RL, Grotendorst GR** 1991 Connective tissue growth factor: a cysteine-rich mitogen secreted by human vascular endothelial cells is related to the SRC-induced immediate early gene product CEF-10. J Cell Biol 114:1285–1294
32. **Martinerie C, Huff V, Joubert I, Badzioch M, Saunders G, Strong L, Perbal B** 1994 Structural analysis of the human nov proto-oncogene and expression in Wilms tumors. Oncogene 9:2729–2732
33. **Degeorges A, Wang F, Frierson Jr HF, Seth A, Sikes RA** 2000 Distribution of IGFBP-rP1 in normal human tissues. J Histochem Cytochem 48:747–754
34. **Kato MV, Sato H, Tsukada T, Ikawa Y, Aizawa S, Nagayoshi M** 1996 A follistatin-like gene, mac25, may act as a growth suppressor of osteosarcoma cells. Oncogene 12:1361–1364
35. **Degeorges A, Wang F, Frierson Jr HF, Seth A, Chung LW, Sikes RA** 1999 Human prostate cancer expresses the low affinity insulin-like growth factor binding protein IGFBP-rP1. Cancer Res 59:2787–2790
36. **Komatsu S, Okazaki Y, Tateno M, Kawai J, Konno H, Kusakabe M, Yoshiki A, Muramatsu M, Held WA, Hayashizaki Y** 2000 Methylation and down-regulated expression of mac25/insulin-like growth factor binding protein-7 is associated with liver tumorigenesis in SV40T/t antigen transgenic mice, screened by restriction landmark genomic scanning for methylation (RLGS-M). Biochem Biophys Res Commun 267:109–117
37. **Umeda F, Ono Y, Sekiguchi N, Hashimoto T, Masakado M, Nakamura K, Chijiiwa Y, Nawata H** 1998 Increased mRNA expression of a novel prostacyclin-stimulating factor in human colon cancer. J Gastroenterol 33:213–217
38. **Kato MV** 2000 A secreted tumor-suppressor, mac25, with activin-binding activity. Mol Med 6:126–135